Modelling subject-specific patellofemoral joint dynamics

by
Jacobus Hendrik Müller

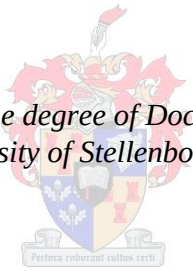

Dissertation presented for the degree of Doctor of Engineering at the University of Stellenbosch

Promoter: Prof. Cornie Scheffer
Co-promoter: Prof. Alex Elvin
Faculty of Engineering
Department of Mechanical and Mechatronic Engineering

December 2010

Declaration

By submitting this dissertation electronically, I declare that the entirety of the work contained therein is my own, original work; that I am the owner of the copyright thereof (unless to the extent explicitly otherwise stated); and that I have not previously in its entirety or in part submitted it for obtaining any qualification.

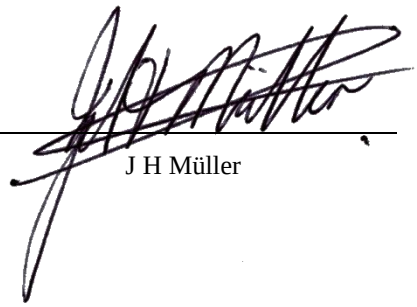

J H Müller

Date: 14 October 2010

Abstract

A methodology to facilitate analysis of dynamic subject-specific patellofemoral function is presented. An enhanced understanding of patellofemoral biomechanics will enable orthopaedic surgeons to identify the mechanisms responsible for imbalances in the joint stabilisers, while also providing objective information on which to base treatment methods. Dynamic patellofemoral function of three volunteers was simulated with a musculoskeletal computational model. The individuals underwent scans from which three-dimensional models of their patellofemoral joints were constructed. Skeletal muscles and soft tissue stabilisers were added to the skeletal models, after which subject-specific motion was simulated.

After trochlear engagement, the patellae of the volunteers followed a lateral path, whereas patella tilt was subject-specific. Comparison of the predicted tilt and mediolateral position values at 30 degrees knee flexion to *in-vivo* MRI values showed a mean accuracy of 62.1 % and 96.9 % respectively. The patellofemoral contact load – quadriceps tendon load ratio varied between 0.7 and 1.3, whereas the mediolateral load component – resultant load ratio ranged between 0 and 0.4. Both parameters' values were similar to previous findings. The medial patellofemoral ligament tension decreased with knee flexion, while the patellar tendon-quadriceps tendon ratio followed a similar trend to that of previous findings (varied between 0.4 and 1.2).

After induction of a tubercle osteotomy in the coronal plane, Volunteer One's patella engaged the trochlear groove at an earlier knee flexion angle, while the patella of Volunteer Two only underwent a small medial displacement. Finite element analyses were employed to investigate the influence of the osteotomy on the patellofemoral pressure distribution. The mean pressure in Volunteer One's patellofemoral joint was alleviated (17 % smaller) at all angles of flexion with the exception of 60 degrees (12 % greater). Pressure in Volunteer Two's joint was alleviated at 30 and 45 degrees knee flexion (6 % smaller), while it was elevated (9.1 % greater) at other angles of flexion.

Two commercial patellofemoral prostheses were tested on the three Volunteers' joints in the virtual environment. Prosthesis Two delivered patella shift and tilt patterns similar to the baseline values. Patellar tendon tension was slightly greater after resurfacing, with the tensions elevated most with Prosthesis Two. Medial patellofemoral ligament tension was reduced most with Prosthesis Two, while lateral retinaculum tension was increased slightly. Prosthesis Two was the best candidate to reproduce patella kinematics, while the patellofemoral kinetics was largely independent from the type of prosthesis used. The prostheses performed worse for Volunteer Three, supporting the need for the development of patient-specific prostheses.

Three validated subject-specific musculoskeletal models facilitated the analysis of the individuals' patellofemoral biomechanics. The technique can potentially be employed by orthopaedic surgeons to visualise the change that an osteotomy or patellofemoral arthroplasty might induce on an individual's patellofemoral joint. This technique might aid in the development of a tool to assist biomedical engineers in the development of new patellofemoral prostheses. Most importantly, the outcome of surgical intervention may be predicted beforehand, and a treatment procedure may be tailored to optimally fit the patellofemoral biomechanics of that individual.

Opsomming

‘n Ondersoekmetode van die dinamiese gedrag van pasiënt-spesifieke patellofemorale gewrigte word beskryf. Indien die patellofemorale biomeganika beter verstaan word, kan ortopediese chirurge die meganismes wat verantwoordelik is vir oneffektiewe stabiliseerders identifiseer en behandeling op objektiewe bevindinge baseer. Die dinamiese patellofemorale funksie van drie vrywilligers is gesimuleer m.b.v. `n spier-skelet rekenaarmodel. Drie-dimensionele modelle van die individue se patellofemorale gewrig is gekonstrueer m.b.v. skanderings. Die skeletspiere en sagte ondersteuningsweefsel is tot die model toegevoeg, voordat vrywilliger-spesifieke beweging gesimuleer is.

Die knieskywe van die vrywilligers het `n laterale pad gevolg nadat dit die groef binnegetree het, met die tiltwaardes uniek vir elke vrywilliger. Vergelyking van die beraamde knieskyf mediolaterale tilt en posisies by 30 grade fleksie met *in-vivo* magnetiese resonansieskandering waardes het `n akkuraatheid van 62.1 % en 96.9 % respektiewelik getoon. Die patellofemorale kontaklas-kwadriseps seningspanning verhouding het gewissel tussen 0.7 en 1.3; asook die mediale komponent – resultante komponent patellofemorale kontaklas wat gewissel het tussen 0 en 0.4. Beide parameters se waardes was soortgelyk aan voorheen-gepubliseerde data. Die mediale patellofemorale ligamentspanning het afgeneem met fleksie. Die patella sening-kwadriseps seningspanning verhouding was soortgelyk aan vorige gepubliseerde waardes en het gewissel tussen 0.4 en 1.2.

Nadat ‘n tuberkel-osteotomie in die koronale vlak aangebring is, het Vrywilliger Een se patella die femorale groef vroeër binnegetree. Vrywilliger Twee se patella het slegs `n mediale verskuiwing ondergaan. Eindige element analises is ingespan om die effek van die osteotomie op die spanningsverspreiding in die patellofemorale gewrig te ondersoek. Die gemiddelde spanning in Vrywilliger Een se gewrig was minder by alle hoeke van fleksie (17 % minder), met uitsondering van die spanning by 60 grade (12 % meer). Die spanning in Vrywilliger Twee se gewrig was minder by 30 en 45 grade (6 % minder), maar hoër by ander hoeke (9.1 % meer).

Twee kommersiële patellofemorale prosteses is getoets op die drie Vrywilligers d.m.v. die model. Prostese Twee het die knieskyf-kinematika die beste nageboots. Die patella-seningspanning was effens groter na die vervanging. Prostese Twee het gesorg vir die grootste toename. Die mediale patellofemorale ligamentspanning was die kleinste toe Prostese Twee gebruik is, maar dit het gesorg vir effense hoër laterale retinakulumlaste. Die analises het getoon dat Prostese Twee die beste kandidaat is om die korrekte kinematika te herbewerkstellig. Die kinetika daarteenoor was onafhanklik van die tipe prostese wat gebruik is. Geeneen van die twee prosteses was geskik vir Vrywilliger Drie nie, wat as motivering vir die ontwikkeling van pasiënt-spesifieke prosteses dien.

Drie bekragtigde vrywilliger-spesifieke spier-skelet modelle het die analise van patellofemorale biomeganika bewerkstellig. Die tegniek het die potensiaal om ortopediste in staat te stel om die effek van `n osteotomie of patellofemorale vervanging te visualiseer. Die tegniek kan verder gebruik word deur biomediese ingenieurs in die vervaardiging van nuwe patellofemorale prosteses. Meer belangrik is die feit dat die resultaat van chirurgiese ingryping voorspel kan word en optimale behandelingsprosedures beplan kan word vir die patellofemorale biomeganika van `n individu.

Department of Mechanical and Mechatronic Engineering Stellenbosch University Declaration

I know that plagiarism is wrong.

Plagiarism is to use another's work (even if it is summarised, translated or rephrased) and pretend that it is one's own.

This assignment is my own work.

Each contribution to and quotation (e.g. "cut and paste") in this assignment from the work(s) of other people has been explicitly attributed, and has been cited and referenced. In addition to being explicitly attributed, all quotations are enclosed in inverted commas, and long quotations are additionally in indented paragraphs.

I have not allowed, and will not allow, anyone to use my work (in paper, graphics, electronic, verbal or any other format) with the intention of passing it off as his/her own work.

I know that a mark of zero may be awarded to assignments with plagiarism and also that no opportunity be given to submit an improved assignment.

I know that students involved in plagiarism will be reported to the Registrar and/or the Central Disciplinary Committee.

Name: Jacobus Hendrik Müller
Student number: 13750666

Signature: 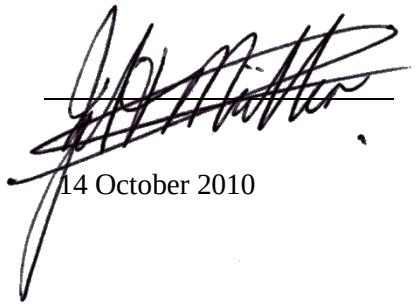

Date: 14 October 2010

Acknowledgements

The author would like to thank the following people or institutions for their contribution:

- Professor Cornie Scheffer and Professor Alex Elvin for their role as promoters.
- Doctor Spike Erasmus and Doctor Edwin Dillon for their assistance in the clinical detail of this report.
- The Department of Mechanical and Mechatronic Engineering for their financial assistance and facilities.
- Tornier for their financial assistance and interest.
- The NRF for their financial assistance.
- Dr. van Wagening and Partners at Stellenbosch Medi-Clinic radiology department for the CT and MRI scans.
- The radiographers at Dr. van Wagening and Partners for their assistance during the CT and MRI scans.
- Smith and Nephew for providing the cadaver knees that were used for the *in-vitro* investigation.
- Doctor Edwin Dillon for his assistance during the *in-vitro* studies.
- The Committee for Human Research at Stellenbosch University for approving the study.
- Mr. Daniel Heunis for designing and testing the cadaver test frame.
- The Mechanical workshop for manufacturing the test frame.
- The volunteers who were willing to take part in the study.
- Stefanie Malan.
- My parents.

Dedication

To the Biomedical Engineering Research Group

(BERG)

Stellenbosch University

Table of Contents

Table of Figures

List of Tables

Nomenclature

Abbreviations

% BW	Percentage bodyweight
ACL	Anterior cruciate ligament
AT	Adductor tubercle
BMI	Body-mass-index
CAD	Computer assisted design
CE	Contractile element
CT	Computed Tomography
DOF	Degrees of freedom
EMG	Electromyogram
FCL	Fibular collateral ligament
FE	Finite element
FEA	Finite element analysis
GT	Gastrocnemius tubercle
HPC	High Performance Cluster / Computer
MCL	Medial collateral ligament
ME	Medial epicondyle
MPFL	Medial patellofemoral ligament
MRI	Magnetic resonance imaging
MVC	Maximum voluntary contraction
N/A	Not applicable
PC	Personal computer
PCL	Posterior cruciate ligament
PE	Passive element
PT	Patellar tendon
Q-angle	Quadriceps-angle
RF	Rectus femoris
SD	Standard deviation
VI	Vastus intermedius
VL	Vastus lateralis
VLL	Vastus lateralis longus
VLO	Vastus lateralis obliquus
VM	Vastus medialis
VML	Vastus medialis longus
VMO	Vastus medialis obliquus
asy	Asymptote

List of Symbols

A	Area
AB	Plane AB
A(t)	Activation state
B	Body reference frame
BO	Bisect offset
CD	Plane CD
E	Elastic modulus
EE	Plane EE
F	Force
G	Global reference frame
X	Cartesian x-axes
Y	Cartesian y-axes
Z	Cartesian z-axes
A	Radius of circular contact area
D	Diameter
I	Cartesian unity vector
J	Cartesian unity vector
K	Cartesian unity vector
K	Passive muscle stress
N	Population size
pCSA	Physiological cross sectional area
Q	Quaternion vector
R	Rotation axis between the body and global reference frame
α	Angle between body axis and reference axis
β	Angle between orientation vectors
ε	Muscle strain
ρ	Correlation coefficient
σ	Passive muscle stress
ν	Poisson ratio
$\mathbf{a}^{\mathbf{B}}$	Body orientation vector
$\mathbf{a}^{\mathbf{G}}$	Reference orientation vector
r^2	Coefficient of determination
CE_{ml}	Maximum relative force (Lengthening)
CE_{sh}	Velocity curve shape (Shortening)
CE_{shl}	Velocity curve shape (Lengthening)
F_{max}	Maximum allowable force
F_{muscle}	Muscle force
F_{CE}	Muscle force contribution from the contractile element
F_{PE}	Muscle force contribution from the passive element
S_k	Active force-length curve shape parameter
S_{free}	No-load sarcomere length
S_{rest}	Resting sarcomere length
$\boldsymbol{Z}_{\boldsymbol{X}_i\boldsymbol{Y}_j}$	Point in three dimensional space
a_i	Orientation vector parameter, $i = 1..3$
d_i	Measurement
f_h	Active force-velocity relationship
f_l	Active force-length relationship
$l_{current}$	Instantaneous muscle length
l_{free}	Free muscle length

l_{rest}	Resting muscle length
l_r	Dimensionless length ratio
q_i	Quaternion parameter, $i = 1..4$
r_i	Rotation axis Cartesian coordinates, $i = 1..3$
v_{max}	Maximum allowable velocity
v_r	Dimensionless velocity ratio
$\mathbf{x_B}$	Cartesian axes body
$\mathbf{y_B}$	Cartesian axes body
y_i	Measurement
$\mathbf{z_B}$	Cartesian axes body
σ_{max}	Maximum allowable stress
$\boldsymbol{A \rightarrow B}$	Line AB
$\boldsymbol{C \rightarrow D}$	Line CD
$\boldsymbol{D \rightarrow E}$	Line DE
$\mathbf{x_B}'$	Rotated Cartesian axis
$\mathbf{x_B}''$	Realigned Cartesian axis
$\mathbf{y_B}'$	Rotated Cartesian axis
$\mathbf{y_B}''$	Realigned Cartesian axis
$\mathbf{z_B}'$	Rotated Cartesian axis
$\mathbf{z_B}''$	Realigned Cartesian axis

Chapter 1

1. Introduction

1.1 Background

"The patella articulates with the femur." This describes the movement of the kneecap relative to the femur, as defined by Henry Gray in the well-known *Gray's Anatomy: Descriptive and Surgical Theory* (Gray (1918)).

Since 1918, various surgeons and biomedical engineers have attempted a more thorough description of the patella's behaviour during knee flexion. Various techniques falling into three categories, namely *in-vivo*, *in-vitro* and computational, have been applied. The first two entail measurements gathered directly from the knee joint, with *in-vivo* referring to measurements obtained from living persons, and *in-vitro* to measurements obtained from deceased persons. Computational techniques are used to predict the response of a mathematical equivalent of the patellofemoral joint as a function of user-defined model inputs. These inputs can be based on measurements obtained through either *in-vivo* or *in-vitro* techniques. Application of these techniques is strongly influenced by the complexity associated with the knee joint and its biomechanics.

In layman's terms, biomechanics can be defined as the science of the mechanical phenomena in living beings (Kapandji (2007)). The study of biomechanics is a discipline that integrates engineering principles with clinical sciences, whereby the behaviour of a biological system is described in terms of its kinetics and kinematics. There is much variability in the results of studies reporting on patellofemoral kinematics (Feller *et al.* (2007); Katchburian *et al.* (2003)). These variations and the lack of objective results complicate the generalisation of patellofemoral function in terms of its biomechanics (Amis *et al.* (2006)). Orthopaedic surgeons therefore face a difficult task in making sense of all the different and often conflicting results from studies on the patellofemoral joint: These **generalised** results need to be interpreted and tailored in an attempt to address patellofemoral pathologies of an **individual**.

1.2 Objectives

This study aims to develop a procedure with which subject-specific patellofemoral biomechanics can be quantified as a function of continuous knee flexion. Patellofemoral function will be simulated with a validated musculoskeletal model generated from and driven according to subject-specific data. The patellofemoral joint model should:

- Be representative of the subject's anatomy in terms of the trochlear groove and patella geometry;
- Include the major soft tissue restraints (medial patellofemoral ligament, lateral retinaculum and the extensor mechanism); and
- Replicate the subject's manner and body motion.

Based on the presented flow chart (Figure 1.1), the following objectives were identified:

- Accurate volumetric imaging of an individual's skeletal geometry, to be used in the generation of subject-specific computer aided design models;
- Accurate representation and placement of the active and passive stabilisers to improve the biofidelity of the musculoskeletal model.
- Subject-specific body motion simulation to enhance the biofidelity of the musculoskeletal models.
- The combination of the musculoskeletal simulation results with finite element analyses (FEA) to predict *in-vivo* patellofemoral contact pressure.
- Validation of the musculoskeletal and finite element model simulation results.
- Demonstration of the clinical relevance of the model with two clinical case studies.

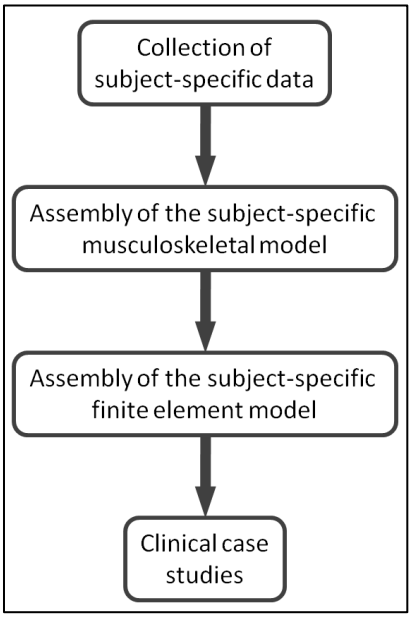

Figure 1.1: Study flowchart (I).

1.3 Motivation

Numerous computational models have been described with which patellofemoral biomechanics were investigated (Besier *et al.* (2005), Elias and Cosgarea (2006), Elias *et al.* (2004, 2010), Fernandez and Hunter

(2005) , Fernandez *et al.* (2008), Mesfar and Shirazi-Adl (2005, 2006), Shirazi-Adl and Mesfar (2007)). Three areas were identified which would improve the predictive ability of the musculoskeletal models:

1) Incorporation of the individual's patellofemoral geometry;
2) Dynamic patellofemoral function analysis; and
3) The inclusion of the peri-patellar stabiliser in the dynamic analysis.

Although one or two of the abovementioned points have been incorporated in the mentioned studies, to the author's knowledge all three were not incorporated in one study. A validated subject-specific musculoskeletal model will enable surgeons to visualise the individual's patellofemoral biomechanics as a function of dynamic knee flexion, as well as the change that a treatment procedure will have on the patellofemoral joint through manipulation of the model parameters. **The outcome of surgical intervention may then be predicted beforehand**, **and a treatment procedure may be based on information related to the patellofemoral biomechanics of that individual.** This will enable more involved experiments than what is possible during *in-vitro* studies (Besier *et al.* (2005)), whereas the need for animal testing and *in-vivo* experiments will be reduced (Fernandez and Hunter (2005)).

1.4 Thesis layout

The thesis has been organised under the following headings:

- **Chapter Two**: A literature review on the current understanding of the patellofemoral joint anatomy and biomechanics is presented, as well as *in-vivo*, *in-vitro*, and computational techniques. The chapter concludes with a discussion on the deficiencies from previous computational models and how these were addressed in this study.
- **Chapter Three**: The collection and processing of the subject-specific measurements necessary for the assembly of the computational and finite element models are described.
- **Chapter Four**: The assembly and results of the musculoskeletal models are discussed.
- **Chapter Five**: The finite element technique that was applied in Chapter 6 is discussed.
- **Chapter Six**: Two case studies are presented to illustrate the use of the technique in the investigation of the effect of surgical intervention of patellofemoral biomechanics.
- **Chapter Seven**: The final conclusions, limitations and future work are discussed.

Chapter 2

2. Literature review

In Chapter 2 the knee joint will be considered in more detail, with the emphasis of the discussion directed towards the knee joint's anatomy, and the interaction between its constitutive parts during normal knee function. It will become clear that the knee joint is a complex multi-degree-of-freedom joint, presenting many difficulties in attempts at analysis / simulation. Although the focus of this study falls on the patellofemoral joint, the anatomy and biomechanics of the tibiofemoral joint will also be considered since it has a direct influence on the patellofemoral joint's behaviour, albeit a minimal influence in terms of patellofemoral kinematics (Seisler and Sheehan (2007)). The last section of this chapter is devoted to a summary of the methods that have been used to analyse the knee joint.

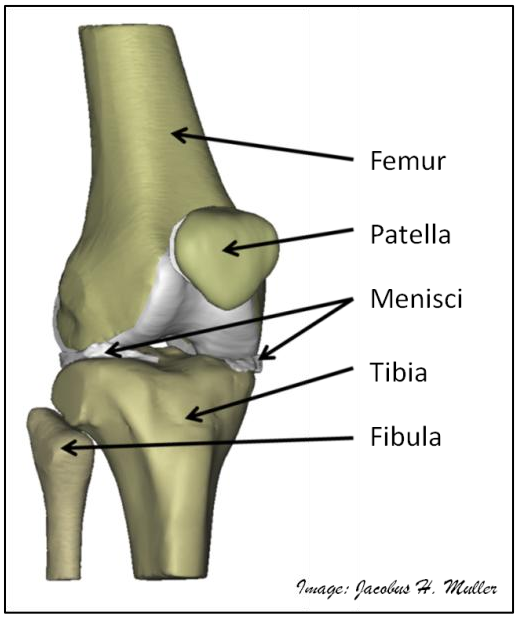

Figure 2.1: The knee joint and its components

2.1 Knee joint anatomy

The knee joint is divided into the patellofemoral joint (patella and anterior femur), the tibiofemoral joint (proximal tibia and distal femur) and the fibulotibial joint (proximal tibia and fibula) (Figure 2.1). Joint stability is provided by soft tissue supporting structures, which are classified as passive stabilisers (ligaments) or active stabilisers (muscle-tendon complex). Stability is further enhanced by the conformity between the contacting bodies, which function in a well-balanced relationship with the active and passive stabilisers. Any imbalance in

this relationship will affect the knee biomechanics, resulting in an unstable joint, leading to joint pain, discomfort and/or immobility.

2.1.1 Skeletal arrangement

The distal femur divides into two convex surfaces, i.e. the lateral and the medial condyles (Figure 2.2). The lateral condyle is the larger of the two, projects more posteriorly and has a flatter distal surface as opposed to the medial condyle (Hamill and Knutzen (2009)). The medial condyle is more distal and covers a shorter anterior-posterior distance than the lateral condyle (Hamill and Knutzen (2009)). The anterior border (front part) of the femoral condyles produces the femoral groove, also referred to as the trochlear groove, which guides the patella during knee flexion (Hamill and Knutzen (2009)) (Figure 2.3). The lateral condyle provides better support to the patella due to its more prominent geometry. Patellofemoral congruency is established through the medial and lateral facets of the patella on its posterior surface (Figure 2.4). Staubli *et al.* (2001) showed that the geometry of the subchondral bone was different to that of the corresponding cartilage. Congruency was therefore largely dependent on the cartilage geometries of the patella and trochlear groove.

The patella is a triangular sesamoid bone[*] functioning as a mechanism which increases the moment arm of the quadriceps tendon, thereby increasing the torque delivered during knee flexion-extension. The patella's articulating area is covered with the thickest cartilage found in the whole body, helping to accommodate the large pressures endured during knee flexion (Hamill and Knutzen (2009)). The medial and lateral facets on the posterior side of the patella are separated by a vertical ridge of bone that can be further divided into the superior, middle and inferior facets, as well as an odd facet on the medial side of the patella (Hamill and Knutzen (2009), Figure 2.5).

[*] A sesamoid bone refers to a bone that is embedded in a tendon.
(http://www.newworldencyclopedia.org/entry/Bone, 29/10/2009)

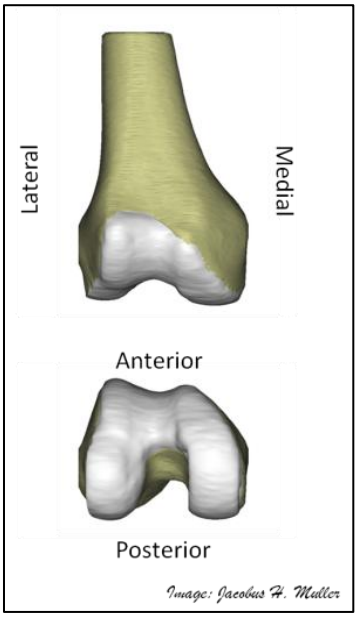

Figure 2.2: The geometry of the distal femur.

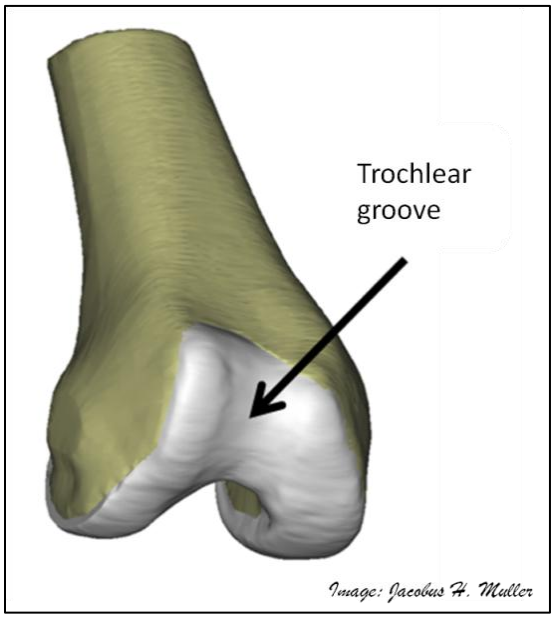

Figure 2.3: The geometry of the trochlear groove.

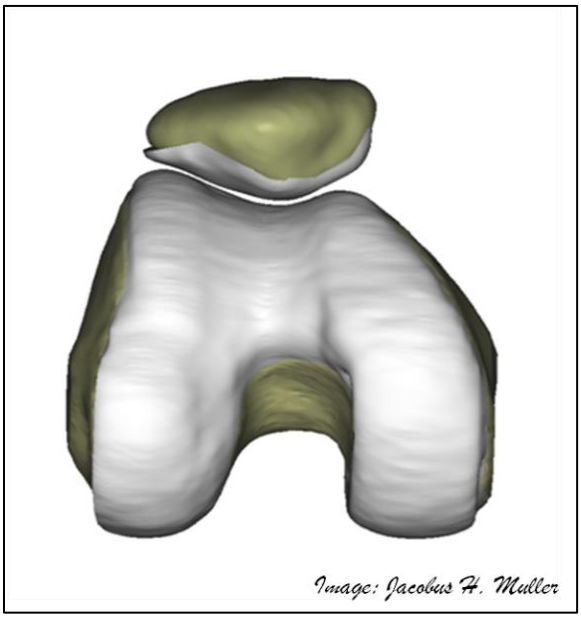

Figure 2.4: The congruency of the patellofemoral joint.

The tibial plateau is divided into a medial and a lateral compartment by a bony ridge that is known as the intercondylar eminence, which indicates the centre of the knee joint and functions as an attachment site for the meniscal ligaments (Hamill and Knutzen (2009), Figure 2.6). It also provides stability when the knee joint is in full extension (Hamill and Knutzen (2009)). The medial compartment is the larger of the two with a longer anterior-posterior dimension. It has an oval appearance and is slightly concave to ensure good contact with the medial condyle of the femur. The lateral plateau is more circular in appearance and has a convex shape. Because of this, the lateral condyle undergoes an anterior-posterior translation relative to the lateral plateau during knee

flexion (sliding-rolling action) (Hamill and Knutzen (2009)). This results in internal rotation of the tibia with respect to the femur during knee flexion, and external rotation during knee extension.

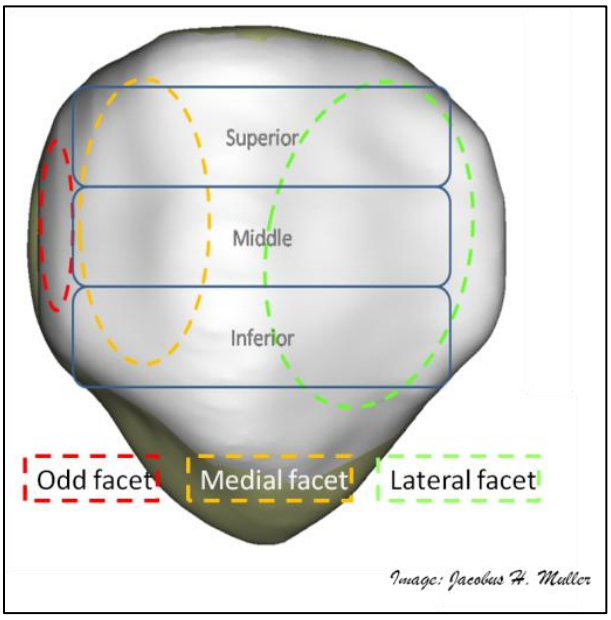

Figure 2.5: The division of the patella's facets.

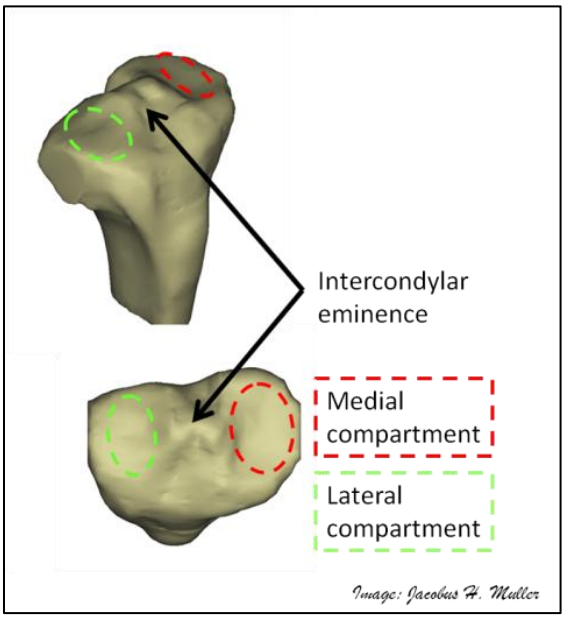

Figure 2.6: The division of the tibial plateau.

The menisci provide additional stability to the tibiofemoral joint (Figure 2.7). The concave geometry of the combination of the tibial plateau and menisci ensure that the tibiofemoral contact is congruent (Figure 2.8). It increases the tibiofemoral contact area, acts as shock absorbers and as additional sources of lubrication by delivering synovial fluids to the joint (Hamill and Knutzen (2009)). Both menisci are wedge-shaped because of their greater thickness at the periphery and they have wide attachment bases at the anterior and posterior horns. The lateral meniscus is oval shaped, whereas the medial meniscus is larger and more crescent shaped. The lateral meniscus does however cover a larger percentage of the lateral tibial compartment (Hamill and Knutzen (2009)). In order to accommodate the anterior-posterior movement of the lateral condyle, the lateral meniscus should be mobile during knee flexion. The lateral meniscus is therefore dynamically less stable, which causes the soft tissues stabilisers, such as the popliteus tendon and meniscal ligaments, to be important dynamic stabilisers to the lateral meniscus.

The fibulotibial joint refers to the contact between the proximal fibula and the posterolateral and inferior aspect of the tibial condyle (Hamill and Knutzen (2009)). The superior fibulotibial joint dissipates the torsional stresses applied by the movement of the foot and it attenuates lateral tibial bending. The fibulotibial joint, in conjunction with the fibula absorb tensile rather than compressive loads, since the middle part of the fibula has more ability to withstand tensile forces than any other part in the human skeleton (Hamill and Knutzen (2009)).

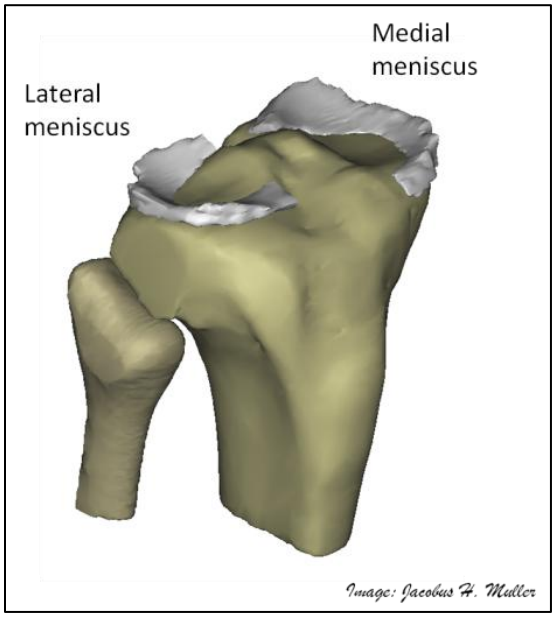

Figure 2.7: The menisci on the tibiofemoral joint.

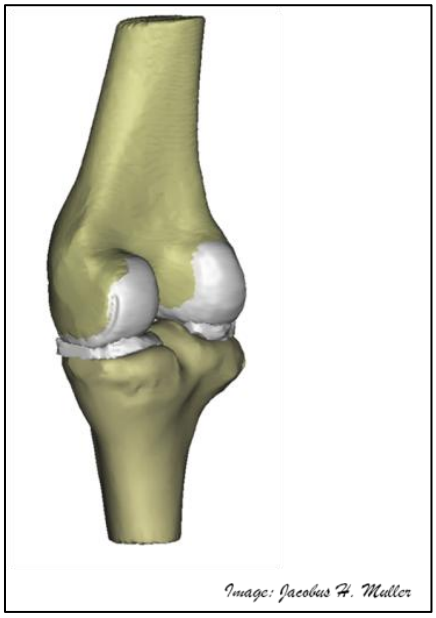

Figure 2.8: The congruency of the tibiofemoral joint.

The surfaces of articulating joints in the human body are coated with a thin layer of articular cartilage which is composed of cells, comprising 2 to 15% of its volume fraction, and an intercellular matrix with a water content of 65 to 80% (Herzog (2006)). It transmits and distributes forces across the joint while providing a smooth and nearly frictionless surface. During articulation, the articulating surfaces move relative to one another, and as a result the points of contact and the magnitude of the contact area change continuously. Composed of collagen fibres (mainly type II with traces of Type VI, IX, X and XI), proteoglycans and non-collagenous proteins, the intracellular matrix is largely responsible for the cartilage's functionality (Herzog (2006)).

Collagen gives the cartilage its tensile strength, as well as its resistance to compressive loading. Although collagen have negligible compressive strength, the combination of the water content inside the cartilage (due to the hydrophilic nature of the proteoglycans), and the collagen fibril arrangement places the collagen under tension when the cartilage is compressed. When the cartilage is under load, water is forced out of the proteoglycans, whereas it is reabsorbed when the load is removed.

2.1.2 Soft tissue arrangement

The passive stabilisers (ligaments) transmit tensile loads between the skeletal structures, while the active stabilisers (tendons) transmit tensile loads between the skeletal muscles and structures. The major ligaments in the knee joint are the anterior and posterior cruciate ligaments (ACL and PCL; Figure 2.9), the fibular collateral and medial collateral ligaments (FCL and MCL; Figure 2.10) and the peri-patellar structures, i.e. the medial and lateral retinaculum (Figure 2.11 and Figure 2.12).

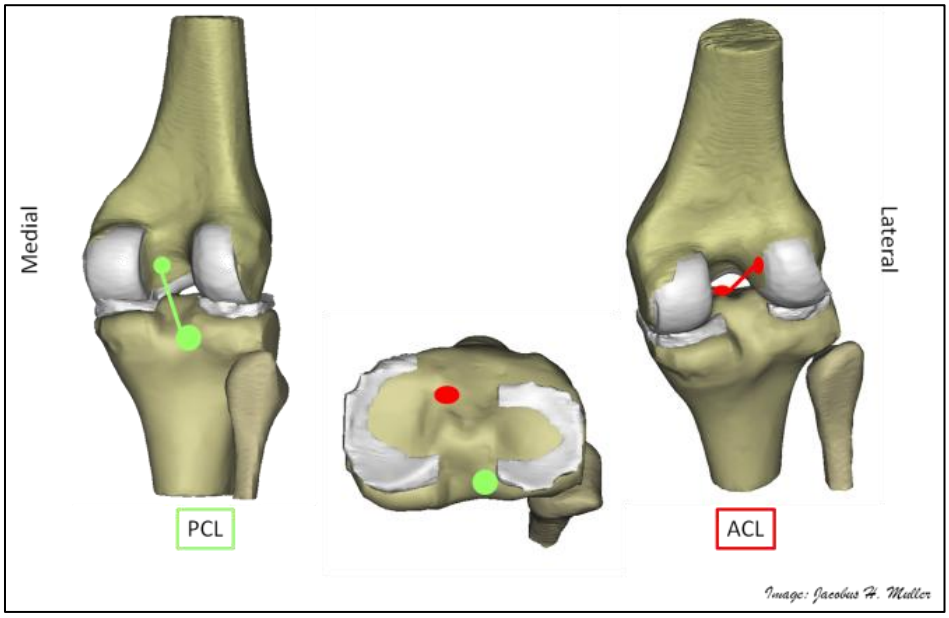

Figure 2.9: The ACL and PCL attachment sites on the tibiofemoral joint.

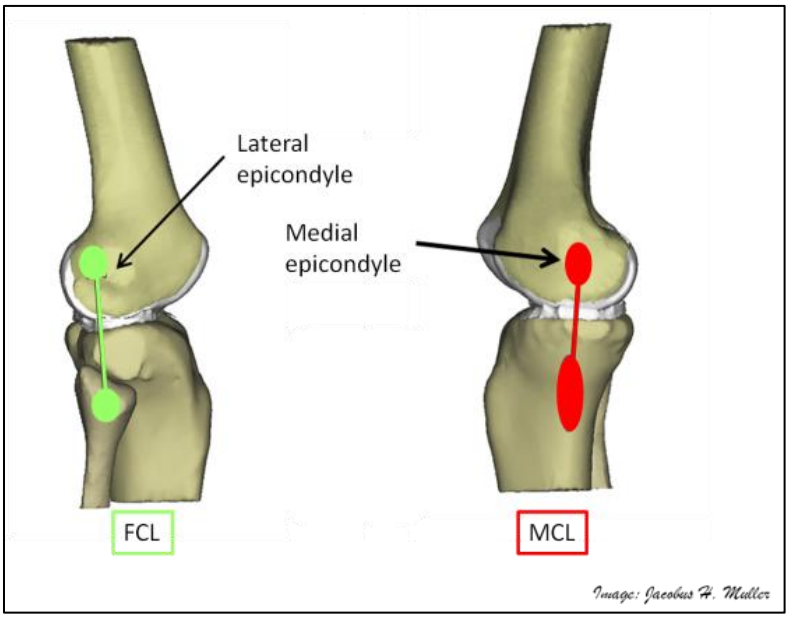

Figure 2.10: The FCL and MCL attachment sites on the tibiofemoral joint.

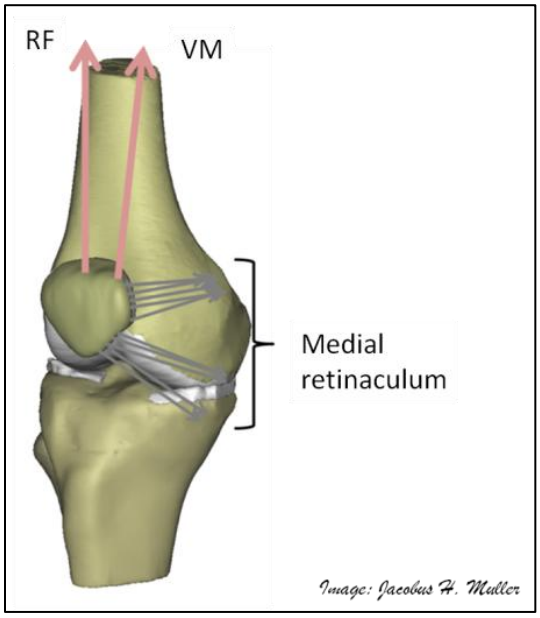

Figure 2.11: The medial retinaculum of the patellofemoral joint.

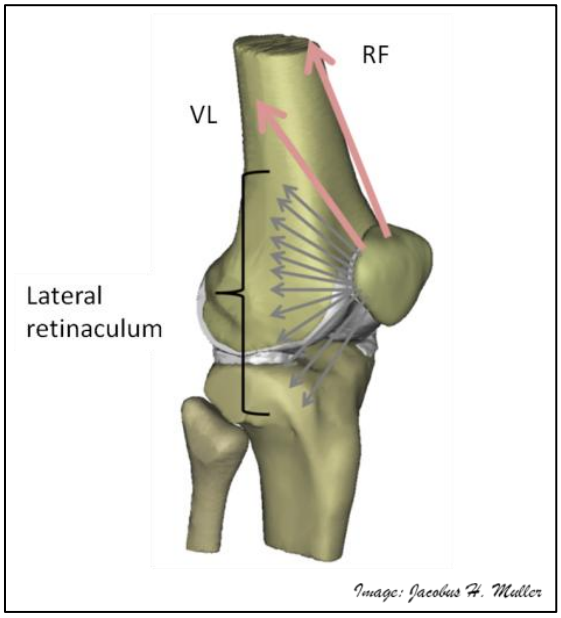

Figure 2.12: The lateral retinaculum of the patellofemoral joint.

The extensor mechanism is composed of the quadriceps muscle complex, the illiotibial tract (since it forms part of the lateral retinaculum), the patellar tendon, the patellofemoral ligaments and fascia. The quadriceps muscle complex is divided into the vastus lateralis (VL), rectus femoris (RF), vastus intermedius (VI) and the vastus medialis (VM). Due to the variance in the muscle fibre orientations of the VL and VM, an additional subdivision can be made: the VL is divided into the vastus lateralis longus (VLL) and the vastus lateralis obliquus (VLO) and the VM into the vastus medialis longus (VML) and the vastus medialis obliquus (VMO) (Figure 2.13). The quadriceps tendon joins the quadriceps muscle complex to the patella, and translates over the patella's anterior border into the patellar tendon, which connects the patella to the tibial tubercle (Figure 2.13).

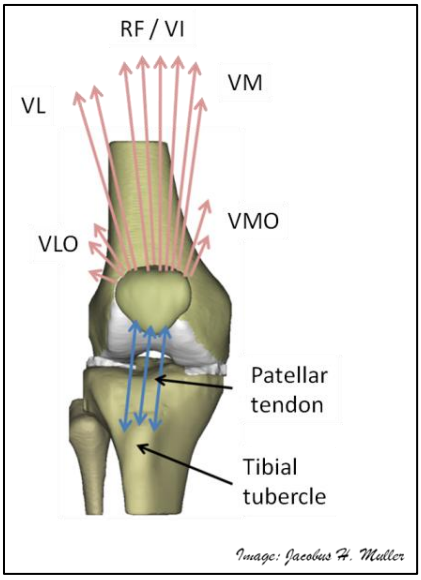

Figure 2.13: The extensor mechanism of the patellofemoral joint.

Andrikoula *et al.* (2006) showed with a dissection study on the extensor mechanism that the RF and VI transform into the quadriceps tendon, which inserts into the posterior-superior pole of the patella. The VI blends partly with the VM medially. The VL leads halfway down the intermediate quadriceps tendon and connects obliquely to the patella. A portion of the VL also connects directly to the tibia through a fibrous expansion that blends with the lateral patellar retinaculum. The majority of distal fibres of the VM pass horizontally into the quadriceps tendon with the VMO inserting into the medial border of the patella. The quadriceps is orientated in a lateral direction with respect to the patellar tendon. This lateral angle is known as the quadriceps-angle (Q-angle) and ranges from 14 degrees (Mesfar and Shirazi-Adl (2005)) to 17 degrees (Elias and Cosgarea (2006)) in normal knees.

The patellar tendon can be divided into a medial, central and lateral section, with each of these having an anterior and a posterior part. The anterior fascicles are longer than the posterior fascicles since they connect more proximally to the patella and distally to the tibial tubercle (Basso *et al.*, 2001). The anterior section attaches to the anterior distal two thirds of the patella, and the medial and lateral fascicles attach more proximally than the central fascicles. Contrary to indications in anatomical texts, the patella's apex does not indicate the longitudinal centre of the patellar tendon, since 61 % of the patellar tendon's width is laterally positioned to the apex (Basso *et al.* (2001). The patellar tendon is wide and thin at the patellar attachment and becomes thick and narrow moving from the patella attachment to the tibial tubercle.

The skeletal muscles and joints are covered by a large thin, fibrous tissue called fascia. Although contributing only minimally to joint stability, it performs an important function allowing for relative motion between the different soft tissue layers in the knee joint. The soft tissue structures around the knee joint are arranged in three layers: the top layer, middle layer and the deep layer (Laprade *et al.* (2007). The retinacula refer to the fascia connecting to the tibia, patella, femur and patellar tendon on the medial and lateral side of the patella.

On the medial side, a layer of fascia forms the top layer which covers the sartorius, gracilis and semitendinosus muscles. In the second layer anterior fascia fibres pass upward to blend into the vastus medialis (VM) muscle, while posterior fascia fibres run from the patella to insert at the medial epicondyle. The superficial medial collateral ligament (MCL) and medial patellofemoral ligament (MPFL) forms part of this middle layer. The knee capsule, the inferior MCL and the capsular ligament connecting the medial meniscus to the tibia, forms the deep layer.

The superficial fibres of the lateral retinaculum originate from the Illiotibial band and the fascia that covers the VL. The illiotibial band consists of a thick sheath of fascia that connects the iliac spine to the anterolateral aspect of the lateral tibial plateau (Sanchez *et al.* (2006)). The lateral retinaculum inserts on the lateral border of the patella and patellar tendon. The deep layer consists of the lateral patellofemoral ligaments as well as the

patellotibial band (Powers *et al.* (2006)). A recent anatomical dissection study found that there is a constant connection to the quadriceps tendon on the superior and lateral side of the patella by the deep fascia (Merican and Amis (2008)). The findings also showed a connection between the deep transverse fibres and the VLO.

The knee capsule (thin fibrous tissue) makes up an important part of the soft tissue support structures. The anterior capsule offers a substantial pocket in which the patella can translate. It contains the fat pad and infrapatellar bursa and is lined by a synovial membrane containing a fold known as the plica (Hamill and Knutzen (2009)), located medially and superior to the patella. The lateral joint capsule is divided into a deep and superficial layer, which includes the FCL and terminates at the fabellotibular ligament while the deep layer extends posterolateral to form the coronary ligament and hiatus of the popliteus tendon (Sanchez *et al.* (2006)). It further translates along the lateral meniscus and extends from the femur to the tibia in a proximal distal direction.

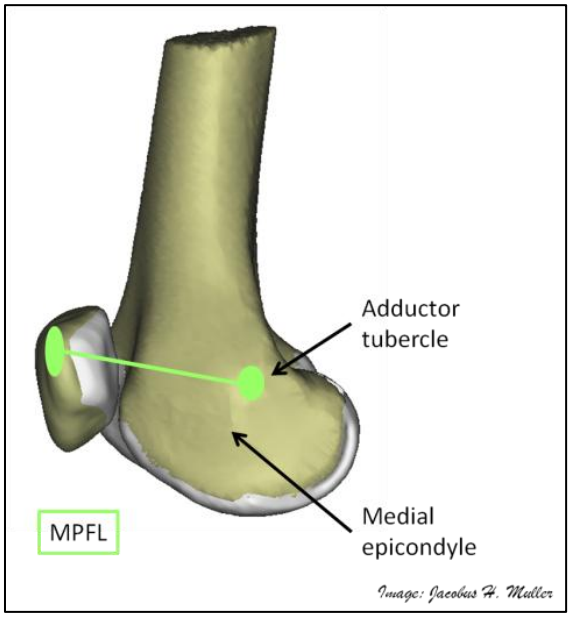

Figure 2.14: The MPFL attachment sites on the patellofemoral joint.

The MPFL is situated in the middle layer of the medial retinaculum and connects the medial edge of the patella to the medial femoral epicondyle. It inserts on the proximal two thirds of the medial patella edge (Bicos *et al.*(2007)). Although there is good correlation between studies on the attachment area of the MPFL on the patella, the same cannot be said of the femoral attachment. In previous studies the femoral attachment has been located anterior to the medial epicondyle (Steensen *et al.* (2004)), posterior to the medial epicondyle, at the adductor tubercle, at the medial collateral ligament attachment (Smirk and Morris (2003)), and at the adductor magnus tendon and superficial MCL attachment (Laprade *et al.* (2007)). In most cases it attaches to the posterior part of the medial epicondyle, approximately 10 millimetres distal to the adductor tubercle (Bicos *et al.* (2007), Figure 2.14).

There also exists some variability in the literature with regards to the shape of the MPFL. It has been described to have a flat and fan-like shape, being larger at the patella attachment, but in some cases an hourglass shape has also been observed (Smirk and Morris (2003)). The MPFL sometimes fuses with the medial longitudinal retinaculum at 15 millimetres medial to the patella and at other times the whole ligament extends proximal to the patella (Steensen *et al.* (2004)). The MPFL's length averages between 47.2 and 70 millimetres (Bicos *et al.* (2007); Elias and Cosgarea (2006); Smirk and Morris (2003)), while its width has been described to vary between 3 to 30 millimetres (Bicos *et al.* (2007)). A fibrous expansion from the VMO blends with the MPFL and this may add an active component to the MPFL (Bicos *et al.* (2007)).

The flexor mechanism consists of the hamstring muscle group. This group includes the long and short biceps femoris on the lateral side (Figure 2.15), and the semimembranosus and pes anseri muscle group consisting of the semitendinosis, gracilis and the sartorius muscles on the medial side (Hamill and Knutzen (2009), Figure 2.16). The hamstring muscles assist the ACL to resist anterior movement of the tibia and also generate joint rotation due to the location of the attachment sites on the knee. As the knee extends, flexion strength diminishes due to hamstring muscles' tendon angle. At full extension the flexion strength is roundabout 50% (Hamill and Knutzen (2009)). Lateral support to the knee joint is provided by the biceps femoris, while the posterior and medial capsule is supported by the semimembranosus. The semitendinosis provides support to the ACL and MCL. When the foot is in the neutral position, the gastrocnemius also contributes to knee flexion.

The popliteus muscle is a weak flexor that assists the PCL in deep flexion (Hamill and Knutzen (2009)), and a dynamic tibial rotator at full extension (Sanchez *et al.* (2006)). It is an obliquely oriented muscle originating from the posteromedial aspect of the proximal tibia and attaches on the lateral condyle. Although it is small (54.5 millimetres in length (Sanchez *et al.* (2006)), it is believed to be an important dynamic stabiliser to the lateral meniscus. This is because it attaches at multiple locations along the posterolateral aspect of the knee. The popliteus unit, along with its ligamentous connections to the fibula, tibia and meniscus are known as the popliteus complex.

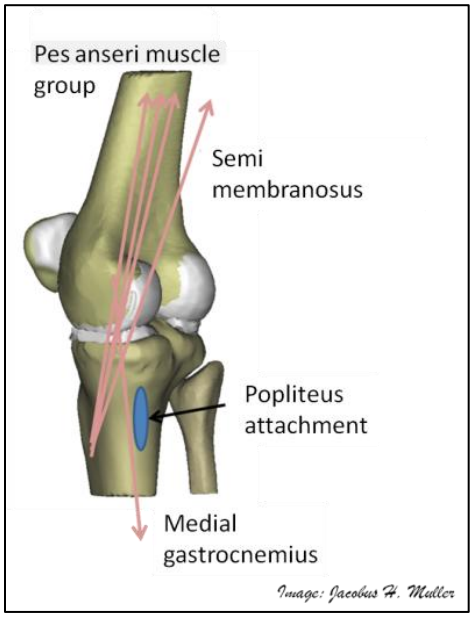

Figure 2.15: The medial flexor mechanism of the tibiofemoral joint.

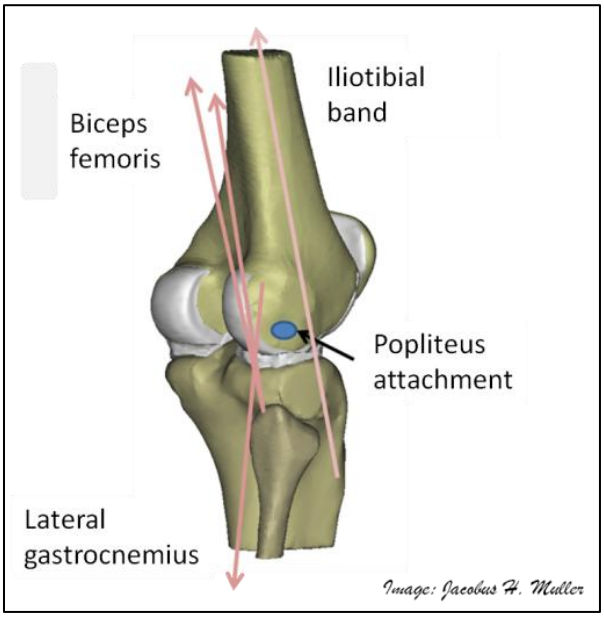

Figure 2.16: The lateral flexor mechanism of the tibiofemoral joint.

2.2 Patellofemoral biomechanics

2.2.1 Patellofemoral kinematics

When the knee flexes or extends (Figure 2.17), both the patellofemoral (Figure 2.18) and tibiofemoral joint (Figure 2.19) translates along and rotates around three principal axes (Hamill and Knutzen (2009)). Knee flexion is dependent on the current hip flexion angle, since there are numerous two-joint muscles that span across the hip and the knee joint, e.g. the RF (Hamill and Knutzen (2009)). Maximum knee flexion is achieved when the hip is in a flexed state, whereas it decreases when the hip is hyper-extended. The normal flexion range of the knee joint is 130 to 145 degrees and it can hyper-extend by one to two degrees.

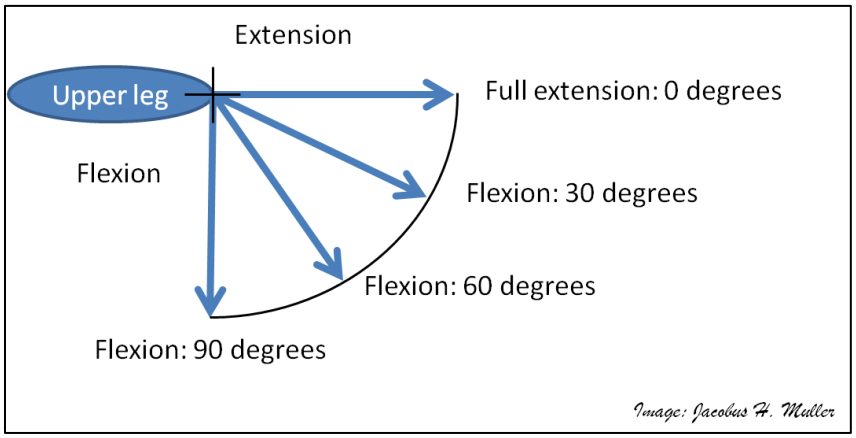

Figure 2.17: Knee flexion-extension convention.

At full knee extension, the patella is above the femoral groove and rests on the suprapatellar fat pad. A recent review (Katchburian *et al.* (2003)) on *in-vitro* and *in-vivo* patellar tracking trends indicated that the patella undergoes an initial medial shift from full extension to roundabout 15 to 40 degrees knee flexion, followed by lateral shift with increasing knee flexion. *In-vitro* studies indicated a medial tilt (between 0.4 and 3.2 degrees) from full extension to between 15 and 30 degrees knee flexion, followed by lateral tilt (between 0.7 and 8.2 degrees from maximum medial tilt) from 30 degrees knee flexion onwards. *In-vivo* tilt patterns showed more variation than *in-vitro* patterns, but the majority of the results indicated initial medial tilt followed by lateral tilt. Some studies did however report results showing an immediate lateral shift and tilt from full extension onwards.

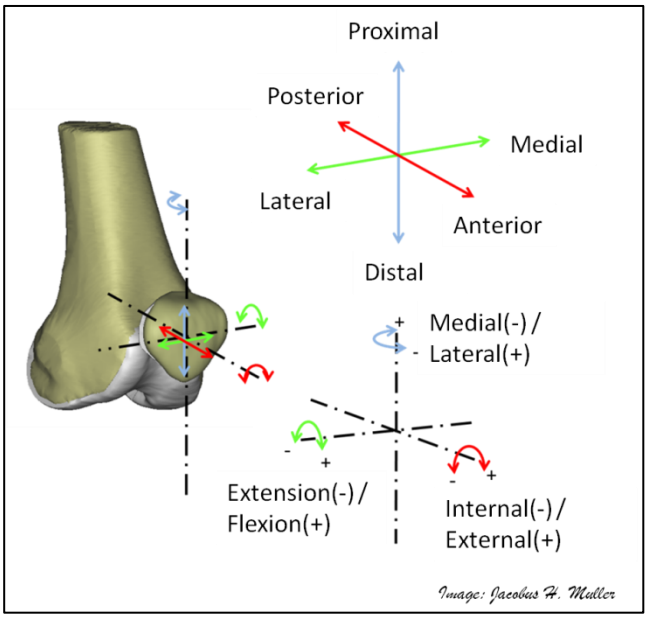

Figure 2.18: The measurement coordinate system of the patellofemoral joint.

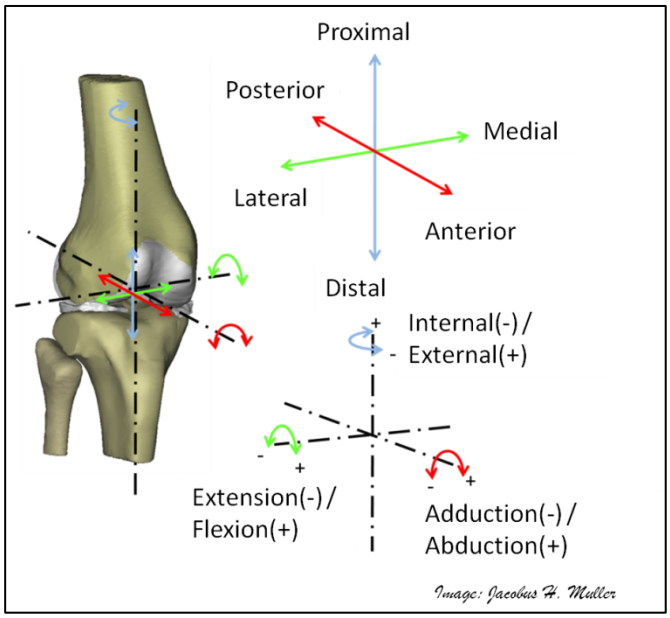

Figure 2.19: The measurement coordinate system of the tibiofemoral joint.

Less important parameters are patellar rotation and flexion (Katchburian *et al.* (2003)). Patellar rotation was found to be highly variable between individuals and as a result no trends could be derived from the *in-vitro* and the *in-vivo* findings. Both *in-vivo* and in-*vitro* studies showed that the patella's flexion angle will generally lag the knee flexion angle during knee flexion. It is important to note that patellar tracking measurements will differ when the knee is extended from full flexion or flexed from full extension (Amis *et al.* (2006)). This moreover complicates the comparisons between different studies.

2.2.2 Patellofemoral kinetics

Everyday activities require the knee joint to endure contact loads far exceeding the bodyweight while allowing for knee joint mobility (Hamill and Knutzen (2009)). Although the skeletal geometry and the cartilage layers

provide means of withstanding these loads, soft tissue stabilisers are still required to improve stability of the articulating parts.

Between knee flexion of 30 and 90 degrees, the patellofemoral contact migrates from an inferior position superiorly on the patellar articular cartilage while it moves from a superior to distal position on the trochlear groove (Feller *et al.* (2007)). The contact area increases with knee flexion while it remains distributed across the medial and lateral patella facets (Von Eisenhart-Rothe *et al.* (2004)). The lateral facet does however contribute more to the total contact area, and from full extension to trochlear engagement, it endures the total contact. When the knee is in full extension, the tibia is in its maximal lateral rotated position, resulting in a laterally displaced tibial tubercle. This, in combination with the Q-angle, draws the patella laterally and a high lateral femoral condyle is thus essential in providing sufficient support during early knee flexion.

It has been shown that an increased Q-angle will lead to an increase in patellofemoral pressures (Li *et al.* (2004) and Elias *et al.* (2004)), and that small alterations in joint alignment will induce significant changes in patellofemoral contact pressures (Feller *et al.* (2007)). Normal patellofemoral pressures range from 2 MPa for level walking to 55 MPa when landing from a jump (Feller *et al.* (2007)). Peak stresses are normally higher during early knee flexion, and more pronounced for patients suffering from patella alta, referring to an abnormally high patella relative to the trochlear groove at full extension. This results in a smaller contact area, which leads to elevated contact pressures. A similar trend is observed where the patella maltracks: patellofemoral stresses have been found to increase outside the physiological range, leading to the onset of cartilage degeneration. It is difficult to give objective values for patellofemoral reaction forces, but studies have reported reaction forces ranging from 350 N for level walking to 6 000 N during landing from a jump (Feller *et al.* (2007)).

2.2.3 Tibiofemoral kinematics

From full extension to 120 degrees knee flexion, the medial condyle undergoes minimal anteroposterior translation (± 1.5 millimetres), whereas the lateral condyle undergoes a posterior translation (± 15 millimetres) by means of a sliding-rolling action across the tibial plateau (Freeman and Pinskerova (2005)). The posterior translation of the lateral condyle causes the medial condyle to rotate on the tibial plateau leading to external femoral rotation (between -5 to 30 degrees from full extension to 90 degrees knee flexion). From 120 degrees knee flexion onwards, both condyles roll back, causing the tibiofemoral joint to subluxate on the lateral side.

The lateral meniscus translates posteriorly with the lateral femoral condyle because of the rolling-sliding action of the lateral condyle in conjunction with the muscular action of the popliteus muscle. As the knee extends, the extensor mechanism assists the patella in drawing the meniscus in an anterior direction. The internal tibial

rotation results in dorsiflexion and pronation at the foot, while external tibial rotation results in plantarflexion and supination at the foot (Hamill and Knutzen (2009)).

2.2.4 Tibiofemoral kinetics

At full extension the tibiofemoral contact is anterior (Li *et al.* (2004)), and shifts posteriorly with knee flexion (Von Eisenhart-Rothe *et al.* (2004)). At 30 degrees flexion, the tibiofemoral contact is both in the medial and lateral compartment, with the medial contact area the larger. The menisci carry half of the load at full extension and a significant portion thereof during knee flexion with the lateral meniscus enduring a greater portion (Hamill and Knutzen (2009)). During low load situations, contact is mainly on the menisci, whereas 70% of the contact is carried by the menisci during high contact situations.

Knee joint kinetics is influenced by the hip flexion angle, since some of the soft tissue stabilisers span across the hip and knee joint. An example is the effect that the hip joint angle has on the moment arm of the biceps femoris: when the hip is extended, the moment arm increases, whereas it will decrease during hip flexion. Another example of the influence of the hip joint angle is that the rectus femoris is able to contribute to knee extension only when the hip joint is at an extended angle (Hamill and Knutzen (2009)).

2.2.5 Soft tissue stabiliser kinetics

During knee flexion/extension, the extensor and flexor mechanism co-contract in order to control knee motion. Eccentric contraction of the extensor mechanism during knee flexion prevents buckling of the knee joint, whereas the flexor mechanism contracts during knee extension in order to slow down a rapidly extending joint. Co-contraction reduces anterior tibial shift, which protects the ACL (for flexion up to 60 degrees) as well as internal tibial rotation (for flexion up to 90 degrees, Li *et al.* (2004)). This results in an increased peak pressure distribution in the patellofemoral joint. The measured role of co-contraction on cruciate ligament forces has however been distorted by the presence of artefact shear forces used to restrain the tibia at a flexion angle during in-vitro and in-vivo investigations (Mesfar and Shirazi-Adl (2006)).

A force differential exists between the quadriceps tendon and the patellar tendon due to the varying geometry and shape of the distal part of the femur and the patella. The changing point of contact between the patella and femur as the knee flexes and extends also contributes to this force differential. The patellar tendon/quadriceps tendon force varies between 1.0 and 1.2 at full extension to between 0.6 and 0.8 at 60 degrees flexion (Powers *et al.* (2006)). On average, patellar tendon load is 8.9% less for flexion between full extension to 60 degrees flexion, when the retinacula is left intact (Powers *et al.* (2006)).

The purpose of the peri-patellar retinaculum is to provide patellofemoral stability in the frontal plane, as well as load sharing with respect to the patellar tendon. The patellofemoral and patellotibial ligaments therefore have a transverse and longitudinal component. It has been shown that patella tilt will increase when the transverse component is deactivated. Since the deactivation on the one side does not alter the transverse loads on the other side, the role of the transverse components has been described to be a passive restraint to dislocation forces on the patella (Feller *et al.* (2007)). The role of the longitudinal components is less clear (Feller *et al.* (2007)), but it has been shown to contribute slightly to the transmission of the extensor mechanism loads (Powers *et al.* (2006)). Between 20 and 40 degrees flexion, there is no difference in patellar tendon load if the retinacula are removed or kept intact. There is however a difference if the flexion range is increased from full extension to 60 degrees knee flexion.

The VL is the strongest of the quadriceps muscles, and it exerts a lateral force on the patella. The VML provides more vertical stabilisation to the patella whereas the VMO provides medial stabilisation to the patella. The quadriceps muscles contract equally throughout the range of motion. During knee extension, the quadriceps muscles not only contribute slightly towards patellar stability, but also pull the menisci anteriorly via the patellomeniscal ligament. Being antagonistic to the ACL, the quadriceps assists the PCL to prevent posterior displacement of the tibia. At small flexion angles (< 45 degrees), anterior patellar tendon pull is resisted by the ACL (Li *et al.* (2004)).

The quadriceps' function depends on tibial rotation (Stoutenberg *et al.* (2005)). The VL and VM is utilised more when the tibia is rotated inwards and least when rotated outwards. The RF on the other hand works harder if the tibia is rotated outwards and less when rotated inwards. When the Q-angle increases, the tibia rotates outward and increases patellofemoral contact pressures (Li *et al.* (2004)). This will also increase utilisation of the RF while utilisation of the VM and VL will decrease. Electromyography (EMG) analyses showed that the levels of RF muscle activation were uniquely independent from those of the VM and VL (Stoutenberg *et al.* (2005)). At full extension, the patella is free to translate in a mediolateral direction when the quadriceps is relaxed. Quadriceps activation draws the patella proximally and laterally and the patella loses its mediolateral mobility. As the knee starts to flex, the MPFL (Bicos *et al.* (2007)) in conjunction with the VMO (Feller *et al.* (2007)) draws the patella in a medial-posterior direction to allow it to be seated in the trochlear groove.

The MPFL is tight at full extension, but slackens during the first 20 degrees of flexion as the patella is pulled medially (Amis *et al.* (2006)). The MPFL is the major passive stabiliser preventing lateral displacement of the patella and contributes 53% of the restraining force (Carmont and Maffulli (2007)). The MPFL fails at 208 N (Carmont and Maffulli (2007); Mountney *et al.* (2005)) and will rupture at approximately 49% strain (Mountney *et al.* (2005)). Changes in its length (Mountney *et al.* (2005)) as well as its isometry (Bicos *et al.* (2007)) are dependent on the location of the femoral attachment. The inferomedial and superomedial fibres of the MPFL

only change 1.1 millimetres during flexion from full extension to 90 degrees flexion (Carmont and Maffulli (2007)).

The PCL resists anterior movement of the tibiofemoral contact point between 60 and 90 degrees flexion (Dennis *et al.*, 1996). When the PCL is deficient, posterior tibial translation and tibial rotation increase, while patellofemoral contact pressures become elevated (Li *et al.* (2004)). An *in-vitro* investigation revealed that the PCL fails at 18% strain (Mountney *et al.* (2005)). The ACL resist posterior movement of the tibiofemoral contact point during flexion (Dennis *et al.* (1996)). A deficient ACL will increase anterior translation and valgus rotation of the tibia and will lead to lateral tilting and shifting of the patella (Von Eisenhart-Rothe *et al.* (2004)). The valgus moments increase ACL strain during weight bearing (Withrow *et al.* (2006)). In a study where the ACL was loaded for both internal and external tibial rotation between full extension and 45 degrees flexion, ACL loads were highest during internal tibial rotation (Woo *et al.* (1999)).

In the previous section, collagen was identified as one of the main components in ligaments and tendons. Collagen chains are arranged in sub fascicles and fascicles that are enclosed by connective tissue sheaths (Atkinson *et al.* (1999)). The smallest units are collagen fibrils, which exist in various degrees of crimp, leading to more fibrils being recruited as the load increases. The collagen chains mainly consist of Type I, although there are trace amounts of Type III, V, X, XII and XIV (Woo *et al.* (1999)). Ligaments also contain other proteins: elastin, fibrillar protein and proteoglycans. Collagen is the major load bearing element, while spacing and lubrication are provided by the water content and proteoglycans. Ligaments and tendons are visco-elastic materials which present properties such as creep[†], stress relaxation[‡] and hysteresis[§], contributing to the ability of the ligaments and tendons to accomplish their function.

2.3 Patellofemoral analysis methods

Patella stability is governed by the articular geometry, action from the active stabilisers and action from the passive stabilisers (Feller *et al.* (2007)). *In-vivo* measurements will provide subject-specific information on an individual's articular geometry, while the contribution of the active stabilisers can be derived from EMG measurements. The contribution from the passive stabilisers remains problematic since it is difficult to monitor all the stabilisers during an experiment. *In-vitro* techniques on the other hand will provide accurate information on the articular geometry, while the contribution from the active and passive stabilisers will be reduced in order to preserve tissue integrity. The joints are also manipulated subjectively to reproduce knee flexion. The combination of *in-vivo, in-vitro* and computational techniques provide a means with which the articular

[†] Elongation of fibres under load.

[‡] Diminishing load under strain.

[§] Energy dissipation with subsequent loading cycles.

geometry can be represented accurately, the active and passive stabilisers can be positioned correctly, and body motion and manner can be based on subject-specific motion recordings. If validated, the computational model can provide a tool with which patellofemoral biomechanics can be analysed objectively.

2.3.1 *In-vivo* methods

During an *in-vivo* investigation, measurements are obtained from an individual either in an invasive or a non-invasive manner. Recent advancements in imaging techniques have provided a means by which the *in-situ* patellofemoral kinematics can be determined non-invasively. Specially adapted sensors enable the *in-situ* measurement of ligament and tendon forces while a volunteer performs an activity, and body motion can be monitored with various motion capturing techniques.

Magnetic resonance imaging (MRI) techniques have allowed researchers to measure patellofemoral kinematics, while the extensor mechanism is loaded or unloaded at various flexion angles (Ward *et al.* (2007); Defrate *et al.* (2007); Freeman and Pinskerova (2005)). This technique produces information on the static behaviour of the joint and requires the volunteer to retain a joint posture for several minutes while the measurement is taken. Seisler and Sheehan (2007) made use of a fast personal computer (PC) MRI technique which enabled the dynamic measurement of patellofemoral and tibiofemoral kinematics all at once, but the range of motion and the inability to load the extensor mechanism during measurement inhibited this technique. Interventional MRI scanning allows a subject to stand upright in the scanner, with the possibility to flex the knee through its entire range of motion. Unfortunately the acquisition of the images also requires the subject to maintain a position for a long time during scanning (static imaging).

Fluoroscopy in combination with computed tomography (CT) provides an alternative with which knee kinematics can be measured dynamically. Tibiofemoral kinematics in the sagittal plane has been reported with accuracy (Fernandez *et al.* (2008)). Single plane fluoroscopy (Fernandez *et al.* (2008); Dennis *et al.* (1996); Komistek *et al.* (2003)) makes use of one fluoroscope tracking the skeleton landmarks in one plane, while bi-plane fluoroscopy (Defrate *et al.* (2007)) utilises two fluoroscopes with which the landmarks can be tracked in two planes. Registration software is used to reposition volumetric images obtained with CT (and in some cases MRI) on the two-dimensional fluoroscope images. In some cases metal beads impregnated into the skeleton are used to assist when segment orientations are calculated from the fluoroscope images.

The advantage of the above mentioned technique is the scanner's ability to move with the subject, while continuously measuring kinematics and without having direct contact with the subject. Although the measurements in the measurement plane deliver good results, inaccuracies occur when the results are extrapolated to the other planes. It is also difficult to track the patella accurately with this technique (Seisler and

Sheehan (2007)). Lin *et al.* (2003) tried to improve on this by coupling fluoroscopy with an optical tracking system monitoring a clamp attached to the patella, but unfortunately the patella could only be tracked from full extension to 20 degrees knee flexion. Another drawback of this technique is the dosages of ionising radiation to which the subject (and test personnel) might be exposed during imaging, and especially so when coupled with CT scanning. Adam *et al.* (2002) made use of Roentgen Stereometric analysis to monitor beads to measure tibiofemoral traction. This technique is similar to fluoroscopy, but a conventional x-ray imager is used instead of the fluoroscope, thus making continuous tracking impossible.

Ultrasound has also been used to dynamically track the patella's mediolateral translation during knee flexion (Shih *et al.* (2004); Shih *et al.* (2003)) as well as for the measurement of ligament and tendon loads (Hansen *et al.* (2006); Pourcelot *et al.* (2005)). This technique gives non-invasive measurement capability and presents no risk in terms of radiation. Unfortunately the knee brace needed for fixation of the probe might influence natural movement of the test subject. Positioning of the probe as well as the prevention of relative motion between the probe and the patella is difficult.

Sensors used to detect soft tissue stabiliser forces or strains include fibre-optic sensors (Arndt *et al.* (1998); Dillon *et al.* (2008); Finni *et al.* (1998); Muller *et al.* (2008)), digital variable reluctance transducers (Cerulli *et al.* (2003)), and buckle transducers (Nicol and Komi (1999)). These sensors are invasive and calibration of the results are challenging. Electromyography (EMG) gives insight into the recruitment patterns of the skeletal muscles (Stoutenberg *et al.* (2005)), and can be used to derive the muscle loads delivered when coupled with a mathematical model (De Luca and Contessa (2009)).

Motion tracking systems, such as camera based and inertial sensor based systems, allow body segment traction. The setup times are usually lengthy and care should be taken to limit cross-talk between sensors. Another drawback might be relative movement between the skin and bony landmarks which will induce measurement errors. Electromagnetic based motion trackers can be used to measure knee biomechanics intra-operatively (Bull *et al.* (2002)). Direct access to the landmarks is therefore possible, limiting the possibility of relative motion between landmark and sensor (Mountney *et al.* (2005)). Unfortunately the obtained measurements relate to passive motion and the knee is therefore manipulated by the surgeon to reproduce knee flexion, which might influence the objectivity of the measurements.

2.3.2 *In-vitro* methods

During a typical *in-vitro* patellofemoral investigation, a cadaver leg is prepared by removing superficial skin and fascia to expose the joint and the active and passive stabilisers. The femur is prepared to be either suspended in a custom designed jig (Amis *et al.* (2006)), a robotic manipulator (Li *et al.* (2004)) or a materials testing machine

(Powers *et al.* (2006)). The extensor mechanism (and sometimes the flexor mechanism), is divided into its constitutive elements and tensioned in its physiological loading directions. These muscle forces can either be applied passively, e.g. through a weight pulley system (Powers *et al.* (2006)), or actively, e.g. a force-controlled hydraulic cylinder (Withrow *et al.* (2006)).

Joint pressures may be measured by pressure sensitive film, e.g. pre-scaled film (Lee *et al.* (2001)), or a suitable pressure sensor, e.g. K-scan (Li *et al.* (2004)) or I-scan (Elias *et al.* (2004)). Passive stabiliser loads can be measured with fibre-optic sensors (Eerdemir *et al.* (2002)) or buckle transducers (Powers *et al.* (2006)). Knee kinematics is measured with an optic tracker (Elias *et al.* (2004)), three dimensional digitizing systems (Powers *et al.* (2006)) or an electromagnetic motion tracker system (Amis *et al.* (2006)).

A major advantage of the *in-vitro* technique is the capability of modifying the joint configuration to gain access to structures that are of interest. Pressure sensors unfit for *in*-vivo studies may be used to gain insight into patellofemoral pressure. *In-vitro* techniques do however present the following difficulties: modifications to the patellofemoral joint may influence the biofidelity of the results; it is impossible to reproduce *in-situ* conditions during an *in-vitro* study since the soft tissue stabilisers and articulate cartilage have a reduced moisture content, resulting in modified material properties post-mortem; muscle loads also need to be adjusted to reduce the risk of muscle tear. Thus, measurements that would be impossible *in-vivo* can therefore be obtained through *in-vitro* techniques, but its relationship with the *in-situ* conditions remains questionable.

2.3.3 Computational methods

The majority of the finite element models of the patellofemoral joint, have been constructed from *in-vitro* measurements (D'Lima *et al.* (2003); Elias and Cosgarea (2006); Elias *et al.* (2004); Mesfar and Shirazi-ADL (2008, 2006, 2005); Shirazi-Adl and Mesfar (2007)), whereas fewer have been based on *in-vivo* conditions (Besier *et al.* (2005); Fernandez *et al.* (2008)). Besier *et al.* (2005) and Fernandez *et al.* (2008) generated the articular geometry of the models from MRI images and Elias and Cosgarea (2006) and Elias *et al.* (2004) from CT scan data. D'Lima *et al.* (2003) digitized commercial replacements while approximating the femoral and patellar skeletal elements through representative solid models. Active soft tissues stabiliser loads (quadriceps and patellar tendon loads) were similar to the *in-vitro* values (D'Lima *et al.* (2003); Elias and Cosgarea (2006); Elias *et al.* (2004); Mesfar and Shirazi-Adl (2008, 2006, 2005); Shirazi-Adl and Mesfar (2007)), whereas active stabiliser loads in the finite element models based on the *in*-vivo studies, were approximated through musculoskeletal models (Besier *et al.* (2005) and Fernandez *et al.* (2008)). Only some of the *in-vitro* models included the patellofemoral passive stabilisers (MPFL and lateral retinaculum) (Elias and Cosgarea (2006); Elias *et al.* (2004); Mesfar and Shirazi-Adl (2008, 2006, 2005); Shirazi-Adl and Mesfar (2007)).

Besier *et al.* (2005) employed a method based on EMG measurements as described by Lloyd and Besier (2003) to derive active stabiliser loads. A generic musculoskeletal model developed by Delp *et al.* (1990) was scaled according to the individual's size and weight, and the muscle tendon lengths and velocities were determined as a function of joint kinematic data measured with a stereophotogrammetry system. The muscle parameters served as input for a Hill-based muscle model[**] from which muscle forces were determined. Fernandez *et al.* (2008) made use of a model described by Anderson and Pandy (2001). The hips, knees and ankles were respectively approximated as ball and socket, hinge and universal joints, while the upper body was modelled as a single entity. The anthropometry of the model was obtained from five volunteers, while the muscles were approximated as EMG driven Hill-type muscles in series with tendons. The model motion was based on video-based motion capture recordings. Patellofemoral posture was derived from single-plane fluoroscopy images.

Other simulation techniques have been described by Fernandez and Hunter (2005) and Powers *et al.* (2006). Fernandez and Hunter (2005) illustrated the use of a patient-specific finite element model which considered muscle geometry (based on generic geometries from a model database), and the bone geometries derived from an anatomical model with indications of the tissue attachments. These generic models were scaled to the individual's anatomy as determined from a MRI by means of a free-form deformation procedure. A camera based system was used to capture volunteer-specific motion, and quasi-static stress analyses were conducted at discrete knee flexion angles.

Powers *et al.* (2006) made use of a computational model to reproduce an *in-vitro* loading condition (at discrete knee flexion angles) to compare the influence of the contact geometry on the measured contact force. That study found that the same reaction force trends were reproduced, although the computational model overestimated the resultant reaction loads by ten percent. There was a difference between the measured and predicted load components: the superior components were overestimated, the lateral components underestimated, whereas the posterior components were similar.

2.3.4 Current work in context of this literature study

The techniques used in this study are similar to the steps followed by Fernandez *et al.* (2008). A skeletal model is generated from volunteer-specific scan data, while soft tissue properties are derived from MRI images. Motion simulation with a musculoskeletal model are based on motion recordings of the volunteers, from which muscle loads are extracted to feed a finite element analysis of the patellofemoral joint at an angle of flexion. This study differs from the study of Fernandez *et al.* (2008) and other previous studies in the following ways:

[**] See Section 4.2.2

- A musculoskeletal model is constructed from the individual's skeletal bone models.

  The musculoskeletal model used by Fernandez *et al.* (2008) consisted of dummy elements (Figure 1 in Anderson and Pandy (2001)), while the musculoskeletal model used by Besier *et al.* (2005) and Fernandez and Hunter (2005) employed generic skeletal elements. Although its influence on patellofemoral reaction forces has been shown to be minimal (Powers *et al.* (2006)), the advantage of subject-specific skeletal geometries would be the better approximation of patella kinematics. It is evident from the study of Feller *et al.* (2007) and Katchburian *et al.* (2003) that patella kinematics are subject-specific, while the patella's traction pattern are also governed mainly by the trochlear groove geometry after 20 degrees knee flexion (Feller *et al.* (2007)). Teichtahl *et al.* (2007) performed a study on 297 healthy subjects and was able to show that the trochlear groove angle varied considerably between volunteers which further suggests that patella tracking will be subject-specific. It is evident from Figure 3.14 on page 36 that the shape of the patellae of the three volunteers is different from each other.

- Dynamic analyses in terms of knee flexion and muscle activation were performed with the musculoskeletal models.

  Amis *et al.* (2006) has advocated the need to perform dynamic analyses to describe patella kinematics while Fernandez and Hunter (2005) expressed the desire to extend their quasi-static analyses to full dynamic analyses in future studies. This would aid in the measurement of the transient behaviour of the patella during maltraction. Although both the musculoskeletal models of Besier *et al.* (2005) and Fernandez *et al.* (2008) were used to perform dynamic analyses, the patella tracking patterns could not be derived from these, but were derived from the FEA. These however were quasi-static analyses. Fernandez *et al.* (2008) did employ single plane fluoroscopy to approximate patellofemoral posture, but the accuracy of this method for patella identification is questionable (Seisler and Sheehan (2007)). Quasi-static simulations were performed with the musculoskeletal model of Fernandez and Hunter (2005). It will be shown in Chapter 4 that traction paths predicted with a dynamic analysis will be different to paths predicted with a quasi-static analysis.

- The lateral retinaculum and medial patellofemoral ligament structures are included in both the musculoskeletal and the FE models.

  These passive stabilisers were not included in the considered musculoskeletal or FE models that were based on *in-vivo* measurements. The passive stabilisers were however included in the *in-vitro* models of Elias and Cosgarea (2006); Elias *et al.* (2004); Mesfar and Shirazi-Adl (2008, 2006, 2005); Shirazi-Adl and Mesfar (2007)). Although the passive stabilisers' only function as primary stabilisers before trochlear groove engagement, their inclusion in the model will increase the utility of the musculoskeletal model in the prediction of soft tissue intervention techniques, similar to that of Elias and Cosgarea (2006).

- The patella will be constrained in the finite element model.

  Patella position was constrained by the action of the active stabilisers and the trochlear groove in the studies of Besier *et al.* (2005), Fernandez *et al.* (2008) and Fernandez and Hunter (2005). Although this was valid for the quasi-static analyses, it would cause the patella to change from a state of dynamic equilibrium to a state of static equilibrium, as will be illustrated in Chapter 4.

Chapter 3

3. Subject-specific measurements

In Chapter 3 the data and information needed to assemble the subject-specific musculoskeletal models are discussed (Figure 3.1). After discussion of the ethical consent for the study in Section 3.1, the method by which the three-dimensional skeletal models were generated from anatomic scans is described in Sections 3.2 and 3.3. Sections 3.4, 3.5 and 3.6 respectively represent the physical, clinical and biomechanical measurements of the volunteers. A motion capturing technique recording volunteer-specific motion is explained in Section 3.7. Chapter 3 concludes with a description of electromyography measurements of a volunteer's quadriceps activity in Section 3.8.

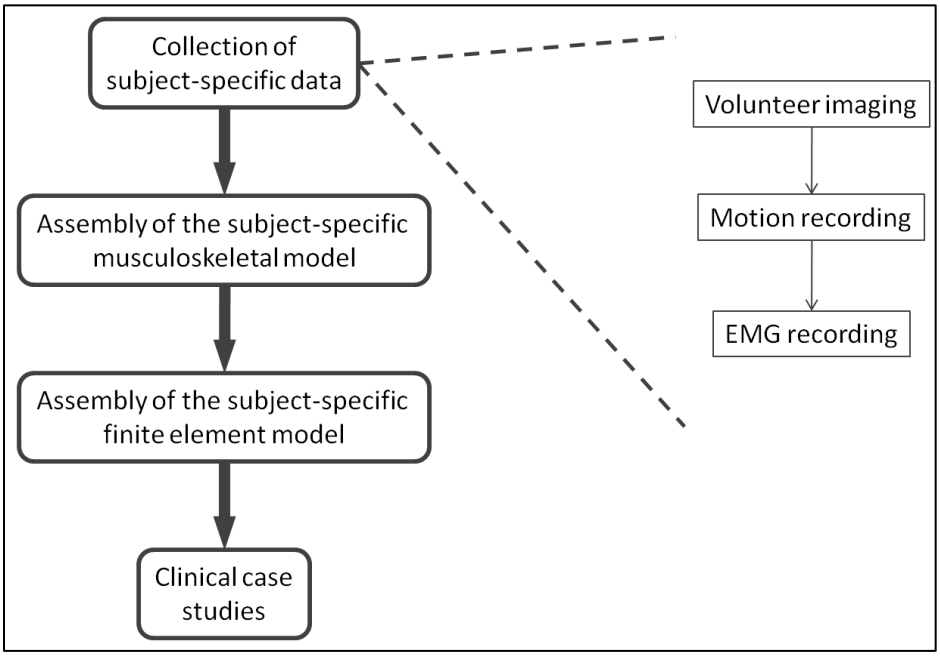

Figure 3.1: Study flowchart (II).

3.1 Ethical consent

Ethical consent, in accordance with the Declaration of Helsinki (1964), was obtained from the Committee for Human Research at Stellenbosch University (project number N08/02/029). Three healthy volunteers were informed of the dosages of radiation they would be exposed to during the computed tomography scans of their lower bodies. Each volunteer was free to abandon the test at any time and was asked to sign an informed consent form.

3.2 Computed tomography and magnetic resonance imaging of the volunteers

3.2.1 Background

CT operates on the principle of x-ray attenuation. Collimated x-rays are produced on the one side of the object and detected on the opposite side. The raw data is then calibrated and post-processed, during which the integrals of the x-ray linear attenuation coefficient distribution are calculated and reconstructed to produce an image. These projections are converted into CT numbers, which are displayed to visualise anatomical features. The scanned object is in other words divided into a series of thin transverse slices, which can then be viewed one after the other (Figure 3.2).

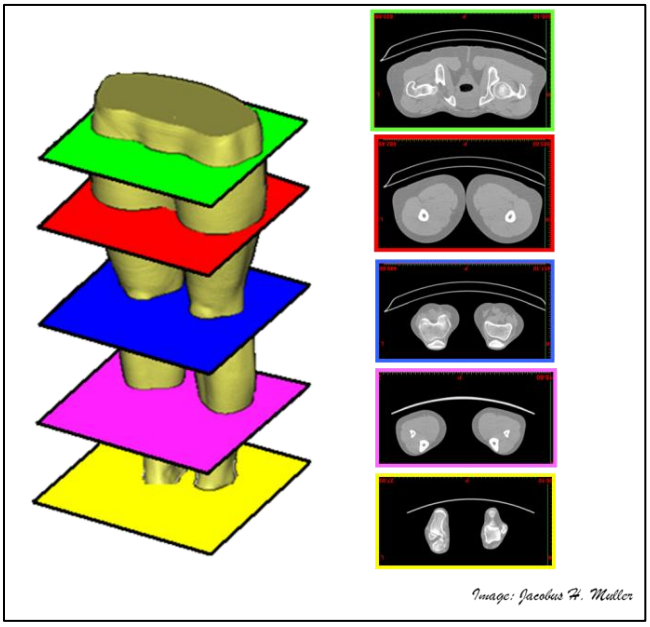

Figure 3.2: CT slices of the lower body.

MRI also produces a series of thin slices (minimum one millimetre thickness) of the scanned object, based on the absorption and emission of energy waves in the electromagnetic frequency range by the different materials in the body. It was originally thought impossible to scan objects with a smaller dimension than the wavelength of the energy waves being used (Hornak (2008)) but this was overcome by exploiting the spatial variation in both the phase and the frequency of the energy being absorbed and emitted by the imaged object. Its working principle is dependent on the hydrogen atom count, making it a suitable modality when scanning tissues with high water content. MRI will therefore deliver good quality images when soft tissues are scanned (Figure 3.3), whereas CT will produce better images of the skeletal structures with a low water content (Figure 3.4).

Figure 3.3: MRI scan of the intact femur, tibia and patella.

Figure 3.4: CT scan of the intact femur, tibia and patella.

3.2.2 Imaging protocol

For the purposes of this study, CT scans (Siemens Emotion 16; 130 kV; Care dose 4D; Table 3.1) from the iliac spine down to the feet, and MRI (Siemens Symphony; 1.5 Tesla; Table 3.2) of the knees, were obtained for the three volunteers. An additional MRI scan was obtained of the volunteers' right knee joint while an isometric leg contraction at 30 degrees knee flexion was applied (5 minutes scan time). A jig was designed and built[††], allowing a person to exert a leg contraction while the MRI is obtained (Appendix A). In order for the jig to be compatible with the MRI scanner, it was manufactured from polyethylene. A load of 25 % bodyweight (% BW) was placed on the jig. This produced a load on a foot piece free to translate along guiding rails, and needed to be balanced by the quadriceps muscles of the volunteer (Figure 3.5). Water-filled plastic bottles (500 ml) were used as weights. The jig was designed with anti-friction rolling and sliding bearings consequently eliminating the effect of friction during the leg contraction.

[††] Designed by Mr. T Cloete, built by the workshop at the Department of Mechanical and Mechatronic Engineering.

Table 3.1: CT scan settings

Parameter		Value
Eff. mAs		105
Acquisition		16 x 0,06 mm
Rotation time		1 second
Pitch		1.5 mm
Slice		5 mm
Reconstruction parameters:		
	Slice	1 mm
	Recon increment	0.7 mm
	Field of view	250 mm
	Kernel / filter	B10s smooth

Table 3.2: MRI scan settings

Parameter		Value
Scan time		9.49 seconds
Contrast:		TR 40
		TE 24
Flip angle		Eight degrees
Resolution:		
	Field of view	200 mm
	Slice thickness	1.5 mm
	Base resolution	512
	Filter	Elliptical
Geometry:	One slab	
	Distance factor	50
	Slices per slab	72
Sequence:	Dimension 3D	
	Bandwidth	132 Hz/Px

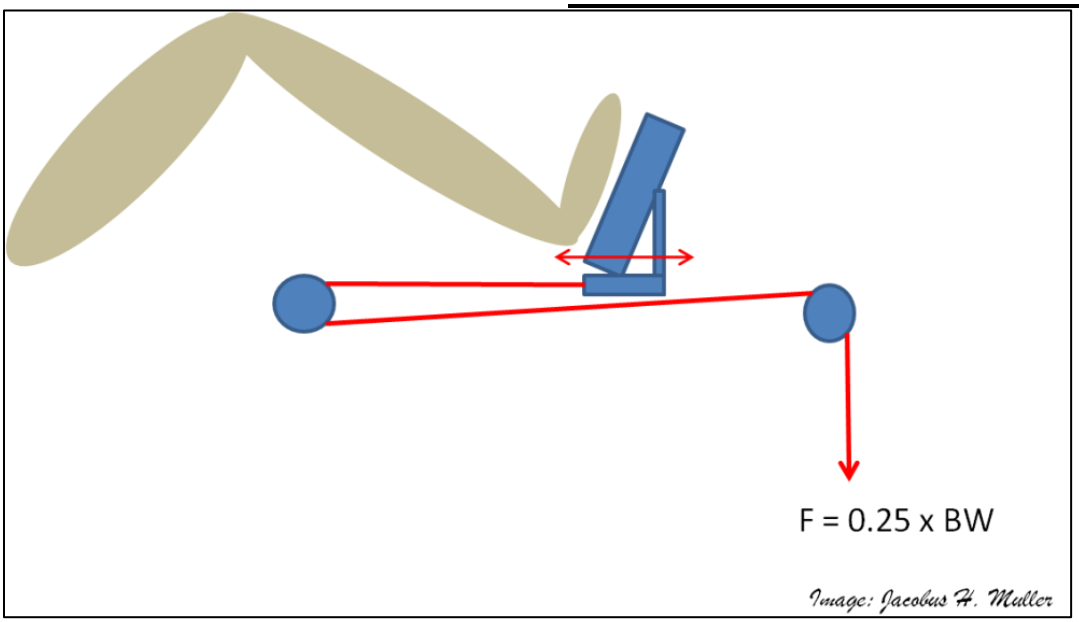

Figure 3.5: The loading jig that enables muscle contraction in the MRI scanner.

3.3 Segmentation procedure

Segmentation is a process during which data is graphically extracted from a scan, and processed to produce a three-dimensional model. Various segmentation techniques exist, for example: region growing, thresholding and manual segmentation. During a manual segmentation process the area of interest (for example the femur) in each CT slice is selected and fused to construct a three-dimensional model (Figure 3.6). The segmentation process can also be automated by means of "thresholding". This entails the selection of voxels[‡‡] with similar Hounsfield numbers. An object's Hounsfield number gives an indication of that object's density, with a higher Hounsfield number pertaining to an object having a higher density. Skeletal bone will therefore have a different Hounsfield

[‡‡] Voxels in three-dimensional space are similar to pixels in two-dimensional space.

number range to that of skeletal muscle. All segmentation and post-processing was done with Mimics (Mimics 12.01, Materialise, Leuven, Belgium).

The three-dimensional models need to be post-processed after the segmentation procedure to remove artefacts that may have resulted from the segmentation procedure. This is achieved through smoothing of the three-dimensional surfaces or by reducing the amount of surface triangles. The artefacts (Figure 3.6) were the result of the slice thickness of the CT scans which were removed with the smoothing function provided by Mimics.

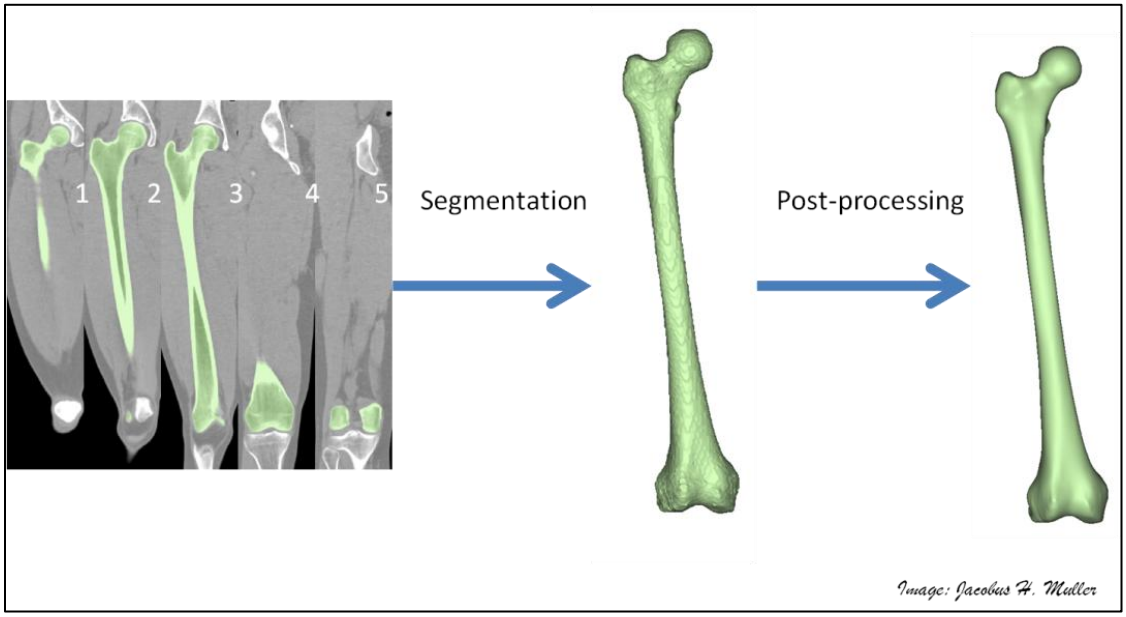

Figure 3.6: Manual segmentation of the femur.

For all three volunteers, the pelvis, femora, patellae, tibiae, fibulae and feet were segmented from the CT images, while the cartilage and menisci were segmented from the MRI scans. The unloaded cartilage geometries were repositioned on the CT images, as well as on the loaded MRI image. Repositioning on the loaded MRI images caused the patellar and femoral cartilage to overlap, which indicated the area of contact (Ward *et al.* (2007)). An approximated contact area magnitude could be derived by measuring the size of the overlapping areas, as explained in Section 3.6 and Appendix C.

3.4 Physical measurements

Two females and one male volunteered for the study. Each volunteer's age, height and mass were recorded (Table 3.3). The body-mass-indexes[§§] (BMI) of the volunteers indicated that they were not overweight (<24). Volunteer One reported mild anterior knee pain when the knee was flexed under load, whereas the other two volunteers reported no pain whatsoever.

[§§] $BMI = mass(kg)/length^2(m^2)$

Table 3.3: Physical measurements of the volunteers.

Volunteer	Gender	Age (years)	Height (millimetres)	Mass (kg)	BMI
Volunteer One	Female	30	1 690	60	21.0
Volunteer Two	Female	23	1 657	63	22.9
Volunteer Three	Male	32	1 898	83	23.0

3.5 Clinical measurements

Clinical measurements were obtained from the CT and the MRI images by the radiographers who assisted in the study[***] (Table 3.4). These parameters were used as a guideline in the determination of the normality of the three volunteers' joints. The trochlear groove-tibial tubercle (TG-TT) distance gave an indication of the lateral offset of the tubercle at full knee extension (Figure 3.7). An increased lateral offset would induce a larger lateral patellar load component on the patella. A distance above 15 millimetres was considered to be pathological, which might have led to patellar instability (Koëter *et al.* (2007)). Volunteer Three had an increased distance of 16.1 millimetres, which was deemed negligible since the slice thickness of the scans was one millimetre. Martino *et al.* (1998) measured an average trochlear groove depth (TG depth) of 5.6 millimetres, considered representative values for male cadavers, which might serve as an explanation for the reduced values recorded for the two female volunteers (Table 3.4).

Table 3.4: Clinical patellofemoral measurements (SD = Standard Deviation).

Measurement	Norm [SD]	Volunteer One	Volunteer Two	Volunteer Three	Mean [SD]
TG-TT, millimetres	< 15[aa]	10.8	10.6	16.1	12.5 [3.1]
TG depth, millimetres	5.6[bb]	4.3	3.8	6.7	4.9 [1.6]
Femoral anteversion, degrees	19.6 [10.2][cc] 24.1 [17.4][dd]	4.0	12.0	12.0	9.3 [4.6]
Femoral axis angle, degrees	5.5 [0.8][ee]	6.0	4.0	5.0	5.0 [1.0]
Femoral condylar – mechanical axis angle, degrees	93.1 [1.6][ee]	91.0	89.0	88.0	89.3 [2.7]

aa: (Koëter *et al.* (2007)); bb: (Martino *et al.* (1998)); cc: (Souza and Powers (2008)); dd: (Strecker *et al.* (1997)); ee**:** (Mullaji *et al.*, 2009)

Femoral anteversion (Figure 3.8) was found to be within the normal range for Volunteers Two and Three (19.6 degrees [SD = 10.2]), whereas it was smaller for Volunteer One. No statistical difference in femoral anteversion between a control group and a group presenting with patellofemoral pain could be found (Souza and Powers

[***] Van Wagening and Partners, Stellenbosch Medi-Clinic

(2008)), whereas Eckhoff *et al.* (1994) showed that higher degrees of anteversion might result in patellofemoral pain.

The femoral axis angle refers to the angle between the femoral shaft (anatomical axis), and the mechanical axis of the lower leg (Figure 3.9). The femoral axis angle plays an important role during total knee arthroplasty, since it is a measure that can be used to avoid misalignment (Farrar *et al.* (1999)). The angle values from all three volunteers fell within the normal range when compared the values obtained by Mullaji *et al.* (2009). The femoral condylar-mechanical axis angle depicts the angular offset between a distal line connecting the femoral condyles and the mechanical offset (Figure 3.9). Values for all three volunteers fell within the normal range; therefore all three volunteers could be classified as having knees with no abnormalities (Mullaji *et al.* (2009)).

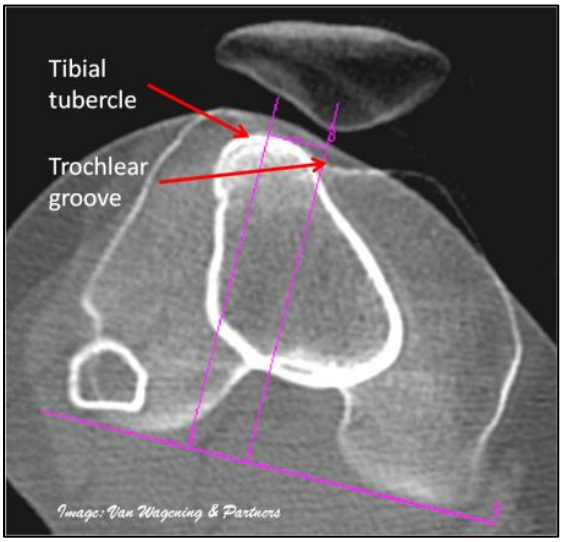

Figure 3.7: Measurement of the tibial tubercle-trochlear groove distance.

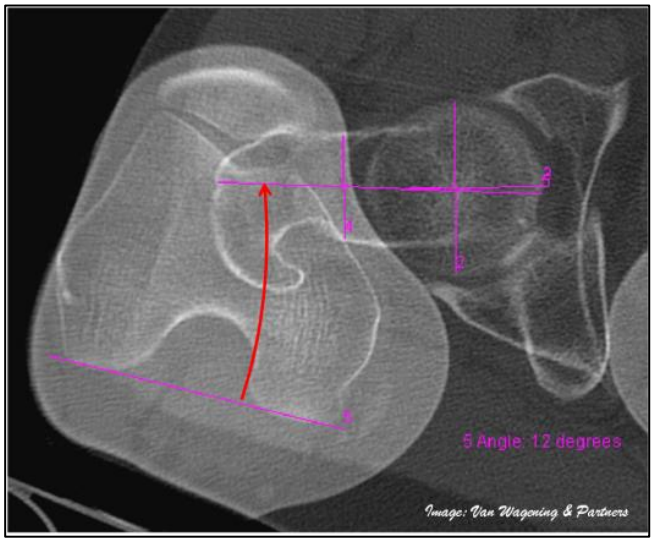

Figure 3.8: Measurement of the angle of femoral anteversion.

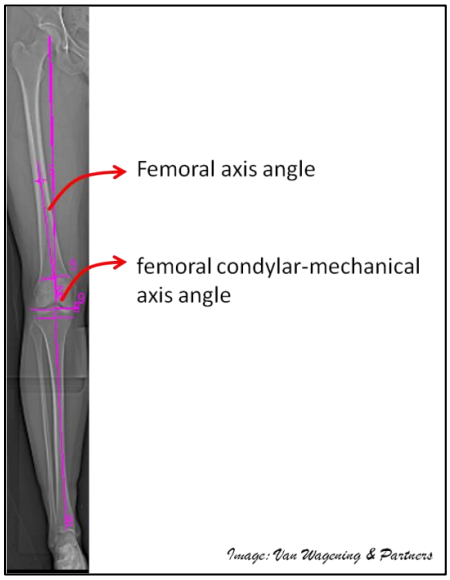

Figure 3.9: Measurement of the femoral axis angle and femoral condylar-mechanical axis angle.

3.6 Biomechanical measurements

The biomechanical measurements were obtained from the CT and MRI scans with the aid of Mimics. The patellotrochlear-index (Biedert and Albrecht (2006)) indicates the magnitude of the overlap between the patella cartilage and the femoral cartilage, and is expressed as a percentage of overlap. This measure can be used as a guideline to determine whether a patient suffers from patella alta or infera. It is measured on an MRI scan in which the quadriceps muscles are isometrically contracted while the knee is fully extended. An index value larger than 50 % indicates patella infera (an abnormally low patella), whereas an index value smaller than 12.5 % indicates patella alta (an abnormally high patella). Patella alta is a recognised pathological condition which might result in patellofemoral disorders, such as patellar instability (Biedert and Albrecht (2006); Dejour *et al.*(1994); Insall *et al.* (1972)) and also might lead to patellofemoral pain (Al-Sayyad and Cameron (2002); Biedert and Albrecht (2006)).

Table 3.5: Biomechanical patellofemoral measurements.

Measurement	Norm	Volunteer One	Volunteer Two	Volunteer Three	Mean [SD]
Modified Patellotrochlear index, %	-	40.84	65.72	54.15	53.57 [12.5]
Patellofemoral moment arm, millimetres	45[aa] and 43[bb]	32.4	36.2	42.2	36.9 [4.9]
Quadriceps muscle cross-sectional area, millimetres^2	-	299.7	285.0	275.0	287.6 [12.4]
Hamstrings muscle cross-sectional area, millimetres^2	-	477.0	437.0	255.3	389.8 [118]
Contact area, millimetres^2	250[cc]	207.0	566.0	297.0	356.7 [186]

aa: (Herzog and Read (1993)); bb: (Smidt (1973)); cc: (Ward *et al.* (2007))

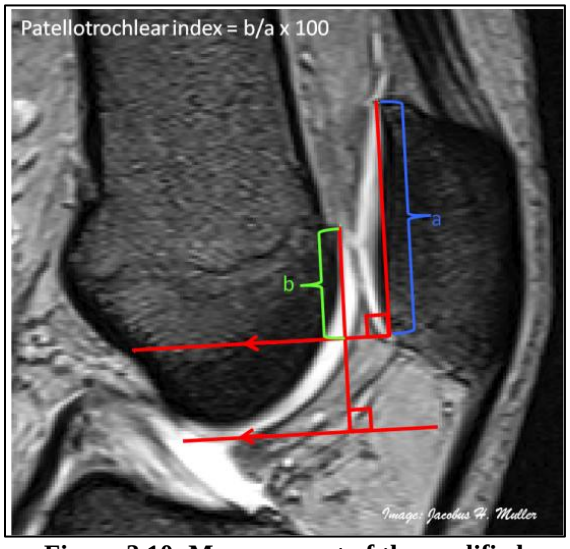

Figure 3.10: Measurement of the modified patellotrochlear index.

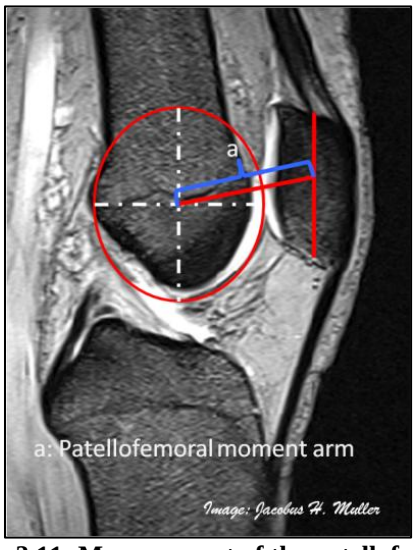

Figure 3.11: Measurement of the patellofemoral moment arm.

A modified patellotrochlear index was used in this study: The quadriceps muscles were relaxed while the MRI was taken with the knee in the fully extended position. Good quality MRI scans were required at full extension, leading to prolonged scan times (in excess of nine minutes) with the volunteers unable to exert the constant muscle load required for such an extended period. The index values were therefore overestimated, since the quadriceps could not be tensioned. It however provided an indication of possible patella alta or patella infera. The index was calculated by following the suggested procedure of (Figure 3.10, Biedert and Albrecht (2006)). The patellotrochlear index of Volunteer Two indicates a possible case of patella infera, whereas the values of Volunteers One and Three indicate normal patella heights.

The muscle model used in the musculoskeletal model software requires a maximum allowable stress level that a skeletal muscle may exert. Zhang *et al.* (1998) measured the maximum voluntary contraction (MVC) during knee flexion and extension on a customised dynamometer. For flexion a mean value of 90.9 N.m [SD = 31.9 N.m], and for extension 133.8 N.m [SD = 31.9 N.m] were obtained. A maximum allowable muscle load was derived from the ratio of the MVC and the patellofemoral moment arm (Eq. 3.1).

$$F_{max} = \frac{MVC}{moment\ arm} \qquad \text{Eq. 3.1}$$

An approximated patellofemoral moment arm was derived for each volunteer by fitting a circle on the femur (Figure 3.11). The circle diameter was varied such that it coincided with the anterior femoral cartilage border. The distance from the centre point of the circle to the point dividing the patella into equal halves (anterior-posterior and proximal-distal), was then taken as an approximate moment arm. Herzog and Read (1993) and Smidt (1973) measured patella moment arms, which would give a better estimate of the actual moment arm. The method used in this study did however provide a reproducible technique that could be applied with ease on the three volunteers. It also provided volunteer-specificity to the moment arms. The drawback of the technique was a reduced moment arm, which would lead to larger maximum muscle loads, but the effect from this was deemed negligible. The values proposed by Herzog and Read (1993) and Smidt (1973) represented normal values for males, and the difference between their average length and that of Volunteer Three was below five millimetres.

The muscle cross-sectional area is an important parameter in the muscle model of the musculoskeletal model. The quadriceps and hamstring cross-sectional areas were derived from the CT scans for each of the three volunteers. The two muscle groups were selected at mid-femur by means of manual segmentation (Figure 3.12). It was possible to calculate the volume of the two segmented groups with the segmentation software. This volume was then divided into the slice thickness (one millimetre), producing an approximated cross-sectional area. The loading ratios applied in *in-vitro* testing is based on the cross sectional ratios of the muscle groups,

used to calculate an approximated cross-sectional area for each muscle in the greater muscle group. The ratio used for the quadriceps and hamstrings was derived from (Table 3.6, Mesfar and Shirazi-Adl (2006))

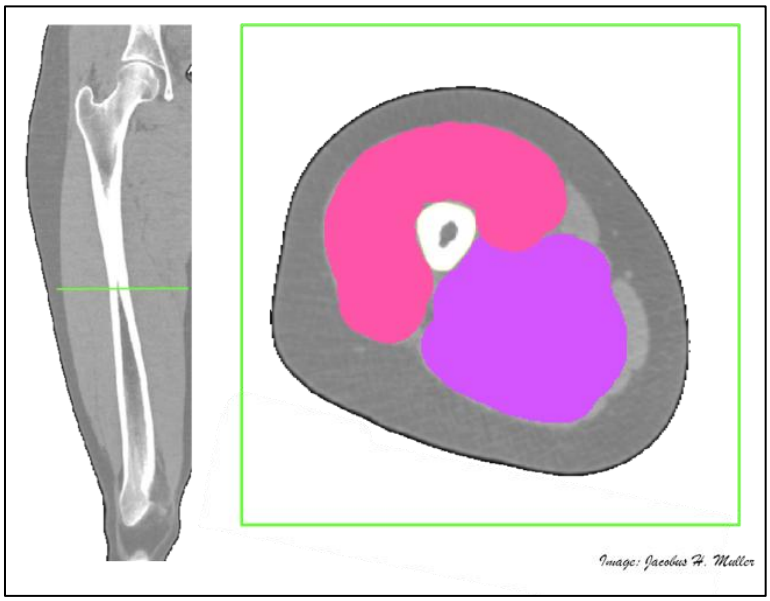

Figure 3.12: Measurement of the cross-sectional area of the quadriceps and hamstrings at mid-femur.

Table 3.6: Muscle loading ratios.

Muscle group	Sub-groups	Loading ratio
Quadriceps	VL:RF/VIM:VM	2.5:3:2
Hamstrings	Short head biceps femoris : Long head biceps femoris : Semitendinosis	1:1:2.6

The patellofemoral contact areas at 30 degrees knee flexion were derived from the loaded MRIs by following the procedure described in Appendix C. The shapes and the contact locations differed between the three volunteers (Figure 3.13 and Figure 3.14). Contact occurred on the lateral facets of the patellofemoral joint for Volunteer One, whereas it was distributed across both the medial and lateral facets of Volunteer Two and Volunteer Three. The contact area was smallest for Volunteer One (207 mm^2, Table 3.5), and largest for Volunteer Two (566 mm^2, Table 3.5). The location of the contact for Volunteer Two confirms patella infera, whereas Volunteer One might run the risk of overloading of the patellofemoral joint since contact occurs only on the lateral facets of the femur and patella which will result in larger pressure values.

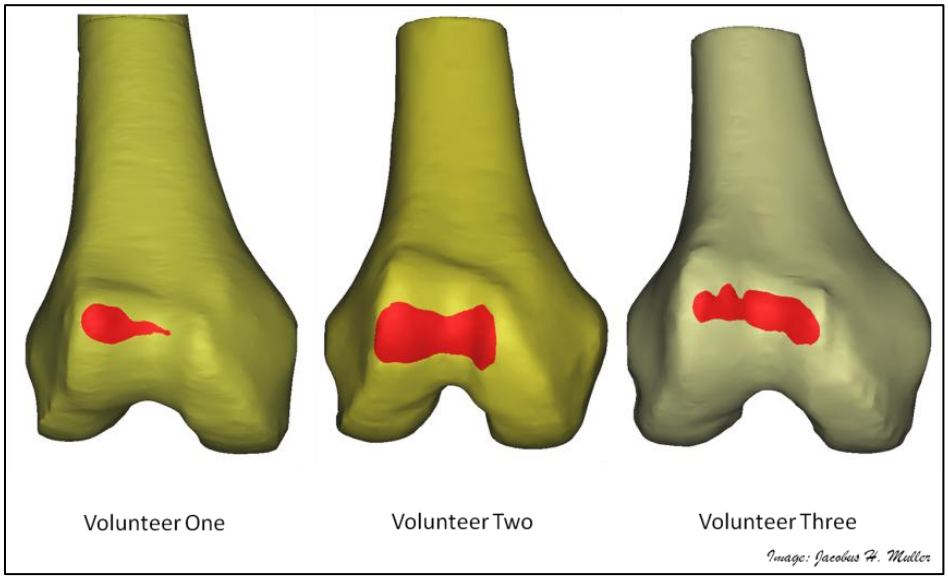

Figure 3.13: Femoral contact area derived from the three volunteers' loaded MRI scans at 30 degrees knee flexion.

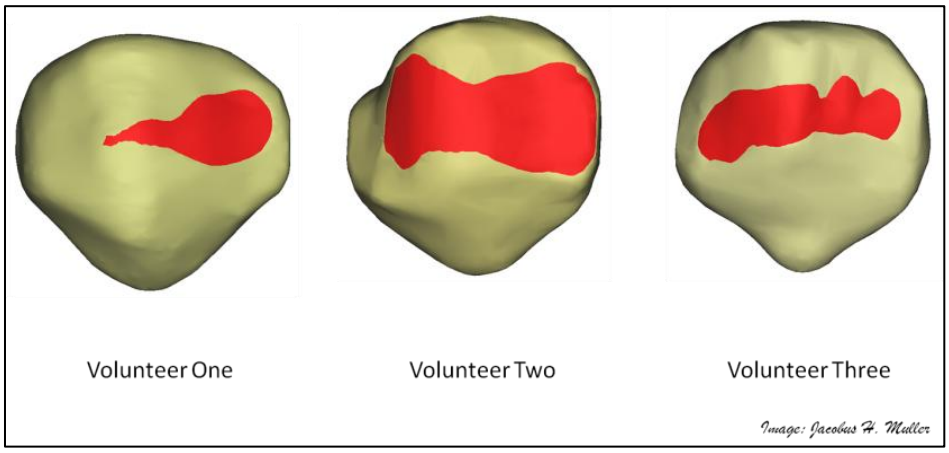

Figure 3.14: Patellar contact area derived from the three volunteers' loaded MRI scans at 30 degrees knee flexion.

The accuracy of the MRI technique presented here and in the study of Ward *et al.* (2007), is dependent on the slice thickness obtainable with MRI. At this stage it is possible to get a slice thickness of one millimetre with a step increment of 0.7 millimetres. This provides an overlapping zone. A slice is produced by taking the "mean" of the Hounsfield numbers in two consecutive increments. It is therefore impossible to identify the border of contact objectively. Brechter *et al.* (2003) showed however that this method produces results comparable to results obtained with pressure sensitive film in an *in-vitro* study.

3.7 Motion capturing

3.7.1 Background

The MVN system is a wireless motion capture system composed of 16 inertial motion sensors (MTx sensors, Xsens Technologies B.V., Enschede, The Netherlands), two Bluetooth transmitter units (Xbus Master, Xsens Technologies B.V., Enschede, The Netherlands) and postprocessor software (MVN studio, Xsens Technologies

B.V., Enschede, The Netherlands). Each inertial sensor is equipped with a tri-axial accelerometer, tri-axial magnetometer and a tri-axial gyroscope. The sensors are located at various landmarks on the volunteer's body, and held in place with either a Lycra suit or Velcro straps.

Before commencement of a recording, a scaled biomechanical model of the volunteer is generated by the postprocessor. This model consists of 23 segments and 22 joints. The positions of the segments and joints are based on calibrations and a regression analysis. The system software converts absolute tri-axial acceleration measurements to tri-axial translations with the aid of the absolute orientation measurements by means of fusion algorithms. The output from the postprocessor consists of the absolute position coordinates as well as the quaternion vectors of each segment at each time step. The segment reference points are located at the joint centres and expressed in terms of a global coordinate reference system. The joint angles are computed by means of quaternion multiplication.

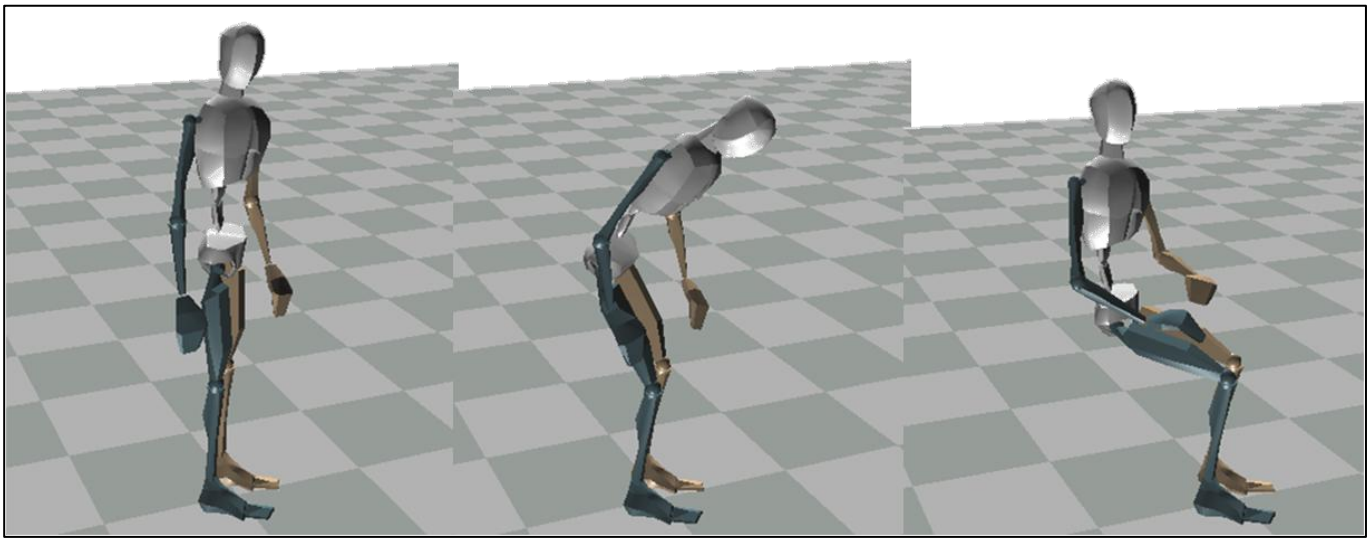

Figure 3.15: Discrete motion capture frames of a volunteer taking a seat.

The three volunteers were asked to take a seat while their body motion was recorded with a motion tracking system (MVN, Xsens Technologies B.V., Enschede, The Netherlands) (Figure 3.15). This was an everyday task that the volunteers could complete with ease, and it allowed patella tracking to be studied over an extensive knee flexion range (full extension to ± 90 degrees flexion).

3.7.2 Segment position and angle calculation

The positions of each segment were contained in the standard output file of the motion capture software (Figure 3.16). This was accompanied with the four quaternion constants for each time step. The orientation of vector $\boldsymbol{a^B}$ in terms of a reference axis system can be calculated with quaternion $\boldsymbol{q}$ as (Baker (2009)):

$$\boldsymbol{a^G} = \begin{bmatrix} (q_1^2 a_1^B + 2q_3 q_1 a_3^B - 2q_4 q_1 a_2^B + q_2^2 a_1^B + 2q_3 q_2 a_2^B + 2q_4 q_2 a_3^B + q_4^2 a_1^B - q_3^2 a_1^B)\boldsymbol{i} \\ (2q_2 q_3 a_1^B + q_3^2 a_2^B + 2q_4 q_3 a_3^B + 2q_1 q_4 a_1^B - q_4^2 a_2^B + q_1^2 a_2^B - 2q_2 q_1 a_3^B - q_2^2 a_2^B)\boldsymbol{j} \\ (2q_2 q_4 a_1^B + 2q_3 q_4 a_2^B + q_4^2 a_3^B + 2q_1 q_3 a_1^B - q_3^2 a_3^B + 2q_1 q_2 a_1^B - q_2^2 a_3^B - q_1^2 a_3^B)\boldsymbol{k} \end{bmatrix} \quad \text{Eq. 3.2}$$

The quaternion $\boldsymbol{q}$ is given by (Baker (2009)):

$$\boldsymbol{q} = [cos(\beta/2) \quad r_1 sin(\beta/2)\boldsymbol{i} \quad r_2 sin(\beta/2)\boldsymbol{j} \quad r_3 sin(\beta/2)\boldsymbol{k}] \quad \text{Eq. 3.3}$$

with $\boldsymbol{r} = [r_1\boldsymbol{i} \quad r_2\boldsymbol{j} \quad r_3\boldsymbol{k}]$ the axis of rotation between vectors $\boldsymbol{a^B}$ and $\boldsymbol{a^G}$:

$$\boldsymbol{r} = \boldsymbol{a^B} \times \boldsymbol{a^G} \quad \text{Eq. 3.4}$$

where × denotes the cross product. β is the angle between $\boldsymbol{a^B}$ and $\boldsymbol{a^G}$:

$$\beta = \cos^{-1}(\boldsymbol{a^B} \cdot \boldsymbol{a^G}) \quad \text{Eq. 3.5}$$

where · denotes the dot product.

If the orientation of **B** in the sagittal plane, that is, the $\mathbf{X_G}$-$\mathbf{Z_G}$ plane, is of interest, the angular offset between the $\mathbf{x_B}$-$\mathbf{Z_G}$ must be determined, but, $\mathbf{x_B}$ and $\mathbf{Z_G}$ must both be in the sagittal plane (Figure 3.17). The quaternion vector, $\mathbf{q_B}$, that describes the orientation of **B** in terms of the global reference frame **G**, (Eq. 3.**2**) can be used to rewrite $\mathbf{x_B}$ and $\mathbf{y_B}$ in terms of the global reference system **G**. The results are $\mathbf{x_B}$**'** and $\mathbf{y_B}$**'** respectively. To ensure that $\mathbf{x_B}$**'** is contained within the sagittal plane, the angle between $\mathbf{y_B}$**'** and $\mathbf{Y_G}$ should be zero.

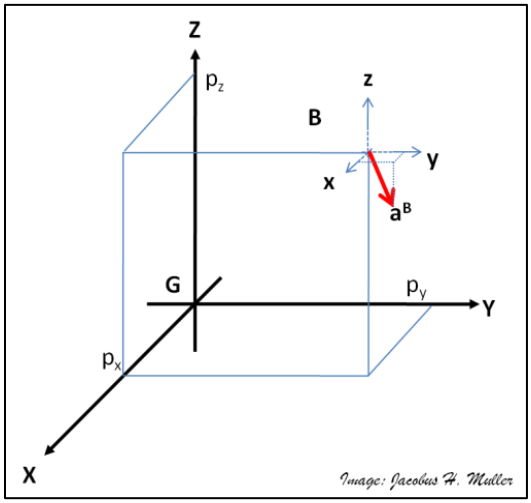

Figure 3.16: Position of body B in the global reference frame G.

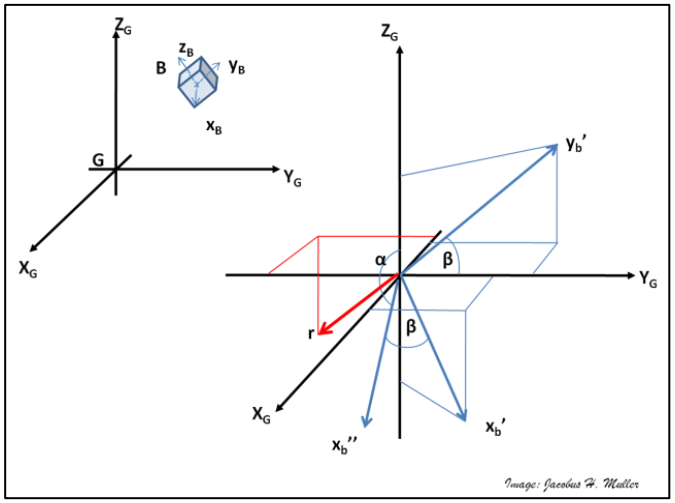

Figure 3.17: Orientation of body B in the sagittal plane in terms of the global reference frame G.

$$\alpha = 90° - \cos^{-1}(\boldsymbol{x}_{\boldsymbol{B}}'' \cdot \boldsymbol{Z}_{\boldsymbol{G}}) \quad \text{Eq. 3.6}$$

If this is not the case, the angle between $\mathbf{y_B'}$ and $\mathbf{Y_G}$, that is, β, can be calculated by means of (Eq. 3.**5**), and then used to calculate a new quaternion vector that describes the orientation of $\mathbf{y_B'}$ in relation to $\mathbf{Y_G}$, by employing (Eq. 3.**3**) and (Eq. 3.**4**). $\mathbf{x_B'}$ can be rotated around axis **r**, by employing (Eq. 3.**2**). $\mathbf{x_B''}$ will then be within the sagittal plane, and the sagittal angle, α, can be calculated with (Eq. 3.**6**). The same approach applies for calculating the coronal and transverse angles, which are the orientations in the $\mathbf{Y_G}$-$\mathbf{Z_G}$ (Figure B.1[†††]) and $\mathbf{X_G}$-$\mathbf{Y_G}$ (Figure B.2) planes, respectively.

3.7.3 Accuracy of motion measurements

The motion capturing system was benchmarked against an optical based motion capturing system (Cloete and Scheffer (2008)). The findings showed that the accuracy of the measurements were comparable between the two modalities. It was shown that artefacts occurred in the results due to relative motion between sensors/markers and the skin. These were minimal for the motions recorded in this study, since the volunteers remained stationary and only took a seat on a chair while their motion was captured.

3.8 Electromyography measurements

3.8.1 Background

A skeletal muscle contains several hundred motor units. A motor unit consists of the motor neuron, its axon and the muscle fibre that is innervated by its axon (Dimitrova and Dimitrov (2006)). When a skeletal muscle is activated, an electrical impulse is produced by a motor neuron through its axon, which stimulates the production of an action potential, or electrical impulse, in the sarcolemma. The sarcolemma (cell membrane of the muscle fibre) contains the functional units known as sarcomeres (Martini and Bartholomew (2003)). It is this action potential that will be measured by a probe under experimental conditions (Dimitrova and Dimitrov (2006)). These potentials can either be monitored with needle or surface electrodes. This is known as electromyography (EMG).

The nerve terminals have different diameters and lengths, leading to consecutive activation of the muscle fibres. With increasing voluntary contraction, the active motor units will fire at increased rates, while motor units with higher threshold values will also start to fire. The potentials that are produced within a motor unit will therefore be desynchronised, and it will be difficult to distinguish between a single motor unit action potential. These

[†††] Appendix B

desynchronised signals are known as an interference pattern (Figure 3.18). The interference pattern contains all the information needed for the activation of the skeletal muscle, but it is of little use in its raw format, and requires post-processing. The raw EMG signal (sampled at 2048 Hz) is first rectified, before being passed through a band pass filter. A running average is then employed giving an indication of the amount of motor units stimulated while the EMG was recorded (Figure 3.19, Towe (2003)).

3.8.2 Muscle activation curves

Unfortunately the EMG device (Nexus-10 system, Mind Media B.V., Roermond-Herten, The Netherlands) was not available while the three volunteers were tested. EMG recordings were obtained from another volunteer who sat down and rose from a chair. The system had two available leads, and the electric activity could therefore be measured at two locations simultaneously. Surface electrodes were placed on the RF, VL and VM, with the reference probe on the patella (Figure 3.20, Cram and Kasman (1998, pp. 360-366)). A rectification and running average algorithm (BioTrace+, Mind Media B.V., Roermond-Herten, The Netherlands) was applied on the EMG interference patterns for the RF (Figure 3.21), VL (Figure 3.22) and VM (Figure 3.23). These activation curves were adapted for the free volunteers with first order polynomials and scaled, as will be explained in Section 4.3, Section 4.4 and Section 4.5.

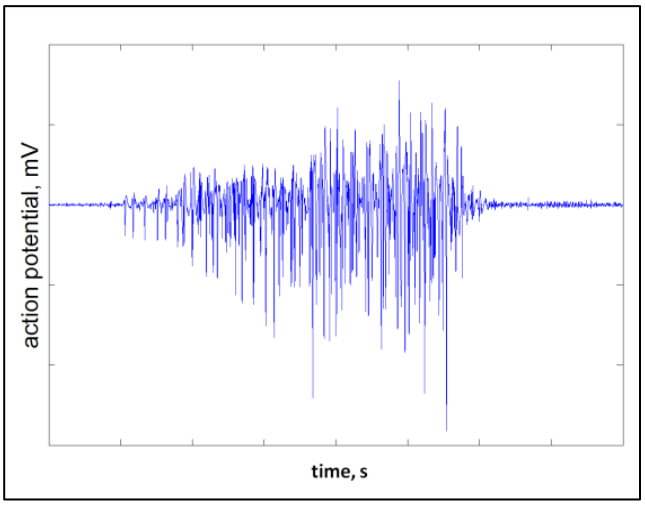

Figure 3.18: Illustration of an EMG interference pattern.

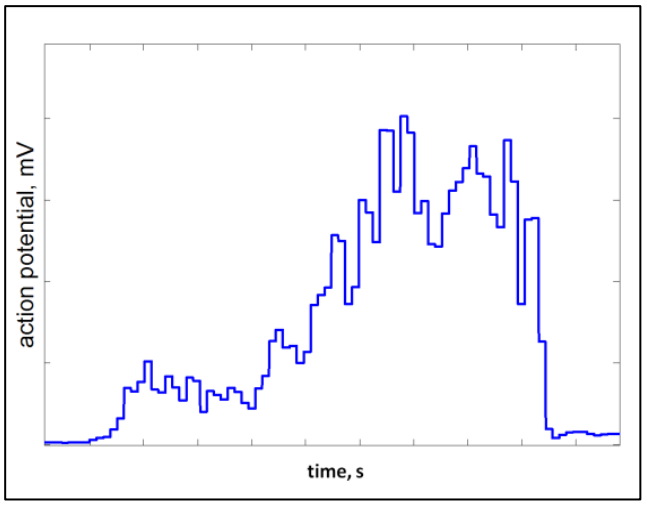

Figure 3.19: A running average of a rectified EMG interference pattern.

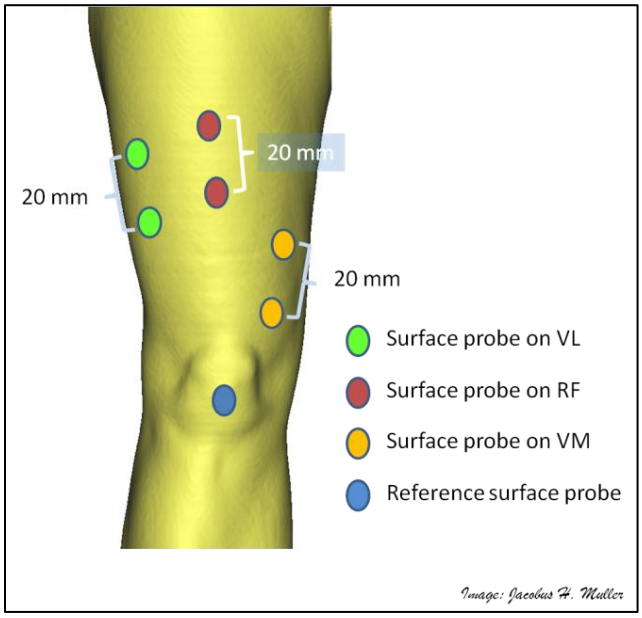

Figure 3.20: Placement of the EMG electrodes on the upper leg.

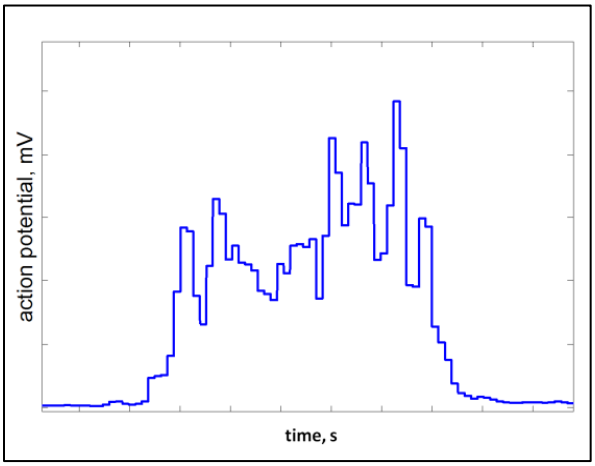

Figure 3.21: EMG of the RF.

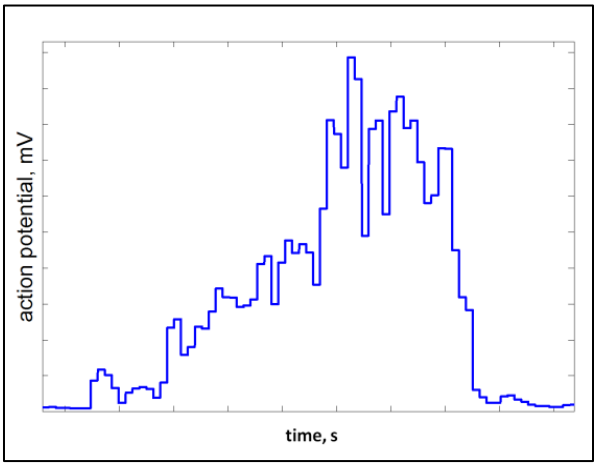

Figure 3.22: EMG of the VL.

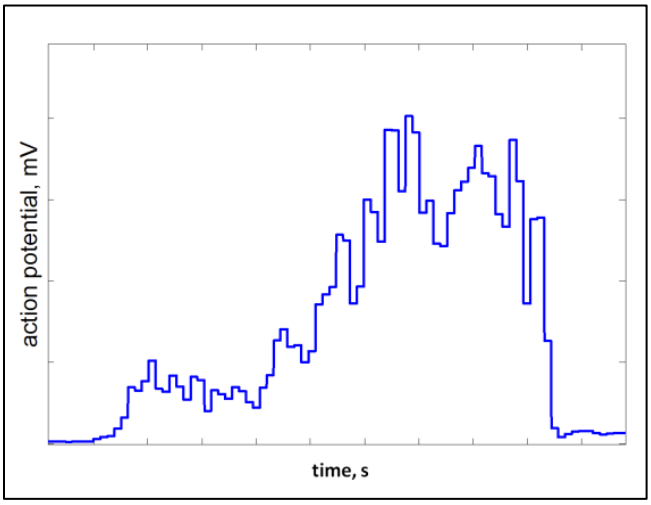

Figure 3.23: EMG of the VM

Chapter 4

4. The musculoskeletal computational model

4.1 Introduction

Chapter 3 described the information and data needed for the assembly of a subject-specific musculoskeletal model. The steps followed during the assembly of these baseline musculoskeletal models are illustrated in Chapter 4, after which their predictive ability is evaluated (Figure 4.1). Published patellofemoral kinematics and kinetics trends, *in-vitro* measurements obtained from a cadaver leg loaded on a test bench, and patellofemoral posture parameters measured with the aid of MRI were compared to the baseline model predictions. These measurements included:

- patella tracking patterns: mediolateral translation / tilt / flexion;
- patellofemoral contact loads;
- MPFL and lateral retinaculum tension;
- patellar tendon / quadriceps tendon tension ratio; and
- tibial transverse rotation.

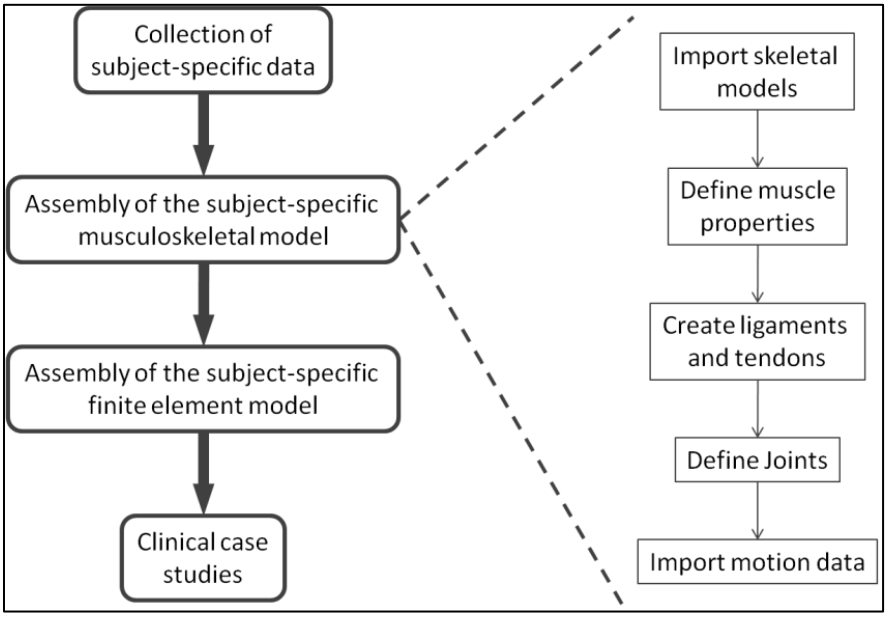

Figure 4.1: Study flowchart (III).

The following section introduces the modelling technique followed by a description of steps to make the models subject-specific. The results obtained with the three baseline models are presented and discussed on the basis of its biofidelity and accuracy.

4.2 LifeModeler technique

LifeModeler (LifeModeler, Inc, San Clemente, California), a human biomechanics simulation tool, uses MSC Adams (MSC Software Corporation, Santa Ana, California) as a platform on which a musculoskeletal model can be constructed and analysed. A generic skeletal model, based on the average between the 5th and 95th percentile of the western civilisation, is scaled to the human subject's weight, length, age and gender. The generic skeleton consists of shell elements, with the body mass embodied in ellipsoids positioned at the inertial centres of the shell elements.

4.2.1 Joints

Three types of joints are available for joint simulation: Hybrid-III joints, passive joints or free-rotating-joints. A Hybrid-III joint's function is governed by a strength model with characteristics based on measurements taken from crash test dummy joints, known as the Hybrid III joints (LifeModeler (2008) b). The strength model is composed of nonlinear stiffness, damping and friction parameters, as well as joint limit stop stiffnesses that incorporate hysteresis. A user-defined scale value regulates the influence of the strength-model on the joint angle. A passive joint consists of torsion springs having user-defined stiffness, damping constant, maximum angular positions, and limit stiffness values, whereas the free-rotating-joints impose no limits on the degrees-of-freedom of the joint.

4.2.2 Soft tissues

Skeletal muscles are either modelled as spring-damper type elements or Hill-type elements. A passive stiffness, passive damping constant and a resting load need to be specified when the spring-damper elements are utilised, whereas the Hill muscle model, developed by Hill (1938), consists of a passive model F_{PE} and an active model F_{CE}. The contributions from the passive and active models result in the exerted muscle load F_{muscle} (Eq. 4.1, LifeModeler (2008) d).

$$F_{muscle} = F_{PE} + F_{CE} \quad \text{Eq. 4.1}$$

$$\sigma = (k \cdot \varepsilon)/\left(1 - {}^{\varepsilon}/_{asy}\right) \quad \text{Eq. 4.2}$$

$$\varepsilon = \left(l_{current} - l_{free}\right)/l_{free} \quad \text{Eq. 4.3}$$

$$l_{free} = l_{rest} \cdot \left(S_{free}/S_{rest}\right) \quad \text{Eq. 4.4}$$

$$F_{CE} = A(t) \cdot F_{max} \cdot f_L(l_r) \cdot f_h(v_r) \quad \text{Eq. 4.5}$$

The passive muscle load F_{PE} is the product of the passive muscle stress σ and the physiological cross-sectional area $pCSA$. The passive muscle stiffness k is multiplied by the passive muscle strain relationship $\varepsilon/\left(1 - {}^{\varepsilon}/_{asy}\right)$ to result in the passive muscle stress σ (Eq. 4.2, LifeModeler (2008) d). Strain ε is based on the instantaneous $l_{current}$ and free length l_{free} difference (Eq. 4.3, LifeModeler (2008) d), whereas a strain asymptote is incorporated with the asy parameter. The free muscle length is the product of the resting muscle length l_{rest} and the ratio of the sarcomere lengths (no-load S_{free} and resting S_{rest}) (Eq. 4.4, LifeModeler (2008) d).

The active force component F_{CE} is equal to a scaled maximum allowable force F_{max} (Eq. 4.5, LifeModeler (2008) d), which is the product of the maximum allowable isometric stress σ_{max} and physiological area. The magnitude of F_{max} depends on the activation state of the muscle $A(t)$, the current length of the muscle $f_L(l_r)$ and the current contraction velocity $f_h(v_r)$. $A(t)$ represents the number of active muscle elements that contribute towards F_{max}, and is implemented by means of a normalised curve based on the EMG measurements described in Section 3.8.

The active force-length relationship $f_L(l_r)$ represents the state at which the muscle will function optimally when at the optimal length. It is based on a dimensionless length ratio l_r of the current muscle length $l_{current}$, sarcomere resting length S_{rest}, the muscle length at no-load l_{rest} and the optimal sarcomere length S_{ref} (Eq. 4.6, LifeModeler (2008) d). When the muscle is at its optimal length, the value of the force-length relationship will be unity, whereas it will decay exponentially according to S_k if the current muscle length deviates from the optimal length (Figure 4.2).

$$l_r = (l_{current} \cdot S_{rest})/\left(l_{rest} \cdot S_{ref}\right) \quad \text{Eq. 4.6}$$

$$v_r = v_{current}/v_{max} \quad \text{Eq. 4.7}$$

The normalised active force-velocity relationship represents the state at which the muscle contraction rate is optimal. This depends on the dimensionless relative velocity ratio v_r, based on the current contraction velocity $v_{current}$ and the maximum allowable contraction velocity v_{max} (Eq. 4.7, LifeModeler (2008) d). There are two possible outcomes of the contraction of muscles (that is when the relative velocity ratio is negative). The first is that if the muscle contracts faster than the maximum allowable velocity, the normalised force-velocity ratio will be zero, deactivating the active force component. The second possibility is that as the contraction speed is reduced relative to the maximum allowable speed, the normalised force-velocity ratio increases to unity. During lengthening, the ratio will increase to a maximum value which is user controlled (Figure 4.3).

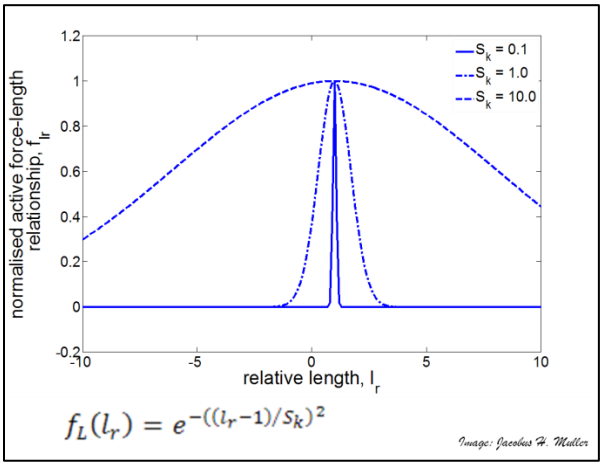

Figure 4.2: Normalised active muscle force-length relationship.

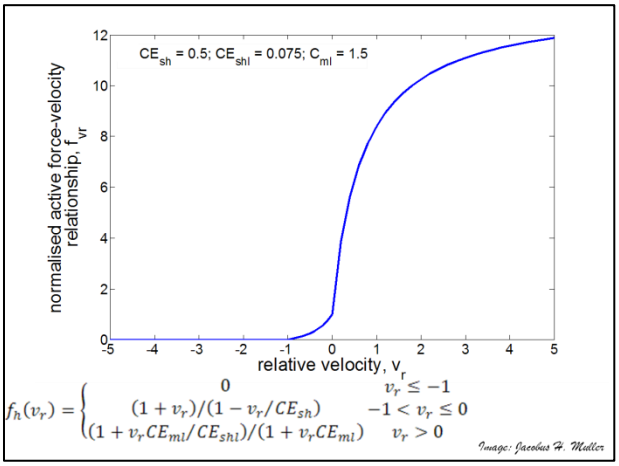

Figure 4.3: Normalised active muscle force-velocity relationship.

Ligaments and tendons are approximated as tension-only spring-damper systems for which the stiffness, damping constants and initial tension need to be specified. A contacting body may be chosen with which the ligament or tendon will interact, enabling the soft tissues to wrap around the body. This improves the biofidelity of the simulation results since the soft tissue tensions will be applied along anatomical directions. When tendons need to be constructed, a mass-less structure is defined at the end of the skeletal muscle to which the muscle and tendon connect. This structure is free to translate and rotate, and serves only as an interface for the muscle and tendon. Its motion is constrained by the muscle-tendon complex.

4.2.3 Contact

Two contact algorithms are available for use when contacts between body segments and the environment need to be defined. A solid-to-solid contact algorithm is used when one or both of the bodies have a complex geometry, while a solid-to-plane contact algorithm is used when one of the bodies can be approximated as a flat plane. Both contact algorithms make use of eight parameters to simulate a contact between two bodies (Table 4.1).

Table 4.1: Contact algorithm parameters.

#	Parameter
1	Contact stiffness value
2	Elasticity exponent
3	Damping coefficient
4	Penetration depth of the damper
5	Static friction constant
6	Dynamic friction constant
7	Stiction velocity
8	Dynamic transition velocity

The contacting bodies are considered to be rigid, and "deformability" is established by means of the damping depth allowing overlap between contacting body surfaces. During the iterative process, the contact detection algorithm computes the volumes of overlap as well as the centroids of these volumes. The shortest distance from the centroid to the surfaces of the bodies are then determined, and multiplied by the stiffness value to calculate an instantaneous reaction force. The elasticity exponent represents the amount of plasticity of the contact: an exponent equal to one will designate a truly elastic contact, whereas an exponent equal to three designates a truly plastic contact. Friction between the contacting bodies' surfaces is dependent on the relative velocity between the articulating parts. If the velocity is greater than the dynamic transition velocity, the friction is based on the dynamic friction constant. The static constant will only come into play if the relative velocity is smaller than the dynamic transition velocity, or decreases below the stiction velocity.

4.2.4 Motion

Motion simulation can occur in one of two ways. The first is called an inverse dynamics analysis, where the musculoskeletal model is manipulated with motion agents (mass-less elements; LifeModeler (2008) c) that connect to the musculoskeletal model with spring-damper systems. The motion agents "pull" the segments along user-defined motion splines. Motion simulation can also occur during a forward dynamics analysis, where the musculoskeletal model is manipulated with the muscles that were "trained" during an inverse analysis. Contraction measurements obtained from an inverse analysis are used as target values by a proportional-integral-differential controller governing muscle activation.

4.3 Subject-specific musculoskeletal model setup

The skeletal segments of the generic model were replaced with the volunteer-specific skeletal elements. The volunteer's pelvis was inserted first and manually repositioned to correspond with the position and orientation of the generic pelvis. Next the femora, tibiae, fibulae, patellae and feet were positioned relative to the centroid of the volunteer's pelvis as determined from the volunteer's CT scan. This ensured that the posture of the subject-specific skeleton was kept intact during this procedure. The next step involved the modification of the generic skeleton posture to coincide with that of the subject-specific skeleton.

The hip, tibiofemoral and ankle joints were modelled as Hybrid-III joints. There was variation between the generic skeletal dimensions and the subject-specific dimensions, which caused the joint centres to be misaligned with the subject-specific centres. The joint axes were manually repositioned to coincide with the subject-specific centres. The new axes' positions were visually verified by flexing the joints. A more refined method in determining the joint centres entails the attachment of a sphere on the femoral head to find the hip centre and the fitment of coaxial cylinders to the femoral condyles (Fernandez *et al.* (2008)). This method was applied to one of

the volunteers and produced similar results to that of the manual approach; hence the manual approach was used for the other volunteers.

A generic simplified muscle set was imported into the model. The extensor mechanism and flexor mechanism were removed to be replaced with subject-specific Hill-type muscles. The Hill-type muscle parameters (cross-sectional area, maximum allowable stress, rest length, free length) were modified to correspond to that of the volunteer. The rest length (minimum length) of each Hill-muscle was determined for the seating exercise by means of a trial simulation, during which the model was taken through the entire range of motion. The minimum length obtained in each muscle was then used as the rest length for that muscle.

Table 4.2: Polynomial fits to quadriceps EMG recordings.

Muscle group	Order of fit	Coefficient of determination, r^2
VL	Sixth order	0.87
RF	Ninth order	0.77
VM	Eighth order	0.89

The activation curves of the Hill-type muscles were approximated with the EMG recordings presented in Section 3.8. The EMG signals were scaled to correspond to the duration of the motion recordings. Polynomials (Table 4.2) were fitted to the EMG recordings for the RF (Figure 4.4), VL (Figure 4.5) and VM (Figure 4.6) to ensure a smooth input to the muscle value. The polynomials with orders between one and ten were considered, after which the polynomial with the best coefficient of determination was chosen. These curves were then normalised with respect to the maximum value reached in each curve (Figure 4.7). This approach was chosen since the EMG recordings for the different muscles were obtained at different times because only two leads were available and as a result the recordings could not be related to one another objectively.

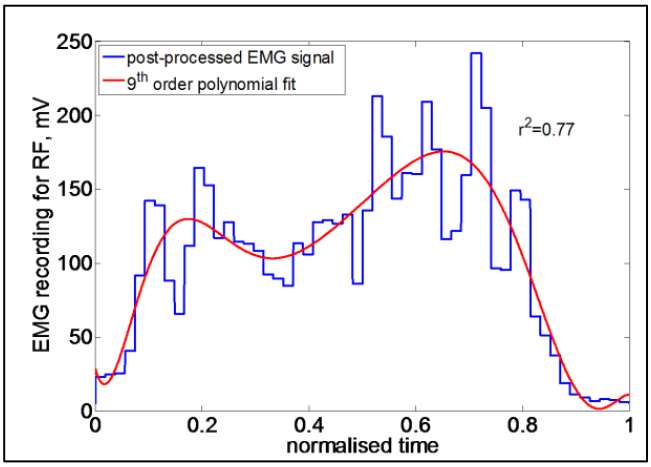

Figure 4.4: Ninth order polynomial fit to RF EMG recording.

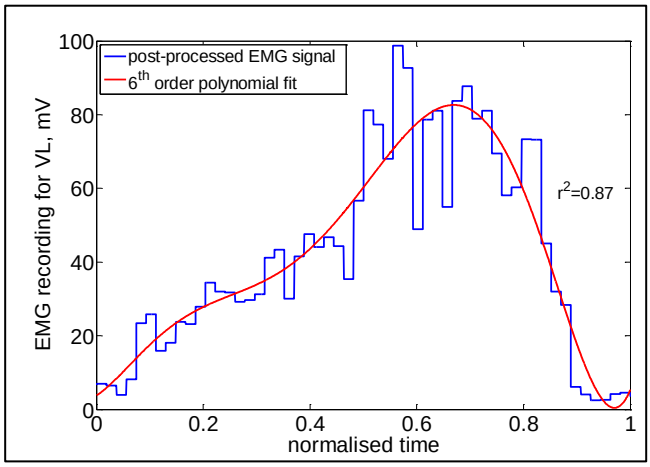

Figure 4.5: Sixth order polynomial fit to VL EMG recording.

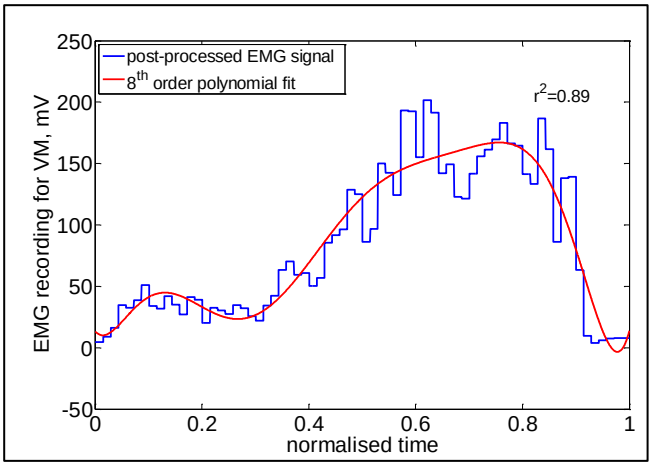

Figure 4.6: Eighth order polynomial fit to VM EMG recording.

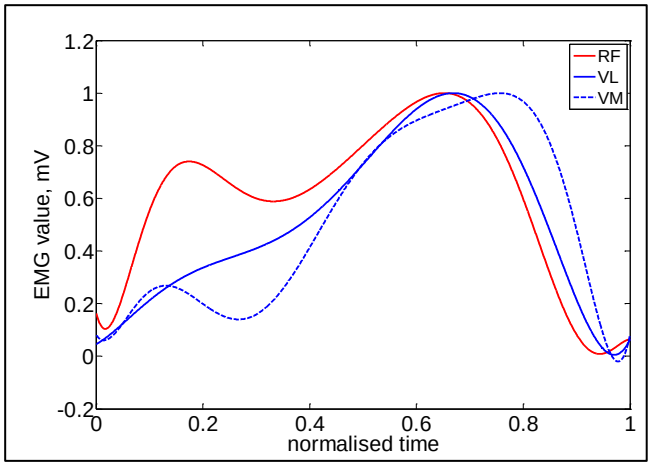

Figure 4.7: Normalised EMG recordings.

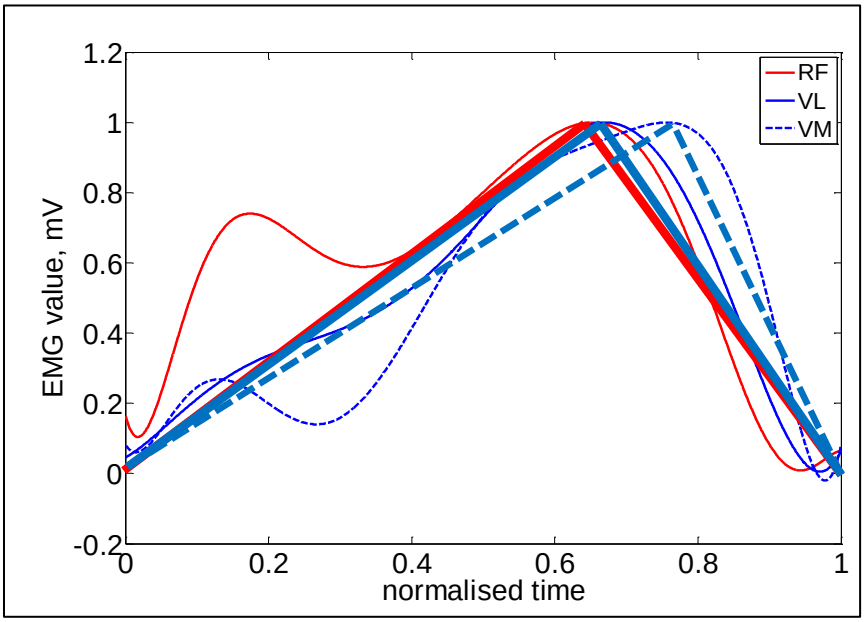

Figure 4.8: First order fits to normalised EMG data.

The curves presented in Figure 4.7 were approximated with first order polynomial fits (Figure 4.8). A preliminary investigation showed that the activation patterns did not have a significant influence on the patella tracking predictions, and a minimal influence on patellofemoral kinetics (Appendix E). Analysis times were however reduced when the activation curves were approximated by first order polynomials.

Mass-less dummy elements were created onto which the quadriceps muscles attached distally. This provided a connection point between the skeletal muscle and quadriceps tendon, which connected the dummy elements to the patella. The quadriceps and patellar tendons, as well as the lateral retinaculum and medial patellofemoral ligament were created next (Table 4.3). The soft tissues stabilisers attached to the designated skeletal landmarks as determined from a cadaver anatomical study (Appendix D), the volunteer MRI scans and supplementary

literature sources (LaPrade *et al.* (2007a, 2007b), Sanchez *et al.* (2006) and Seebacher *et al.* (1982)). The contact bodies were defined to ensure that the ligaments and tendons wrapped around the skeletal elements, which ensured that the tensile forces were exerted in physiological representative directions. The stiffness and initial vales for the tensions in the ligaments and tendons were based on published results (Table 4.3).

Table 4.3: Patellofemoral soft tissue stabiliser parameters.

Soft tissue structure	# elements [aa]	Stiffness (N/mm)	Pre-tension (N)
Patellar tendon	(medial/central/lateral)	734[bb]	137[bb]
Quadriceps tendon	(VL/RF/VM)	734[bb]	137[bb]
Lateral retinaculum	9	4[cc]	1[cc]
MPFL	3	4[cc]	1[cc]

aa: Shirazi-Adl and Mesfar (2007); bb: Hashemi *et al.* (2005); cc: Elias and Cosgarea (2006)

The contact between the patella and the femur (solid-to-solid) was assumed to be a combination of ideally elastic and plastic, hence an exponent of two was chosen. The *in-vivo* contact will be dependent on the viscoelastic nature of the cartilage, but this option was not available in the solver software. The stiffness parameter was based on a simplified two-dimensional FEA in which a uniformly distributed load was applied across a cartilage layer (Appendix H). The compression was recorded and a stiffness value was calculated, $stiffness = applied\ load/compression$. The damping coefficient was increased to reduce vibration between the contacting bodies; while a damping depth equal to the cartilage thickness was chosen, being two to three millimetres (Koo *et al.* (2005)). Friction was assumed to be negligible (friction constants were <<1) between the two contact bodies (Mow *et al.* (1993)).

Contact between the feet and the floor was established by using the default barefoot-hard floor settings (solid-to-plane; LifeModeler (2008) a). A solid model of a chair was imported and repositioned relative to the model and the contact was defined between the lower body and the chair (solid-to-solid, LifeModeler (2008) a). The ellipsoids on the legs approximated the contact geometry of the legs whereas the chair's actual geometry represented the chair's contact geometry. The ellipsoids provided a good approximation of the geometry of the leg circumference since it is scaled according to the model length and weight that would make contact with the chair during actual performance of the exercise.

Seven motion agents were defined and positioned to correspond with the landmarks used in biomechanical models of the motion capturing software, that is: the sacrum, hip centre, knee centre and ankle centre. The motion agents translated and rotated along motion splines on the two principal horizontal axes. The vertical displacement and transverse rotation of the skeletal segments were governed by the muscle forces and gravitation.

An equilibrium analysis was performed during which the motion agents and the joints were fixed in space and the muscle activation was disabled, for the model to reach a state of equilibrium. After the equilibrium analysis was concluded, the ligament and initial tendon tensions were adjusted to the values obtained during the equilibrium analysis. An inverse dynamics analysis followed, during which the motion agents were allowed to manipulate the model's posture. The partial differential equations of motion were solved by employing the GSTIFF integrator (default integrator for Adams Solver) with Standard Index-2 (SI2) formulation with a maximum step size of 1×10^{-4}. The GSTIFF integrator used backward differential formulas as well as fixed coefficients for the prediction and correction procedures. The SI2 formulation enables the GSTIFF integrator to monitor the error of velocity variables since it takes the derivatives of the constraint variables into account. At small step sizes, the Jacobian matrix remains stable, which improves stability and robustness.

Patella flexion was expressed in terms of the initial flexion of each volunteer's patella. The mediolateral tilt and shift were standardised for the three volunteers by incorporating the method used by Ward *et al.* (2007). A vertical plane $\boldsymbol{AB}$ was fitted on the post-condylar line $\boldsymbol{A \rightarrow B}$ and a plane $\boldsymbol{CD}$ on the patellar width line $\boldsymbol{C \rightarrow D}$ (Figure 4.9). The angle between planes $\boldsymbol{AB}$ and $\boldsymbol{CD}$ was used as the initial value for lateral patella tilt. A plane $\boldsymbol{EE}$, perpendicular to the postcondylar plane, was fitted through the deepest point E on the trochlear groove. The distance from the lateral point $\boldsymbol{C}$ to the intersection $\boldsymbol{EE \cap CD}$ of plane $\boldsymbol{EE}$ and plane $\boldsymbol{CD}$, was used in the calculation of the lateral patella bisect offset, Eq. 4.8.

$$BO = \frac{\boldsymbol{C \rightarrow EE \cap CD}}{\boldsymbol{C \rightarrow D}} \times 100 \qquad \text{Eq. 4.8}$$

$$Accuracy = \left(1 - \sqrt{\left(\frac{Parameter_{prediction} - Parameter_{MRI}}{Parameter_{MRI}}\right)^2}\right) \times 100\% \qquad \text{Eq. 4.9}$$

This datum was chosen to ensure better repeatability between measurements. The initial positions of the gravitational centres of the patellae were used as the origin of the reference axis frame on the patella to which the measurements (kinematics and kinetics) were related. The patella tilt and bisect offset for each baseline model were compared to the values obtained from the MRI measurements at 30 degrees knee flexion. These values were used to approximate the accuracy of the simulation technique (Eq. 4.9).

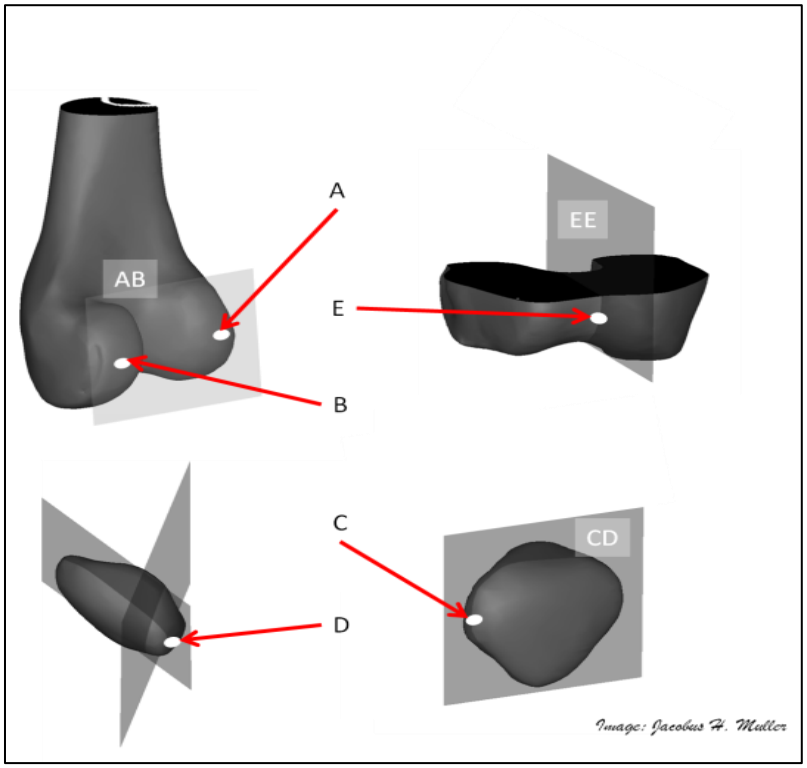

Figure 4.9: Determination of the patella bisect offset and lateral patella tilt.

The correlation between tibial rotation and patellar tilt was calculated by means of Pearson's rank coefficient of correlation (Myers and Well (2003)). The rank coefficient rather than the linear coefficient was used to avoid the assumption of the two variables being linearly dependent. Rank values were assigned to the patella tilt and tibia rotation measures, with the patella tilt rank values rearranged to form a monotonic increasing function. The corresponding tibia rotation rank values were rearranged in the same order as the patella tilt rank values. The average of the rank values of the tilt or rotation values that were equal replaced the ranks of the similar values.

$$\rho = 1 - \frac{6\sum_{i=1}^{n} d_i^2}{n(n^2-1)} \qquad \text{Eq. 4.10}$$

The difference of the corresponding rank values ($d_i, = amount\ of\ measures$; $n = population\ size$) was then computed and used to calculate the rank correlation coefficient ρ (Eq. 4.10). A correlation value $0.5 < |\rho| \leq 1$ indicates a strong correlation between the two variables. The student t method (confidence interval of 95%, Vining (1998)) was used to determine if the correlations were statistically significant.

Additional quasi-static analyses (at 30, 60 and 90 degrees knee flexion) were performed to determine their effect on patella shift and tilt prediction as compared to the dynamic analysis prediction. Patellofemoral contact loads as well as soft tissue tensions were also compared to the dynamic analysis results. The musculoskeletal models'

joints were fixed at the desired flexion angles, while the muscle activation was similar to the corresponding values of the dynamic analysis.

4.4 Results

4.4.1 Baseline model properties

The initial lateral tilt angles and bisect-offsets were subject-specific and differed from the values obtained from the CT scans (Table 4.4) (will be explained in Section 4.5). Volunteer One's patella started to track more laterally and at a greater tilt angle whereas the lateral tilt and bisect-offset were smallest for Volunteer Three. Volunteers One and Two's patella ridge (area that separates the medial facet from the lateral facet), had a lateral offset with respect to the trochlear centre, whereas Volunteer Three's patella ridge had a medial offset. Visual inspection showed that Volunteers One and Three's patellae engaged the trochlear groove after knee flexion began, whereas Volunteer Two's patella was engaged in the trochlear groove at the start of knee flexion.

Table 4.4: Initial position of patellae with regards to the trochlear groove centre at full extension.

	Tilt angle, degrees		Bisect offset, % patella width	
	Prediction	CT Scan	Prediction	CT scan
Volunteer One	24.0	14.2	85	65
Volunteer Two	10.7	5.2	55	47
Volunteer Three	0.9	10.4	42	62

4.4.2 Patellofemoral kinematics

The volunteers performed the exercises at differed speeds, with Volunteer Two performing a faster knee flexion than Volunteers One and Three at early knee flexion (< 20 degrees knee flexion). At mid-flexion (20 degrees < knee flexion < 60 degrees), Volunteer One performed a faster knee flexion movement, which had an effect on the active model of the Hill-muscle model.

Volunteer One's patella shifted medially, and engaged the trochlear groove at 30 degrees knee flexion, after which it shifted laterally again. Volunteers Two and Three's patellae followed a lateral traction pattern from the start of knee flexion (Figure 4.10 and Figure 4.11). The tilt trends appeared subject-specific (Figure 4.12): before trochlear engagement, Volunteer One's patella tilted medially with respect to the post-condylar line. After trochlear engagement, the lateral tilt angle changed minimally. The lateral tilt angle of Volunteer Two's patella increased with knee flexion (up to 65 degrees), after which it decreased again for the remainder of knee flexion. Volunteer Three's patella tilted medially to 45 degrees knee flexion, after which it tilted laterally again. The

initial (at trochlear engagement) and final tilt angles did however remain constant for Volunteers One, Two and Three.

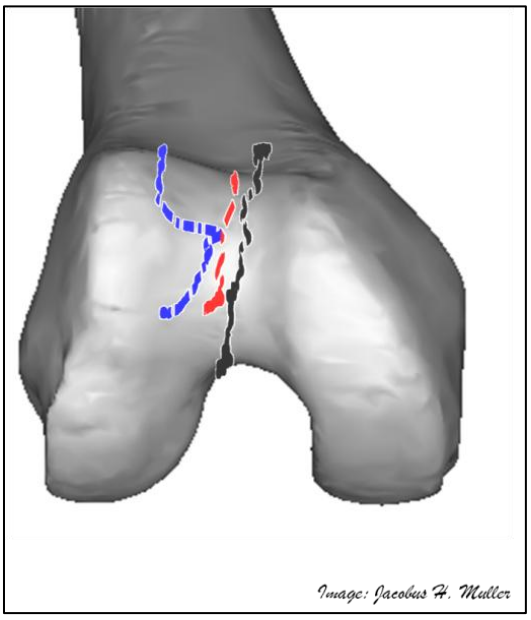

Figure 4.10: Patella tracking along the trochlear groove.

(Blue: Volunteer One; Red: Volunteer Two; Black: Volunteer Three)

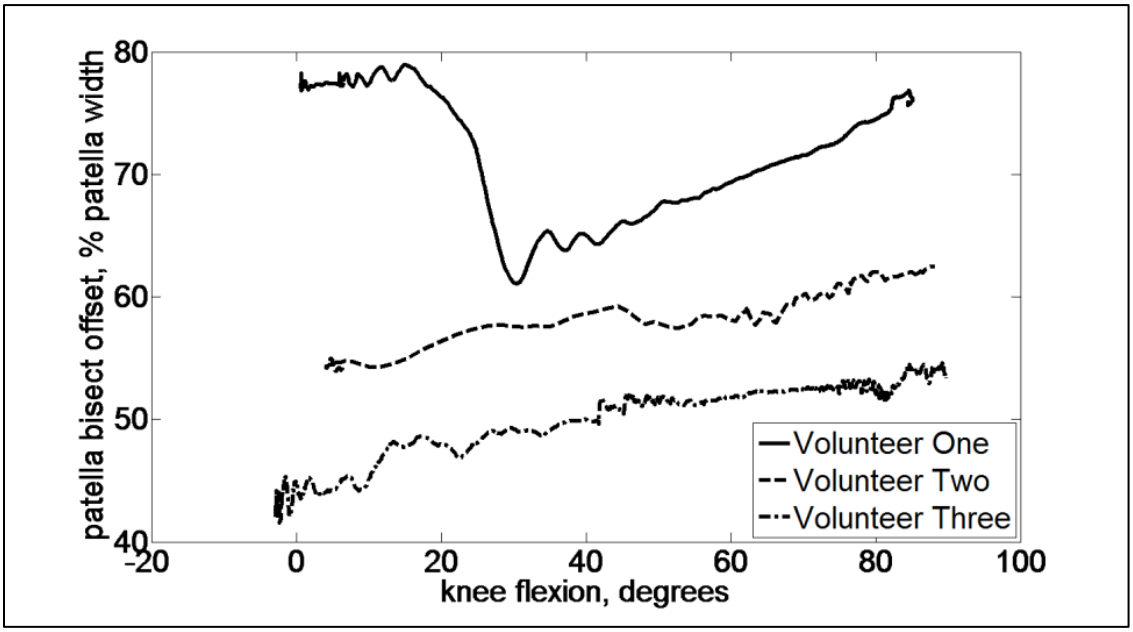

Figure 4.11: Patella bisect offset as a function of knee flexion (+: lateral; -: medial).

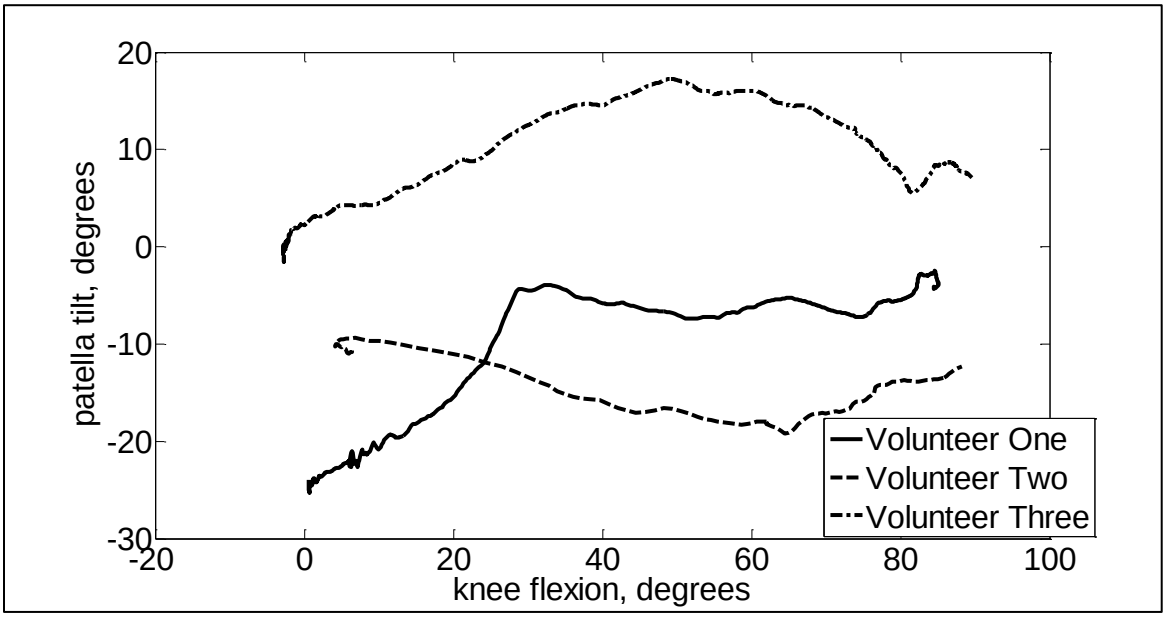

Figure 4.12: Patella tilt as a function of knee flexion (+: medial; -: lateral).

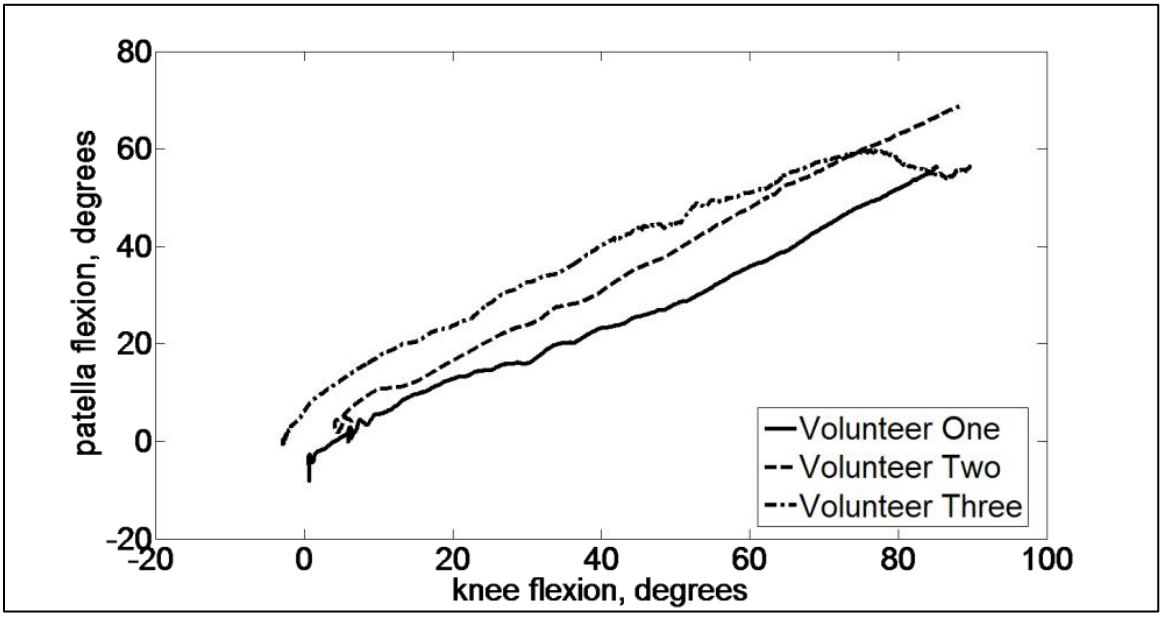

Figure 4.13: Patella flexion as a function of knee flexion.

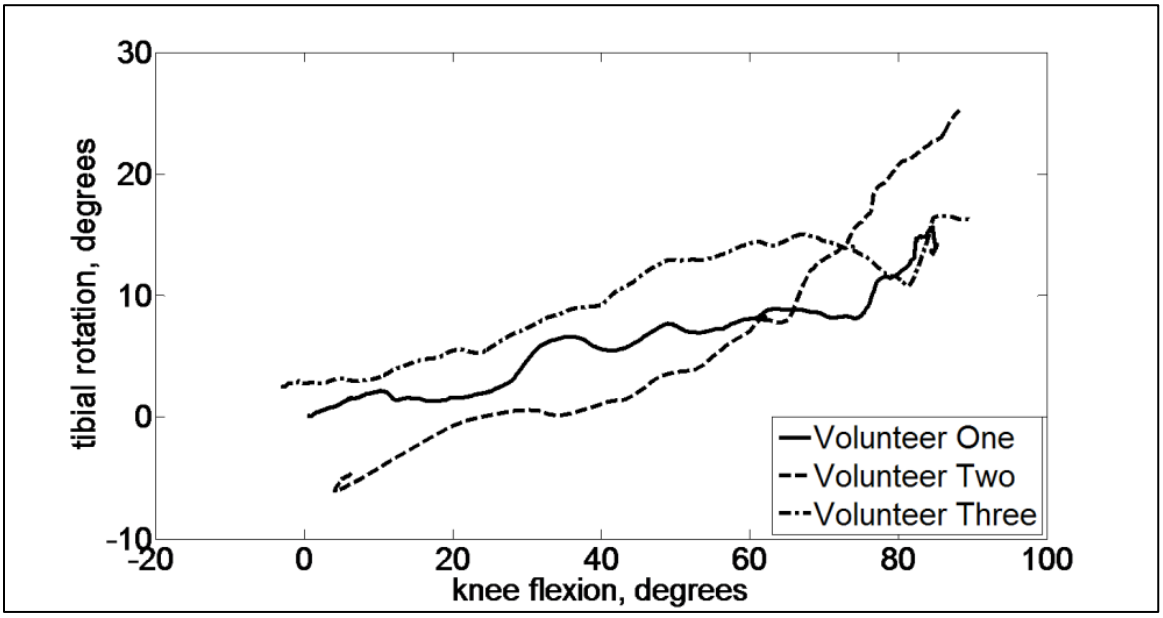

Figure 4.14: Internal tibial rotation as a function of knee flexion (+: internal; -: external).

The mean accuracy in terms of the bisect offset was 96.9 % (SD = 3.5 %), while the accuracy of the predicted tilt angles was lower at 62.1 % (SD = 27.7 %) (Table 4.5). The latter value was influenced by the low accuracy attained for Volunteer One's patella tilt. Patella flexion lagged knee flexion for all three volunteers (Figure 4.13). All three volunteers' tibiae rotated inwards relative to the femur as the knee flexion angle increased (Figure 4.14). There was good correlation ($\rho > 0.5$ ($p < 0.05$)) between patella tilt and tibial rotation for Volunteers One and Three, but the correlation was weak ($\rho < 0.5$ ($p < 0.05$)) for Volunteer Two (Table 4.6).

Table 4.5: Comparison between the *in-vivo* and the predicted patella bisect offset and tilt at 30 degrees flexion.

	Tilt angle, degrees			Bisect offset, % patella width		
	Prediction	MRI	**Accuracy, %**	Prediction	MRI	**Accuracy, %**
Volunteer One	-4.52	-14.5	**31.1**	61.17	59.9	**97.9**
Volunteer Two	-13.43	-19.0	**70.7**	57.57	61.9	**93.0**
Volunteer Three	12.51	14.8	**84.5**	49.12	49.2	**99.8**

Table 4.6: Correlation between internal tibial rotation and patella tilt.

	Correlation factor (ρ)	Probability (p)
Volunteer One	0.92	$p < 0.05$
Volunteer Two	0.39	$p < 0.05$
Volunteer Three	0.67	$p < 0.05$

The difference in patella mediolateral position as well as the mediolateral patellofemoral load component prediction with a dynamic or quasi-static analysis was examined for Volunteer One. The results indicate that there was a maximum 53.4 % (with respect to the dynamic value) difference in the mediolateral position prediction at 30 degrees. A maximum difference of 23.3 % occurred in the mediolateral load prediction at 30 degrees. The differences between the static and dynamic predictions decreased as the knee was flexed from full extension to 90 degrees flexion.

Table 4.7: Differences in mediolateral position and patellofemoral load predictions by the quasi-static and dynamic simulations (Volunteer One).

Knee flexion angle	Mediolateral position, % of the dynamic value	Mediolateral load component, % of the dynamic value
30 degrees	53.4 %	23.3 %
60 degrees	21.2 %	5.2 %
90 degrees	4.7 %	9.2 %

4.4.3 Patellofemoral kinetics

Patellofemoral contact load (normalised in terms of the weight of each volunteer) increased with knee flexion for all three volunteers (Figure 4.15). The contact load increased more sharply for Volunteer One than for Volunteers Two and Three. The mediolateral patellofemoral load component varied for all three volunteers (Figure 4.16). The patellofemoral contacts were maintained on the lateral patella facet of Volunteers One and Three after trochlear engagement, and were balanced between the lateral and medial facet of Volunteer Two.

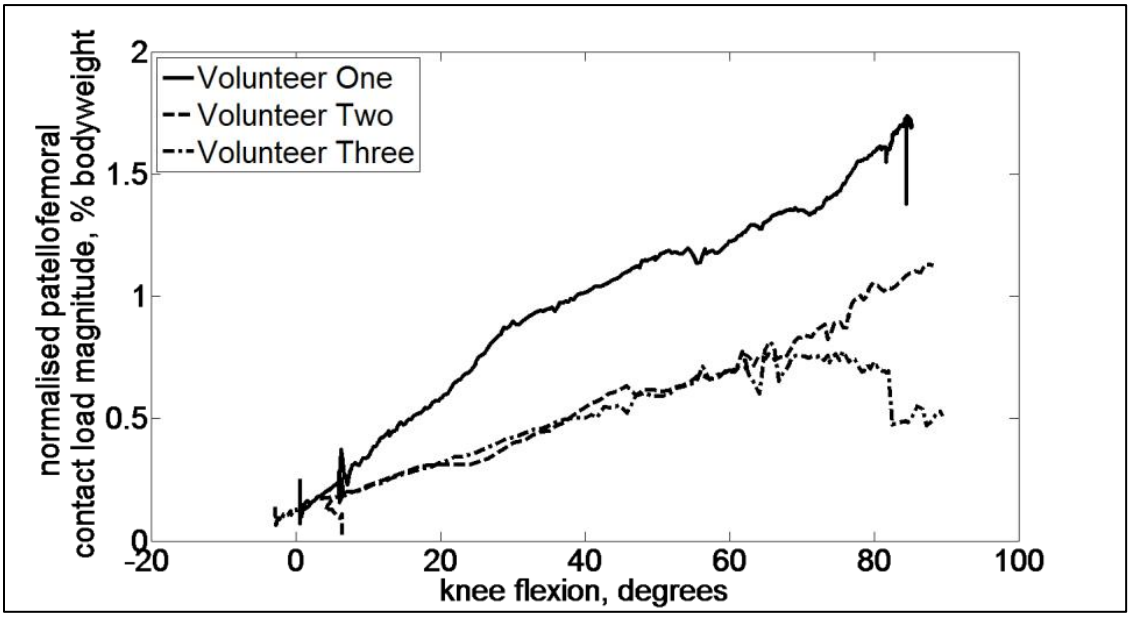

Figure 4.15: Patellofemoral resultant contact load as a function of knee flexion.

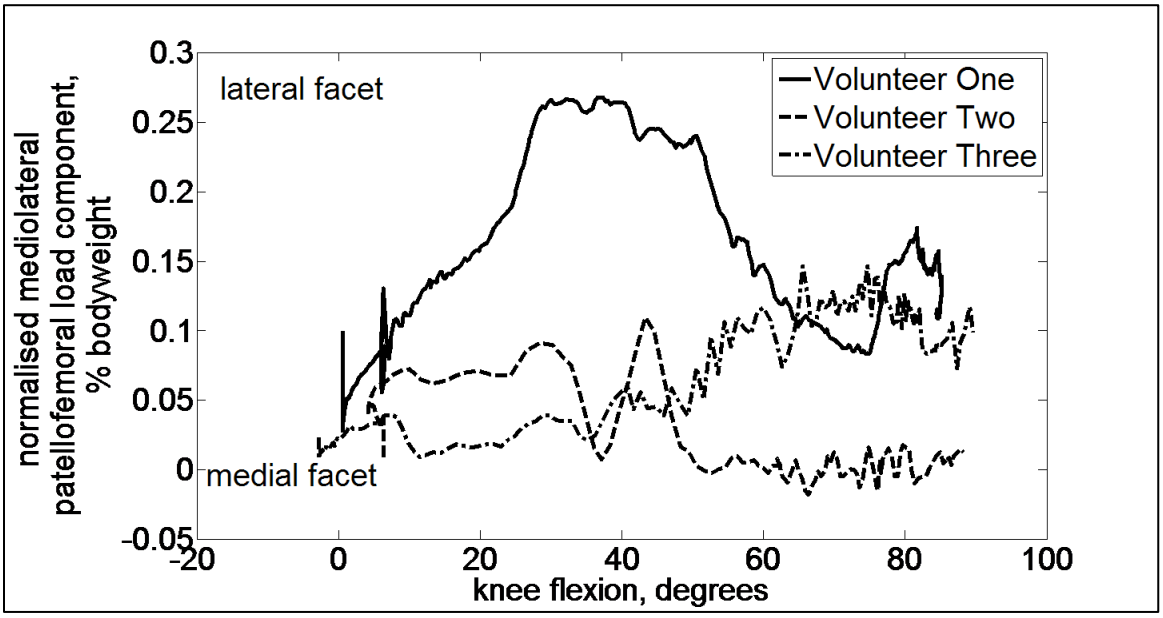

Figure 4.16: Patellofemoral mediolateral contact load component as a function of knee flexion.

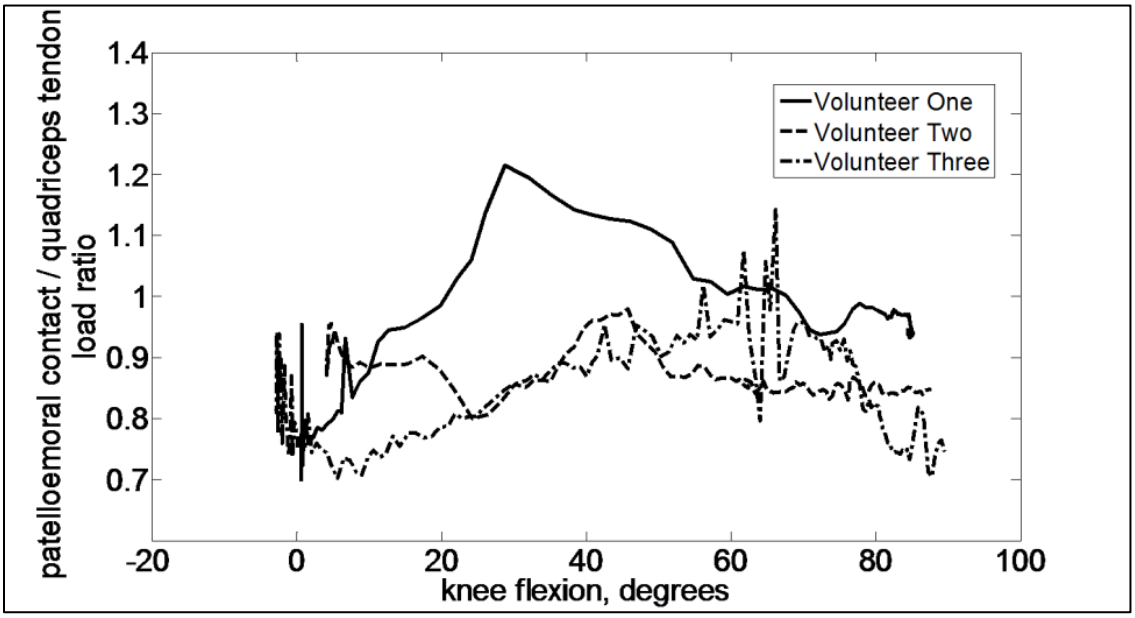

Figure 4.17: Patellofemoral contact-quadriceps tendon load ratio as a function of knee flexion.

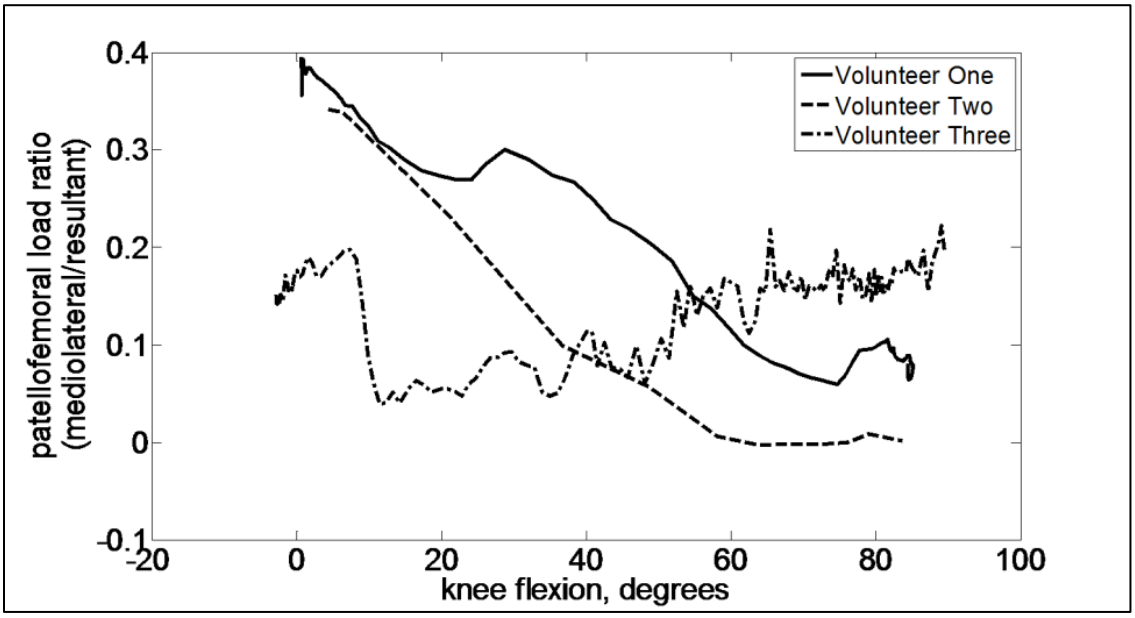

Figure 4.18: Patellofemoral mediolateral contact load – patellofemoral contact magnitude ratio as a function of knee flexion.

The patellofemoral contact-quadriceps tendon load ratio (Figure 4.17) was maintained between 0.7 and 1.3 through the entire range of flexion. The ratio was highest for Volunteer One at 30 degrees knee flexion when the patella engaged the trochlear groove. The percentage of the lateral load component contributing towards the patellofemoral contact load decreased with knee flexion for Volunteer One and Two, whereas it increased for Volunteer Three (Figure 4.18).

To better visualise the effect of the soft tissue stabiliser tensions on the patella, the tension components (mediolateral, anteroposterior and proximal-distal) were calculated (defined as an output by the simulation software) for the MPFL, lateral retinaculum, quadriceps tendon (VM, RF and VL) and the patellar tendon. The resultant load in the coronal (Figure 4.19), sagittal (Figure 4.20) and transverse planes (Figure 4.21) for each volunteer was then plotted. The tension values are expressed as a percentage of the volunteer's bodyweight.

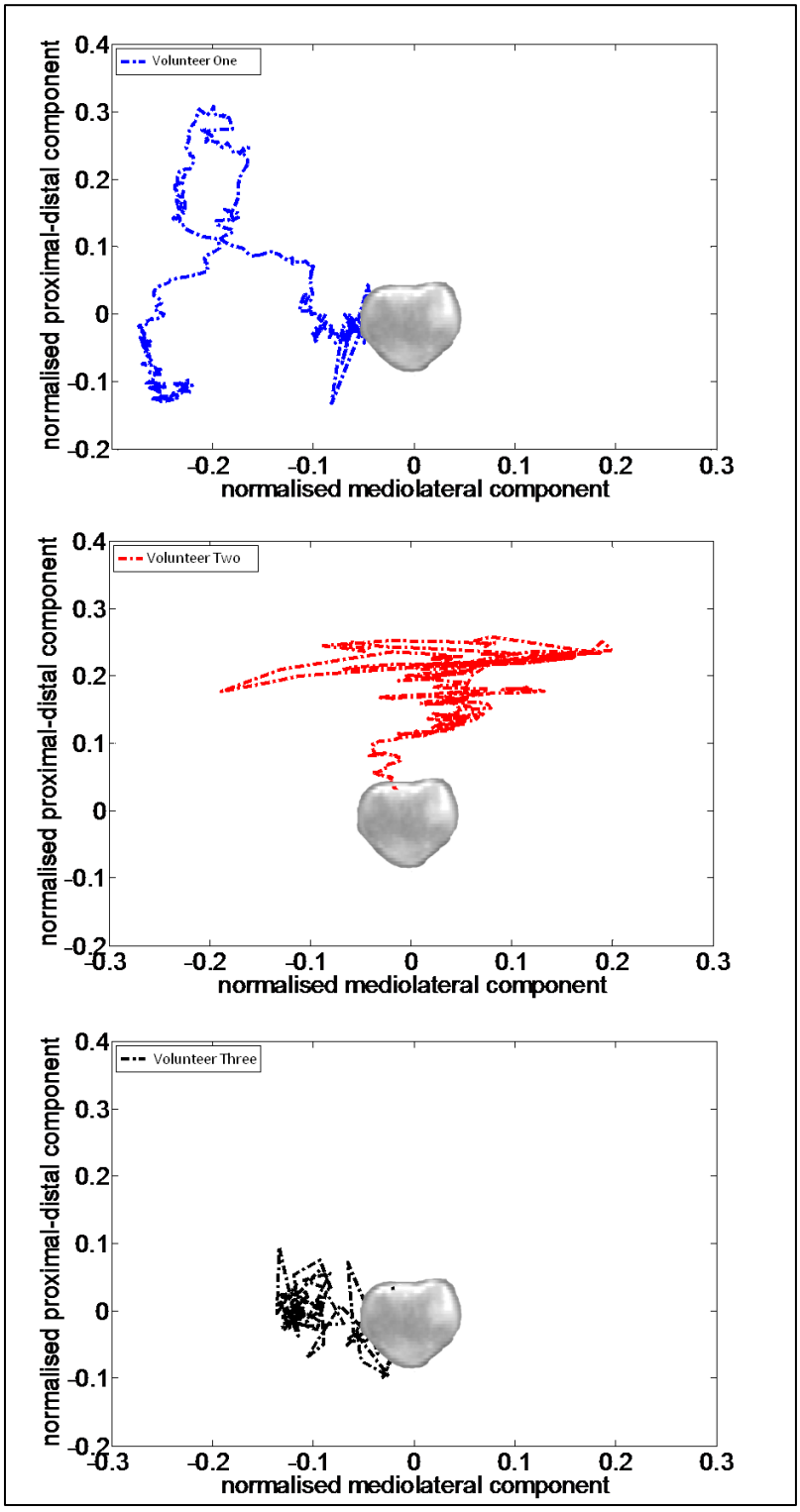

Figure 4.19: Soft tissue stabiliser load in the coronal plane (+: medial / proximal; -: lateral / distal).

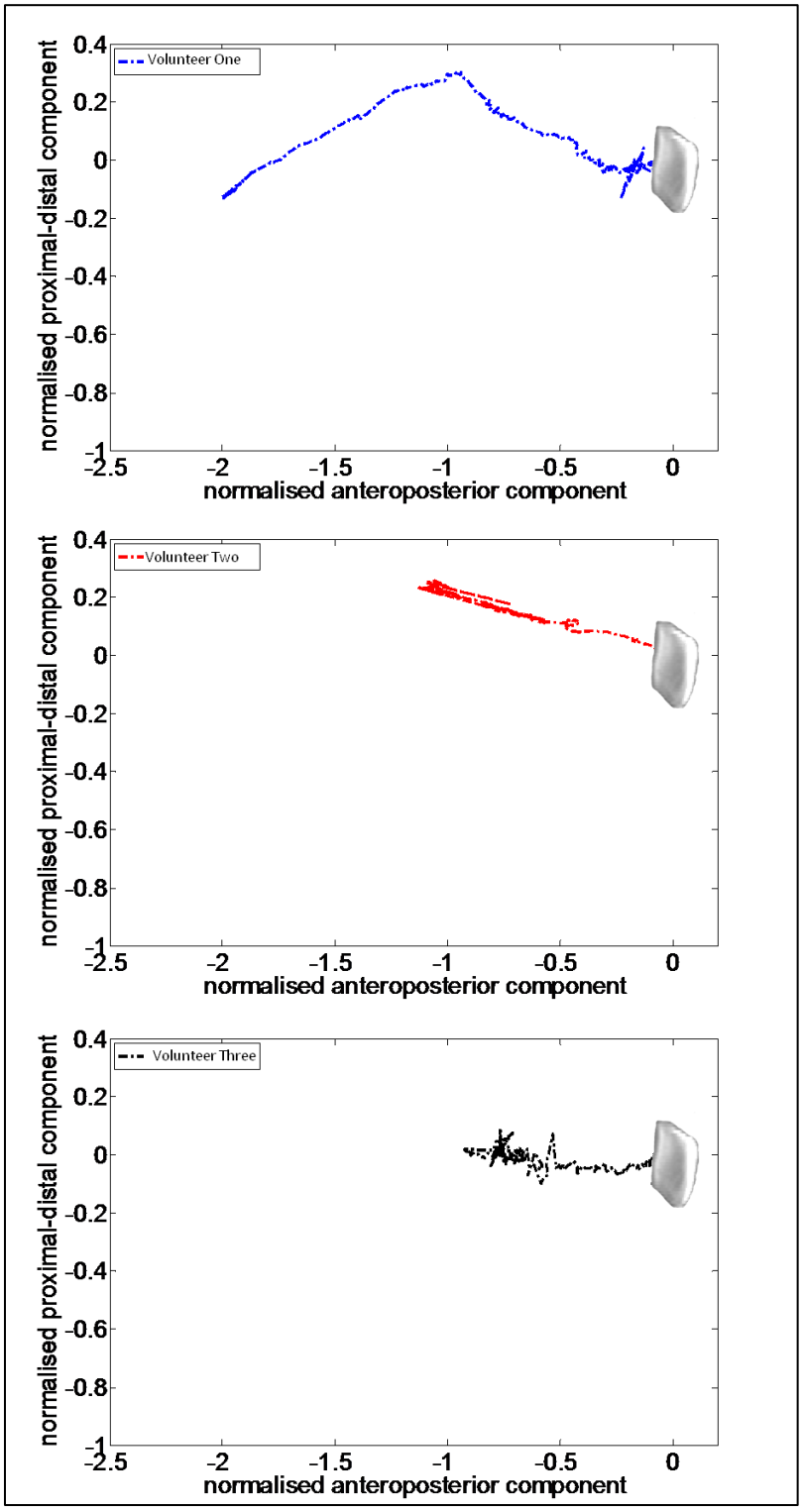

Figure 4.20: Soft tissue stabiliser load in the sagittal plane (+: anterior / proximal; -: posterior / distal).

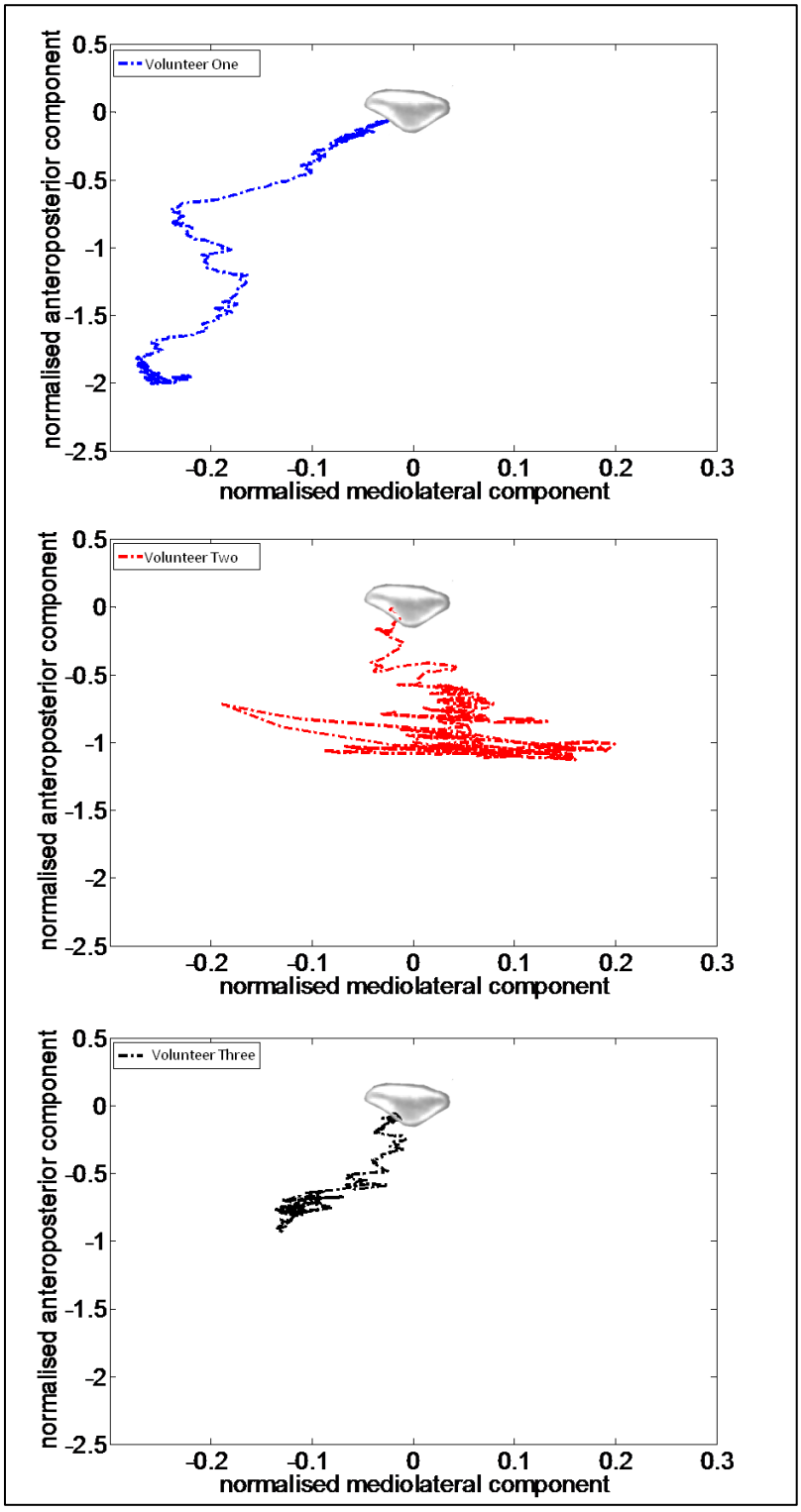

Figure 4.21: Soft tissue stabiliser load in the transverse plane (+: medial / anterior; -: lateral / posterior).

The soft tissue stabilisers pulled Volunteer One's patella in a lateral and posterior direction throughout the entire range of knee flexion. The load component in the proximal direction increased at early knee flexion, but decreased again after 45 degrees knee flexion. The mediolateral load component on Volunteer Two's patella varied for the duration of the exercise, while it was laterally directed on the patella of Volunteer Three. The

angles of impact in the sagittal plane remained constant for both Volunteers Two and Three's patellae through the entire range of flexion.

The tension in the MPFL of all three volunteers diminished after trochlear engagement (Figure 4.22). Volunteer Three experienced an increased MPFL tension below ten degrees knee flexion, before its tension decreased. The lateral retinaculum load of Volunteer One increased sharply before trochlear engagement, after which the tension diminished again (Figure 4.23). The patellar tendon-quadriceps tendon tension ratio decreased with knee flexion for Volunteers One and Three, whereas it remained constant for Volunteer Two (Figure 4.24).

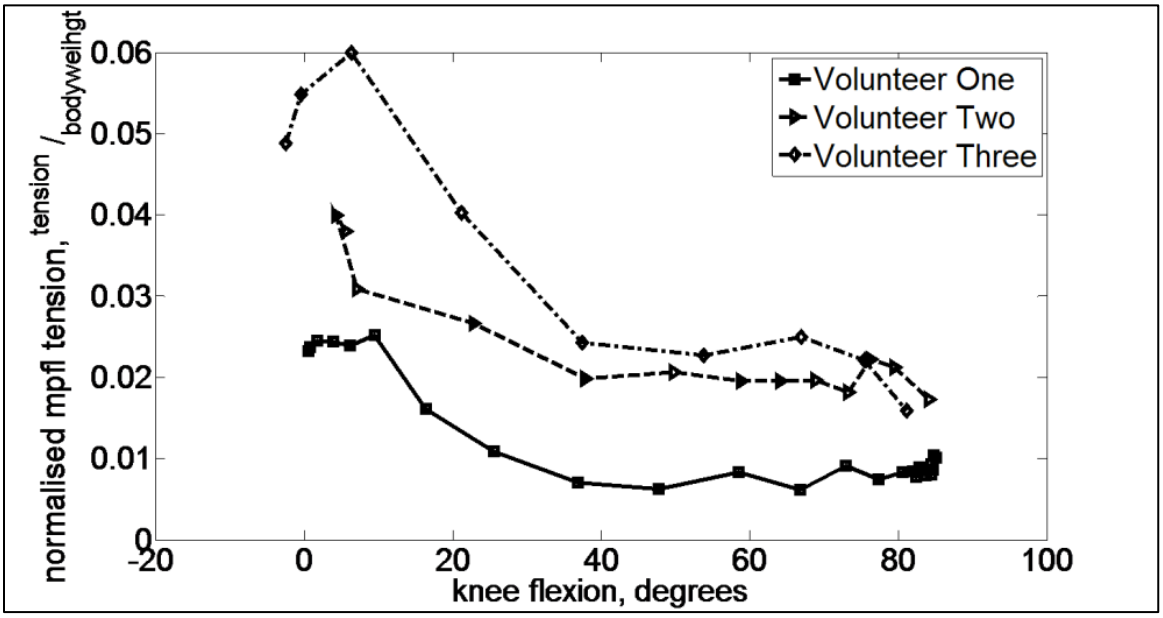

Figure 4.22: MPFL tension as a function of knee flexion.

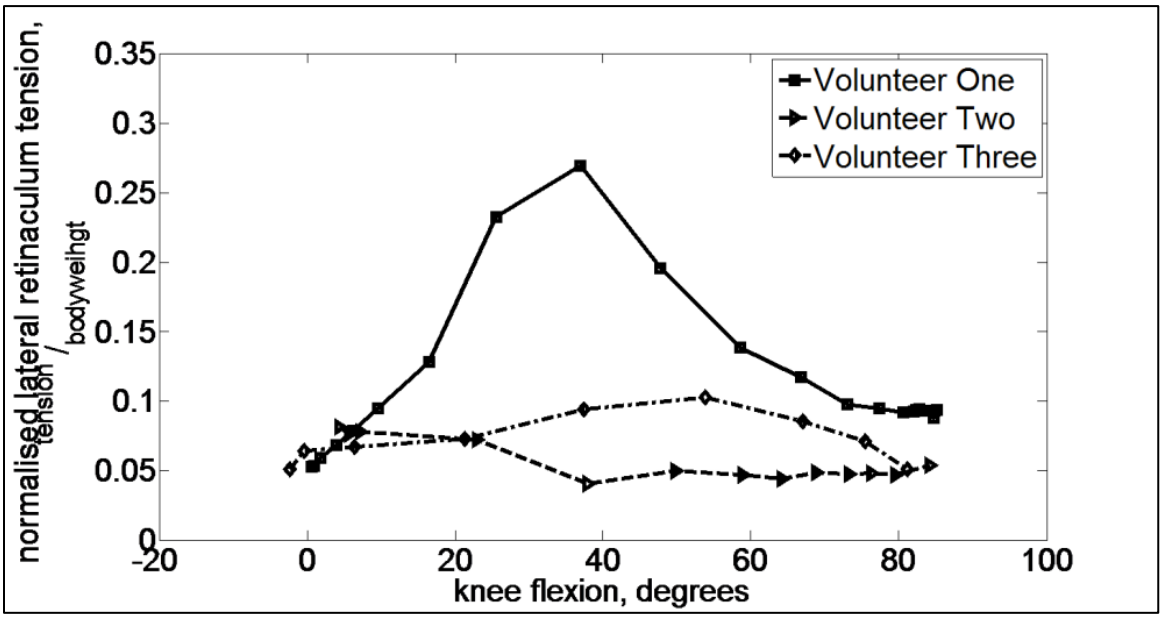

Figure 4.23: Lateral retinaculum tension as a function of knee flexion.

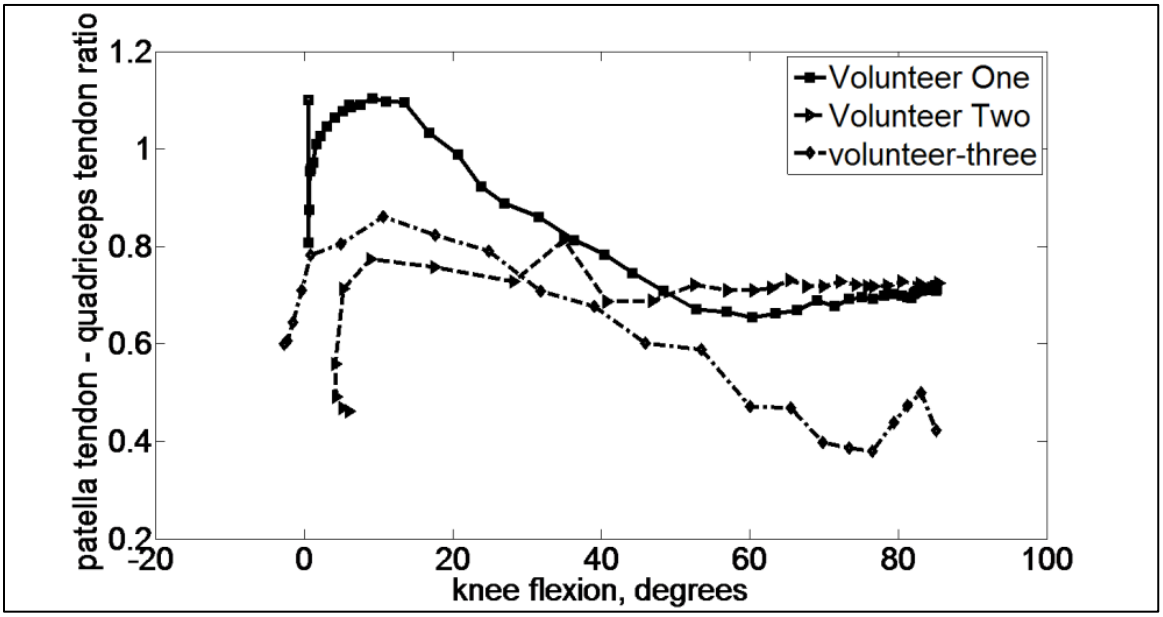

Figure 4.24: Patellar tendon-quadriceps tendon tension ratio as a function of knee flexion.

4.5 Discussion

4.5.1 Baseline model properties

During the CT scans, the extensor mechanisms of the volunteers were relaxed and their hips were rotated inwards to ensure that the trochlear grooves were directed vertically. When the musculoskeletal model was created, the posture was modified to correspond to that of the motion recordings. This caused the initial position and orientation of the patellae as seen in the CT scans to differ from that of the musculoskeletal model.

The inter-volunteer variability in the initial patella positions can be related to the variability in the bisect-offset, vertical ridge position and patellar height (measured in Chapter 3, Table 3.5). Ward *et al.* (2007) measured a bisect-offset of 71.3% [SD = 3.0%] and a mean lateral tilt angle of 15 degrees [SD = 2 degrees] at full extension in a control group (n = 13). The bisect-offsets calculated from the CT scans were smaller than the values obtained by Ward *et al.* (2007), while the tilt values with the exception of values obtained for Volunteer Two were closely related to control group measurements. The former might have been the result of the extensor mechanism not being excited during the CT scan. The small tilt angle measured on Volunteer Two's CT scan might have been the result of the low patella height, which caused the patella to be seated in the trochlear groove at full extension.

4.5.2 Patellofemoral kinematics

The infra-patellar fat pad was not included in the musculoskeletal models. At full extension, the patella will rest on the fat pad, and therefore will not make contact with the femur (with the exception of the trochlear groove). The exclusion of the fat pad in the models resulted in the patellae having no posterior support, which led to direct contact with the femur. This caused initial tilt angles (especially for Volunteer One) to be exaggerated, but as the patellae engaged the trochlear grooves, the patellofemoral posture was similar to the *in-vivo* posture at 30 degrees flexion. The lower accuracy obtained for the tilt angles might have been the result of the exaggerated tilt angles at full extension. The accuracy parameters in Table 4.5 do however prove that the musculoskeletal models are able to provide useful and accurate information on the patella kinematics, especially after trochlear engagement.

There is large variability between results reporting on patella tilt (Katchburian *et al.* (2003)). Two recent *in-vivo* studies measured patella tracking under weight-bearing conditions with a specially designed patella clamp (Wilson *et al.* (2009)) and the other with the aid of MRI image registration techniques (Ward *et al.* (2007)). The former (ten subjects) showed that the patella will tilt medially from full extension to approximately 45 degrees knee flexion, after which it will tilt laterally to 90 degrees knee flexion. The latter (13 subjects) showed that the patella will continue to tilt medially after 45 degrees knee flexion to 60 degrees knee flexion. A recent *in-vitro* (Amis *et al.* (2006)) study (eight subjects) showed that the patella will follow a lateral tilt pattern from full extension to 90 degrees knee flexion. This result was also obtained in a computational modelling study (one subject, Fernandez *et al.* (2008)), as well as the *in-vitro* study described in Appendix A.

Published results on mediolateral patella shift are also conflicting. Katchburian *et al.* (2003) stated that the majority of studies showed the patella to undergo an initial medial shift after which it translated laterally for the remainder of knee flexion. The two *in-vivo* studies reported that the patella will follow a medial shift pattern from full extension to 90 degrees knee flexion (Wilson *et al.* (2009)) and 60 degrees knee flexion (Ward *et al.* (2007)). Amis *et al.* (2006) concurred with the findings of Katchburian *et al.* (2003) while Fernandez *et al.* (2008) reported that the patella will translate laterally as knee flexion increases.

Commenting on the reasons for the variability between the four considered studies is problematic. Katchburian *et al.* (2003) suggested that patella tilt and shift might be both subject-specific and dependent on the chosen reference frame to which the measurements are related. The reference frame utilised in this study is similar to the one used by Ward *et al.* (2007), but different results were obtained. The two *in-vivo* studies and the *in-vitro* study considered patient-specificity, but still managed to obtain results representing a generalised tilt and shift trend for each subject. The variability between those studies and this study therefore might be the result of the inherent characteristics of the applied investigation methods.

In the study of Wilson *et al.* (2009), a specially designed clamp was fixed to the patella by means of an elastic band which would exert compression around the patellofemoral joint. Similarly, a coil would have been fixed around the patellofemoral joint during the MRI scan, also exerting compression on the patellofemoral joint in the study of Ward *et al.* (2007). These additional compressive forces might therefore have influenced the recorded patella tilt and shift measures, and may serve as an explanation for the low correlation between the predicted tilt and measured tilt patterns in this study.

Amis *et al.*, (2006) used a sensor on the patella to record its motion during the *in-vitro* study. The knee was rotated and the sagittal plane was parallel to the horizontal, and knee flexion occurred in the horizontal plane. The added weight to the patella might also have played a role in the measurements.

Fernandez *et al.* (2008) derived the patella position from single-plane fluoroscopy measurements on which a FEA was based. Seisler and Sheehan (2007) reported difficulty in accurately deriving the patella's mediolateral position from fluoroscopy images. The reported medial translation might also be related to the trochlear groove being the reference when the mediolateral translation is measured.

When the anatomy of the patellofemoral joint is considered, the extensor mechanism will induce a lateral component on the patella when excited. This is due to the lateral orientated Q-angle of the quadriceps muscles. The trochlear groove is orientated laterally when viewed from a distal-anterior position, (Figure F.7); when the patella engages the trochlear groove, the trochlear groove centre slants laterally as the patella displaces distally. Amis *et al.* (2005) reported a lateral deviation equal to 16 degrees from the axis of the femoral shaft. It is therefore probable that the patella will displace laterally as the knee flexion angle increases due to the combined effect of the lateral load component and the lateral slanted trochlear groove.

Tibial internal rotation might however also influence patella tracking (Katchburian *et al.* (2003)). As the tibia rotates internally with knee flexion, the tibial tubercle to which the patellar tendon attaches will displace in a medial direction. This will decrease the Q-angle which might pull the patella in a medial direction. When the patella is properly seated in the trochlear groove, tibial rotation will however have a reduced influence on its traction (medial translation, Lee *et al.* (2001)). Seisler and Sheehan (2007) indicated that patella tilt could be related to tibial rotation in only 28% of cases, which might be the reason for Volunteer Two's weak correlation between tilt and tibial rotation, since it was securely seated in the trochlear groove at the start of flexion.

4.5.3 Patellofemoral kinetics

Although the implementation of the Hill-model is advantageous due to its simplicity, it is not an accurate predictor of muscle force. Perreault *et al.* (2003) conducted an investigation into the model's ability to predict

muscle loads that were experimentally measured. The findings showed that a maximum error of 50 % was made at low activation rates, with the error attributed to the model's inability to account for the collaboration between muscle activation and force velocity properties. It is therefore possible that the magnitudes of the muscle loads might have been overestimated, since the seating exercise was performed at slow flexion rates. The accuracy was further influenced by the crude approximations of the activation curves.

The inability to accurately estimate muscle loads was partly overcome by using the predicted muscle loads only as a basis on which different patellofemoral configurations can be compared. The purpose was therefore not to report on the absolute muscle loads that would occur during the *in-vivo* exercise, but rather to obtain the trends when the patellofemoral joint is loaded. Comparison of the patellofemoral posture at 30 degrees knee flexion between MRI measurements and the model prediction does show that the model was able to predict patella kinematics accurately.

The increasing patellofemoral contact load as a function of knee flexion was also observed during other studies (Fernandez *et al.*, (2008); Mesfar and Shirazi-Adl (2005); Powers *et al.* (2006) and Zavatsky *et al.* (2004)). The mediolateral component predicted for Volunteers Two and Three also relate well to the literature (Fernandez *et al.* (2008); Mesfar and Shirazi-Adl (2005); Powers *et al.* (2006) and Zavatsky *et al.* (2004)). The different trend predicted for that of Volunteer One would have been the result of the predisposed lateral bisect-offset and the lateral traction pattern on the lateral trochlear facet.

Comparison of the patellofemoral contact load – quadriceps tendon load ratio to published data revealed similar results to that of Fernandez *et al.* (2008). The mediolateral load components in terms of the percentage of the resultant load components were also similar to the results of Powers *et al.* (2006) who reported a maximum percentage of 30 % at full extension which would diminish to 10 % at 60 degrees knee flexion. The increasing percentage of Volunteer Three resulted from the medialised patella bisect-offset. The patella moved from the medial facet to the lateral facet, which led to the lateral facet enduring greater loads as the knee flexion angle increased. It is evident that the dynamic analysis gives insight into the transient behaviour of the patellofemoral contact loads when the graphs of Figure 4.17 are compared to the results of Fernandez *et al.* (2008, Figure 8.D).

The predicted contact load of Volunteer One was larger than that of Volunteers Two and Three, which might have been induced by the elevated lateral load component and the larger force-velocity relation coefficients. It is unclear what caused the elevated coefficients. A possible explanation might be the knee flexion speed. Except for the initial degrees of knee flexion (<40 degrees), Volunteer One's knee flexion angle changed the fastest. This might have induced elevated lengthening speeds of the extensor muscles, which increased the muscle load and therefore the patellofemoral contact loads.

The diminishing MPFL load as a function of knee flexion concurs with the findings of Bicos *et al.* (2007) who reviewed the anatomy, mechanical function and treatment of the MPFL. The lateral retinaculum load for Volunteer One's patella was closely related to the mediolateral displacement of the patella, while the load remained constant for Volunteers Two and Three's patellae. Feller *et al.* (2007) showed that the patella is able to displace laterally more easily when the lateral retinaculum is removed. This is contradictory to what might be assumed, but Feller *et al.* (2007) reasoned that the lateral retinaculum rather prevented the patella from travelling laterally over the elevated lateral facet. Its mediolateral stability might therefore be secondary to its role in providing anterior-posterior stability. The patella did not only displace medially, but also anteriorly during early flexion, which might serve as an explanation for the elevated lateral retinaculum load.

The oscillations in the reported loads might have been induced by the rigidity of the patella and femur. The contacting surfaces were not enabled to deform, and this had a negative impact on the conformity of the patellofemoral joint. The lateral soft tissue stabiliser load components exerted on Volunteers One and Three's patellae served as an indication that the resultant contact was on the lateral facets of the patella and trochlear groove. The oscillating mediolateral component on Volunteer Two's patella suggests that the patella was tracking in the centre of the trochlear groove, and that the contact resultant was therefore shared between the medial and lateral facets as the knee flexed. For both Volunteers One and Two's patellae, the proximal-distal component was directed in the proximal direction, which suggested that the patellar tendon load needed to balance an increased quadriceps load component. An improved load balance existed between the quadriceps and patellar tendon of Volunteer Three.

It is difficult to determine the reason for the variability between the orientations of the stabiliser loads. It might be dependent on the trochlear groove geometry, the conformity between the patella and trochlear groove, the patella tracking path and the attachment locations of the supporting soft tissue stabilisers. The patella and trochlear groove geometries differed between the three volunteers, which had an effect on the conformities of the patellofemoral joints (Figure F.1, Figure F.3 and Figure F.5). The patella tracking patterns differed and volunteer-specificity were implemented in the placement of the attachment sites as far as possible. Therefore, it is fair to suspect that the biomechanical trends between the volunteers will not necessarily match.

Chapter 5

5. Finite element analysis

5.1 Introduction

Chapter 4 described the measurements obtained from the musculoskeletal models to potentially quantify patellofemoral function. This information can be applied to perform a finite element analysis (FEA) of the joint to calculate the resulting contact pressures during articulation. It is not sufficient to only consider the magnitude of the patellofemoral contact loads, since changes in patella articulation might change the contact area. These changes in contact area will result in alterations in the patellofemoral contact pressure, and an increased contact pressure might indicate a possible risk for the onset of osteoarthritis.

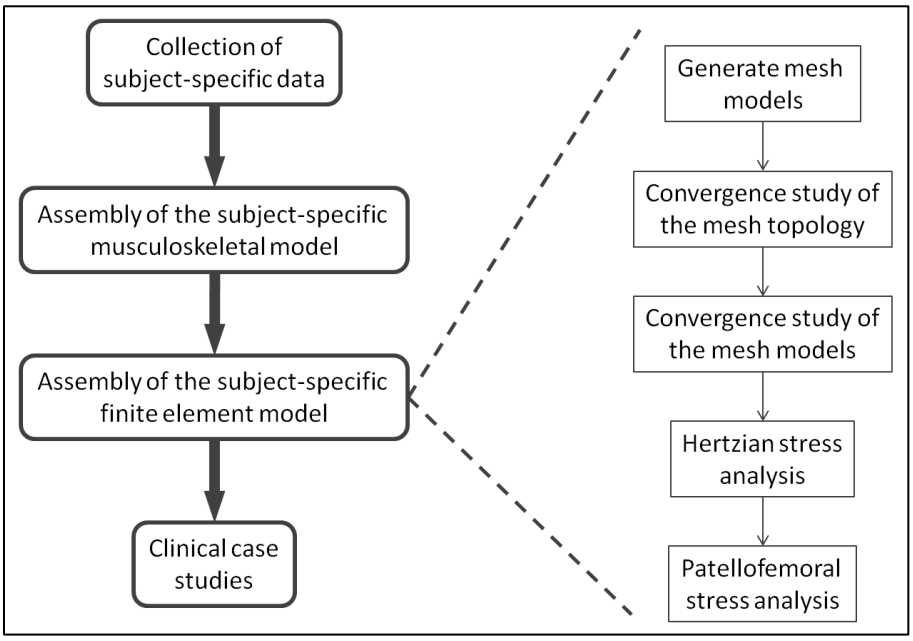

Figure 5.1: Study flowchart (IV).

The approach followed during assembly of a typical finite element model to analyse patellofemoral pressure is described and illustrated for one case (Figure 5.1). The accuracy of the element topology used in the finite element meshes is quantified through two Hertzian contact simulations, after which a spatial convergence analysis is performed for both the Hertzian and the test case. The presented approach is applied in Section 6.1 to evaluate the effect of a tubercle osteotomy procedure on patellofemoral pressure at five discrete knee flexion angles.

5.2 Finite element model setup

5.2.1 Analysis software and hardware

The FE analyses were conducted on the high performance cluster (HPC) at Stellenbosch University. The Rhasatsha Cluster consists of 168 cores, each having access to 2 GB random access memory. A job is sent to the head node, after which it is distributed to the amount of cores as specified by the user. Pre- and post-processing (on PC) was done on MSC Patran 2008r1 (MSC Software Corporation, Santa Ana, California) and MSC Mentat 2007r1 (MSC Software Corporation, Santa Ana, California), while processing (on HPC) was done in MSC Marc 2008r1 (MSC Software Corporation, Santa Ana, California).

5.2.2 Hertzian contact analysis

Hertzian contact analyses were performed to evaluate the accuracy of the chosen mesh topology and the analysis. The contact was simulated between two flat surfaces (Figure 5.2, Case One with E = 15 MPa and ν = 0.45 and Figure 5.3) and between two spheres (Figure 5.4, Case Two with E = 15 MPa and ν = 0.45 and Figure 5.5), resulting from an externally applied 100 N compression load. Two mesh topologies (eight node brick elements (brick-8) and 20 node brick elements (brick-20) (Figure 5.6)) were compared to one another on the basis of the maximum predicted pressure, as well as the accuracy of the pressure magnitude in terms of the analytical solutions of Cases One and Two.

The cube and the plate were generated with the pre-processor geometry toolbox. The hexahedral automesher provided in the mesh toolbox was used to generate the two mesh sets of the FE model (Table 5.1). In Case One the resulting pressure was considered to be uniformly distributed, a valid assumption since the loading condition satisfies the following requirements (Budynas and Nisbett (2008, pp. 84)):

- the line of action of the force is contained in the centroid of the section; and
- the pressure is sampled in the centre of the contacting area, away from the edges of the block.

Case One therefore depicts a pure compression condition, and the resulting pressure is equal to the compression force F, divided by the contact area A (Eq. 5.1, Budynas and Nisbett (2008, pp. 84)):

$$\sigma = \frac{F}{A} \qquad \text{Eq. 5.1}$$

In Case Two, a Hertzian contact results since each body has a curvature. These contact situations can be addressed with the aid of two assumptions, as presented by Boresi and Schmidt (2003, pp. 591 - 592):

- each body should comprise of a homogenous, isotropic material with elasticity properties in accordance with Hooke's law; and
- a common tangent plane to the contacting surfaces of the two bodies should exist near the point of contact.

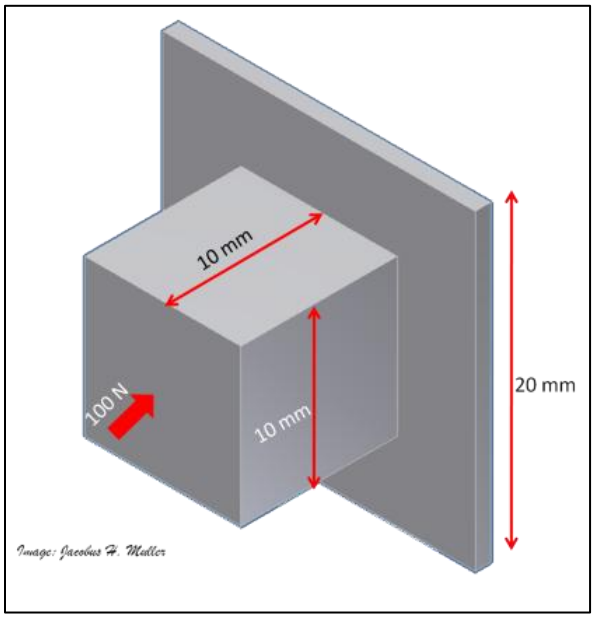

Figure 5.2: Cube in contact with the plane.

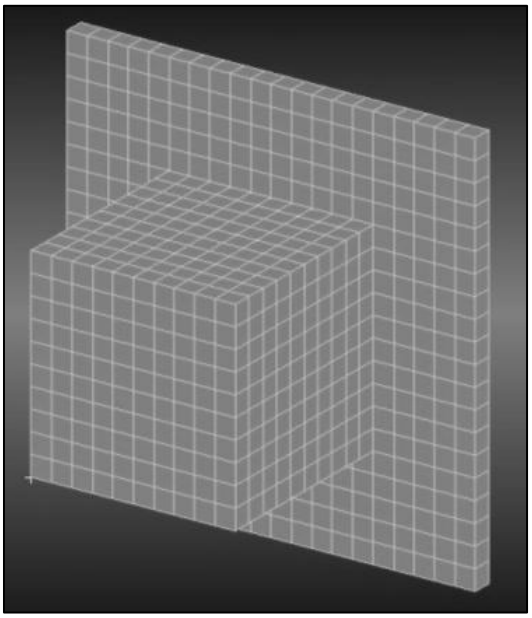

Figure 5.3: Cube and plane mesh (# nodes: 7 964 / # elements: 1 400).

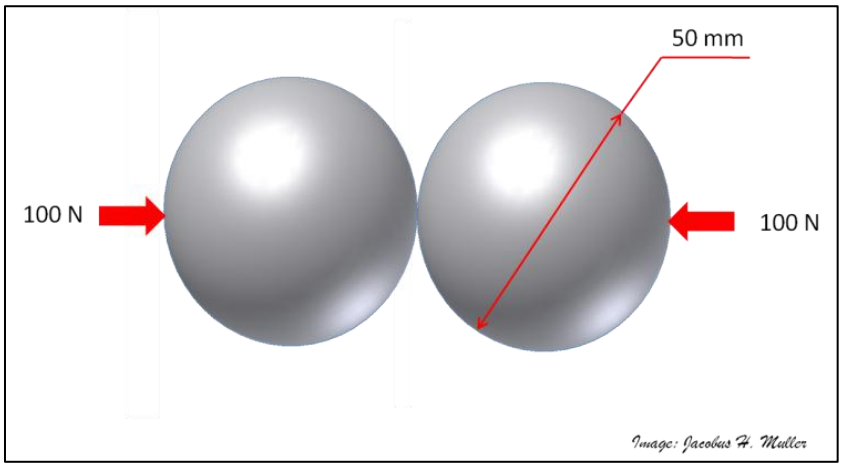

Figure 5.4: Two spheres in contact.

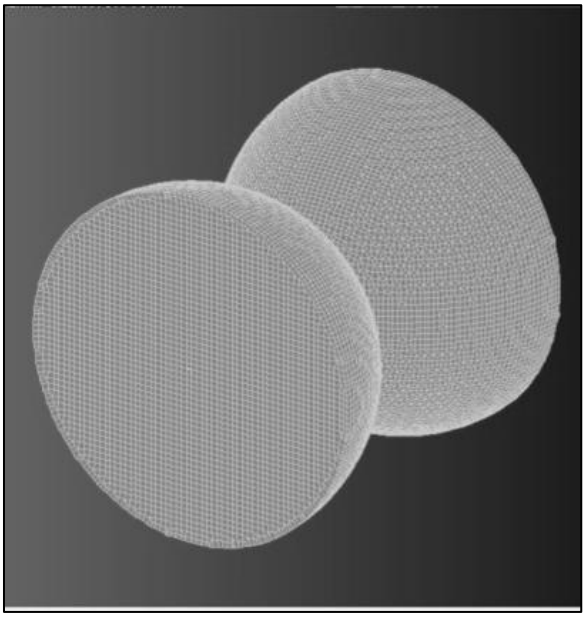

Figure 5.5: Spheres mesh (# nodes: 137 907 / # elements: 126 266).

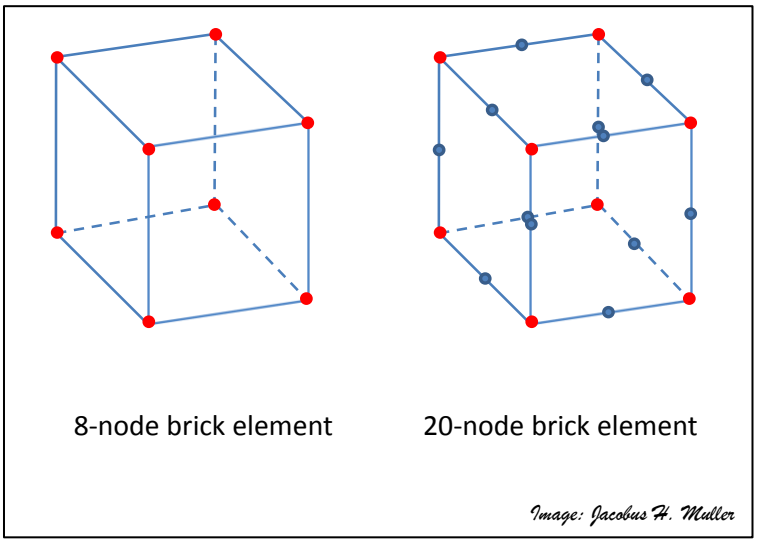

Figure 5.6: Element topologies evaluated during the Hertzian contact analysis.

Table 5.1: Finite element model mesh topologies for Cases One and Two.

Model	Edge length, millimetres	# nodes	# elements
	Case One		
Brick-8	1.0	2 213	1 400
	0.5	14 304	11 200
	0.25	101 726	89 600
Brick-20	1.0	7 964	1 400
	0.5	53 966	11 200
	0.25	394 490	89 600
	Case Two		
Brick-8	1.0	137 907	126 266

The latter condition is needed to calculate the deformation resulting from the contact. Distances between corresponding points on the two bodies, whose line of contact is perpendicular to the tangent plane, are used in

the derivation of the area of contact and its shape. The maximum pressure resulting when two spheres are pressed together can be computed with Eq. 5.2 (Budynas and Nisbett (2008, pp. 117)), which is a simplified version of the derivation of Boresi and Schmidt (2003, pp. 592 - 598). The mesh topologies consisted of brick-8 elements having a maximum edge length of one millimetre (Table 5.1). The edge lengths could not be reduced further due to computer memory limitation restrictions.

$$\sigma_{max} = \frac{3F}{2\pi a^2} \qquad \text{Eq. 5.2}$$

$$a = \sqrt[3]{\frac{3F}{8}\frac{d(1-\nu)}{E}} \qquad \text{Eq. 5.3}$$

The two spheres (Figure 5.4) are pressed together with a force F, having a diameter d, an elastic modulus E, and a Poisson ratio ν. The radius a of the circular contact area is calculated from Eq. 5.3 (Budynas and Nisbett (2008, pp 117)).

5.2.3 Patellofemoral joint pressure prediction

The instantaneous patellofemoral posture at a specific flexion angle, as well as the soft tissue stabiliser tensions predicted with the musculoskeletal models, were used to assemble a finite element model. Volume meshes were created from the three dimensional CAD models of the distal femur and its cartilage, as well as the patella and its cartilage. The meshes consisted of eight node brick elements (Figure 5.7) that were produced in MSC Mentat 2007r1 (MSC Software Corporation, Santa Ana, California)[‡‡‡]. The eight node brick elements have been used in numerous FEA studies on the patellofemoral joint (Fernandez *et al.* (2008); Mesfar and Shirazi-Adl (2005); Mesfar and Shirazi-Adl (2006); Shirazi-Adl and Mesfar (2007); Laz *et al.* (2006) and Rawlison *et al.* (2006))[§§§]. The model of Volunteer One consisted of 670 509 nodes and 502 500 elements. From the discussion on the FE technique in Section 2.3.3, it follows that the pressures produced by a static analysis might be different to the transient pressures that occur during a dynamic analysis. It has also been shown in Chapter 4 that the patellofemoral posture at dynamic equilibrium is different to the posture at static equilibrium.

[‡‡‡] The complete meshes with illustrations of the boundary conditions are presented in Appendix I.

[§§§] Other elements that have been used in past studies include rigid surface elements (Laz *et al.* (2006) and Rawlison. *et al.* (2006)) and tetrahedral elements (Au *et al.* (2005)).

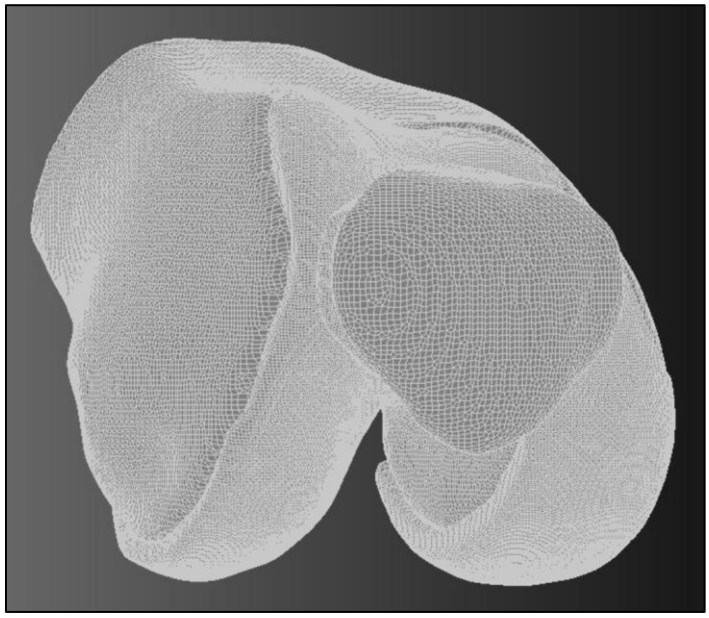

Figure 5.7: Patellofemoral joint consisting of eight node brick elements (# nodes: 670 509 / # elements: 520 500).

Steps have been taken to improve the validity of the static analyses. These steps included the preservation of the dynamic patellofemoral posture and the soft tissue load configuration obtained from the dynamic analyses. The relative position and orientation of the patellofemoral joint remained intact: the femur and patella's degrees of freedom (DOF) were constrained, with the patella allowed to translate only along the resultant loading direction, whereas the femur was held in place. This limited relative movement and preserved the dynamic patellofemoral posture.

The soft tissue tensions (patellar tendon, MPFL, lateral retinaculum and quadriceps tension (three load vectors)) were implemented as assigned vectors to the corresponding nodes on the patella. In order to reproduce the instantaneous loading condition of the dynamic analysis, the landmarks of the patellofemoral soft tissues needed to relate to that of the dynamic analysis. This was achieved by using spheres (one millimetre in diameter) indicating the implant locations in both the FE model and the musculoskeletal model. The force vectors were applied to a surface node in the closest proximity of the sphere.

The cartilage and skeletal bone were modelled as two separate entities, each having elastic isotropic material properties (Table 5.2). This approach is similar to that of previous studies of Fernandez *et al.* (2008), Mesfar and Shirazi-Adl (2005, 2006) and Shirazi-Adl and Mesfar (2007). According to Fernandez *et al.* (2008), a simplified isotropic cartilage material model will suffice if the duration of load application during the analysis is short. As soon as the analysis time exceeds two seconds, the fluid contents of the cartilage will influence its behaviour. It is difficult to obtain a value for the elastic modulus of cartilage from literature, since different values have been used. Elias *et al.* (2004) used a value of 4 MPa, while Mesfar and Shirazi-Adl (2006, 2005) and Shirazi-Adl and

Mesfar (2007) used a value of 15 MPa. Fernandez *et al.* (2008) used a value of 40 MPa. The value chosen for this study was 15 MPa, since this range was used in a study published in a clinical journal.

Table 5.2: Material properties of the skeletal bone and cartilage.

	Elastic modulus, MPa	Poisson ratio	Source
Bone	17 000	0.19	Guo (2001)
Cartilage	15	0.45	Shirazi-Adl and Mesfar (2007)

Since the bone and cartilage were modelled as separate entities, a multipoint constraint (MPC) needed to be created between the cartilage and bone surface elements. This entailed the specification of an independent node on the native bone volume mesh, with a set of dependent surface nodes on the native cartilage volume mesh. The relative position and orientation of the dependent nodes were coupled to that of the independent node by using a rigid MPC definition. The cartilage surface was therefore "fixed" to the bone surface.

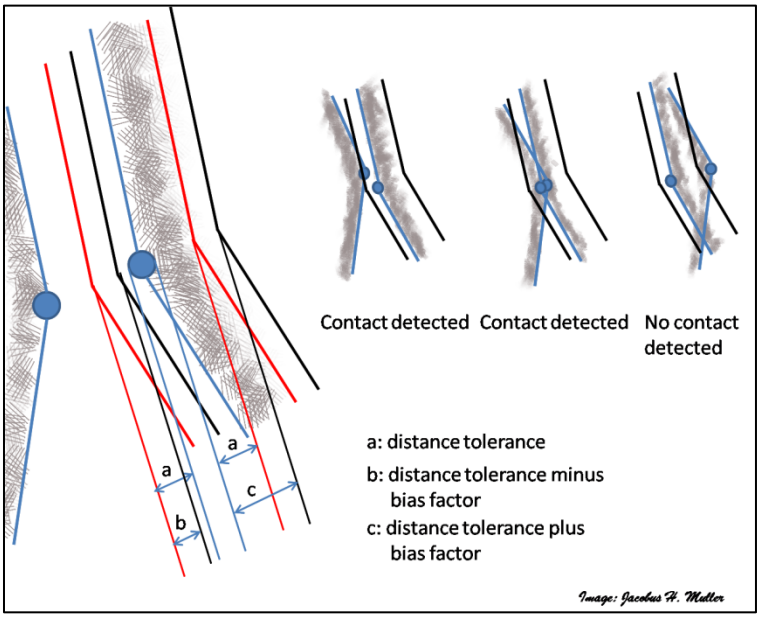

Figure 5.8: Contact detection with the distance tolerance and bias factor.

The contact between the femoral and the patellar cartilages was modelled by the "touching-body" function. Contact was determined by defining a distance tolerance and bias factor. When the distance (adjusted by the bias factor) between the nodes of Body One and Body Two was within the distance tolerance on either side of Body Two, the nodes were considered to be in contact (Figure 5.8). This resulted in a discrete contact which depended on the nodes. To improve on this, coons surface patches (Daintith (2004)) were fitted through the nodes of the contacting surfaces, allowing improved definition of the curved surfaces of the patellofemoral joint.

A sensitivity analysis of the distance tolerance's influence on the predicted pressure was performed with the finite element model of Volunteer One. The analysis was repeated for different distance tolerance values, while

its influence on the maximum pressure was noted. The FE models of Volunteers One and Two were also used to perform a spatial convergence study on the volume meshes. When the analyses were repeated with elements twice as small, it resulted in elements having a maximum edge length of 0.5 millimetres. If the maximum pressure was within ten percent of the maximum pressure value obtained with the previous mesh, the mesh was considered to be sufficiently fine for this analysis. The relative position of contact between the patella and trochlear groove was compared to the images obtained with the MRI scans when Volunteers One and Two exerted an isometric quadriceps contraction at 30 degrees flexion (Appendix A).

5.3 Results

5.3.1 Hertzian contact analysis

The spatial convergence study for Case One indicates that the results with the brick-8 elements with a maximum edge length of one millimetre produced an outcome closest to the analytical solution (2 % difference, Table 5.3). Convergence was best for the brick-20 elements, whereas the difference in terms of the analytical solution was greatest. A 4.51 % difference occurred between the maximum pressure prediction and the analytic maximum pressure value for Case Two (Table 5.4). When the model was setup with brick-20 elements, convergence could not be attained.

Table 5.3: Spatial convergence measurements for Case One.

Topology	Edge length, mm	Analysis time, seconds	Maximum Pressure, MPa	Convergence	% Difference
Brick-8	1.0	4.41	1.02		2.0 %
	0.5	52.28	1.16	13.7 %	16.0 %
	0.25	744.00	1.09	6.0 %	9.0 %
Brick-20	1.0	55.18	1.12		12.0 %
	0.5	491.77	1.25	11.6 %	25.0 %
	0.25	6667.79	1.19	5.0 %	19.0 %

Table 5.4: Comparison of the Hertzian contact results to the analytical solution of Case Two.

	Maximum pressure, MPa
Brick-8	2.32
Analytical solution	2.22
Error %	4.51 %

5.3.2 Patellofemoral pressure prediction

Variability was noted between the patellofemoral pressures derived for Volunteers One and Two (Table 5.5). As a result, the mean pressure distributions differed for the two volunteers, with Volunteer One enduring a mean pressure of 2.29 MPa (SD = 2.22) and Volunteer Two a mean pressure of 0.66 MPa (SD = 0.60). The distance

tolerance had a maximum influence of 2.3% on the contact pressure predictions of Volunteer One (Table 5.6). The contact area locations in the FE models were different to the locations seen on the MRI scans (Figure 5.9), while there was some agreement between the MRI and FEA results of the contact location on Volunteers One and Two's trochlear grooves. The contact locations on the patellae of Volunteers One and Two were more proximal and lateral on the MRI than what was predicted by the FEA. The predicted maximum pressure did not change by more than 2.08 % (Volunteer Two) when the mesh topology was refined (Table 5.7).

Table 5.5: Patellofemoral pressure at 30 degrees flexion.

	Maximum pressure, MPa [SD]		Mean pressure, MPa [SD]		
	Trochlear groove	Patella	Trochlear groove	Patella	Mean
Volunteer One	11.2	13.0	2.00 [2.23]	2.57 [2.21]	2.29 [2.22]
Volunteer Two	2.89	2.73	0.58 [0.60]	0.73 [0.60]	0.66 [0.60]

Table 5.6: Sensitivity of the mean pressure (MPa) as a function of the distance tolerance.

	0.1 millimetres	0.05 millimetres	0.01 millimetres	Percentage difference
Trochlear groove	2.57	2.52	2.51	2.3 %
Patella	2.29	2.27	2.28	0.9%

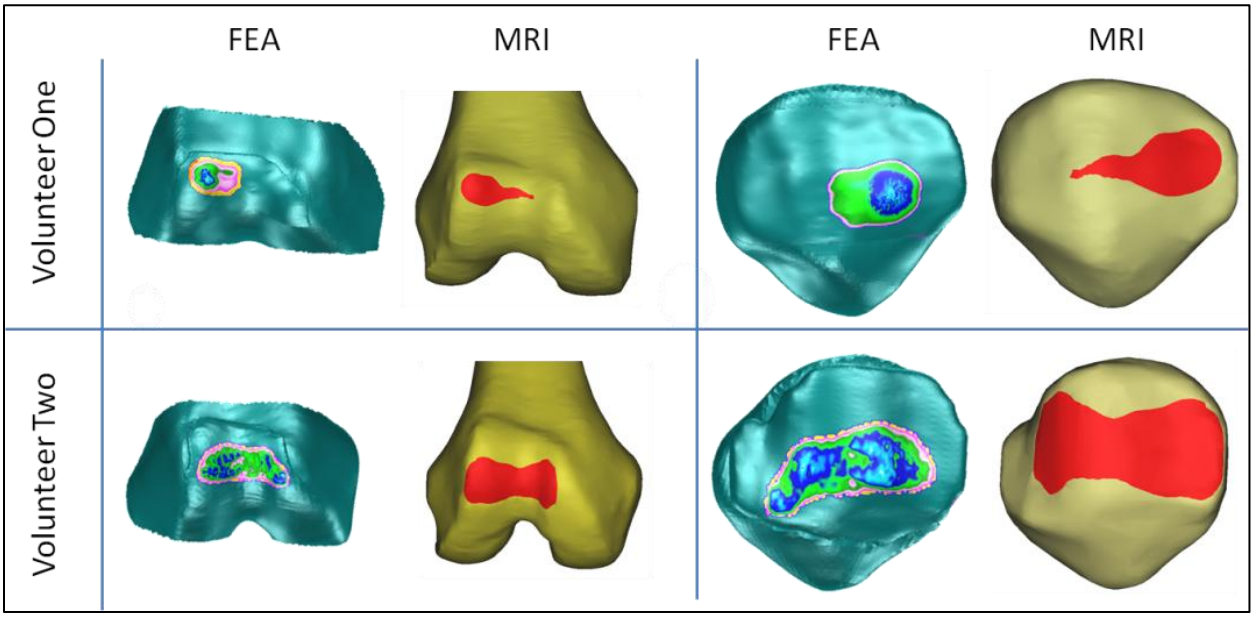

Figure 5.9: Comparison of MRI and FEA contact areas.

Table 5.7: Spatial convergence of the mesh topology.

	Volunteer One		Volunteer Two	
	1 millimetres	0.5 millimetres	1 millimetres	0.5 millimetres
Number of elements[****]	242 718	531 583	83 280	650 931
Number of nodes	287 527	600 466	116 029	787 395
Maximum pressure, MPa	6.66	7.17	2.89	2.95
% difference	7.66 %		2.08 %	

5.4 Discussion

5.4.2 Hertzian contact analysis

It was expected that the brick-20 elements used during the analysis of Case One would produce a better spatial convergence $\left(\frac{previous\ result\ (element\ edge = a\ mm)}{current\ result\ (element\ edge = b\ mm)}, a > b\right)$ than the brick-8 elements. The former is therefore ideal since spatial convergence will be attained faster. When the model of Case Two was assembled with brick-20 elements, the model would not converge on a solution; irrespective of the contact tolerance or the element size (possible reasons are discussed in the next paragraphs). This was unfortunate since the brick-20 elements in theory would suit the contact analysis on the patellofemoral joint best because of the improved spatial convergence rate.

There were limitations imposed on the FEA. Firstly, due to the geometrical appearance of the models in Case Two, and the patellofemoral joints, the hexahedral mesher of Patran failed since the geometries were not tri-parametric. The Mentat pre-processor was able to construct hexahedral elements by means of a grid based method, but the boundary elements were of poor quality because they were not aligned with the elements in the volume. During a contact analysis, the extent of cartilage deformation would cause a reduced quality of the elements, which in turn often resulted in the solver being unable to achieve stress recovery, or elements penetrating one another. This phenomenon was further enhanced when parabolic elements such as the brick-20 elements were used. One remedy for this would be to employ re-meshing strategies during the analysis, but this could unfortunately not be implemented successfully, due to constant failure of the mesher. After consultation with the software support team, they suggested that the re-meshing module should only be used on TET-4 elements.

Another problem might be the way in which the algorithm searches for contact during the analysis. Some of the models would not converge if the incorrect combination of the distance tolerance and bias factor was chosen. When the brick-20 elements were implemented in Case Two, the models would not converge for the same set of

[****] Relates to the number of elements and nodes of the cartilage volume meshes.

boundary and initial values, even after the mid-side nodes' degrees of freedom were frozen and different combinations of distance tolerance and bias factors were tested. This indicates a problem with the contact algorithm when brick-20 elements are used in combination with curved contact geometries. This same condition occurred with other parabolic elements such as ten node tetrahedral elements (Tet-10).

Although the contact analyses were performed with brick-8 elements, the results show that an acceptable level of accuracy and convergence could be attained. Since the aim was to use the FEA to compare pressures resulting from different soft tissue configurations, the accuracy in terms of the absolute pressure was of secondary importance to the repeatability of the chosen mesh topologies. The convergence analyses for both Cases One and Two, as well as the patellofemoral analyses showed that the meshes would provide repeatable results. It was therefore possible to indicate with certainty if the pressure would be increased or relieved for different loading conditions.

5.4.2 Patellofemoral pressure prediction

The elevated patellofemoral pressure of Volunteer One is expected, since the patella articulated on the lateral facet of the trochlear groove, resulting in a reduced contact area. There was good correlation between the pressures at 30 degrees knee flexion measured during the *in-vitro* analysis (Appendix A) and the mean pressure computed for Volunteers One and Two. The maximum pressures also relate well to the findings of Fernandez *et al.* (2008), who reported peak pressures ranging between 5 MPa and 10 MPa for a stair ascending exercise, and Elias *et al.* (2004) who reported peak pressures between 3.6 MPa and 4.4 MPa for a loading exercise on a cadaver test rig. Both these studies were conducted on knees exhibiting distributed loads on both facets of the trochlear grooves.

The difference between the simulated FE contact area and the MRI measurements may have resulted from the influence of the coil used during the MRI. The MRI measurements further pertain to a static loading condition, which will be different to the simulated loading condition. A correlation exists between the proximal-distal locations of the FE and MRI contact, as well as with the findings of other studies at small flexion angles (Elias *et al.* (2004); Fernandez *et al.* (2008).

Although the volume meshes consisted of brick-8 elements, a convergence study showed the mesh sizes to be suitable. These volume meshes have been applied in Section 6.1 to compare the relative peak and mean pressures that would occur before and after a tubercle osteotomy in the coronal plane at different degrees of flexion. The technique would therefore produce results that can be compared objectively, since the boundary conditions would remain the same with only the initial conditions changing due to the varying degrees of flexion and the tubercle position.

Chapter 6

6. Clinical case studies

The use of the musculoskeletal models in the investigation of patellofemoral disorders and treatment techniques will be demonstrated by two case studies in Chapter 6 (Figure 6.1). In Section 6.1 the effect of a tibial tubercle osteotomy on subject-specific patellofemoral kinematics and kinetics will be illustrated. The musculoskeletal model results were combined with the findings of finite element analyses to evaluate the effect of an osteotomy on patellofemoral kinematics, kinetics and contact pressure. Section 6.2 will evaluate the capability to reproduce subject-specific patellofemoral kinematics and kinetics by two commercial patellofemoral prostheses. The differences for a particular volunteer between Prostheses One, Two and the native joint were quantified on the basis of joint kinematics and kinetics. The information may help an orthopaedic surgeon to choose which one of the two prostheses will reproduce the patellofemoral joint biomechanics best.

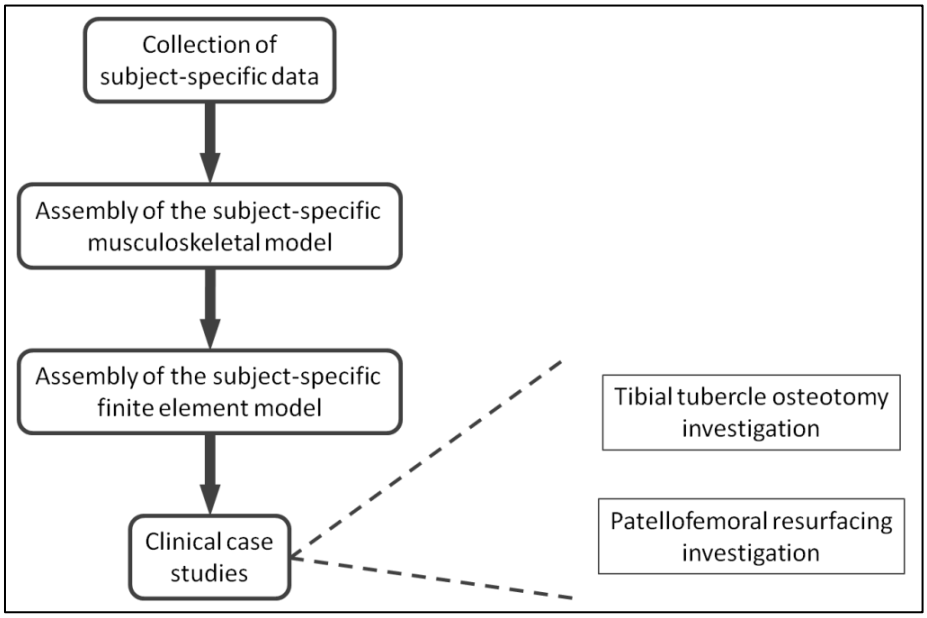

Figure 6.1: Study flowchart (V).

6.1 Tibial tubercle osteotomy

6.1.1 Background

Tibial tubercle osteotomies have received much attention regarding their ability to relieve patellofemoral pain (Fulkerson *et al.* (1990)), relieve excessive patellofemoral contact pressure (Benvenutti *et al.* (1997); Cameron *et al.* (1986); Cox (1982); Fulkerson (1983); Elias *et al.* (2004); Ramappa *et al.* (2006)), correct abnormal Q-angles

(Kuroda *et al.* (2001)), improve abnormal patellar tracking (Benvenutti *et al.* (1997); Cameron *et al.* (1986); Chrisman *et al.* (1979); Cosgarea *et al.* (1999); Cox (1982); Farahmand *et al.* (1998); Fulkerson (1983); Kuroda *et al.* (2001); Ramappa *et al.* (2006)), and correct an abnormally lateral positioned tibial tubercle (Koëter *et al.* (2007)). Five tubercle transfer techniques have been described:

- the flat osteotomy or Elmslie-Trillat procedure (Äärimaa *et al.* (2008); Cosgarea *et al.* (1999); Cox (1982); Fulkerson *et al.* (1990); Riegler (1988); Shelbourne *et al.* (1994));
- the oblique osteotomy (Cosgarea *et al.* (1999));
- the Maquet procedure or Fulkerson procedure (Cosgarea *et al.* (1999); Fulkerson *et al.* (1990); Fulkerson (1983));
- the Roux-Goldthwait procedure (Äärimaa *et al.* (2008); Chrisman *et al.* (1979); Cox (1982)); and
- the Hauser procedure (Chrisman *et al.* (1979)).

A tubercle osteotomy in the coronal plane entails medialisation of the tibial tubercle, whereas it is also anteriolised during an oblique osteotomy or distalised during the Hauser procedure. During the Roux-Goldthwait procedure, the distal attachment of the lateral patellar tendon half is released and re-implanted posteriorly to the medial half of the patellar tendon. The outcomes of these techniques are measured against the alteration in patellar traction (Ramappa *et al.* (2006)), the alteration in patellofemoral contact pressure (Benvenutti *et al.* (1997); Fulkerson *et al.* (1990); Kuroda *et al.* (2001); Ramappa *et al.* (2006)), the improvement or deterioration of clinical measurements (Äärimaa *et al.* (2008); Koëter *et al.* (2007)) or patient comfort in terms of pain relief (Äärimaa *et al.* (2008); Fulkerson *et al.* (1990); Koëter *et al.* (2007)).

Patients are evaluated frequently postoperatively according to an evaluation grid to determine the success rate of an osteotomy (Äärimaa *et al.* (2008); Cameron *et al.* (1986); Chrisman *et al.* (1979); Cox (1982); Fulkerson *et al.* (1990); Fulkerson (1983); Koëter *et al.* (2007) and Riegler (1988)). The advantage of this is the longer evaluation periods available to measure the effects of the procedure on the patellofemoral joint, but the success of the procedure can only be determined after completion. Äärimaa *et al.* (2008) showed that the patients in their study were pleased with the results of the procedures (pain was relieved and dislocations and subluxation did not occur), but the chances for the development of osteoarthritis increased due to shortening of the patellar tendon. Cox (1982) reported that only 66% of the procedures performed in their study were rated good to excellent.

In-vitro models (Fulkerson *et al.* (1990); Kuroda *et al.* (2001); Ramappa *et al.* (2006)) have been used to examine the effect of tibial tubercle medialisation on patellofemoral and tibiofemoral contact pressure as a function of passive muscle excitation. The cadaver legs used in the *in-vitro* studies did not display abnormal Q-angles and deficiency was either induced (Kuroda *et al.* (2001); Ramappa *et al.* (2006)) or the influence of the

procedure was measured on a normal knee (Fulkerson *et al.* (1990)). A drawback of the *in-vitro* investigative technique is its incapability to simulate active muscle function (Kuroda *et al.* (2001)), and the vastus lateralis and vastus medialis are frequently sacrificed while only the quadriceps tendon is loaded (Fulkerson *et al.* (1990); Ramappa *et al.* (2006)). Other studies were able to simulate patella kinematics as a function of approximated active muscle activation (Ostermeier *et al.* (2007); Withrow *et al.* (2006); Yoo *et al.* (2004)), but no *in-vitro* studies have been published that investigated the effect of tibial tubercle transfer on patellofemoral biomechanics as a function of active muscle load. Another drawback was the mean age of the specimens available for *in-vitro* studies, since the specimens were usually from old donors whose knees might present other pathologies, such as osteoarthritis (Yamada *et al.* (2007)).

Elias *et al.* (2004) calculated patellofemoral contact pressure at various knee flexion angles as a function of the Q-angle by means of a discrete element method. The computational model input values were obtained from *in-vitro* test results. The analyses did not exceed a knee flexion angle of 70 degrees due to the inability to go beyond 70 degrees during the *in-vitro* test. To measure the patellofemoral forces *in-vitro*, it was necessary to remove the medial and lateral retinacula top quarters to insert the pressure sensor. As a result, these soft tissues were also not included in the discrete element model. The patella's position relative to the femur was based on an algorithm which did not compensate for patella shift or tilt.

The challenge remains to objectively evaluate the outcomes from a tubercle osteotomy, with the goal of predicting the success of the procedure before it is performed. The aim of this study was to utilise the subject-specific computational models of Volunteers One and Two to illustrate the effect of tibial tubercle medialisation on the patellofemoral joint. Volunteer One had a minor case of patella dysplasia and reported anterior knee pain as the knee was flexed during a one-leg squat. Volunteer Two presented with no pain, but had a mild case of patella infera. Volunteer Three was not considered for this study since his patella had a medial offset. The effect of a tubercle osteotomy in the coronal plane on patellofemoral biomechanics was quantified by measuring the effect on medial patellofemoral ligament tension, mediolateral patellofemoral load component, mediolateral patella tilt and shift, and patellofemoral pressure distribution.

6.1.2 Methods

The tubercles in the baseline musculoskeletal models were moved ten millimetres medially from their native positions in the coronal plane by moving the distal attachments of the three patellar tendon elements (Figure 6.2). Before the dynamic simulations presented in Chapter 4 were repeated, the models were allowed to reach a new state of equilibrium to nullify the transient effects that might have resulted from the new tissue

configuration. Finite element models were assembled at 30, 45, 60, 75 and 90 degrees[††††] for both the medialised and the neutral tibial tubercles using the methodology presented in Chapter 5.

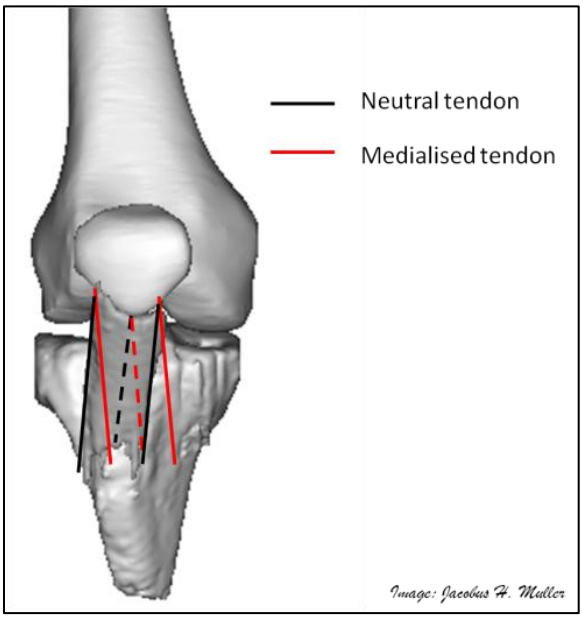

Figure 6.2: Medialisation of the distal patellar tendon attachment.

6.1.3 Results

6.1.3.1 Patellofemoral kinematics

Tubercle medialisation caused Volunteer One's patella to engage the trochlear groove at an earlier knee flexion angle, but the effect of the medialised tubercle on the mediolateral shift was negligible after trochlear groove engagement (Figure 6.3). The patella maintained its laterally tilted orientation, but the mediolateral tilt angles remained more stable after the tubercle was medialised (Figure 6.4). Volunteer Two's patella experienced a medial offset relative to its position in the baseline model after the tibial tubercle was medialised (Figure 6.5). The tilt pattern changed from a medial tilt during early knee flexion to a lateral tilt, although the patella maintained an overall laterally tilted orientation (Figure 6.6).

[††††] The maximum knee flexion angle achieved with the computational model.

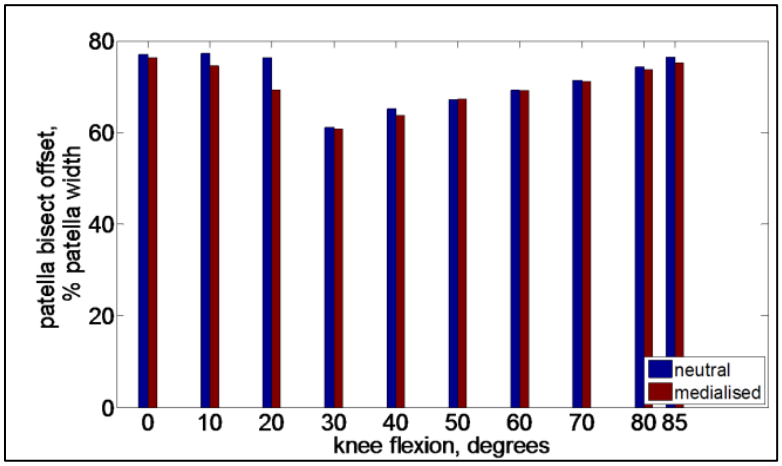

Figure 6.3: Patella bisect offset of Volunteer One before and after the osteotomy (-: medial / +: lateral).

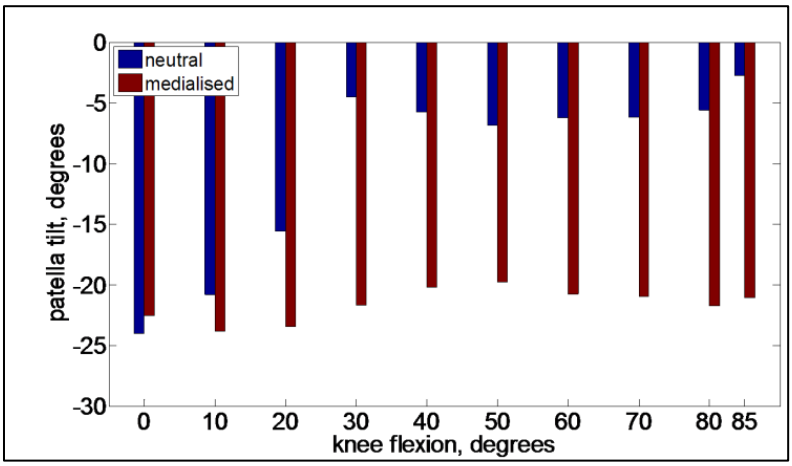

Figure 6.4: Patella tilt of Volunteer One before and after the osteotomy (+: medial / -: lateral).

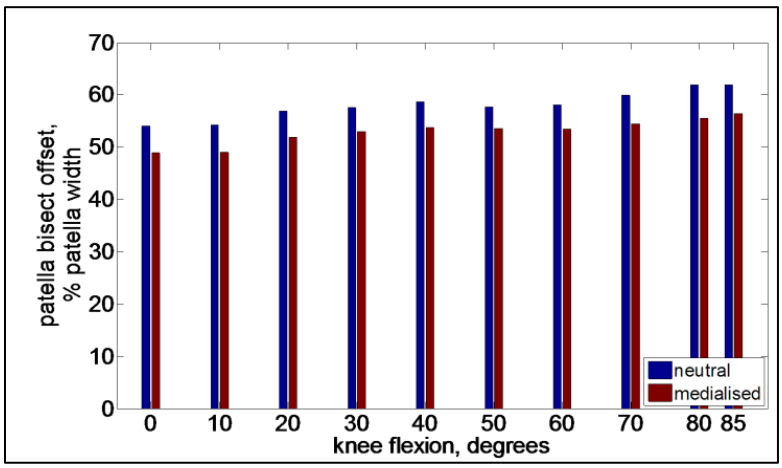

Figure 6.5: Patella bisect offset of Volunteer Two before and after the osteotomy (-: medial / +: lateral)

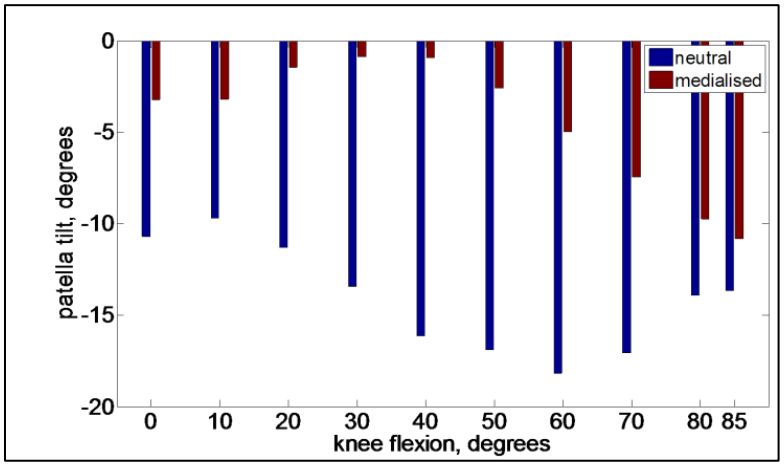

Figure 6.6: Patella tilt of Volunteer Two before and after the osteotomy (+: medial / -: lateral).

6.1.3.2 Patellofemoral kinetics

The tension in Volunteer One's MPFL was relieved (a maximum of 80 % at ten degrees knee flexion) prior to trochlear engagement when the tubercle was medialised (Figure 6.7). The MPFL tensions remained similar between the neutral and medialised configuration after the patella engaged the trochlear groove. Tubercle medialisation had a negligible effect on Volunteer Two's MPFL tension (Figure 6.8). There was a negligible change in both Volunteers One (Figure 6.9) and Two's (Figure 6.10) lateral retinaculum load after tubercle medialisation, with the exception of a 50 % elevated tension at 20 degrees knee flexion in Volunteer One's lateral retinaculum. The tension in both the patellar tendon and quadriceps tendon diminished when Volunteer One's tubercle was medialised (Figure 6.11 and Figure 6.13). The tension in Volunteer Two's patellar tendon increased in particular after trochlear engagement when the tubercle was medialised (Figure 6.12), whereas the quadriceps tendon tension remained the same (Figure 6.14).

The medialisation of Volunteer One's tubercle caused a decrease in soft tissue tensions and resulted in a smaller patellofemoral contact load (Figure 6.15). The resultant mediolateral contact load component on the lateral patella and trochlear groove facet was reduced, and changed its orientation towards the medial facet at 70 degrees knee flexion. The contact load on Volunteer Two's patellofemoral joint did not change when the tubercle was medialised (Figure 6.16), whereas the mediolateral load component was changed as follows (Figure 6.18): the resultant load was exerted in a medial direction during early knee flexion (knee flexion < 30 degrees), and elevated after 30 degrees knee flexion. The mediolateral load component during the neutral configuration was negligible from 50 degrees knee flexion onwards.

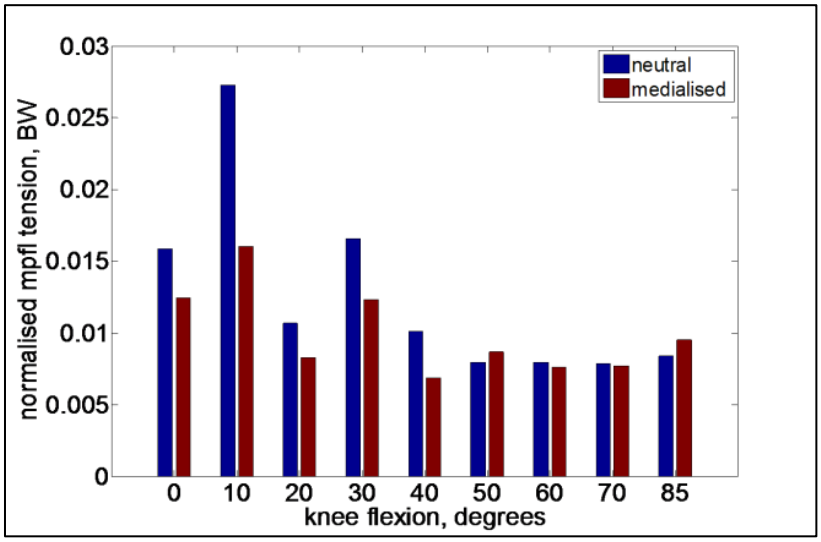

Figure 6.7: MPFL tension before and after the osteotomy (Volunteer One).

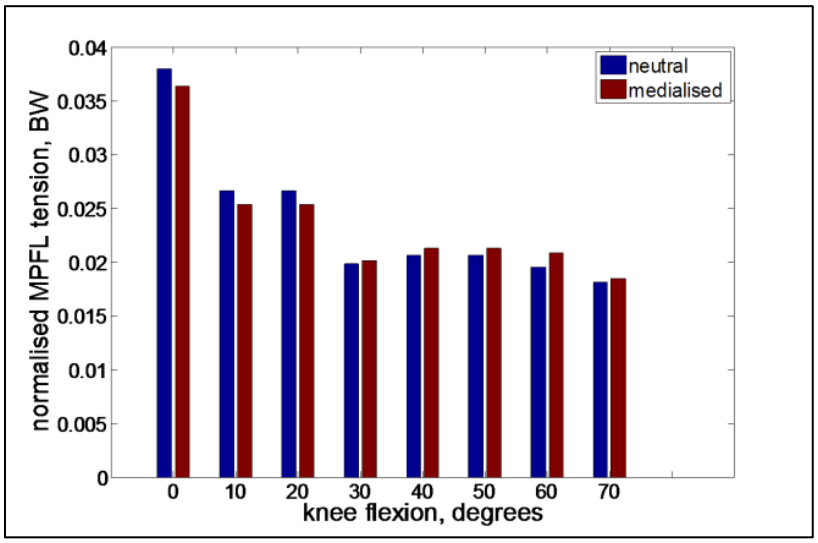

Figure 6.8: MPFL tension before and after the osteotomy (Volunteer Two).

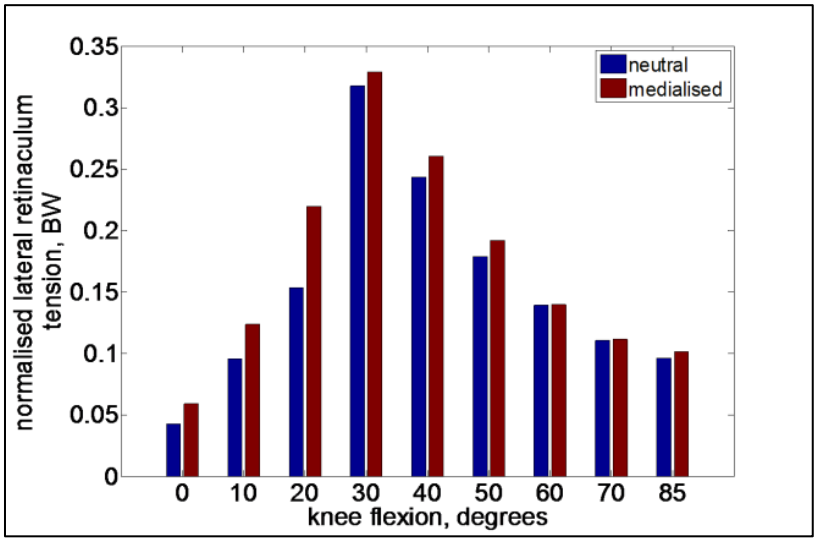

Figure 6.9: Lateral retinaculum tension before and after the osteotomy (Volunteer One).

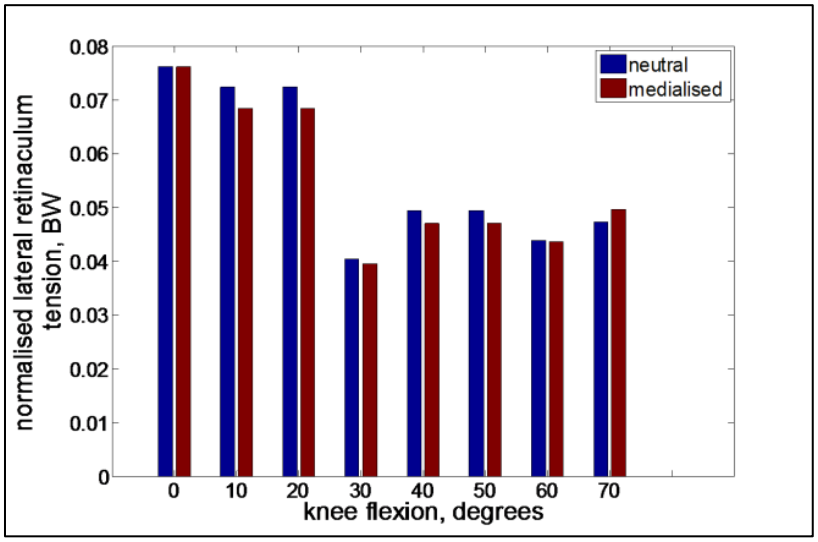

Figure 6.10: Lateral retinaculum tension before and after the osteotomy (Volunteer Two).

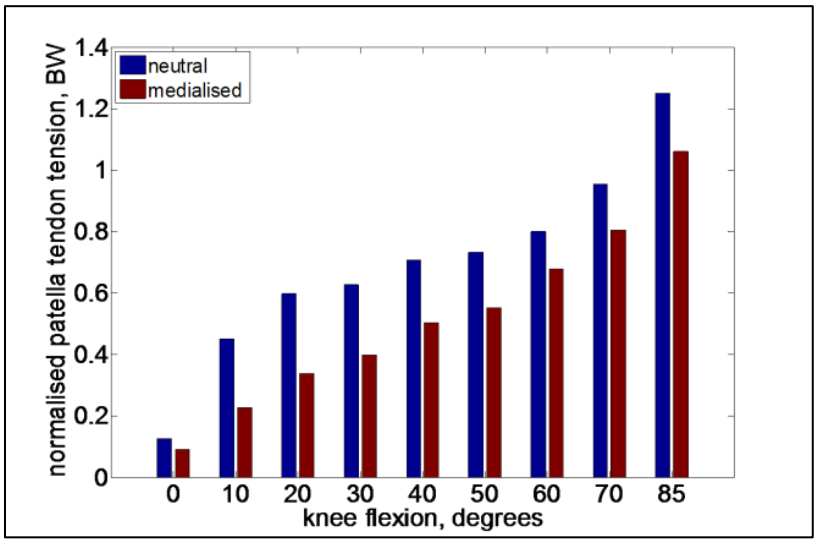

Figure 6.11: Patellar tendon tension before and after the osteotomy (Volunteer One).

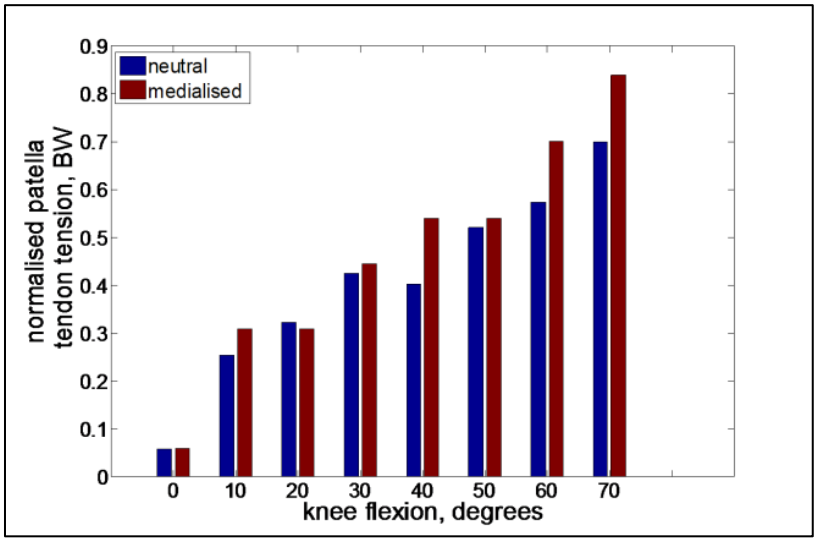

Figure 6.12: Patellar tendon tension before and after the osteotomy (Volunteer Two).

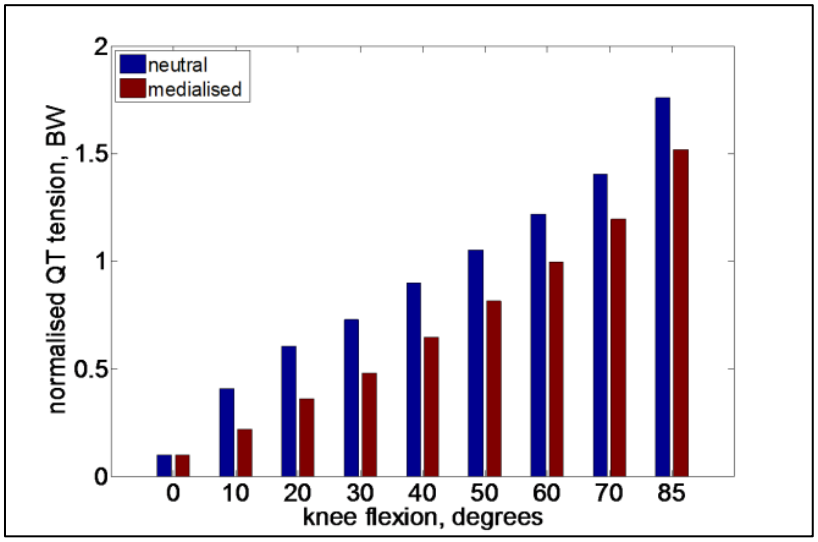

Figure 6.13: Quadriceps tendon tension before and after the osteotomy (Volunteer One).

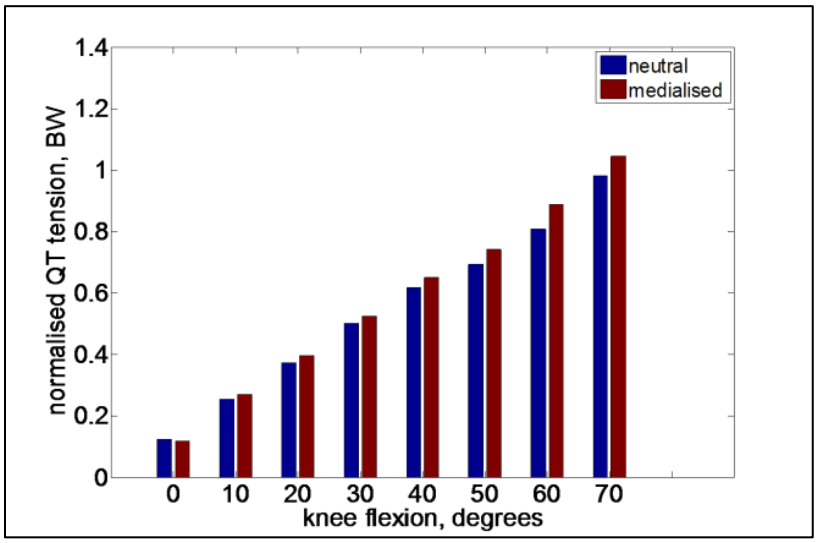

Figure 6.14: Quadriceps tendon tension before and after the osteotomy (Volunteer Two)

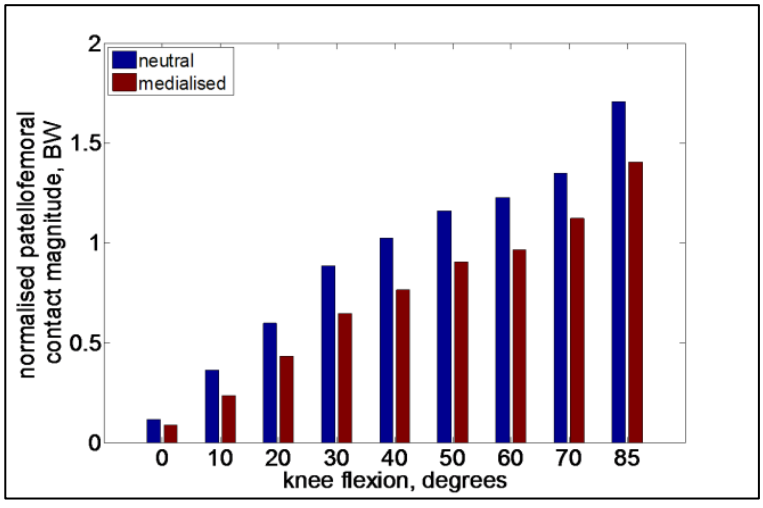

Figure 6.15: Patellofemoral contact magnitude before and after the osteotomy (Volunteer One).

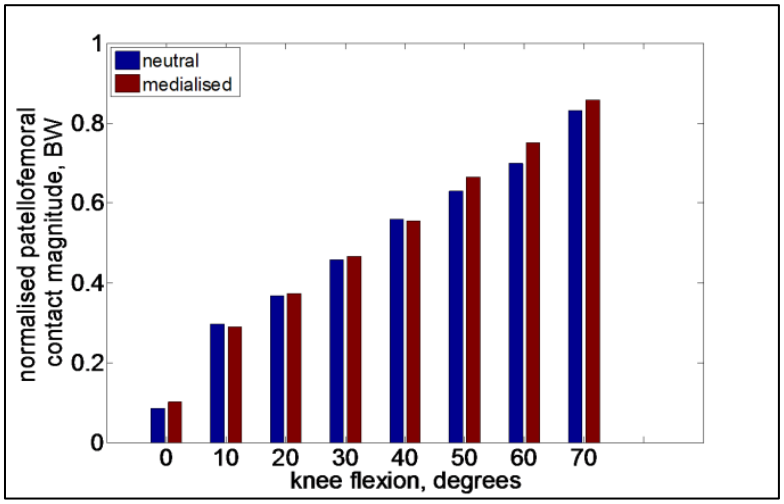

Figure 6.16: Patellofemoral contact magnitude before and after the osteotomy (Volunteer Two).

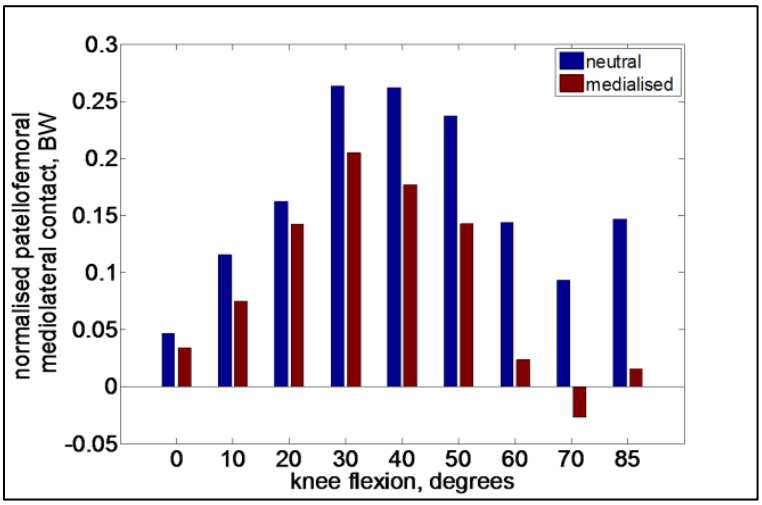

Figure 6.17: Patellofemoral mediolateral contact component before and after the osteotomy (Volunteer One; +: lateral facet / -: medial facet).

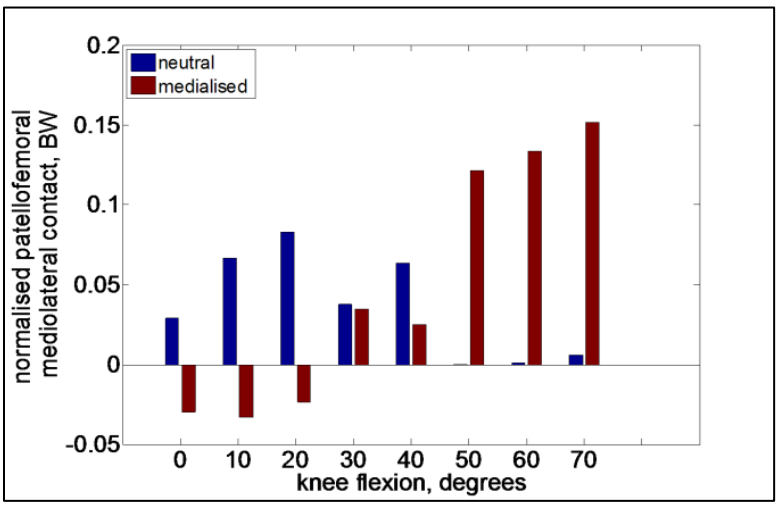

Figure 6.18: Patellofemoral mediolateral contact component before and after the osteotomy (Volunteer Two; +: lateral facet / -: medial facet).

6.1.3.3 Patellofemoral contact pressure

The mean patellofemoral pressures in Volunteer One's patellofemoral joint were decreased at all degrees of flexion after the tubercle was medialised (Figure 6.19 and Figure 6.20). The effect of medialisation on the mean patellofemoral pressure was less profound for Volunteer Two (Figure 6.21 and Figure 6.22). Since the mediolateral load component was changed after the medialisation of the tibial tubercle, the pressure distribution on the medial and lateral facets would be influenced. The pressure distribution on the trochlear groove (Figure G.1 to Figure G.5) and patella (Figure G.6 to Figure G.10) of Volunteer One indicated the following:

- The contact across the lateral and medial facets of the trochlear groove and patella was distributed more evenly, especially at early degrees of flexion (30 and 45 degrees).
- The pressure increased on the medial facets.
- The contact on the patella migrated from a more distal to a more proximal location across the patella cartilage, while it changed from a predominantly lateral distribution to become more evenly distributed across both the facets.
- The maximum pressure increased at 60 (by 8.0 %) and 85 degrees (by 20.3 %) after the tubercle was medialised.

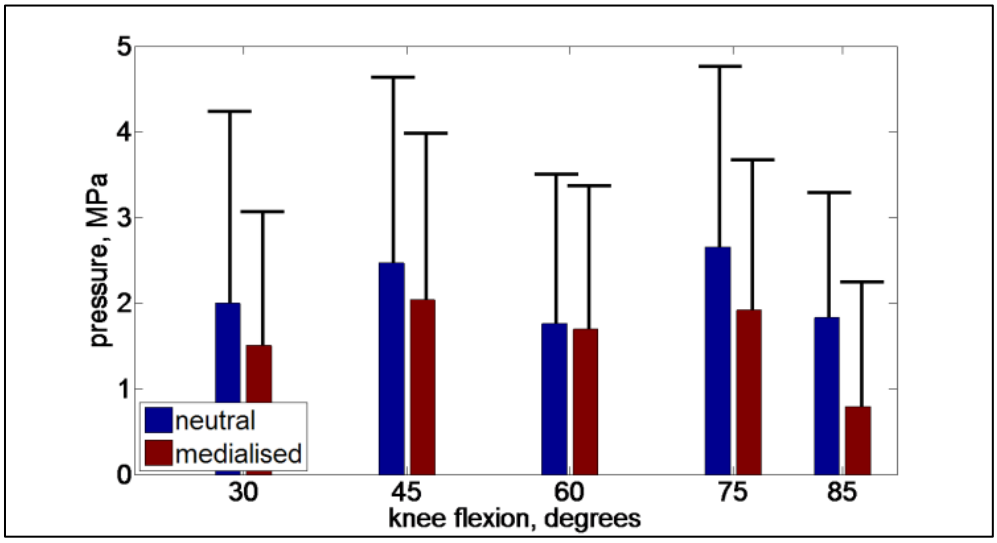

Figure 6.19: Mean pressure distribution across the trochlear groove (Volunteer One).

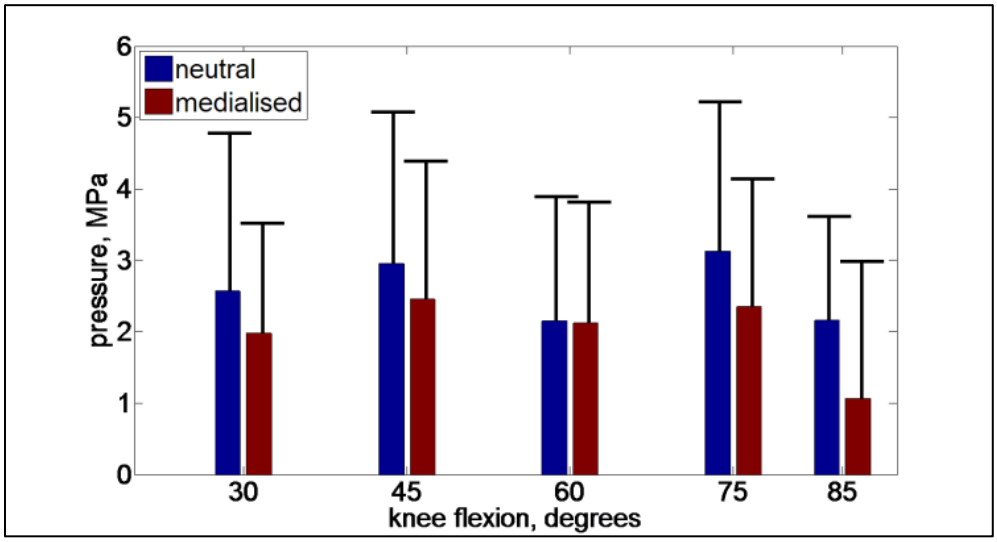

Figure 6.20: Mean pressure distribution across the patella (Volunteer One).

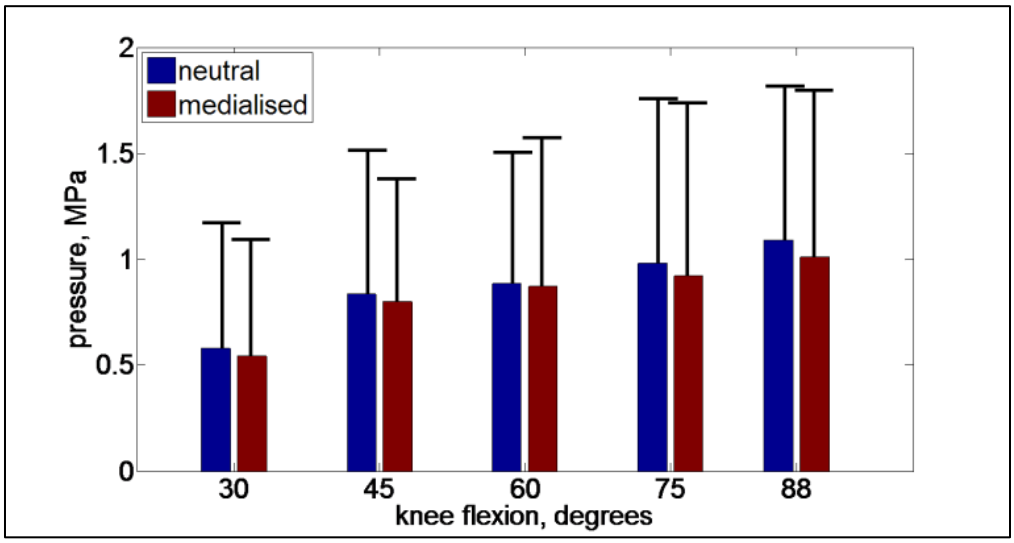

Figure 6.21: Mean pressure distribution across the trochlear groove (Volunteer Two).

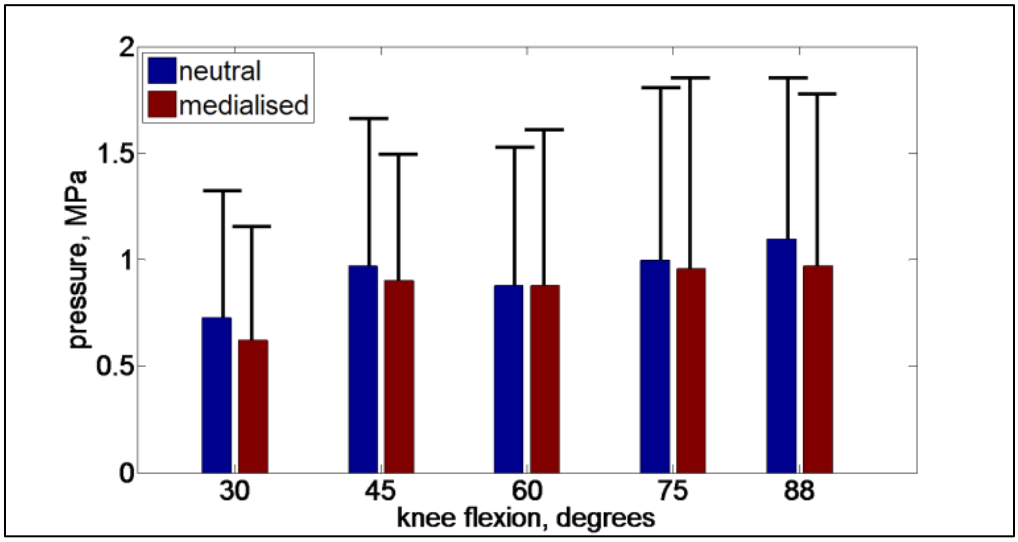

Figure 6.22: Mean pressure distribution across the patella (Volunteer Two).

The pressure distribution on the trochlear groove (Figure G.11 to Figure G.15) and patella (Figure G.16 to Figure G.20) of Volunteer Two indicated the following:

- The contact remained the same across the lateral and medial facets of the trochlear groove and patella.
- The maximum pressure increased at 60 (by 15.0 %), 75 (by 2.3 %) and 85 degrees (by 16.0 %) after the tubercle was medialised, while the pressure was increased on the medial facets of the trochlear groove and patella.
- The contact on the patella migrated from a more distal to a more proximal location across the patella cartilage, while it changed from a predominantly lateral distribution to become more evenly distributed.

Boxplots (Vining (1998)) of the pressure distribution of Volunteers One (Table G.1) and Two (Table G.2) were constructed to determine the effect of tubercle medialisation on the pressure distribution. The pressure distribution in Volunteer One's joint was diminished at 30, 75 and 85 degrees while it remained the same at 45 degrees, and was increased at 60 degrees. The median of the boxplots were smaller at all degrees of flexion after the tubercle was medialised. The pressure distribution across Volunteer Two's patellofemoral joint was increased at 60 and 75 degrees, remained the same at 30 and 85 degrees and was smaller at 45 degrees knee flexion. The median was decreased at 30, 45 and 85 degrees while it was unchanged at 60 and 75 degrees.

6.1.4 Discussion

The findings suggest that tubercle medialisation is more effective at earlier angles of flexion, than deeper angles of flexion. A patella which starts to articulate outside of the trochlear groove will be forced to enter the trochlear groove at a smaller angle of flexion, which will improve patellofemoral stability. Hence, patella tilt will become more regular. The effect of medialisation on the resultant patellofemoral contact load is negligible, but it has an effect on the mediolateral component, especially at deeper angles of flexion. The reduction in the mediolateral component resulted from the decreased Q-angle of Volunteer One, and was shifted from a lateral direction to a medial direction. If the patella is however already articulating in the central trochlear groove, as was the case with Volunteer Two, the medial component might increase. The FEA showed that the pressure on the medial facet might increase, and that the maximum pressure might even become larger than what it was for the neutral tubercle, even though the mean pressure might decrease. This stresses the importance of not only considering contact load, but also its effect on the joint pressure.

The effect of medialisation on soft tissue stabiliser dynamics showed that the MPFL load would decrease. The increase in lateral retinaculum tension after medialisation for Volunteer One can be ascribed to the pronounced lateral facet of Volunteer One's trochlear groove. Since the patella was forced to enter the trochlear groove at an earlier angle of flexion, it needed to displace in an anterior direction over the facet which resulted in the

increased lateral retinaculum tension. The patellar tendon and quadriceps tendon tensions of Volunteer One decreased due to the decrease in the moment arm of the patellofemoral joint: the patella displaced medially, to the centre of the trochlear groove, which resulted in a decreased moment arm.

The results of this study correlate with the findings of Elias *et al.* (2004) who predicted a decrease of lateral pressure, while an increase in medial pressure would occur when the Q-angle is decreased. They did however show that the mean pressure would stay the same regardless of the Q-angle. In contrast, this study showed the mean pressure to decrease after medialisation (reduction of the Q-angle). The findings of Elias *et al.* (2004) relate to a static loading condition, which will be different to the dynamic condition. Since the patella will most likely come into a similar state of equilibrium during a static analysis, the same cannot be said of a dynamic state of equilibrium. During the FEA, the patella was constrained to translate only along the resultant loading direction. The dynamic posture was therefore maintained, which might have resulted in different computed mean pressures.

The study confirmed that patellofemoral contact pressure can be relieved by means of an osteotomy (Benvenutti *et al.* (1997); Cameron *et al.* (1986); Cox (1982); Fulkerson (1983); Elias *et al.* (2004); Ramappa *et al.* (2006)) but surgeons should be concerned about the possibility of increasing the maximum pressure on the medial facet at deeper angles of flexion after the osteotomy. Patella tilt was also improved after the osteotomy, and the patella of Volunteer One entered the trochlear groove at an earlier angle of flexion. This suggests that abnormal patellar tracking can be improved with an osteotomy (Benvenutti *et al.* (1997); Cameron *et al.* (1986); Chrisman *et al.* (1979); Cosgarea *et al.* (1999); Cox (1982); Farahmand *et al.* (1998); Fulkerson (1983); Kuroda *et al.* (2001); Ramappa *et al.* (2006)). It is difficult to objectively quantify the *in-vivo* pressures that will occur inside the patellofemoral joint during dynamic flexion. This technique does however provide a means to investigate probable outcomes when the patellofemoral configuration is changed.

6.2 Patellofemoral replacement biomechanics

6.2.1 Background

Abnormalities in patellofemoral anatomy caused by trauma or anatomical variations might result in an unstable patellofemoral joint. Anatomical variations seem to be produced by genetic assimilation and can therefore not be classified as an acquired pathology (Lancaster *et al.* (2007)). Although anterior knee pain is a common ailment, the current understanding of the underlying causes for pain is limited (Herrington and Al-Shehri (2006)).

Patellofemoral pain syndrome is an idiopathic chronic pain disorder characterised by the gradual onset of poorly localised pain in the anterior aspect of the knee (MacIntyre *et al.* (2006)). Activities such as squatting and prolonged sitting with the knee in a bent position can intensify pain. Herrington and Al-Shehri (2006) suggest that patients who suffer from long term patellofemoral pain syndrome will ultimately develop patellofemoral osteoarthritis, which is a degenerative disease causing pain and stiffness in synovial joints, as a result of articular cartilage damage and degeneration.

If non-surgical treatment of osteoarthritis fails, an arthroplasty (joint replacement) is the recommended treatment. During a total knee replacement, the patella, and both the distal femur and the proximal tibia are resurfaced while a patellofemoral arthroplasty entails the resurfacing of the patella and trochlear groove (Hollinghurst *et al.* (2007); Sisto and Sarin (2006)). The proposed advantage of a patellofemoral arthroplasty above a total knee arthroplasty is the preservation of the structural integrity of the joint (Sisto and Sarin (2006)). Long term studies (Ackroyd *et al.* (2007); Eisenhuth *et al.* (2006)) have shown that more than 50 % of patellofemoral arthroplasties deliver good results, although this is inferior to the success rate of 90 % achieved with traditional total knee arthroplasties (Southern California Orthopaedics Institute, 2008). Failure of the patellofemoral prosthesis can be ascribed to the patella running off the femoral prosthesis beyond 90 degrees of flexion (Amis *et al.* (2005)); or residual malalignment of the prosthesis (Amis *et al.* (2005)); or wear of the polyethylene used to resurface the patella (3% of cases according to Ackroyd *et al.* (2007)).

Another problem is the onset of arthritis in the rest of the joint after surgery (iatrogenic causes). Underlying abnormalities in the patellofemoral joint, which have led to a degenerative condition such as an unstable patella, might not be adequately addressed by the present available prostheses and procedures used during the replacement surgery (Amis *et al.* (2005)). Patients having replacement surgery normally present with abnormal soft tissue configurations which should be attended to correctly during surgery. Patellofemoral instability after a total knee arthroplasty is a common result and it is one of the leading reasons for surgical revision (Eisenhuth *et al.* (2006); Hollinghurst *et al.* (2007)).

Patellofemoral prostheses biomechanics have received little attention. Amis *et al.* (2005) reviewed four types of prostheses on the basis of joint kinematics, kinetics, contact mechanics, bone preservation during implantation and the instrumentation used during surgery. Their study however described the factors to be considered when doing a patellofemoral arthroplasty and did not report on the behaviour of the prosthesis in a dynamic situation. In the current study, two commercial prostheses[‡‡‡‡] were compared on the basis of patellofemoral kinematics, soft tissue tension, and patellofemoral kinetics as a function of dynamic knee flexion. The baseline models of the

[‡‡‡‡] Referred to as Prosthesis A (Smith and Nephew) and Prosthesis B (Avon).

three volunteers were used as reference values for a normal knee's condition. A virtual replacement was done for each volunteer and the simulations presented in Chapter 4 were repeated for Prosthesis A and Prosthesis B.

6.2.2 Methods

It was necessary to reverse engineer the prostheses, since the computer aided design (CAD) models were not available from the manufacturer. A desktop laser scanner (NextEngine, Inc., Santa Monica, California) capable of generating three-dimensional models of scanned objects was used to generate three-dimensional models of the two respective prostheses size ranges (four trochlear sizes of the Avon and four sizes of the Smith and Nephew range were scanned). The laser scanner has been shown to have an accuracy of ± 0.127 millimetres (Van Sxhalkwyk (2010)). The scanned models were used only for the purposes of this study and access to the models was restricted.

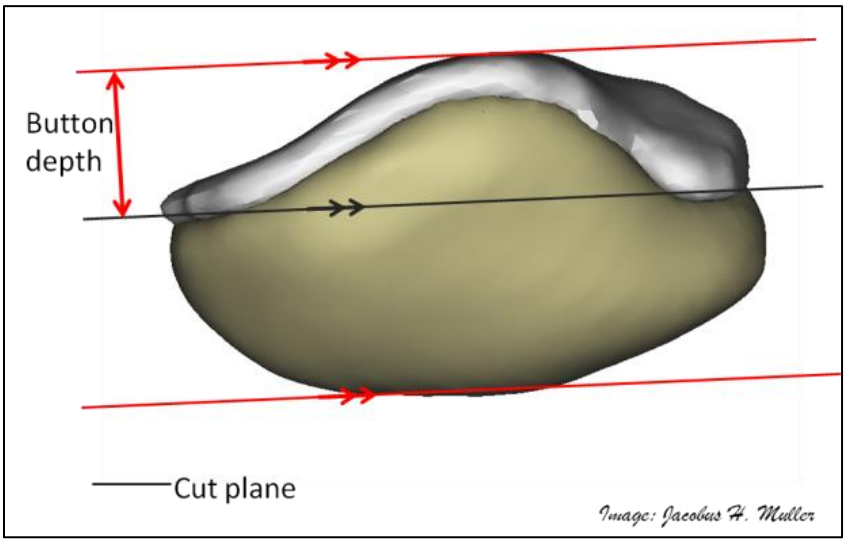

Figure 6.23: Cut plane on patella for button placement.

Two orthopaedic surgeons assisted during the virtual resurfacing of the patella and femur. A patella button was used to resurface the patella[§§§§]. The major advantage of the button was the ease with which it could be aligned. Unfortunately the geometry of the button will result in a point contact (at best a line contact) during articulation, which might lead to elevated contact pressures. A cut plane, parallel to the anterior patella border, was defined and had an offset equal to the button depth (Figure 6.23 and Figure 6.24). After the button was medialised, the patella and button were exported as one part. By medialising the button, the lateral load component from the extensor mechanism would be better accommodated during knee flexion (Amis *et al.* (2005)). Three button sizes were available (Table 6.1).

[§§§§] In practice, both prostheses are used in conjunction with a patella resurfacing geometry that is more conforming, but these were unfortunately not available.

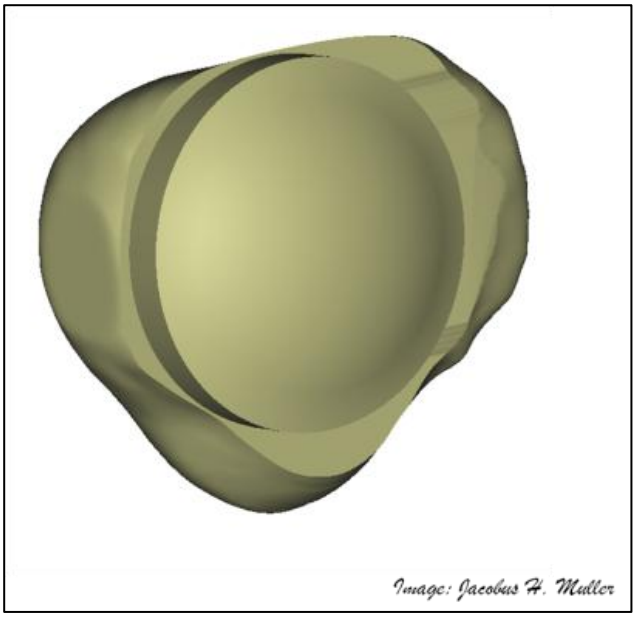

Figure 6.24: Patella resurfaced with the button.

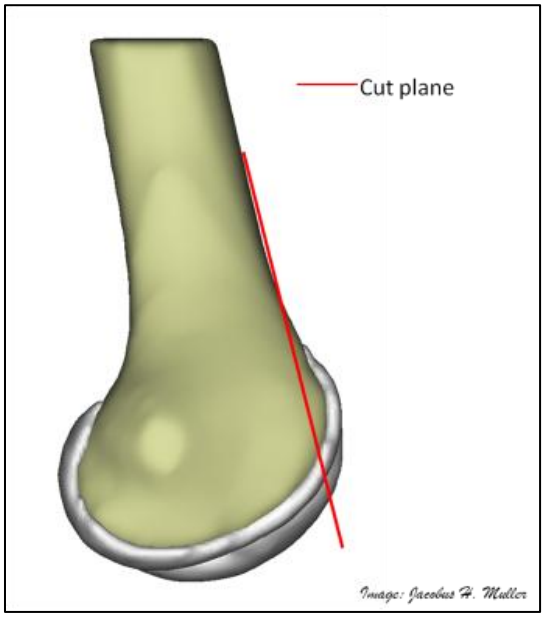

Figure 6.25: Cut plane on the femur.

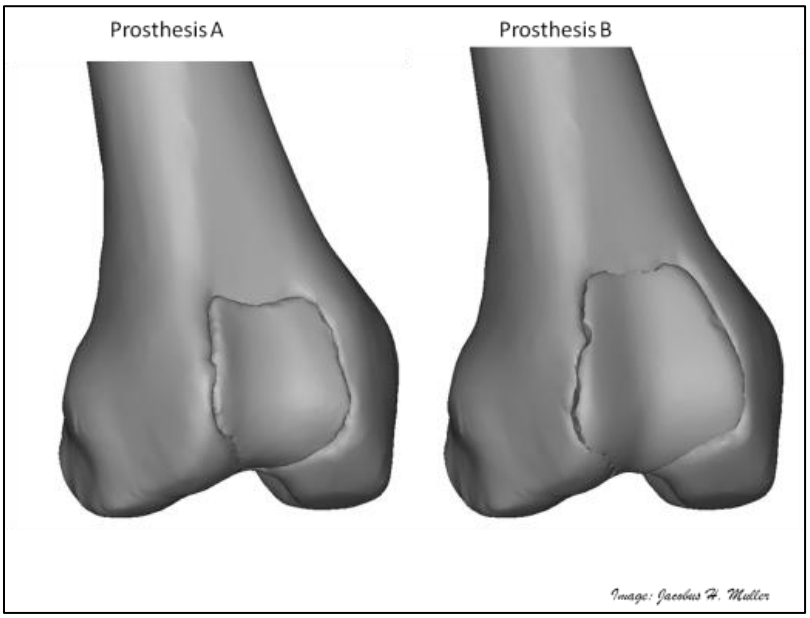

Figure 6.26: Resurfaced femora.

Table 6.1: Patella button sizes.

Button	Diameter, millimetres	Depth, millimetres
Small	23	6.90
Medium	26	7.31
Large	29	8.16

During resurfacing of the trochlear groove, a cut plane parallel to the anterior femoral shaft was defined. The plane was positioned to allow the interface between the femur and trochlear groove prosthesis to be flush (Figure 6.25 and Figure 6.26). The internal-external rotation of the prosthesis was adjusted to ensure that the distal ridge was flush with the native cartilage. A fair amount of bone had to be removed in order for the prosthesis to have a

good fit since the trochlear grooves of all three volunteers had normal depths. Amis *et al.* (2005) reported that it is desirable for a minimal amount of bone to be removed, especially for revision purposes. In practice, patients will present with some form of trochlear groove dysplasia, that is shallow trochleae, and less bone will have to be removed than what was necessary in this investigation.

The resurfaced femur and patella replaced the native femur and patella in the baseline musculoskeletal models. The seating exercise was repeated for both Prostheses A and B. Comparison of the patella tilt and bisect offset between the two prostheses as well as the native patellofemoral joint was made. Patellofemoral contact (magnitude and mediolateral component) as well as soft tissue stabiliser loads (Patellar tendon, quadriceps tendon, MPFL and lateral retinaculum) were also compared between the two prostheses and to the baseline results.

6.2.3 Results

6.2.3.1 Geometric appearance

Prosthesis A possessed a more prominent medial facet than that of Prosthesis B (Figure 6.27). This was accompanied by a lateralised trochlear groove, while the groove was more neutrally placed on Prosthesis B. Prosthesis B covered a larger distance in a proximal distal direction while the difference between mediolateral distances was minimal.

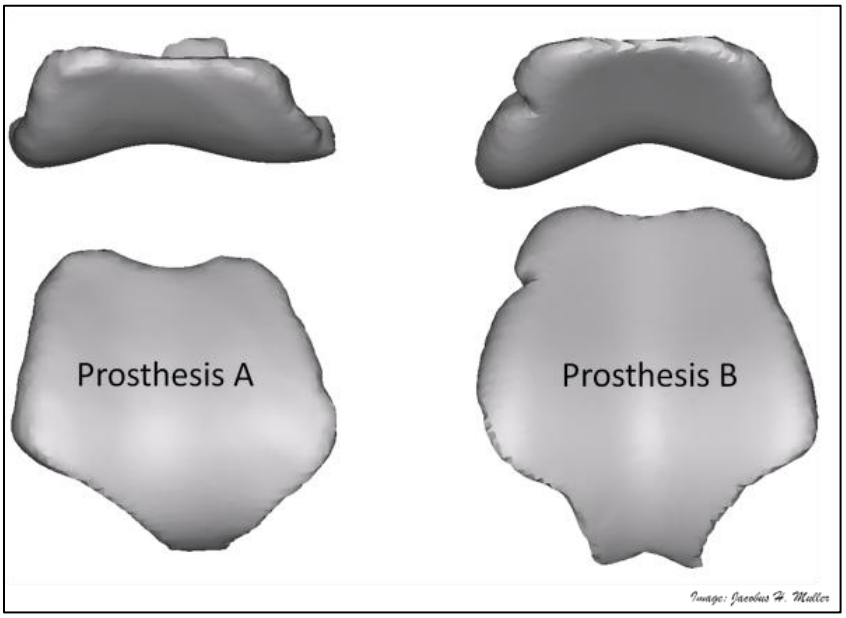

Figure 6.27: Prosthesis A and Prosthesis B (largest available sizes).

6.2.3.2 Kinematics

The traction patterns of Volunteer One's patella were reproduced by both prostheses after trochlear engagement (Figure 6.28 and Figure 6.29). The mediolateral shift when Prosthesis B was implanted was closest to the baseline values prior to trochlear engagement. The mediolateral shift when Prosthesis A was implanted remained more stable through the entire range of flexion. Lateral tilt during early knee flexion was reduced at a faster rate when the prostheses were implanted, and a difference in tilt was maintained after trochlear engagement.

The initial mediolateral shift of Volunteer Two's patella was reduced after Prosthesis B was implanted and reduced further when Prosthesis A was implanted (Figure 6.30). The mediolateral shift patterns varied, with the predominantly lateral shift for the baseline model changing to a lateral shift up to 30 degrees knee flexion, after which the patella shifted medially when Prosthesis A was implanted. Volunteer Two's patella shifted laterally and maintained its mediolateral position after 40 degrees knee flexion. The tilt pattern stayed the same for both prostheses (Figure 6.31). Prosthesis B reproduced the baseline tilt pattern best, while the tilt orientation was more medial when Prosthesis A was implanted.

Volunteer Three's patella were displaced medially after resurfacing with both Prosthesis A and B (Figure 6.32). The medial shift between 20 and 40 degrees knee flexion in the neutral joint, changed to a lateral shift, after which the patella shifted medially again. The medial tilt posture changed to a lateral tilt posture, but the patella followed a similar tilt pattern as was the case for the neutral joint: medial tilt between full extension and 50 degrees and a lateral tilt from 50 degrees to 90 degrees knee flexion (Figure 6.33).

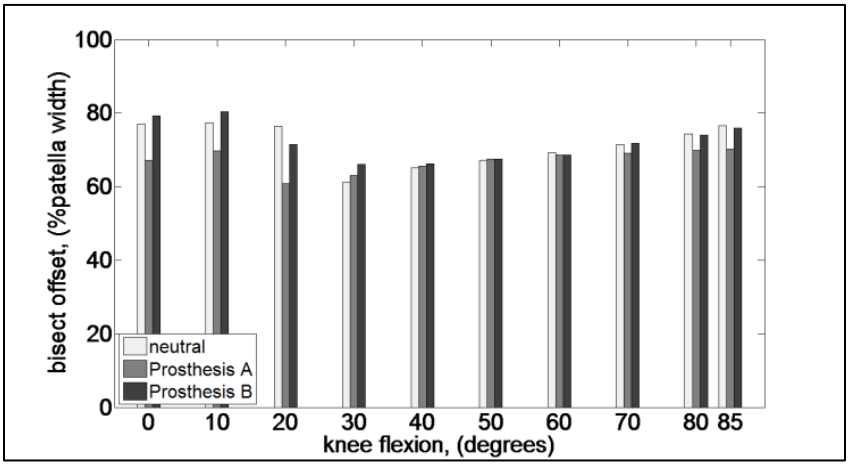

Figure 6.28: Patella bisect offset of Volunteer One (+: medial / -: lateral).

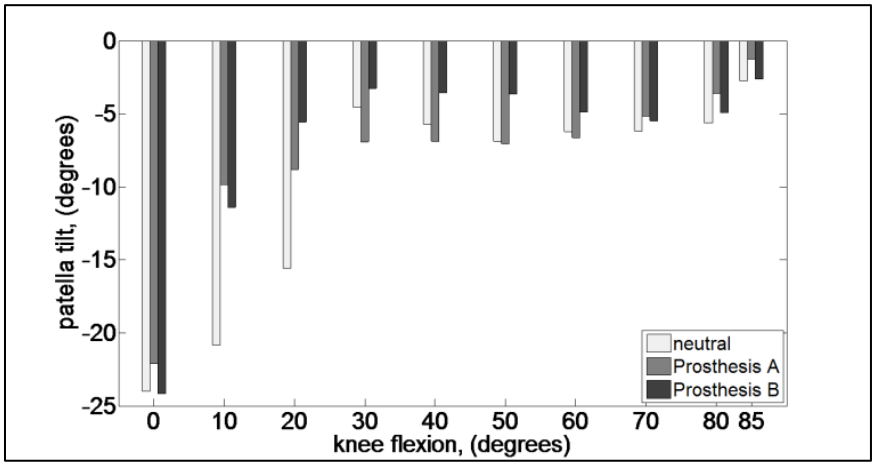

Figure 6.29: Patella tilt of Volunteer One (+: medial / -: lateral).

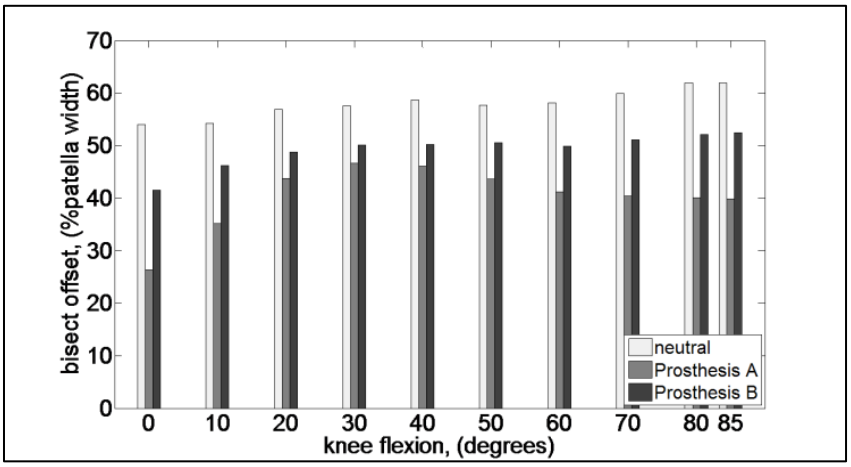

Figure 6.30: Patella bisect offset of Volunteer Two (+: medial / -: lateral).

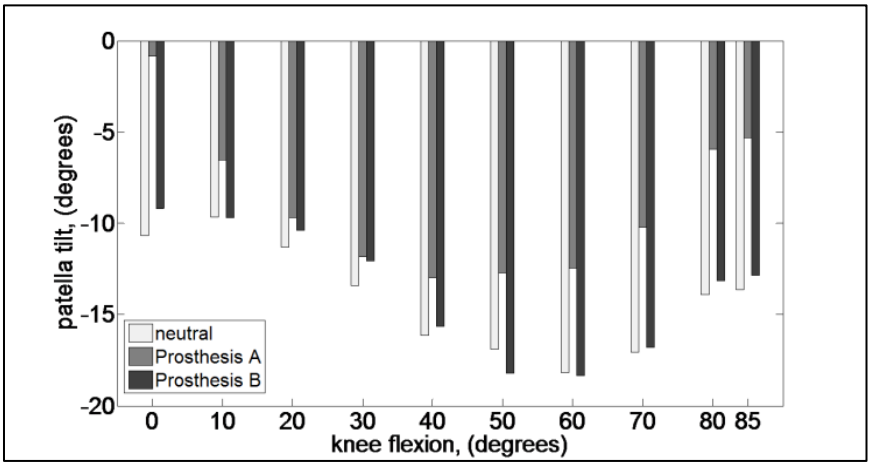

Figure 6.31: Patella tilt of Volunteer Two

(+: medial / -: lateral).

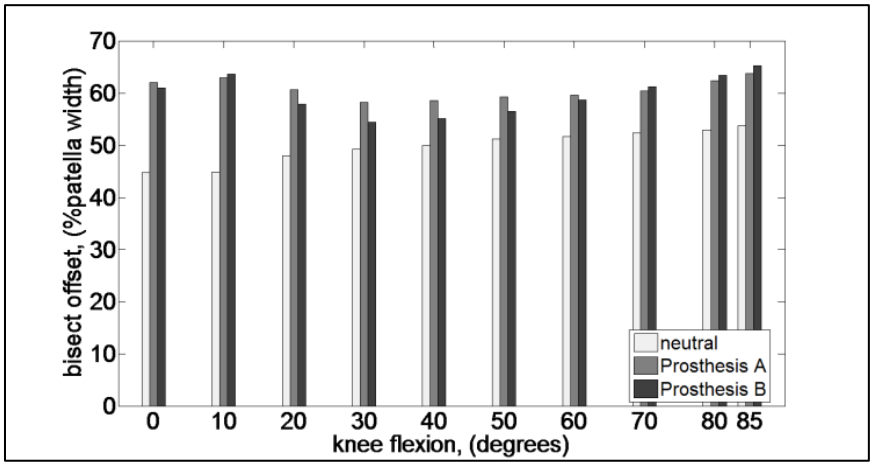

Figure 6.32: Patella bisect offset of Volunteer Three (+: medial / -: lateral).

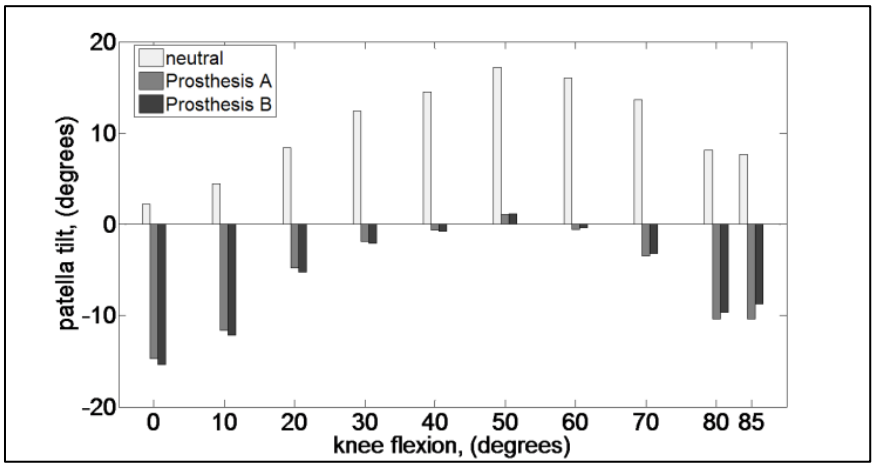

Figure 6.33: Patella tilt of Volunteer Three (+: medial / -: lateral).

6.2.3.3 Kinetics

The patellofemoral resultant contact magnitudes for all three volunteers were independent of the type of prosthesis that was implanted (Figure 6.34, Figure 6.36 and Figure 6.38). The opposite was true of the mediolateral load components. The resultant mediolateral component on Volunteer One's patella was reduced and transferred from the lateral facet to the medial facet between 50 and 85 degrees knee flexion (Figure 6.35). When Prosthesis A was implanted in Volunteer Two, the resultant mediolateral component was similar to the baseline values up to 50 degrees knee flexion. The resultant mediolateral load was transferred to the medial facet and back to the lateral facet after 40 degrees knee flexion when Prosthesis B was implanted (Figure 6.37). The resultant mediolateral component trend of Volunteer Three was maintained, but the load values increased relative to the baseline values (Figure 6.39). Prosthesis A endured the largest mediolateral load between 70 and 80 degrees knee flexion.

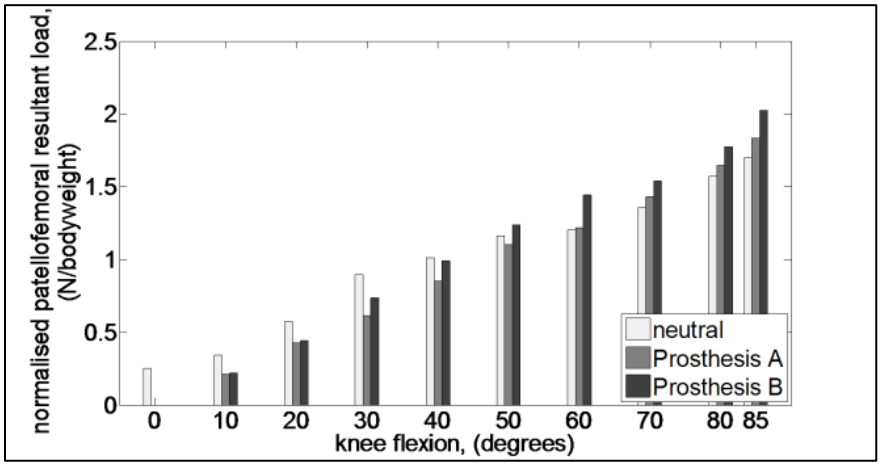

Figure 6.34: Patellofemoral contact magnitude (Volunteer One).

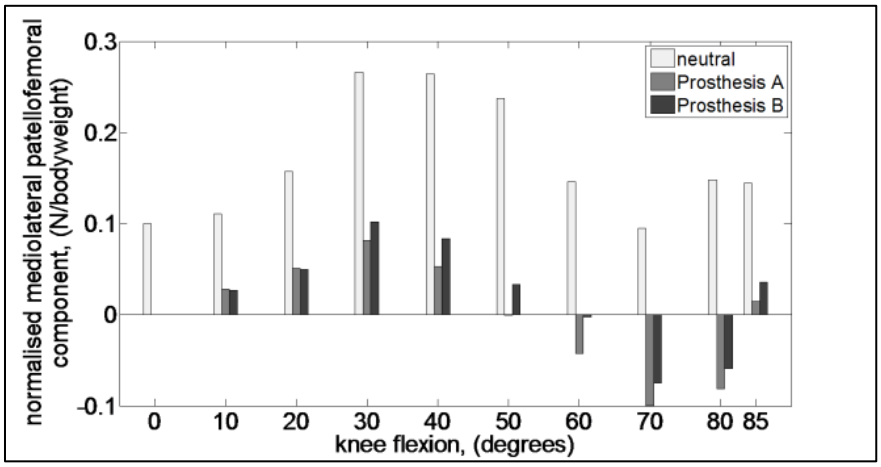

Figure 6.35: Patellofemoral mediolateral contact component (Volunteer One).

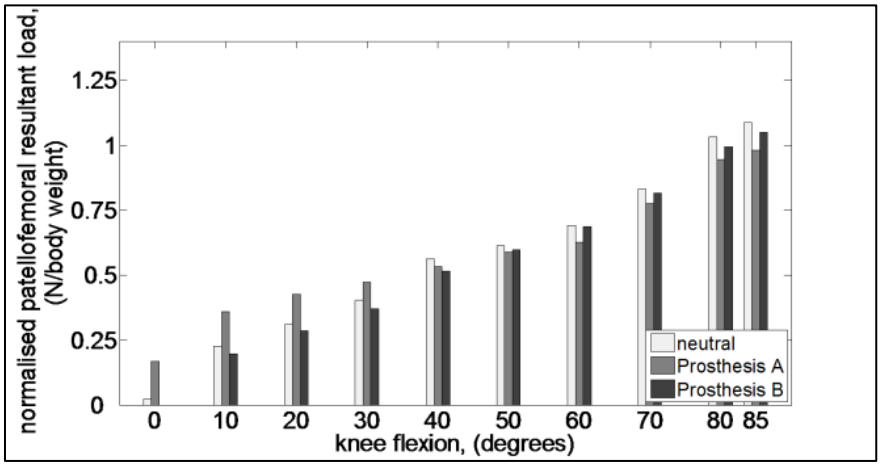

Figure 6.36: Patellofemoral contact magnitude (Volunteer Two).

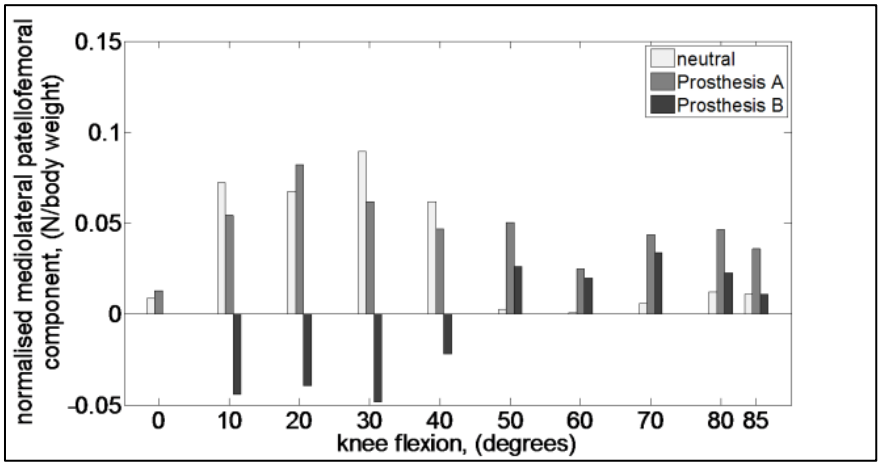

Figure 6.37: Patellofemoral mediolateral contact component (Volunteer Two).

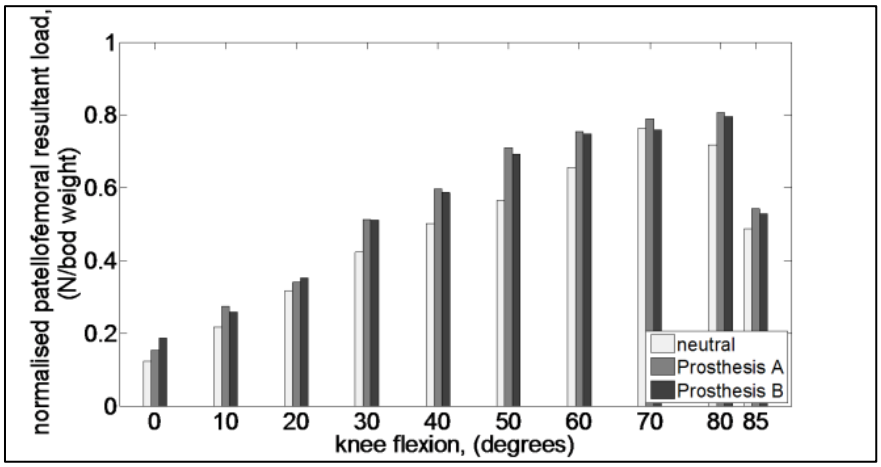

Figure 6.38: Patellofemoral contact magnitude (Volunteer Three).

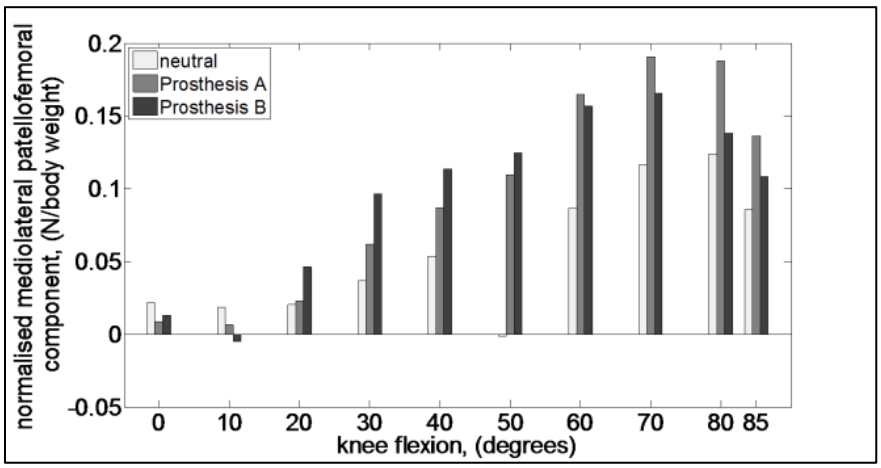

Figure 6.39: Patellofemoral mediolateral contact component (Volunteer Three).

The patellar tendon (Figure 6.40, Figure 6.42 and Figure 6.44) and quadriceps tendon (Figure 6.41, Figure 6.43 Figure 6.45) tensions were also independent from the type of prosthesis that was implanted. The retinaculum loads did however vary considerably. The MPFL and lateral retinaculum tensions of Volunteer One were reduced when the prostheses were implanted, with Prosthesis A causing the largest reduction in lateral retinaculum tension (Figure 6.46 and Figure 6.47). Volunteer Two saw a large increase in MPFL and lateral

retinaculum tension during early flexion when Prosthesis A was implanted. The tensions were comparable to the baseline values when Prosthesis B was implanted (Figure 6.48 and Figure 6.49). The initial MPFL tension in Volunteer Three was increased, but was less for the remainder of knee flexion when compared to the baseline values (Figure 6.50). The lateral retinaculum load did increase when the prostheses were implanted (Figure 6.51).

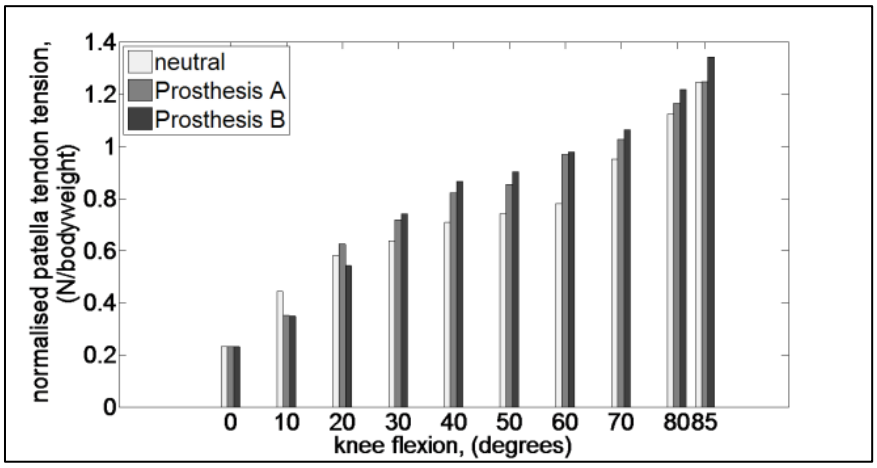

Figure 6.40: Patellar tendon tension (Volunteer One).

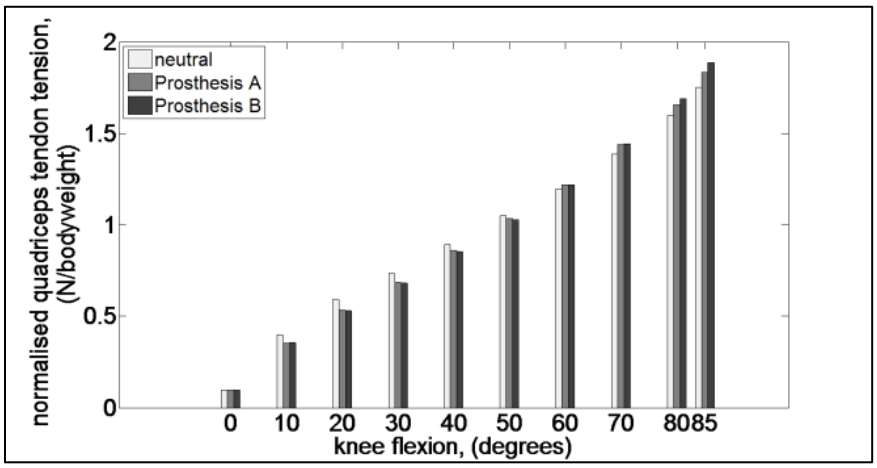

Figure 6.41: Quadriceps tendon tension (Volunteer One).

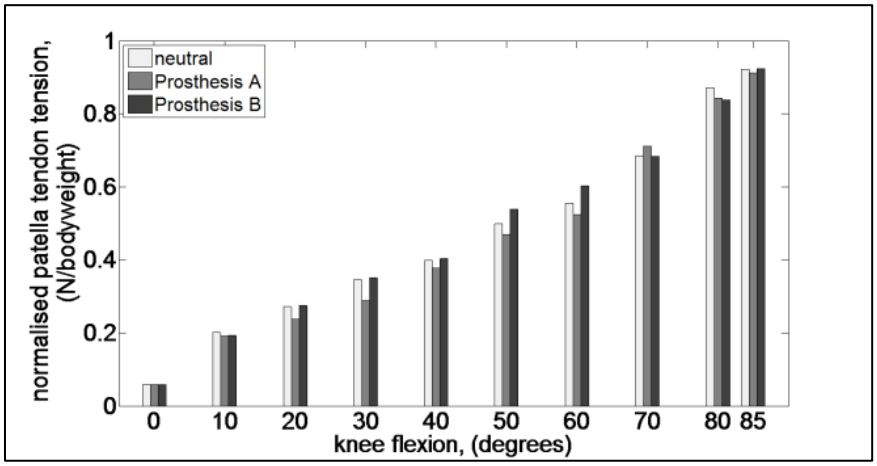

Figure 6.42: Patellar tendon tension (Volunteer Two).

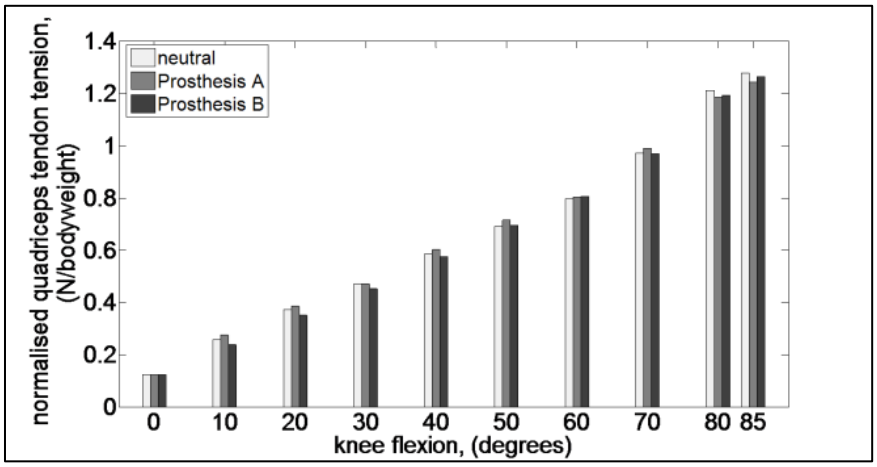

Figure 6.43: Quadriceps tendon tension (Volunteer Two).

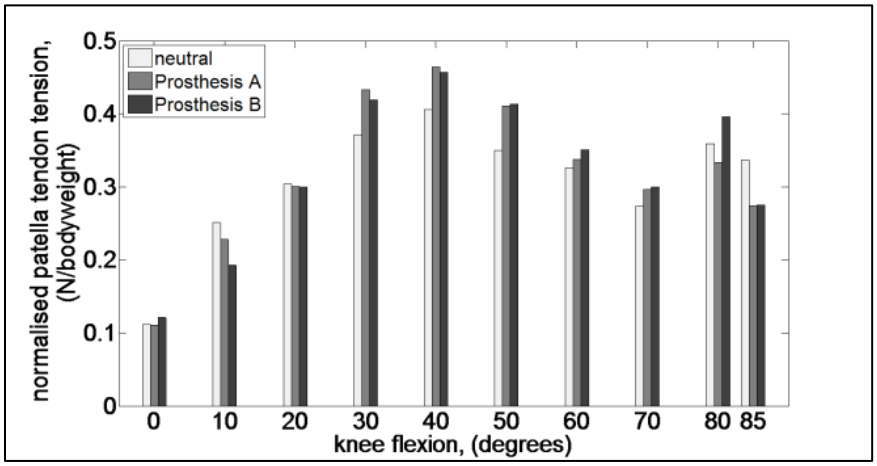

Figure 6.44: Patellar tendon tension (Volunteer Three).

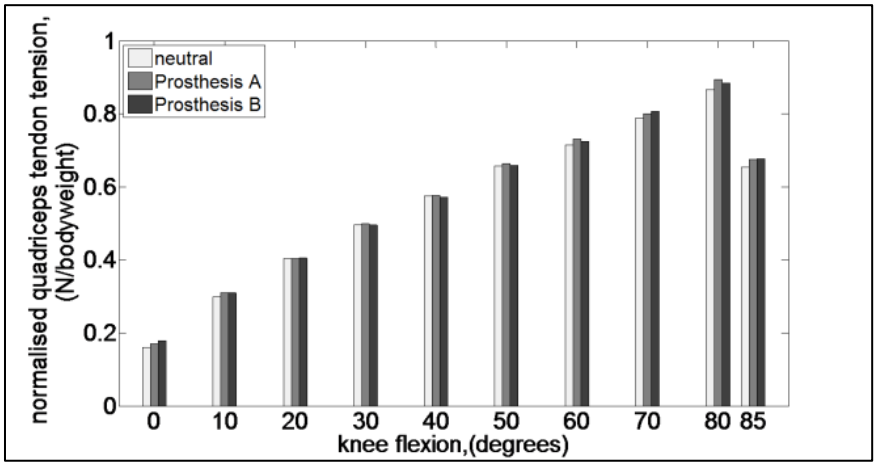

Figure 6.45: Quadriceps tendon tension (Volunteer Three).

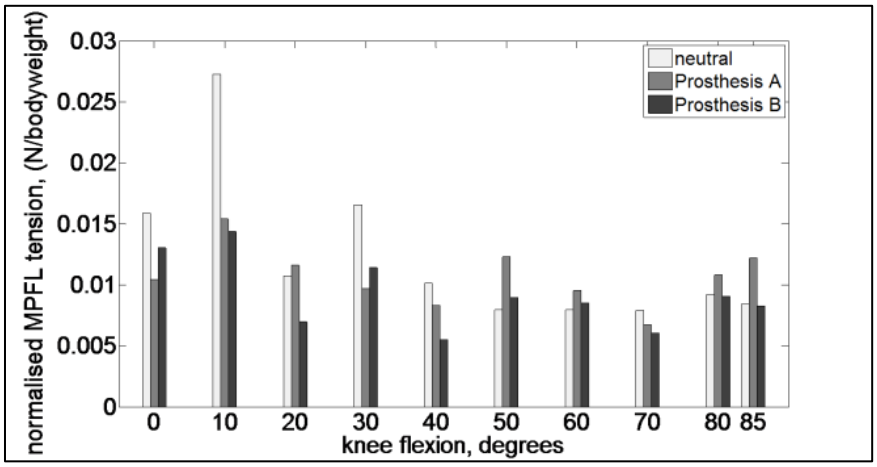

Figure 6.46: MPFL tension (Volunteer One).

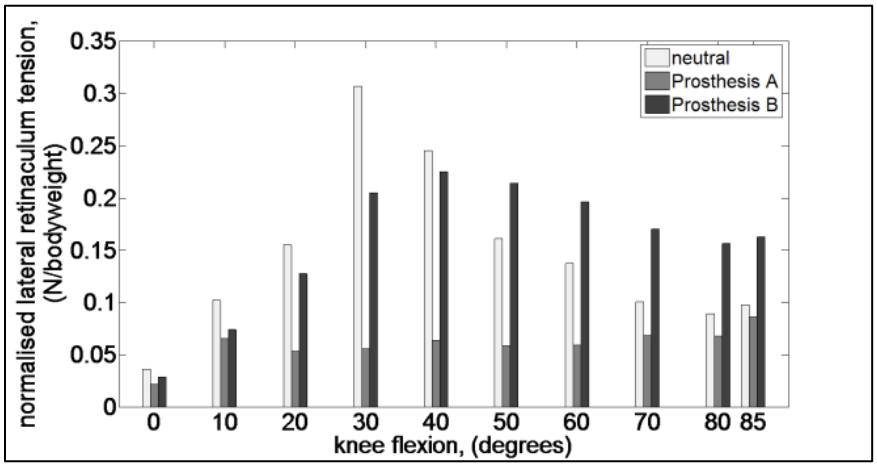

Figure 6.47: Lateral retinaculum tension (Volunteer One).

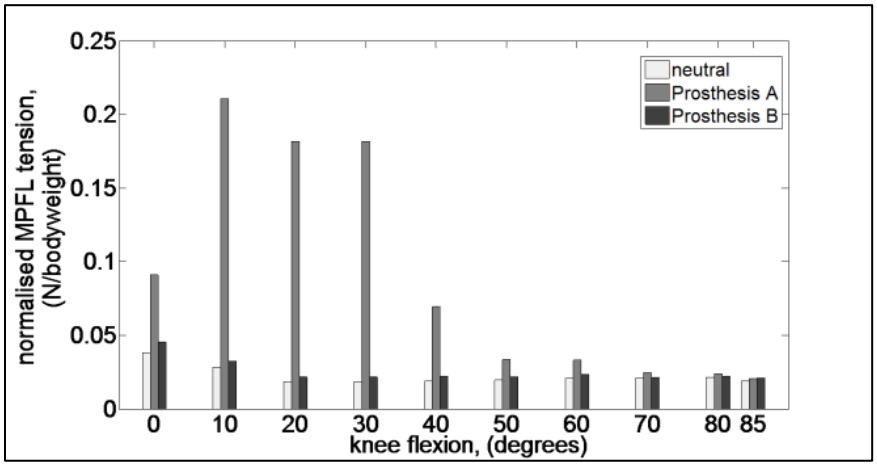

Figure 6.48: MPFL tension (Volunteer Two).

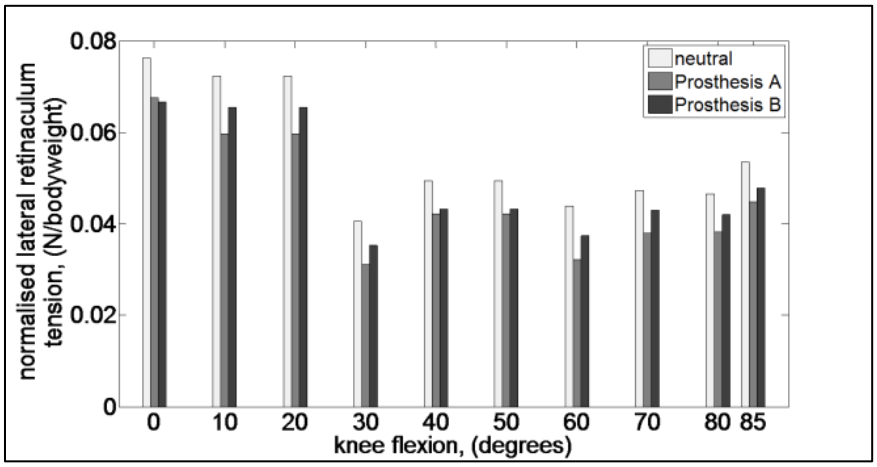

Figure 6.49: Lateral retinaculum tension (Volunteer Two).

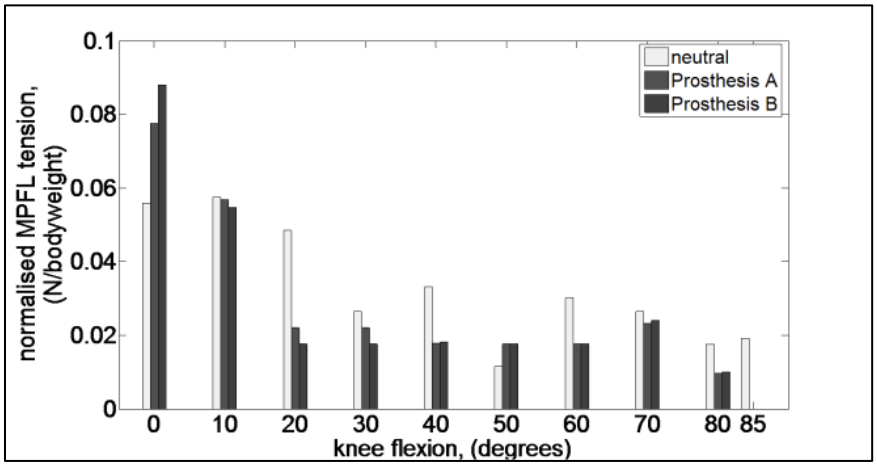

Figure 6.50: MPFL tension (Volunteer Three).

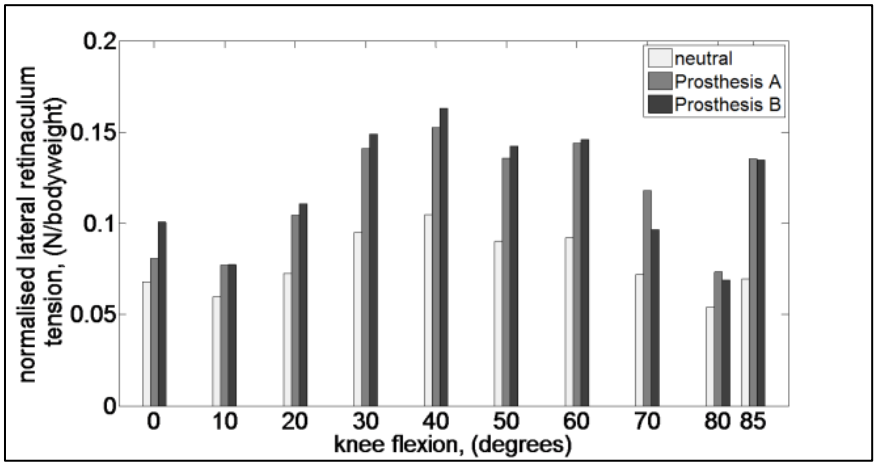

Figure 6.51: Lateral retinaculum tension (Volunteer Three).

6.2.4 Discussion

It is difficult to objectively judge which prosthesis will provide the best solution on the basis of the results on the patellofemoral kinematics provided. Prosthesis B seemed to have reproduced Volunteer One's patella mediolateral shift the best, while tilt was better reproduced by Prosthesis A. Prosthesis B seemed to be the desirable option for Volunteer Two in terms of the kinematics, while neither of the two prostheses yielded good results for Volunteer Three.

When considering the kinetics, it is evident that Prosthesis B gave better support to the MPFL (especially for Volunteer Two), while the lateral retinaculum was better supported by Prosthesis A. The mediolateral load component seemed to be more stable when Prosthesis B was implanted. The prominent medial condyle and lateralised trochlear groove of Prosthesis A might have resulted in the elevated MPFL load and the different mediolateral load components. Therefore patients receiving Prosthesis A might run the risk of over-straining their MPFL's which might cause the need for additional treatment and possible revision surgery. Amis *et al.* (2005) showed that revision on Prosthesis A is a strong possibility when special attention is not given to extensor mechanism alignment during surgery. Ackroyd *et al.* (2007) reported good results at five year follow up with Prosthesis B. Maltracking and wear of the components were lower than what was reported for other prostheses. The broad trochlear groove of Prosthesis B accommodates the patella better in full extension, as well as patellae with a tendency to track laterally (Ackroyd *et al.* (2007)). This is best illustrated for Volunteer One who had such a laterally tracking patella.

Hollinghurst *et al.* (2007) used fluoroscopy to compare sagittal plane kinematics in knees that were resurfaced with Prosthesis B, to that of normal knees. The findings of that study suggested that the only difference between the normal and resurfaced knees was a slightly increased patellar tendon angle. This caused the patella to be displaced anteriorly by 1.6 millimetres. This finding is not supported by the results presented here. Instead, the

patellar tendon angle would be reduced at early knee flexion due to the fair amount of bone that needed to be removed in order to ensure a flush fit between prosthesis and bone.

Since this was a computational study, it was not possible to simulate patient adjustment to the prosthesis; and the patellofemoral kinematics and kinetics might be improved with rehabilitation. However, this study gave an indication of the ability of the prostheses to reproduce patellofemoral dynamics when subjected to the same conditions as the baseline knees. The prostheses were also only tested below 90 degrees knee flexion and the patellae did therefore not run off the resurfaced material. Amis *et al.* (2005) stated that the distal border in the proximity of the intercondylar notch is an important design feature since the patella should be enabled to run off from the prosthesis unto the native cartilage without a step.

On the basis of the kinematics and kinetics results presented, Prosthesis B will provide a better alternative than Prosthesis A. When the geometry of the two prostheses was considered, Prosthesis B represented "normal" patellofemoral geometry more accurately. Neither of the two prostheses provided a good solution with regards to the patella kinematics of Volunteer Three. This suggests that there might be room for improvement or even a need to consider the customisation of patellofemoral prostheses.

Chapter 7

7. Conclusions

The aim was to develop a procedure by which subject-specific patellofemoral biomechanics could be quantified as a function of continuous knee flexion. This was achieved with three musculoskeletal models, representative of the individuals' anthropometric and anatomic appearance. The patellofemoral models:

- consisted of three-dimensional models of the trochlear groove and patella generated from CT and MRI scans of the individual's knee;
- included the medial patellofemoral ligament, lateral retinaculum and the extensor mechanism, which were modelled as spring-damper systems capable of wrapping around the individual's femora; and
- replicated the individuals' manner and body motion as recorded with a wireless inertial motion capturing system.

Six milestones were identified for the successful completion of the study, outlined below.

7.1 Milestones

Milestone 1: **Accurate volumetric imaging of an individual's skeletal geometry.** Each individual underwent a CT (lower body) and MRI scans (knees) from which three dimensional models of the skeletal elements were generated with the aid of segmentation techniques. CT scans have been applied in a variety of studies to provide accurate volumetric images from which subject-specific finite element models could be created. A previous study by Van Schalkwyk (2010) inspected the accuracy of the CT-segmentation process by scanning a geometry of known dimensions, and creating a three dimensional model from the scan data. A spatial accuracy of 99.71 % was obtained.

Table 7.1: Volume differences between the models generated from CT and the MRI scans.

	Patella volume (CT), mm^3	Patella volume (MRI), mm^3	% difference
Volunteer One	13 466	14 217	5.58 %
Volunteer Two	15 560	16 668	7.12 %
Volunteer Three	22 629	23 418	3.49 %

MRI on the other hand requires user intervention during the segmentation procedure since it is difficult to identify the border between the patella cartilage and the infra-patellar fat-pad, as well as the femoral cartilage and tibial cartilage. This might induce errors in the models, which could be exacerbated by the geometric

distortion effects of MRI (Fernandez *et al.* (2008)). The volumes of the models generated from the CT and MRI scans were different, albeit small (Table 7.1). These differences translated into dimensional errors of 0.58 millimetres, and therefore did not influence the geometrical accuracy, since the error was smaller than the spatial resolution obtainable with the CT and MRI scans. The CT and MRI scans therefore provided sufficiently accurate data from which three-dimensional models of the patellofemoral joint could be accurately constructed.

Milestone 2: Accurate representation and placement of the active and passive stabilisers to improve the biofidelity of the musculoskeletal model. Guidelines for the placement of the passive soft tissue stabilisers (MPFL and lateral retinaculum) were derived from published data on cadaver dissection studies. The patellar attachment of the quadriceps tendon and the attachments of the patellar tendon were identified from the MRI scans of the volunteers. The proximal attachments of the extensor mechanism muscles (RF, VL and VM) and the flexor mechanism muscles (Biceps femoris long and short head, and the Semitendinosus) were derived from McMinn and Hutchings (1988). This ensured repeatability of the placement of soft tissue structures. Unfortunately, only the placement of the patellar tendon and quadriceps tendon was subject-specific, but after comparison with McMinn and Hutchings (1988), the attachments were found to differ minimally.

Milestone 3: Subject-specific body motion simulation to enhance the biofidelity of the musculoskeletal models. The incorporation of the motion recordings enabled the musculoskeletal model to reproduce subject-specific body motion. Hip, knee and ankle flexion were governed by the motion recordings, while rotation among the other joint axes was governed by the muscles of the body. Motion agents controlled the horizontal motion of the pelvis and feet according to the translational measures recorded with the motion capturing system, while translation in the vertical plane was governed by the muscles and gravity. The motion agents' influence on the model was managed by a spring-damper system with which the motion agents were attached to the body. An iterative procedure was followed during which the stiffness and damping was increased to a point during which the model motion was stable.

Milestone 4: The combination of the musculoskeletal simulation results with finite element analyses (FEA) to predict *in-vivo* patellofemoral contact pressure. The musculoskeletal model delivered results in relation to dynamic patellofemoral function, from which patella kinematics and patellofemoral kinetics could be quantified as a function of continuous knee flexion. The finite element technique was employed with the purpose of determining the resulting contact pressure at specific angles of flexion. The patellofemoral posture, as well as the soft tissue stabiliser loads provided the initial and boundary values for the finite element models. The contact pressure could be determined while the dynamic patellofemoral postures were maintained.

The accuracy of the predicted pressures in terms of the actual *in-vivo* values were influenced by the calculated soft tissue stabiliser loads, the simplified material models that were employed, as well as the mesh topology that

was used. The soft tissue stabiliser loads were derived from the spring-damper elements with which the soft tissue stabilisers' function was approximated in the musculoskeletal model. The stiffness values were derived from published values, and the damping constants were chosen iteratively to minimise vibration of the soft tissues. The loading directions were anatomical since the tissues wrapped around the femur. The calculated forces might therefore be different in magnitude from the *in-vivo* values, but the loading directions would be similar.

Both the cartilage and skeletal bone material models were isotropic in nature, with the modulus of elasticity and Poisson values similar to published values. The loading durations were kept below two seconds, and therefore the moisture content of the cartilage needn't be considered (Fernandez *et al.* (2008)). The bone was considered as a homogenous structure, which was a valid approximation because only the cartilage contact pressure and not the bone stresses were of interest.

Convergence studies on the mesh topologies and element sizes showed that the pressure predictions' accuracy would be acceptable (Section 5.3). The predicted pressure values were compared to results from other studies as well as *in-vitro* measurements and found to be of the same order of magnitude. Although this does not prove the capability of the FEA to reproduce *in-vivo* pressure, it gives confidence in the ability of the technique to reproduce values similar to previous published values. The convergence study showed that the technique would produce repeatable estimations, and it would therefore be possible to compare the relative pressures from different loading configurations to one another.

Milestone 5: Validation of the musculoskeletal and finite element model simulation results. Comparison of the musculoskeletal models' patellofemoral posture at 30 degrees flexion to the *in-vivo* postures as determined from the MRI measurements indicated a mean accuracy of 96.9 % with respect to the bisect offset, while the accuracy of the tilt angle was less at 62.1 %. The latter value was expected since the patella tilt angle would be influenced by the coil attached round the knee during the MRI scan. At 30 degrees knee flexion, the patella might not be seated securely in the trochlear groove, possibly leading to the coil changing the tilt angle. This was the case for Volunteer One (31 %) who had a patella tracking on the lateral facet. The accuracy of Volunteers Two and Three's tilt predictions were respectively 71 % and 85 %.

It is difficult to compare the predicted contact loads to that of the *in-vivo* case since it could not be measured. Comparison of the patellofemoral contact load – quadriceps tendon load ratio to published data revealed similar results to that of Fernandez *et al.* (2008). The mediolateral load components in terms of the percentage of the resultant load components were also similar to the results of Powers *et al.* (2006), who reported a maximum percentage of 30 % at full extension which would diminish to 10 % at 60 degrees knee flexion.

The MPFL's tension decreased with knee flexion as was predicted by Bicos *et al.* (2007). The patellar tendon-quadriceps tendon ratio followed a similar trend to that of Fernandez *et al.* (2008), who reported a ratio of one at full extension which diminished with knee flexion to a value of 0.65 at 60 degrees knee flexion. The musculoskeletal model therefore reproduced similar loading trends to that of previous studies, while reproducing subject-specific *in-vivo* patellar kinematics. It could therefore be used as a valid tool in the investigation of dynamic patellofemoral biomechanics.

The finite element analyses produced pressures comparable to previous published values. A mean pressure of 2 MPa was measured during the *in-vitro* study (Appendix A), while Fernandez *et al.* (2008) reported peak pressures to range between 5 and 10 MPa during a stair ascending exercise. Since the patella articulated on the lateral facet, similar maximum pressure values were obtained with the model of Volunteer One (even though the exercise was less demanding). The maximum pressure values of Volunteer Two were within a range of 2 MPa to 5 MPa, comparable to the findings of Elias and Cosgarea (2006). Validation of both the musculoskeletal and FE model results enabled the simulation of clinical procedures to predict the effect of the procedures on the patellofemoral parameters.

Milestone 6: Demonstration of the clinical relevance of the model with two clinical case studies. A tibial tubercle osteotomy was induced in the models of Volunteer One and Volunteer Two. This entailed medialisation of the tibial tubercle by ten millimetres in the coronal plane. The exercises were repeated and revealed a reduction in the contact pressures on the lateral facet of Volunteer One. The MPFL tension was reduced while the effect on the lateral retinaculum was negligible since its primary function was to act as an anterior stabiliser to the patella. The patella was forced to enter the trochlear groove at an earlier flexion angle, increasing patellar stability during flexion. The models revealed that the patient might run a risk of elevated patellofemoral pressures on the medial facet at deeper angles of flexion after the tubercle was medialised. This might give rise to the onset of osteoarthritis.

The results of the osteotomy investigation were compared to published results. A previous study (Fernandez and Hunter (2005)) also investigated the effect of tubercle translation by means of a computational model. The tubercle was medialised and anteriolised (Maquet procedure). A disadvantage of that study was the assumption that the patella kinematics would remain unchanged after the osteotomy, which this study proved to be incorrect. This study is therefore, to the knowledge of the author, one of the first to explore the effect of an osteotomy on the dynamic subject-specific patellofemoral biomechanics and its effect on the peri-patellar structures.

Various knee replacements are available to orthopaedic surgeons. Patellofemoral replacements are ideally more suitable to address patellofemoral disorders, since they replace only the affected area, while the healthy joint remains intact. Different designs have been presented with many studies conducting FEA on the prostheses to

prove their biofidelity. One study also investigated the considerations from a surgical perspective when these prostheses need to be implanted. In this investigation two commercial prostheses were compared to one another in terms of their capability to reproduce normal patellofemoral biomechanics as predicted by the musculoskeletal models.

The results showed that one of the prostheses was superior to the other in terms of its ability to reproduce patella tracking, while reducing the strain on the patella soft tissue stabilisers. It was therefore possible to expose the prostheses to the same boundary and initial values, while testing them in a subject-specific environment. The technique therefore provides the capability to test different prosthesis designs on a patient, enabling a surgeon to identify a suitable candidate before the surgery takes place.

The milestones set out at the start of the research paper have been achieved. A strategy has been established enabling the accurate simulation of an individual's patellofemoral joint as a function of knee flexion. The technique will enable surgeons to gain insight into a patient's patellofemoral biomechanics, thereby identifying possible causes for malfunction. The technique also enables investigation into the outcomes of surgical interventions, by aiding surgeons in identifying possible causes of malfunction, and allowing testing of different treatments on the model before implementation. The next step would be to test this strategy on a patient.

7.2 Limitations

Segmentation of the cartilage from MRI remains problematic, especially in the identification of the patellar cartilage. The procedure is subjective and results may be different for different users. In this study only one person performed the segmentation, and the final models were the product of many segmentation iterations.

The starting posture of the musculoskeletal models at setup was similar to the posture of the volunteers during the CT scan. The posture was then modified to correspond to the volunteer's posture as measured during the start of the motion capturing sequence. During this step, the patella's orientation relative to the trochlear groove was locked to maintain the patellofemoral posture. Only during the first equilibrium analysis was the patella allowed to move to a static equilibrium state. The resulting patellofemoral posture might therefore be different to the *in-vivo* posture when the quadriceps is excited at full extension; firstly because the initial soft tissue stabiliser tensions are determined from the equilibrium analysis, and secondly since the fat pad is not included in the model. It was however shown that the models were able to recover and predict the *in-vivo* posture correctly at 30 degrees knee flexion. It would have been advantageous if more *in-vivo* postures could be measured, but unfortunately this was impossible due to the size of the tunnel in the MRI scanner.

Although the implementation of the Hill-model is advantageous due to its simplicity, the accuracy of its muscle force predictions is not ideal. Perreault *et al.* (2003) investigated the Hill model's ability to predict muscle loads that were also measured experimentally. Their findings showed that a maximum error of 50% occurred at low activation rates. This error was attributed to the model's inability to account for the collaboration between muscle activation and force velocity properties, therefore the magnitudes of the muscle loads might be overestimated.

The Hill-model did however produce more physiologically representative results compared to the simplified spring-damper elements which predicted muscle loads of an order magnitude greater (results not included). This inability to accurately estimate muscle loads was partly overcome by the fact that the generated baseline models, replicated the subject-specific patellofemoral configurations as closely as possible. It was not possible to determine the absolute muscle loads that would occur during the exercise, but muscle loads of different joint configurations can be compared to one another for the same exercise (comparisons on relative loads).

EMG measurements of one volunteer were used for all three volunteers. Since the simulated exercise could be controlled in terms of stance position and the position of the feet, the muscle activation curves would differ minimally between the three volunteers. The effect of this would therefore be negligible in terms of the accuracy of the patellofemoral biomechanics, which is evident in the accuracy of the prediction of the patella kinematics. An improvement to the muscle model would be the addition of calibrated subject-specific EMG recordings.

It would be beneficial if deformable bodies were used during the dynamic contact analysis. This fell outside the scope of this examination, but need to be explored in future. The contact was however improved by means of the damping depth, possibly accounting for the deformability of the cartilage. Soft tissue stabiliser loads could therefore still be used to conduct a finite element analysis on the patellofemoral joint when it consisted of deformable bodies.

Unfortunately the FE solver could not be used to conduct a contact analysis when the mesh was comprised of parabolic elements. The reason for this was probably the contact algorithm used by the solver. It was however proved that the eight node brick elements would produce repeatable results. In order to reproduce the dynamic patellofemoral postures, the patella needed to be constrained in all its degrees of freedom with the exception of the loading direction. This could be avoided if a dynamic FE analysis could be conducted, which was impossible with the available resources.

Another limitation is the implementation of simplified material properties in both the musculoskeletal model and during the FEA. The skeletal bone and cartilage were assumed to be isotropic in nature whereas in reality skeletal bone consists of different zones, exhibiting different elastic moduli. Ligaments and tendons were

approximated with spring-damper systems, while both the soft tissue stabilisers and the cartilage are classified as visco-elastic materials.

7.3 Future work

The current model should be improved in the following ways:

- The ligaments and tendons in the musculoskeletal model should be implemented as deformable bodies approximating the geometry of the actual *in-vivo* tissues and incorporating their viscoelastic nature.
- The material models (bone and cartilage) in the FE model should be improved to enhanced correspondence to the *in-vivo* materials, as described in Section 7.2.
- The cartilage function should be approximated through deformable bodies in the musculoskeletal model.
- The use of parabolic elements in the FEA should be further investigated.
- The proposed strategy should be tested on an actual patient in the following way:
    - A musculoskeletal model should be constructed for the patient using the proposed technique.
    - The malfunction must be identified from the simulation results.
    - Different treatment techniques should be tested.
    - The patient undergoes surgery during which the malfunction will be treated.
    - The patient should be monitored post-operatively to compare the results to the predictions of the musculoskeletal model.

7.4 Contribution to the field

A technique is presented to facilitate analysis of the **dynamic** behaviour of a **subject-specific** patellofemoral joint, providing information on patella kinematics as well as patellofemoral and soft tissue stabiliser kinetics. Orthopaedic surgeons would be able to investigate the impact of a surgical procedure on the joint function by visualising the changes in patella tracking, soft tissue tension and patellofemoral contact loads and pressure. Biomedical engineers can utilise the musculoskeletal model to compare different prosthesis designs to one another while orthopaedic surgeons can determine the optimal positioning of the prosthesis during surgery in order to restore patellofemoral function.

8. References

Äärimaa, V., Ranne, J and Mattila K. *et al.* 2008. Patellar Tendon Shortening after Treatment of Patellar Instability with a Patellar Tendon Medialization Procedure. Scandinavian Journal of Medicine & Science in Sports. 18, pp.442-446.

Ackroyd, C. E., Newman, J. H. and Evand, R. *et al.* 2007. The Avon Patellofemoral Arthroplasty, Five-Year Survivorship and Functional Results. The Journal of Bone and Joint Surgery, Br. 89, pp.310-315.

Adam, F., Pape, D., Kohn, D. and Seil, R. 2002. Length of the Patellar Tendon After Anterior Cruciate Ligament Reconstruction With Patellar Tendon Autograft: A Prospective Clinical Study Using Roentgen Stereometric Analysis. Arthroscopy: The Journal of Arthroscopic and Related Surgery. 18, pp.859-864.

Al-Sayyad, M. and Cameron, J. 2002. Functional Outcome after Tibial Tubercle Transfer for the Painful Patella Alta. Clinical Orthopaedics. 396, pp.152-162.

Amis, A. A., Senavongse, W. and Bull, A. M. W. 2006. Patellofemoral Kinematics during Knee Flexion-Extension: An In vitro Study. Journal of Orthopaedic Research. 24, pp.2201-2211.

Amis, A. A., Senavongse, W. and Darcy, P. 2005. Biomechanics of Patellofemoral Joint Prostheses. Clinical Orthopaedics and Related Research. 436, pp.20-29.

Anderson, F. C. and Pandy, M. G. 2001. Dynamic Optimization of Human Walking. Journal of Biomechanical Engineering. 123, pp.381-390.

Andrikoula, S., Tokis, A., Vasiliadis, H. S., and Georgoulis, A. 2006. The Extensor Mechanism of the Knee Joint: An Anatomical Study. Knee Surgery Sports Traumatol Arthrose. 14, pp.214-220.

Arndt, A. N., Komi, P. V., Brüggemann, G.-P., and Lukkariniemi, J. 1998. Individual Muscle Contributions to the In-vivo Achilles Tendon Force. Clinical Biomechanics. 13, pp.532-541.

Atkinson , T. S., Ewers, B. J., and Haut, R. C. 1999. The Tensile and Stress Relaxation Response of Human Patellar Tendon Varies with Specimen Cross-Sectional Area. Journal of Biomechanics. 32, pp.907-914.

Au, A. G., Raso, V. J., and Liggons, A. B. *et al.* 2005. A Three-Dimensional Finite Element Stress Analysis for Tunnel Placement and Buttons in Anterior Cruciate Ligament Reconstructions. Journal of Biomechanics. 38, pp.827-832.

Baker, M. J. 2009. Maths - Transformations using Quaternions. [online]. [Accessed 13 10 2009]. Available form World Wide Web: <http://www.euclideanspace.com/maths/algebra/realNormedAlgebra/quaternions/transforms/ index.htm>

Baldwin, M. A., Chaddclary, C., Maletsky, L. P. and Rullkoetter, P. J. 2009. Verification of Predicted Specimen-Specific Natural and Implanted Patellofemoral Kinematics during Simulated Deep Knee Bend. Journal of Biomechanics. 42, pp.2341-2348.

Barink, M., Van Kampen, A., De Waal Malefijt, M. and Verdonschot, N. 2005. A Three-Dimensional Dynamic Finite Element Model of the Prosthetic Knee Joint: Simulation of Joint Laxity and Kinematics. Proceedings of the Institution of Mechanical Engineers, Part H: Journal of Engineering in Medicine. 219, pp.415-542.

Basso, O., Johnson, D. P. and Amis, D. P. 2001. The Anatomy of the Patellar Tendon. Knee Surgery, Sports Traumatology and Arthroscopy. 9, pp.2-5.

Besier, T. F., Gold, D. E., Beaupré, G. S. and Delp, S. L. 2005. A Modeling Framework to Estimate Patellofemoral Joint Cartilage Stress In vivo. Medicine and Science in Sports and Exercise. 37(1), pp.1924-1930.

Bicos, J., Fulkerson, J. P., and Amis, A. A. 2007. The Medial Patellofemoral Ligament. American Journal of Sports Medicine. 35, pp.484-492.

Biedert, R. and Albrecht, S. 2006. The Patellotrochlear Index: A New Index for Assessing Patellar height. Knee Surgery, Sports Traumatology and Arthroscopy. 14, pp.707-712.

Boresi, A. P. and Schmidt, R. J. 2003. Contact Stresses. In: Hayrton, J., (ed). Advanced Mechanics of Material, New York: Wiley & Sons Inc., pp.589-623.

Budynas, R. G. and Nisbett, J. K. 2008. Load and Stress Analysis. In: Holman, J. P. and Lloydd, J. R., (eds). Shigley's Mechanical Engineering Design, Eighth International Edition, New York: McGraw Hill, pp.68-139.

Bull, A. M. J., Earnshaw, P. H., and Smith, A. *et al.* 2002. Intraoperative Measurement of Knee Kinematics in Reconstruction of the Anterior Cruciate Ligament. The Journal of Bone and Joint Surgery - British Edition. 84, pp.1075-1081.

Carmont, M. R. and Maffulli, N. 2007. Medial Patellofemoral Ligament Reconstruction: a New Technique. BMC Musculoskeletal Disorders. 8, p.nr 22.

Cerulli, G., Benoit, D. L., and Lamontagne, M. *et al.* 2003. In-vivo Anterior Cruciate Ligament Strain Behaviour During a Rapid Deceleration Movement: Case Report. Knee Surgery, Sports Traumatology and Arthroscopy. 11, pp.307-311.

Chrisman, O. D., Snook, G. A., and Wilson, T. C. 1979. A Long-Term Prospective Study of the Hauser and Roux-Goldthwait Procedures for Recurrent Patellar Dislocation. Clinical Orthopaedics and Related Research. 144, pp.27-30.

Cloete, T. and Scheffer, C. 2008. Benchmarking of a Full-body Inertial Motion Capture System for Clinical Gait Analysis. In: 30th Annual International IEEE EMBS Conference, 2008. Vancouver, British Columbia, Canada: IEEE EMBS, pp.4579-4582.

Cohen, Z. A., Roglic, H., and Grelsamer, R. P. *et al.* 2001. Patellofemoral Stresses during Open and Closed Kinetic Chain Exercises: An Analysis using Computer Simulation. The American Journal of Sports Medicine. 29(4), pp.480-487.

Cosgarea, A. J., Schatzke, M. D., Seth, A. K., and Litsky, A. S. 1999. Biomechanical Analysis of Flat and Oblique Tibial Tubercle Osteotomy for Recurrent Patellar Instability. The American Journal of Sports Medicine. 27, pp.507-512.

Cox, J. S. 1982. Evaluation of the Roux-Elmslie_Trillat Procedure for Knee Extensor Realignment. American Journal of Sports Medicine. 10, pp.303-310.

Cram, J. R. and Kasman, G. S. 1998. Electrode Placements. In: Colilla, J., (ed). Introduction to Surface Electromyography, Gaithersburg: Aspen Publishers Inc, pp.360-366.

D'Lima, D. D., Chen, P. C., Kester, M. A., and Colwell JR., C. W. 2003. Impact of Patellofemoral Design on Patellofemoral Forces and Polyethylene Stresses. The Journal of Bone and Joint Surgery, American edition. 85, pp.85-93.

Daintith, J. 2004. A Dictionary of Computing. [online]. [Accessed 2 February 2010]. Available form World Wide Web: <http://www.encyclopedia.com/doc/1O11-Coonspatch.html>

Dao, T. T., Marin, F., and Christine, M. 2009. Sensitivity of the Anthropometrical and Geometrical Parameters of the Bones and Muscles on a Musculoskeletal Model of the Lower Limbs. In: I. EMBS, (ed). 31st Annual International Conference of the IEEE EMBS, 2009. Minneapolis, Minnesota, USA: IEEE EMBS, pp.5251-5254.

De Luca, C. J. and Contessa, P. 2009. A Muscle-Force Model with Physiological Bases. In: XXII Congress of the International Society of Biomechanics, 2009. Cape Town, South Africa: International Society of Biomechanics.

Defrate, L. E., Nha, K. W., and Papanagari, R. *et al.* 2007. The Biomechanical Function of the Patellar Tendon during In-vivo Weight-bearing Flexion. Journal of Biomechanics. 40, pp.1716-1722.

Dejour, H., Walch, G. and Nove-Josserand, L. 1994. Factors of Patellar Instability: An Anatomic Radiographic Study. Knee Surgery, Sports Traumatology and Arthroscopy. 2, pp.19-26.

Delp, S. L., Loan, J. P., and HOY, M. G. *et al.* 1990. An Interactive Graphics-based Model of the Lower Extremity to Study Orthopaedic Surgical Procedures. IEEE Transactions on Biomedical Engineering. 37(8), pp.757 - 767.

Dennis, D. A., Komistek, R. D., Hoff, W. A. and Gabriel, S. M. 1996. In-vivo Knee Kinematics Derived Using an Inverse Perspective Technique. Clinical Orthopaedic and Related Research. 331, pp.107-117.

Dillon, E. M., Erasmus, P. J., and Muller, J. H. *et al.* 2008. Differential Forces Within the Proximal Patellar Tendon as an Explanation for the Characteristic Lesion of Patellar Tendinopathy. An In Vivo Descriptive Experimental Study. The American Journal of Sports Medicine. 36, pp.2119-2127.

Dimitrova, N. A. and Dimitrov, G. V. 2006. Electromyography (EMG) Modelling. In: Akay, M., (ed). Wiley Encyclopedia of Biomedical Engineering - Volume 2, Hoboken, New Jersey: John Wiley and Sons, pp.1397-1416.

Eckhoff, D. G., Montgomery, W. K., Kilcoyne, R. F., and Stamm, E. R. 1994. Femoral Morphometry and Anterior Knee Pain. Clinical Orthopaedics and Related Research. 302, pp.64-68.

Eisenhuth, S. A., Saleh, K. J., CUI, Q. J., and CLARK, C. R. B. T. E. 2006. Patellofemoral Instability after Total Knee Arthroplasty. Clinical Orthopaedics and Related Research. 446, pp.149-160.

Elias, J. J. and Cosgarea, A. J. 2006. Technical Errors during Medial Patellofemoral Ligament Reconstruction could Overload Medial Patellofemoral Cartilage. American Journal of Sports Medicine. 34, pp.1478-1485.

Elias, J. J., Kilambi, S., and Cosgarea, A. J. 2010. Computational Assessment of the Influence of Vastus Medialis Obliquus Function on Patellofemoral Pressures: Model evaluation. Journal of Biomechanics. 43, pp.612-617.

Elias, J. J., Wilson, D. R., Adamson, R., and Cosgarea, A. J. 2004. Evaluation of a Computational Model Used to Predict the Patellofemoral Contact Pressure Distribution. Journal of Biomechanics. 37, pp.295-302.

Erdemir, A., Piazza, S. J, and Sharkey, N. A. 2002. Influence of Loading Rate and Cable Migration on Fiberoptic Measurement of Tendon Force. Journal of Biomechanics. 35, pp.857-862.

Farrar, M. J., Newman, R. J., Mawhinney, R. R., and KING, R. 1999. Computed Tomography Scan Scout Film for Measurement of Femoral Axis in Knee Replacement. The Journal of Arthroplasty. 14, pp.1030-1031.

Feller, J. A., Amis, A. A., and Andrish, J. T. *et al.* 2007. Surgical Concepts of the Patellofemoral Joint. Arthroscopy: The Journal of Arthroscopic and Related Surgery. 23, pp.542-553.

Fernandez, J. W., Akbarshahi, M., Kim, H. J., and Pandy, M. G. 2008. Integrating Modelling, Motion Capture and X-ray Fluoroscopy to Investigate Patellofemoral Function During Dynamic Activity. Computer Methods in Biomechanics and Biomedical Engineering. 11, pp.41-53.

Fernandez, J. W. and Hunter, P. J. 2005. An anatomical Based Patient-specific Finite Element Model of Patella Articulation: Towards a Diagnostic Tool. Biomechanics and Modeling in Mechanobiology. 2005(4), pp.20-38.

Finni, T., Komi, P. J., and Lukkariniemi, J. 1998. Achilles Tendon Loading During Walking: Application of a Novel Optic Fiber Technique. European Journal of Applied Physiology. 77, pp.289-291.

Freeman, M. A. R. and Pinskerova, V. 2005. The Movement of the normal Tibiofemoral Joint. Journal of Biomechanics. 38, pp.197-208.

Fulkerson, J. P. 1983. Anteromedialization of the Tibial Tuberosity for Patellofemoral Malalignment. Clinical Orthopaedics and Related Research. 177, pp.176-181.

Fulkerson, J. P., Becker, G. J., and Meaney, J. A. *et al.* 1990. Anteromedial Tibial Tubercle Transfer without Bone Graft. American Journal of Sports Medicine. 18, pp.490-497.

Gray, H. 1918. Osteology, The Patella. In: Anatomy of the Human Body, Philadelphia: Lea & Febiger, pp.191-192.

Guo, X. E. 2001. Mechanical Properties of Cortical Bone and Cancellous Bone Tissue. In: S. C. COWIN, (ed). Bone Mechanics Handbook, 2nd Edition, Florida: CRC Press, p.10.8.

Hamill, J. and Knutzen, K. 2009. In: T. EDITION, (ed). Biomechanical Basis of Human Movement, Lippincott, Williams & Wilkins, p.210.

Hansen, P., Bojsen-Moller, J., and Aagaard, P. *et al.* 2006. Mechanical Properties of the Human Patellar Tendon, In-vivo. Clinical Biomechanics. 21, pp.54-58.

Hashemi, J., Chandrashekar, N., and Slauterbeck, J. 2005. The Mechanical Properties of the Human Patellar Tendon are Correlated to its Mass Density and are Independent of Sex. Clinical Biomechanics. 20, pp.645-652.

Brechter, H. J., Powers, C. M., and Terk, M. R. *et al.* 2003. Quantification of Patellofemoral Joint Contact Area using Magnetic Resonance Imaging. Magnetic Resonance Imaging. 21, pp.955-959.

Herrington, L. and Al-Shehri, A. S. 2006. Comparison of Single and Multiple Joint Quadriceps Exercise in Anterior Knee Pain Rehabilitation. Physical Therapy in Sport. 7, pp.171-180.

Herrington, L., McEwan, I., and Thom, J. 2006. Quantification of Patella Position by Ultrasound Scanning and its Criterion Validity. Ultrasound in Medicine & Biology. 32(12), pp.1833-1836.

Herzog, W. 2006. Articular Cartilage. In: Akay, M., (ed). Wiley Encyclopedia of Biomedical Engineering: Volume 1, Hoboken, New Jersey: John Wiley & Sons, pp.121 - 130.

Herzog, W. and Read, L. J. 1993. Lines of Action and Moment Arms of the Major Force-Carrying Structures Crossing the Human Knee. Journal of Anatomy. 182, pp.213-230.

Heunis, P. D. 2008. Final year project report: In vitro Knee Fitting Frame. Department of Mechanical and Mechatronic Engineering, Stellenbosch University.

Hill, A. V. 1938. The Heat of Shortening and the Dynamic Constants of Muscle. Proceedings of the Royal Society of Biological Sciences. 126, pp.136-195.

Hirokawa, S. 1991. Three-dimensional mathematical model analysis of the patellofemoral joint. Journal of Biomechanics. 24, pp.659-671.

Hollinghurst, D., Stoney, J., and Ward, T. *et al.* 2007. In vivo Sagittal Plane Kinematics of the AVON Patellofemoral Arthrosplasty. Journal of Arthroplasty. 22, pp.117-123.

Hornak, J. P. 2008. The Basics of MRI. [online]. [Accessed 3 September 2009]. Available form World Wide Web: <http://www.cis.rit.edu/htbooks/mri/>

Insall, J., Salvati, E., and Goldberg, V. 1972. Recurrent Dislocation and High-Riding Patella. Clinical Orthopaedics and Research. 88, p.67.

INSTITUTE, S. C. O. 2008. Total Knee Replacement. [online]. [Accessed 26 01 2010]. Available form World Wide Web: <http://www.scoi.com/tkr.htm>

Kapandji, A. 2007. You said biomechanics? It's 'fuzzy' mechanics! [online]. [Accessed 26 August 2009]. Available form World Wide Web: <http://www.maitrise-orthop.com/corpusmaitri/orthopaedic/mo64_fuzzy_mechanics/>

Katchburian, M. V., Bull, A. M. J., and Shih, Y.-F. *et al.* 2003. Measurement of Patellar Tracking: Assessment and Analysis of the Literature. Clinical Orthopaedics and Related Research. 412, pp.241-259.

Koëter, S., Diks, M. J. F., Anderson, P. G., and Wymenga, A. B. 2007. A Modified Tibial Tubercle Osteotomy for Patella Maltracking. The Journal of Bone and Joint Surgery, B. 89, pp.180-185.

Komistek, R. D., Douglas, D., and Mohamed, M. 2003. In-vivo Fluoroscopic Analysis of the Normal Knee. Clinical Orthopedics. 410, pp.69-81.

Koo, S., Gold, G. E., and Andriachi, T. P. 2005. Considerations in Measuring Cartilage Thickness using MRI: Factors Influencing Reproducibility and Accuracy. OsteoArthritis and Cartilage. 13, pp.782-789.

Kuroda, R., Kambic, H., Valdevit, A., and Andrish, J. T. 2001. Articular Cartilage Contact Pressure after Tibial Tuberosity Transfer. The American Journal of Sports Medicine. 29, pp.403-409.

Lancaster, A. R., Nyland, J., and Robert, C. S. 2007. The Validity of the Motion Palpation Test for Determining Patellofemoral Joint Articular Cartilage Damage. Physical Therapy in Sport. 8, pp.59-65.

Laprade, R. F., Engebretsen, A. H., and Ly, T. V. *et al.* 2007. The Anatomy of the Medial Part of the Knee. The Journal of Bone and Joint Surgery. 89, pp.2000-2010.

Laprade, R. F., Morgan, P. M., and Wentorf, F. A. *et al.* 2007. The Anatomy of the Posterior Aspect of the Knee. An Anatomic Study. Journal of Bone and Joint Surgery, Br. 89, pp.758 - 764.

Laz, P. J., Pal, S., and Fields, A. *et al.* 2006. Effects of Knee Simulator Loading and Alignment Variability on Predicted Implant Mechanics: A Probabilistic Study. Journal of Orthopaedic Research. 24, pp.2212-2221.

Lee, T. Q., Yang, B. Y., Sandusky, M. D., and McMahon, P. J. 2001. The Effects of Tibial Rotation on the Patellofemoral Joint: Assessment of the Changes in In-situ Strain in the Peripatellar Retinaculum and the Patellofemoral Contact Pressures and Areas. Journal of Rehabilitation Research and Development. 38, pp.463-469.

Li, G., Defrate, L. E., and Zayontz, S. *et al.* 2004. The effect of tibiofemoral joint kinematics on patellofemoral contact pressures under simulated muscle loads. Journal of Orthopaedic Research. 22, pp.801-806.

LifeModeler. 2008. Contacts. [online]. [Accessed 14 05 2010]. Available form World Wide Web: <http://www.lifemodeler.com/LM_Manual/modeling_contact.shtml>

LifeModeler. 2008. Joints. [online]. [Accessed 14 05 2010]. Available form World Wide Web: <http://www.lifemodeler.com/LM_Manual/modeling_joints.shtml>

LifeModeler. 2008. Motion. [online]. [Accessed 14 05 2010]. Available form World Wide Web: <http://www.lifemodeler.com/LM_Manual/modeling_motion.shtml#j2>

LifeModeler. 2008. Muscle formulation. [online]. [Accessed 14 05 2010]. Available form World Wide Web: <http://www.lifemodeler.com/LM_Manual/A_musclesform.shtml>

Lin, F., Makhsous, M., and Chang, A. H. *et al.* 2003. In-vivo and Non-invasive Six Degree of Freedom Patellar Tracking During Voluntary Knee Movement. Clinical Biomechanics. 18, pp.401-409.

Lloyd, D. G. and Besier, T. F. 2003. An EMG-driven Musculoskeletal Model to Estimate Muscle Forces and Knee Joint Moments In-vivo. Journal of Biomechanics. 36, pp.765-776.

Lu, D., Bai, E.-W., and Wang, G. 2006. Computed Tomography. In: Akay, M., (ed). Wiley Encyclopedia of Biomedical Engineering - Volume 2, Hoboken, New Jersey: John Wiley and Sons, pp.940-952.

MacIntyre, N. J., Hill, N. A., and Fellows, R. A. *et al.* 2006. Patellofemoral Joint Kinematics in Individuals with and without Patellofemoral Pain Syndrome. The Journal of Bone and Joint Surgery, Am. 88, pp.2596-2605.

Martini, F. H. and Bartholomew, E. F. 2003. The Muscular System. In: Snavely, S. L., (ed). Essentials of Anatomy and Physiology, Third Edition, Upper Saddle River, New Jersey: Prentice Hall, pp.177-223.

Martino, F., De Serio, A., and Macarini, L. *et al.* 1998. Ultrasonography versus Computed Tomography in Evaluation of the Femoral Trochlear Groove Morphology: a Pilot Study on Healthy, Young Volunteers. European Radiology. 8, pp.244-247.

McMinn, R. M. H. and Hutchings, R. T. 1988. A Colour Atlas of Human Anatomy, 2nd edition. London: Wolfe Medical Publications.

Merican, A. and Amis, A. A. 2008. Anatomy of the Lateral Retinaculum of the Knee. The Journal of Bone and Joint Surgery - British Volume. 90-B, pp.527-534.

Mesfar, W. and Shirazi-Adl, A. 2005. Biomechanics of the Knee Joint in Flexion under Various Quadriceps Forces. The Knee. 12, pp.424-434.

Mesfar, W. and Shirazi-Adl, A. 2008. Computational Biomechanics of Knee Joint in Open Kinetic Chain Extension Exercises. Computer Methods in Biomechanics and Biomedical Engineering. 11(1), p.55–61.

Mesfar, W. and Shirazi-Adl, A. 2006. Knee Joint Mechanics Under Quadriceps-Hamstrings Muscle Forces are Influenced by Tibial Restraint. Clinical Biomechanics. 21, pp.841-848.

Mountney, J., Senavongse, W., Amis, A. A., and Thomas, N. P. 2005. Tensile Strength of the Medial Patellofemoral Ligament Before and After Repair or Reconstruction. Journal of Bone and Joint Surgery. 87, pp.36-40.

Mow, V. C., Teshian, G. A., and Spilker, R. L. 1993. Biomechanics of Diarthrodial Joints: A Review of Twenty Years of Progress. Journal of Biomechanical Engineering. 115, pp.460-467.

Mullaji, A. B., Marawar, S. V. and Mittal, V. 2009. A Comparison of Coronal Plane Axial Femoral Relationships in Asian Patients With Varus Osteoarthritic Knees and Healthy Knees. The Journal of Arthroplasty. 24, pp.861-867.

Muller, J. H., Scheffer, C., and Elvin, A. 2008. In-vivo Detection of Patellar Tendon Creep using a Fibre-optic Sensor. International Journal of Medical Engineering and Informatics. 1, pp.155-173.

Myers, J. L. and Well, A. D. 2003. Research Design and Statistical Analysis (second edition ed.). Philadelphia: Lawrence Erlbaum.

Nicol, C. and Komi, P. V. 1999. Quantification of Achilles tendon force enhancement by passively induced dorsiflexion stretches. Journal of Applied Biomechanics. 15, pp.221-232.

Ostermeier, S., Holst, M., and Bohnsak, M. *et al.* 2007. Dynamic Measurement of Patellofemoral Contact Pressure following Reconstruction of the Medial Patellofemoral Ligament: An In Vitro Study. Clinical Biomechanics. 22, pp.327-335.

Perreault, E. J., Heckman, C. J., and Sandercock, T. G. 2003. Hill Muscle Model Errors during Movement are Greatest within the Physiologically Relevant Range of Motor Unit Firing Rates. Journal of Biomechanics. 36, pp.211-218.

Pourcelot, P., Defontaine, M., and Ravary, B. *et al.* 2005. A Non-invasive Method for Tendon Force Measurement. Journal of Biomechanics. 38, pp.2124-2129.

Powers, C. M., Chen, Y.-J., Farrokhi, S., and Lee, T. Q. 2006. Role of Peripatellar Retinaculum in Transmission of Forces within the Extensor Mechanism. The Journal of Bone and Joint Surgery. 88 A, pp.2042-2048.

Powers, C. M., Chen, Y.-J., Scher, I., and Lee, T. Q. 2006. The Influence of Patellofemoral Joint Contact Geometry on the Modeling of Three Dimensional Patellofemoral Joint Forces. Journal of Biomechanics. 39, pp.2783-2791.

Radon, J. 1917. Über die Bestimmung von Funktionen durch ihre Integralwerte längs gewisser Mannigfaltigkeiten. Berigte Sächsische Akademie der Wissenscahfte. 69, pp.262-267.

Ramappa, A. J., Apreleva, M., and Harrold, F. R. *et al.* 2006. The Effects of Medialization and Anteromediaization of the Tibial Tubercle on Patellofemoral Mechanics and Kinematics. The American Journal of Sports Medicine. 34, pp.749-756.

Rawlison, J. J., Furman, B. D., and Li, S. *et al.* 2006. Retrieval, Experimental, and Computational Assessment of the Performance of Total Knee Replacements. Journal of Orthopaedic Research. 24, pp.1384-1394.

Sanchez, A. R., Sugalski, M. T., and Laprade, R. F. 2006. Anatomy and Biomechanics of the Lateral Side of the Knee. Sports Medicine Arthroscopy Rev. 14, pp.2-11.

Sandwell, D. T. 1987. Biharmonic Spline Interpolation of GEOS-3 and SEASAT Altimeter Data. Geophysical Research Letter. 14, pp.139-142.

Seebacher, J. R., Inglis, A. E., Marshall, J. L., and Warren, R. F. 1982. The structure of the posterolateral aspect of the knee. Journal of Bone and Joint Surgery, Am. 64, pp.536-541.

Seisler, A. R. and Sheehan, F. T. 2007. Normative Three-Dimensional Patellofemoral and Tibiofemoral Kinematics: A Dynamic, in Vivo Study. IEEE Transactions on Biomedical Engineering. 54, pp.1333-1341.

Shih, Y.-F., Bull, A. M. J., McGreggor, A. H., and Amis, A. A. 2004. Active Patellar Tracking Measurement: A Novel Device Using Ultrasound. American Journal of Sports Medicine. 32, pp.1209-1217.

Shih, Y.-F., Bull, A. M. J., and McGreggor, A. H. *et al.* 2003. A Technique for the Measurement of Patellar Tracking during Weight-bearing Activities using Ultrasound. Proceedings for the Institution for Mechanical Engineers. 217, pp.449-457.

Shirazi-Adl, A. and Mesfar, W. 2007. Effect of Tibial Tubercle Elevation on Biomechanics of the entire Knee Joint under Muscle Loads. Clinical Biomechanics. 22, pp.344-351.

Sisto, V. J. and Sarin, V. K. 2006. Custom Patellofemoral Arthroplasy of the Knee. The Journal of Bone and Joint Surgery, Am. 88, pp.1475-1480.

Smidt, G. L. 1973. Biomechanical Analysis of Knee Flexion and Extension. Journal of Biomechanics. 6, pp.79-92.

Smirk, C. and Morris, H. 2003. The Anatomy and Reconstruction of the Medial Patellofemoral Ligament. The Knee. 10, pp.221-227.

Souza, R. B. and Powers, C. M. 2008. Predictors of Hip Internal Rotation During Running. The American Journal of Sports Medicine. 37, pp.579-587.

Stasiulaitis, P. and Eidukynas, V. 2006. 3D human Gait Modelisation and Analysis. In: Mechanika 2006. Proceedings of the 11th International Conference, 2006. Kaunas, Lithuania: Kaunas University of Technology, Kaunas, Lithuania, pp.324-329.

Staubli, H. U., Durrenmatt, U., Porcellini, B., and Rauschning, W. 2001. Articular Cartilage Surfaces and Osseous Anatomy of the Patellofemoral Joint in the Axial Plane. Sports Medicine and Arthroscopy Review. 9, pp.282-287.

Steensen, R. N., Dopirak, R. M., and MacDonald, W. G. 2004. The Anatomy and Isometry of the Medial Patellofemoral Ligament: Implications for Reconstruction. American Journal of Sports Medicine. 32, pp.1509-1513.

Stoutenberg, M., Pluchino, A. P., and Ma, F. *et al.* 2005. The Impact of Foot Position on Electromyographical Activity of the Superficial Quadriceps Muscles During Leg Extension. Journal of Strength and Conditioning Research. 19, pp.931-938.

Strecker, W., Leppler, P., Gebhard, F., and Kinzl, L. 1997. Length and torsion of the lower limb. The Journal of Bone and Joint Surgery, Br. 79, pp.1019-1023.

Teichtahl, A. J., Parkins, K., and Hanna, F. *et al.* 2007. The relationship between the angle of the trochlear groove and patella cartilage and bone morphology e a cross-sectional study of healthy adults. OsteoArthritis and Cartilage. 15, pp.1158-1162.

Towe, B. C. 2003. Bioelectricity and its Measurement. In: Kutz, M., (ed). Standard Handbook of Biomedical Engineering and Design, New York: McGraw-Hill, pp.17.42-17.45.

Van Schalkwyk, E. P. 2010. Thesis: Determining Femoral Component Goodness-of-Fit using Computer Segmentation and Numerical Simulation. Department of Mechanical and Mechatronic Engineering, Stellenbosch University.

Vining, G. G. 1998. Data Displays. In: Kugshev, A., and Hinrichs, C., (eds). Statistical methods for engineers, Pacific Grove, California: Duxbury Press, pp.42-49.

Von Eisenhart-Rothe, R., Siebert, M., and Bringmann, C. *et al.* 2004. A New In vivo Technique for Determination of 3D Kinematics and Contact Areas of Patellofemoral and Tibio-femoral Joint. Journal of Biomechanics. 37, pp.927-934.

Von Eisenhart-Rothe, R., Vogl, T., Eenglmeierd, K.-H., and Graichen, H. 2007. A new in vivo technique for determination of femoro-tibial and femoro-patellar 3D kinematics in total knee arthroplasty. Journal of Biomechanics. 40, pp.3079 - 3088.

Ward, S. R., Terk, M. R., and Powers, C. M. 2007. Patella Alta: Association with Patellofemoral Alignment and Changes in Contact Area During Weight-Bearing. Journal of Bone and Joint Surgery - American Edition. 89, pp.1749-1755.

Wilson, N. A., Press, J. M., and Koh, J. L. *et al.* 2009. In Vivo Noninvasive Evaluation of Abnormal Patellar Tracking During Squatting in Patients with Patellofemoral Pain. The Journal of Bone and Joint Surgery. 91, pp.558-566.

Withrow, T. J., Huston, L. J., Wojtys, E. M., and Ashton-Miller, J. A. 2006. The Effect of an Impulsive Knee Valgus Moment on In-vitro Relative ACL Strain During a Simulated Jump Landing. Clinical Biomechanics. 21, pp.977-983.

Woo, S.-Y., Debski, R. E., Withrow, J. D., and Janaushek, M. A. 1999. Biomechanics of Knee Ligaments. The American Journal of Sports Medicine. 27, pp.532-543.

Yamada, Y., Toritsuka, Y., and Horibe, S. *et al.* 2007. In Vivo Movement Analysis of the Patella using a Three-Dimensional Computer Model. The Journal of Bone and Joint Surgery - B. 89, pp.752-760.

Zavatsky, A. B., Oppolt, P. T., and Price, A. J. 2004. Simultaneous In Vitro Measurement of Patellofemoral Kinematics and Forces. Journal of Biomechanical Engineering. 126, pp.351-356.

Zhang, L.-Q., Nuber, G., and Butler, J. *et al.* 1998. In-vivo Human Knee Joint Dynamic Properties as Functions of Muscle Contraction and Joint Position. Journal of Biomechanics. 31, pp.71-76.

Appendices

Appendix A: In-vitro patellofemoral loading in a custom-built knee loading frame

A.1 Background

A test frame was designed and built with which patellofemoral function on a cadaver could be simulated while the extensor-mechanism was under load. The purpose of this study was to obtain data on patella tracking and patellofemoral contact pressures. This could be used for validation of the musculoskeletal and finite element simulation results. A pulley-weight system was used to tension the quadriceps muscles in their physiological directions. Knee flexion was established by constraining the femur and flexing the tibia by hand.

A.2 Experimental procedure

A.2.1 Dissection

After removal of the skin and superficial fat tissue from the thawed cadaver leg, the quadriceps muscles were isolated into the vastus lateralis group, the rectus femoris and vastus intermedius group, and the vastus medialis group. A gauze noose was stitched to each muscle group, and a cable carrying weight was attached to the noose, forming the pulley-weight system, (Figure A.1). Before the patella was split into a medial and a lateral part, two three millimetre holes were drilled from the medial border in a mediolateral direction in the proximal and distal halves, (Figure A.2). An oscillating saw was used to cut through the patella bone, after which the cartilage layer was split with a scalpel. This ensured a smooth cut. Two self tapping screws (five millimetres in diameter) were used to fix the medial halve to the lateral halve.

Figure A.1: Gauze noose stitched to muscles.

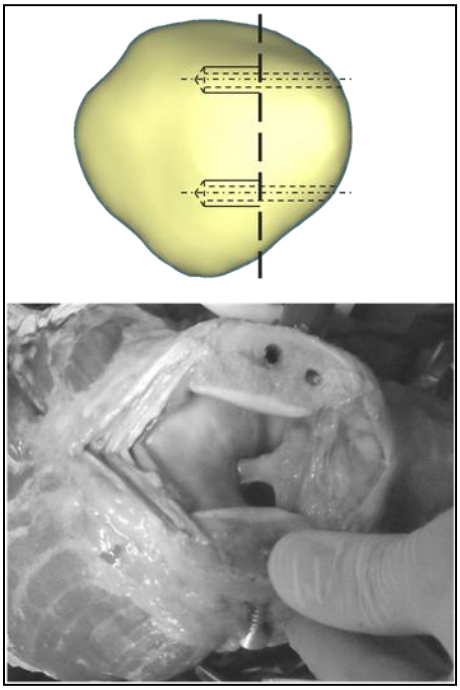

Figure A.2: Right patella with the cut plane.

A.2.2 Setup and test procedure

A customised intercondylar rod[*****] was inserted into the femoral shaft and fixed in place with an adhesive (Pratley putty, Pratley Group South Africa). The intercondylar rod was then fitted into a slot on the test frame. The pulleys were repositioned to ensure that the muscle loading directions remained in the correct physiological orientations. Inertial orientation sensors (Xsens Technologies, Enschede, The Netherlands) were fixed to the femur, patella and tibia, which provided patella orientation recordings as a function of knee flexion (Figure A.3). The loads could then be applied, after which the knee was flexed.

After completion of the dynamic measurements, the loads were removed, and the tibia was fixed at discrete flexion angles. At each flexion angle, a pre-scale pressure film (Tekscan, Inc., South Boston, Massachusetts) was inserted into the patellofemoral joint and the load was reapplied (Figure A.4). Pressure readings were obtained at 30, 45, 60, and 90 degrees knee flexion.

[*****] Mild steel rod having a diameter equal to ten millimetres

Figure A.3: Inertial orientation sensors.

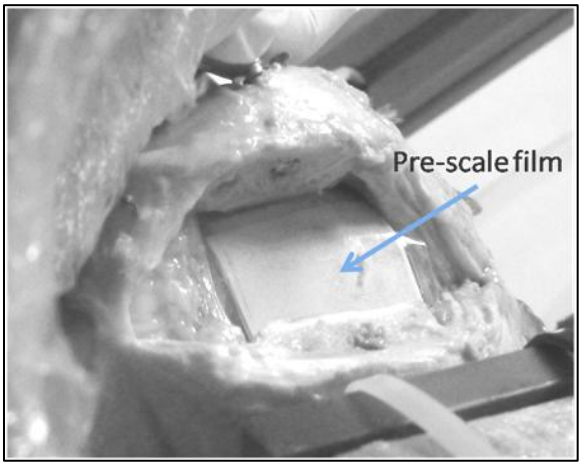

Figure A.4: Pre-scale film inserted in between the patella and femur.

A.3 Results

As the knee was flexed from full extension to 90 degrees flexion, the patella flexion lagged knee flexion (Figure A.5), while it tilted laterally (Figure A.6). Patella spin was found to be irregular, (Figure A.7). At 30 degrees knee flexion, the patellofemoral contact occurred on the lateral patella facet. The contact shifted from the lateral facet to be on both the lateral and medial facets from 45 degrees onwards. The contact pressure increased as the flexion angle was increased, with the maximum pressure (between 2.5 and 3 MPa) occurring on the lateral side at 90 degrees knee flexion (Figure A.8).

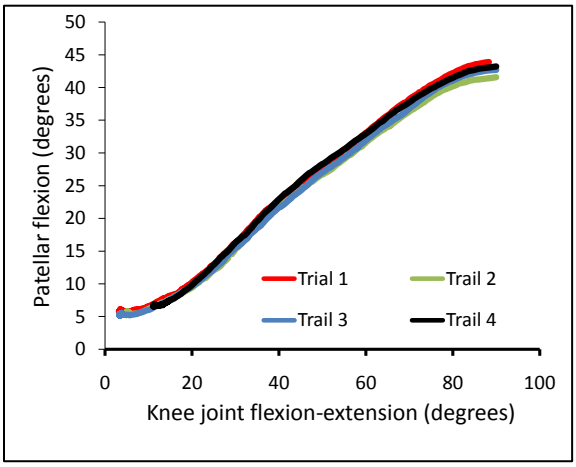

Figure A.5: Patella flexion (Adopted from Heunis (2008))

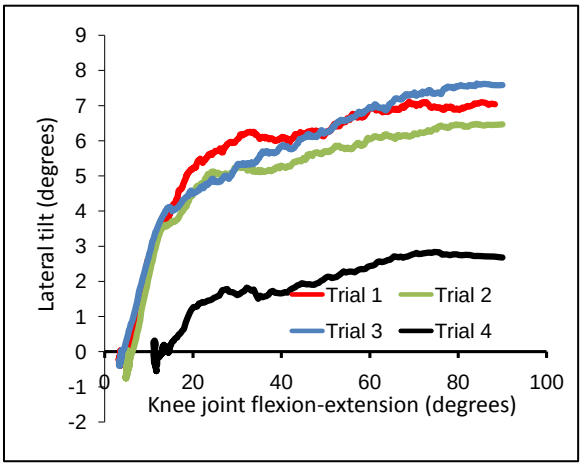

Figure A.6: Patella tilt (Adopted from Heunis (2008)).

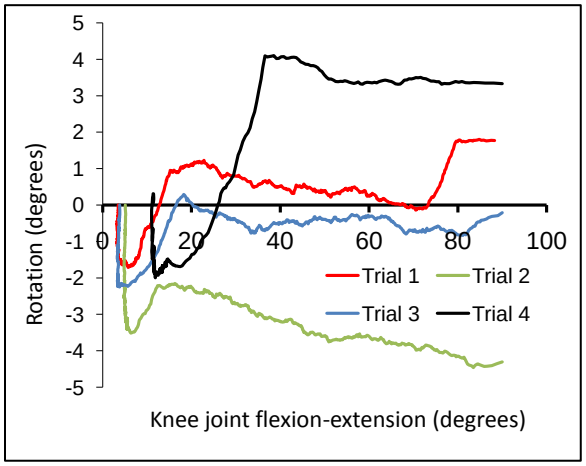

Figure A.7: Patella rotation (Adopted from Heunis (2008)).

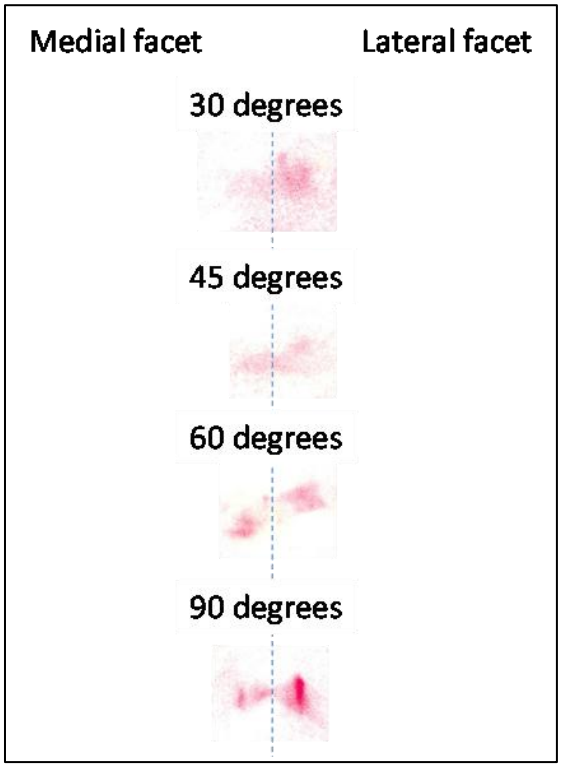

Figure A.8: Pre-scale film measurements.

A.4 Conclusion

A test frame was designed and built which enabled the patellofemoral joint to be studied while the extensor mechanism was loaded. Patella tracking was monitored by measuring patella orientation as a function of knee flexion. Patellofemoral contact pressure readings were obtained at discrete knee flexion angles with the aid of pre-scale pressure sensitive film. The kinematic measurements concur with the findings of Amis *et al.* (2006). During the fourth trial, the extensor mechanism started to tear, which lead to the decreased lateral tilt measure in Figure A.6.

The pressure readings relate well to the findings of Hirokawa (1991). There is some controversy with regards to the contact pressure as a function of knee flexion (Mesfar and Shirazi-Adl (2005)). In this study, the contact pressure increased with knee flexion. Hirokawa (1991) found a similar result, but after 90 degrees knee flexion, the pressure decreased. Elias and Cosgarea (2006) found the pressure to increase up to 50 degrees knee flexion, after which it stayed constant up to 60 degrees and increasing again up to 90 degrees knee flexion. Ostermeier *et al.* (2007) on the other hand indicated a decreasing patellofemoral pressure from full extension to 40 degrees knee flexion, and an increasing pressure from 70 degrees onwards.

Appendix B: Calculation of coronal and transverse orientation of a segment in three-dimensional space

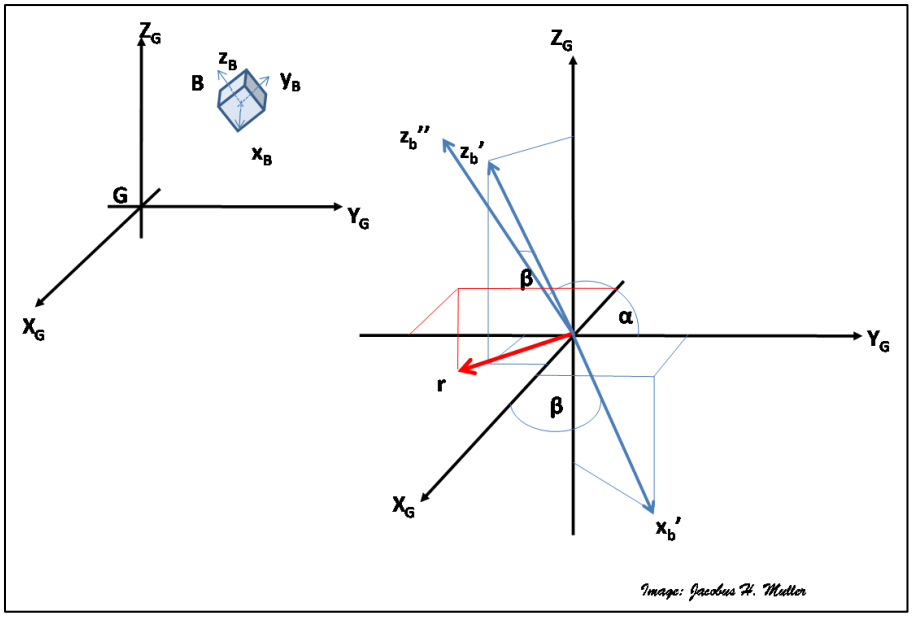

Figure B.1: Orientation of body B in the coronal plane in terms of the global reference frame G.

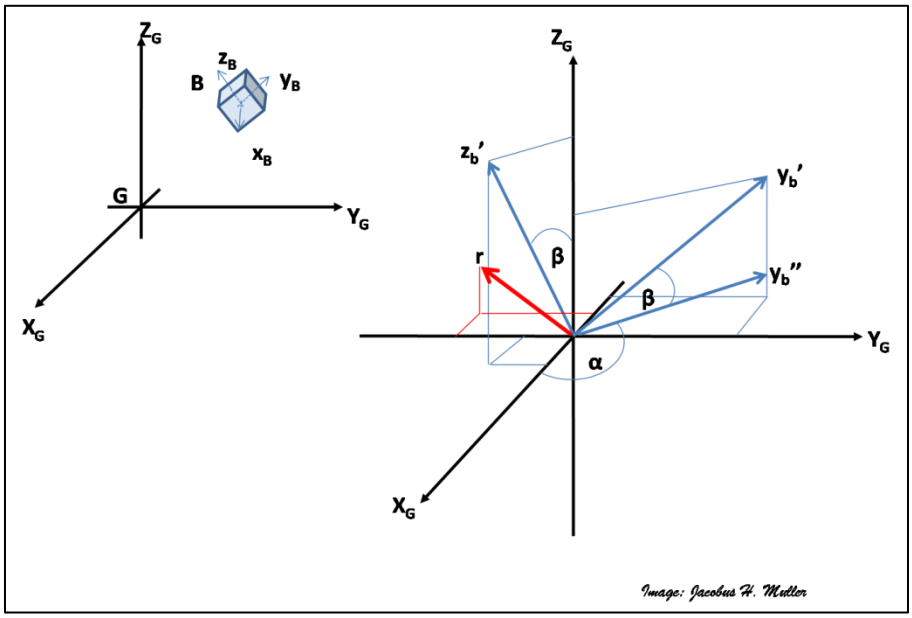

Figure B.2: Orientation of body B in the transverse plane in terms of the global reference frame G.

Appendix C: Calculation of the *in-vivo* contact areas from loaded MRI scans

C.1 Background

Ward *et al.* (2007) derived patellofemoral contact areas at full extension, 20, 40 and 60 degrees knee flexion from axial MRI scans. An external load equal to 25% the volunteer's body weight ($0.25 \times BW$) needed to be balanced by the volunteer's extensor mechanism (Figure C.1). The patellofemoral contact was identified in each slice where no separation between the femur and patella was visible. The length of a line along the contact border was then multiplied with the slice thickness, and the summation of the contact areas of each slice provided the patellofemoral contact areas.

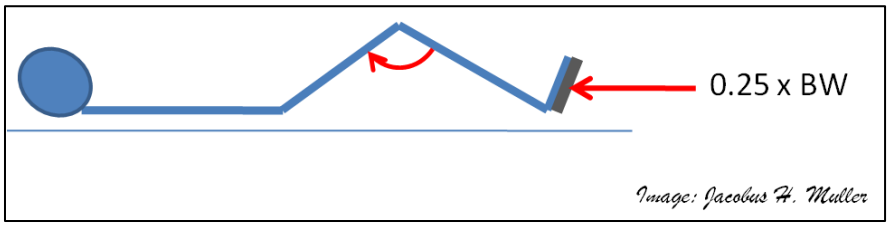

Figure C.1: Extensor mechanism loading configuration in MRI.

C.2 Methodology

A similar approach was followed in this study. A MRI of each volunteer's right knee at 30 degrees knee flexion was obtained, while the extensor mechanism was loaded. A load equal to $0.25 \times BW$ was applied at the volunteer's right foot. Instead of axial images, sagittal images were obtained. These provided better visualisation of the patellofemoral joint.

The three-dimensional models of the femur and patella that were obtained from the unloaded MRIs were repositioned on the loaded MRI scan. The quality of the loaded MRI scan was inferior to that of the unloaded scan since the scan times needed to be shorter for the loaded case. The shorter scan time enabled the volunteers to maintain the extensor mechanism load, while keeping still for the scan to be taken. Relative movement of the volunteers did however produce small artefacts on the loaded MRI images.

Visual inspection showed that the manual repositioning technique was satisfactory. The areas of contact on the three-dimensional models overlapped, since the cartilage was deformed on the loaded MRI at the contact points. A Boolean subtraction function was used to construct a volume of intersection. The surface area of the volume of intersection was calculated and approximated the patellofemoral contact area.

A surface was fit through points that were positioned on the surface of the intersection. The griddata-function (Matlab R2007b, Mathworks, Natic, Massachusetts) fits a surface ($Z = f(X,Y)$) through a set of points with x, y and z coordinates. Four methods are available, namely a linear, cubic, nearest and v4. The v4 method (Sandwell (1987)) were utilised for the purposes of this study since it proved to be the most stable for all three volunteers. The contact area A was calculated as, (Figure C.2):

$$A = \sum_{i=0}^{n-1}\sum_{j=0}^{m-1}\left\{\left[\frac{1}{2}\left(\left(\boldsymbol{Z}_{\boldsymbol{X_{i+1},Y_j}} - \boldsymbol{Z}_{\boldsymbol{X_i,Y_j}}\right) + \left(\boldsymbol{Z}_{\boldsymbol{X_{i+1},Y_{j+1}}} - \boldsymbol{Z}_{\boldsymbol{X_i,Y_{j+1}}}\right)\right)\right] \times \left[\frac{1}{2}\left(\left(\boldsymbol{Z}_{\boldsymbol{X_{i+1},Y_{j+1}}} - \boldsymbol{Z}_{\boldsymbol{X_{i+1},Y_j}}\right) + \left(\boldsymbol{Z}_{\boldsymbol{X_i,Y_{j+1}}} - \boldsymbol{Z}_{\boldsymbol{X_i,Y_j}}\right)\right)\right]\right\} \quad \text{Eq C.1}$$

An iterative procedure was followed in which X and Y were refined until the contact area converged.

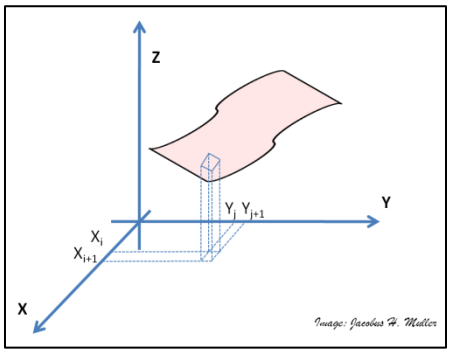

Figure C.2: Surface in three-dimensional space.

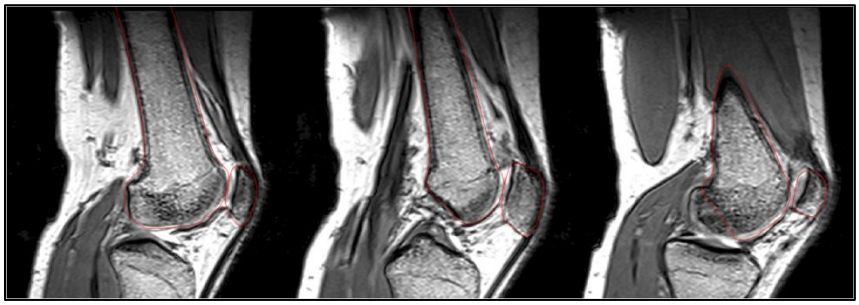

Figure C.3: Positioning of three-dimensional models (red line) on the MRI image.

C.3 Discussion

This technique provided a means with which the contact area between the patella and femur could be calculated *in-vivo*. It is an improvement on the technique proposed by Ward *et al.* (2007), since the contact area is approximated through a smoothed surface rather than the discrete lengths in each slice. There is however some limitations associated with this technique.

It is difficult to reposition the patella and femur on the loaded MRI scan due to the movement artefacts in the loaded MRI (Figure C.3), and the best fit was visually established. The resolution of the images also induced error in the measurements. The Hounsfield number of each voxel is an average of the Hounsfield numbers inside the voxel. The boundary of a structure will therefore be defined within a tolerance equal to the voxel depth. Ward *et al.* (2007) has however shown that the accuracy of their discrete method still produced accurate results when compared to *in-vitro* measurements.

Appendix D: Anatomical dissection study

In order to ensure accurate positioning of the implantation sites of the ligaments and tendons, another cadaver knee was dissected by removing its three layers step by step and indicating the relevant structures (medial patellofemoral ligament (MPFL) and medial collateral ligament (MCL)) and their attachment sites on the medial side (Figure D.1). The cadaver leg was CT scanned after which the relative distances and ratios between the different landmarks were measured and calculated (Table D.1).

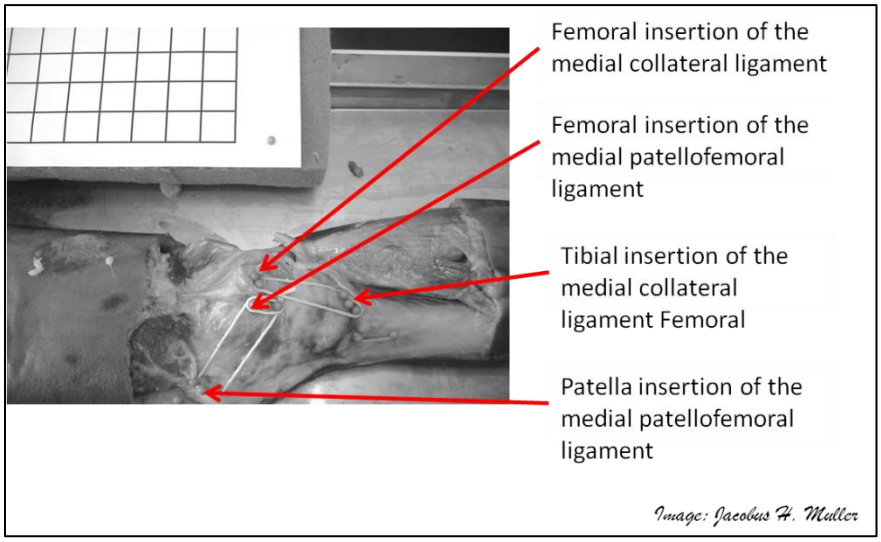

Figure D.1: Landmarks of the soft tissue attachments on the medial side.

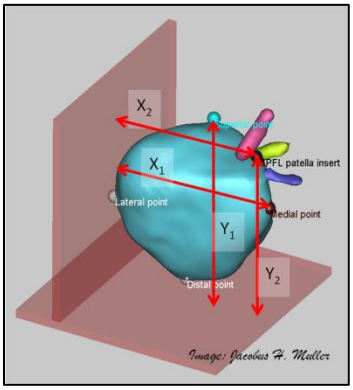

Figure D.2: MPFL attachment on the patella.

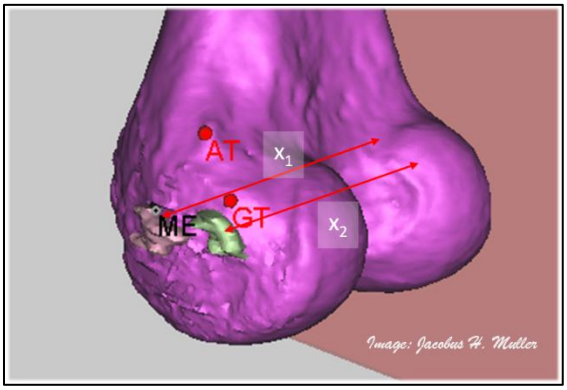

Figure D.3: MPFL and MCL attachment distance from the lateral plane.

Table D.1: Landmark locations of the soft tissue stabiliser attachments.

Soft tissue structure	Measurement	Value
MPFL patella attachment	Ratio of patella medial-lateral distance to MPFL lateral distance, Eq D.1 (Figure D.2)	0.826
	Ratio of patella superior-inferior distance to MPFL inferior distance, Eq D.2 (Figure D.2)	0.851
MPFL femur attachment	Ratio of epicondylar distance to MPFL lateral distance, Eq D.3 (Figure D.3)	0.972
	Ratio of epicondylar distance to MPFL distal distance, Eq D.4 (Figure D.4)	0.407
	Ratio of epicondylar distance to MPFL posterior distance, Eq D.5 (Figure D.5)	0.335
MCL femur attachment	Ratio of epicondylar distance to MCL lateral distance, Eq D.6 (Figure D.3)	0.926
	Ratio of epicondylar distance to MCL distal distance, Eq D.7 (Figure D.4)	0.245
	Ratio of epicondylar distance to MCL posterior distance, Eq D.8 (Figure D.5)	0.320

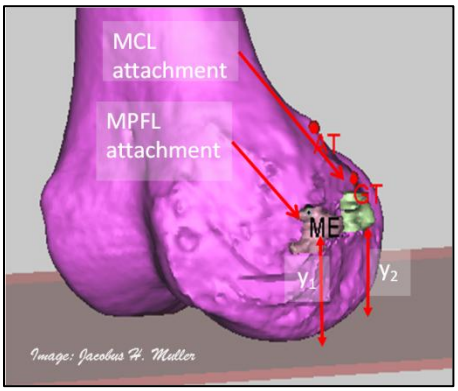

Figure D.4: MPFL and MCL attachment distance from the distal plane.

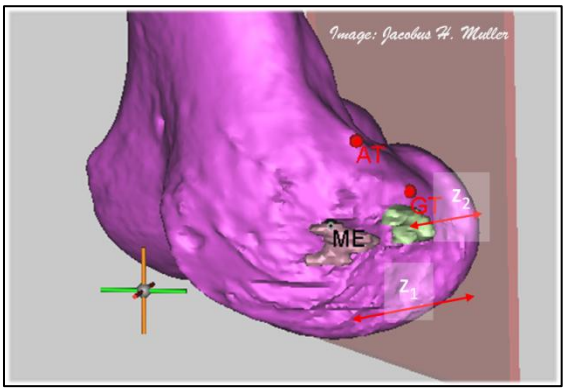

Figure D.5: MPFL and MCL attachment distance from the posterior plane.

$$MPFL_{Lateral\ distance} = \frac{x_2}{x_1}$$ Eq D.1

$$\text{Ratio of patella superior} - \text{inferior distance to MPFL inferior distance} = \frac{y_2}{y_1}$$ Eq D.2

$$\text{Ratio of epicondylar distance to MPFL lateral distance} = \frac{x_1}{epicondylar\ distance}$$ Eq D.3

$$\text{Ratio of epicondylar distance to MPFL distal distance} = \frac{y_1}{epicondylar\ distance}$$ Eq D.4

$$\text{Ratio of epicondylar distance to MPFL posterior distance} = \frac{z_1}{\text{epicondylar distance}}$$ Eq D.5

$$\text{Ratio of epicondylar distance to MCL lateral distance} = \frac{x_2}{\text{epicondylar distance}}$$ Eq D.6

$$\text{Ratio of epicondylar distance to MCL distal distance} = \frac{y_2}{epicondylar\ distance}$$ Eq D.7

$$\text{Ratio of epicondylar distance to MCL posterior distance} = \frac{z_2}{epicondylar\ distance}$$ Eq D.8

Appendix E: Simplified muscle activation curves

E.1 Introduction

The sensitivity of the baseline model predictions as a function of the muscle activation curves were tested for two sets of curves. The first set consisted of the polynomials that were fitted to the EMG data recorded in Section 3.8. The second set consisted of simplified first order approximations of the EMG data. If the first order approximation did not induce large errors as compared to the first set of curves, it could be used instead. This would reduce the times needed to complete the analyses.

E.2 Materials and methods

A baseline model was setup for the two curve sets by following the procedure in Section 4.3. The analysis time was recorded for each analysis, as well as the test parameters. The test parameters included the:

- Patella tracking trends: Translation and rotation along and about the three principal axes.
- Soft tissue tension trends: MPFL, lateral retinaculum, patellar tendon and quadriceps tendon
- Patellofemoral contact load
- Tibial rotation.

A mean error (Eq E.1) and standard deviation was computed for each parameter, with n equal to the number of values for that parameter through the range of flexion.

$$error = \sum_{i=1}^{n} \left| \frac{y_i^{set\ 1} - y_i^{set\ 2} \Big/ \max\left(y_i^{set\ 1}\right)}{n} \right| \qquad \text{Eq E.1}$$

E.3 Results

The mean patella tracking errors (Figure E.1) induced by the simplified activation curves were 7.75 % [SD = 13.4]. This was high because of the error induced in the prediction of patellar rotation. Patellar rotation does not play a major role in patellofemoral kinematics, since it has been shown to be highly variable for a subject and between subjects (Amis *et al.* (2006)). If the value for patella rotation is excluded, the induced error decreases to a value of 2.33 % [SD = 1.51] (Table E.1). The mean soft tissue tension error was 4.52% [SD = 1.13], with the

largest error occurring in the prediction of the quadriceps tendon tension (5.74 % [SD = 4.97]) (Table E.2 and Figure E.2).

Table E.1: Patella tracking errors.

Parameter	% Error [SD]
Mediolateral shift	4.30 [3.05]
Anteroposterior displacement	1.38 [0.871]
Proximal-distal displacement	0.983 [0.518]
Tilt	3.60 [1.71]
Flexion	1.40 [0.717]
Rotation	34.9 [22.2]
Mean error	7.75 [13.4]
Mean error (Rotation excluded)	2.33 [1.51]

Table E.2: Soft tissue tension errors.

Parameter	% Error [SD]
Patellar tendon tension	5.10 [4.97]
Quadriceps tendon tension	5.74 [5.00]
Lateral retinacula tension	4.08 [3.24]
MPFL	3.17 [5.60]
Mean error	4.52 [1.13]

Table E.3: Total error resulting from the simplified muscle activation curves.

Parameter	% Error [SD]
Patella tracking error	2.33 [1.51]
Soft tissue error	4.52 [1.13]
Patellofemoral contact error	6.31 [5.05]
Tibial rotation error	0.193 [0.111]
Mean error	3.34 [2.65]
Mean error (Tibial rotation excluded)	4.38 [1.99]

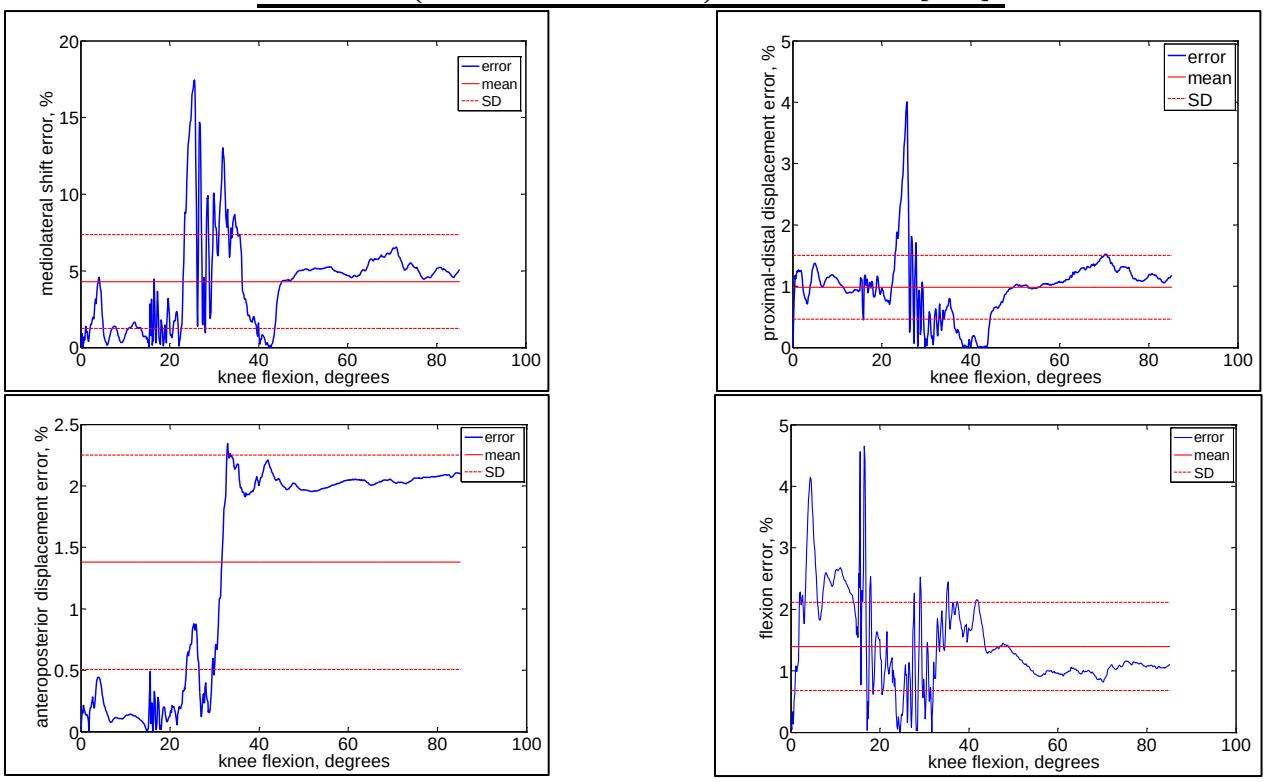

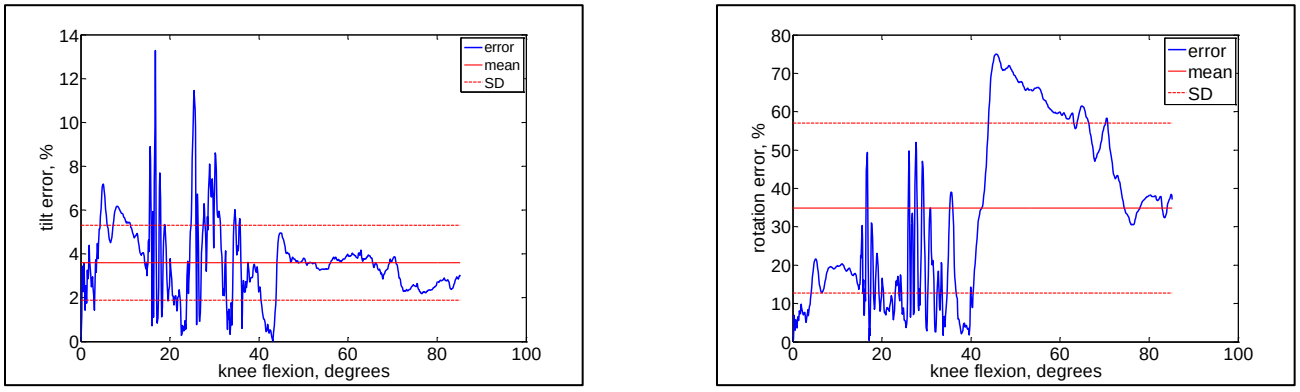

Figure E.1: Patella tracking error.

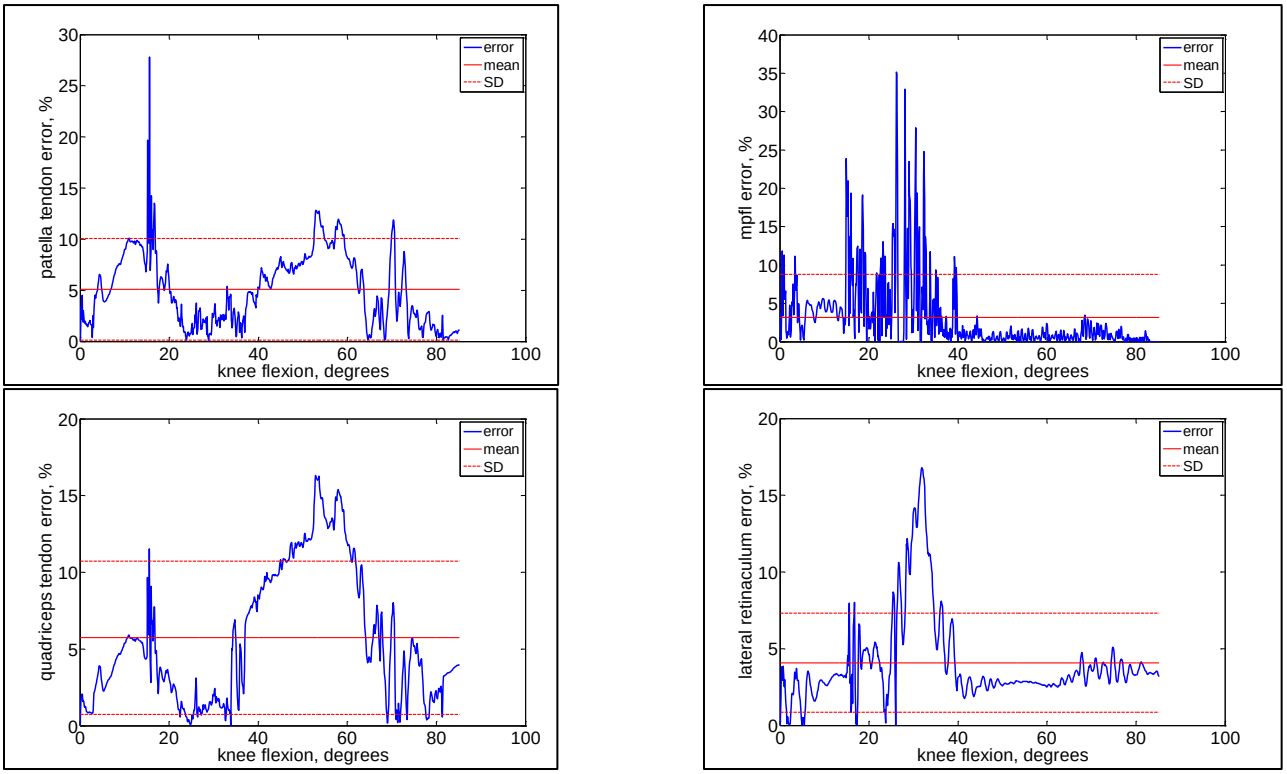

Figure E.2: Soft tissue tension error.

The mean error (Figure E.3) in the patellofemoral contact load prediction was calculated as 6.34 % [SD = 5.05] (Table E.3). If one ignores the error in patella rotation, the largest error occurred in the prediction of patellofemoral contact load. There was little difference in tibial internal rotation prediction between the two analyses (Figure E.4). A mean error of 0.139 % [SD = 0.111] was made. When the errors for the test parameters were combined, a representative mean error of 3.34 % [SD = 2.65] was computed. When the small error resulting from tibial rotation was not considered, this error increased to 4.38 % [SD = 1.99].

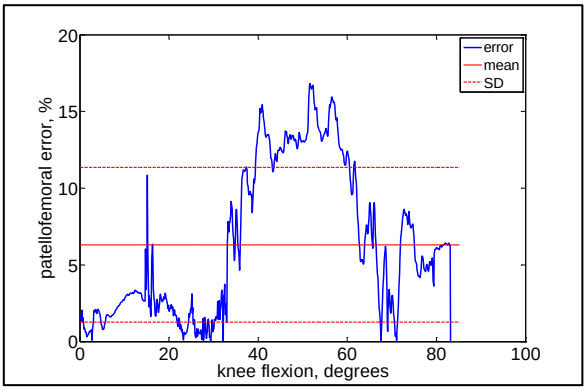

Figure E.3: Patellofemoral contact load magnitude error.

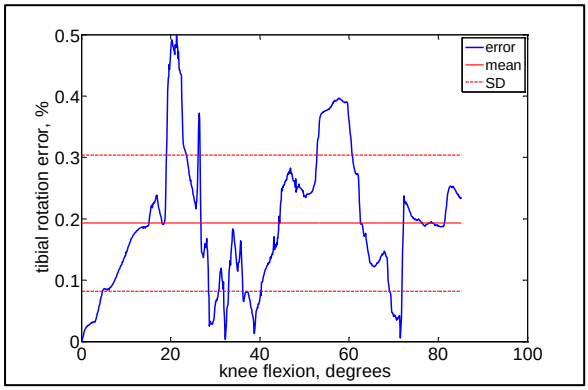

Figure E.4: Tibial rotation error.

E.4 Discussion

The results show that the activation curves have a negligible influence on patella tracking patterns (with the exception of patella rotation). This result is expected, since patella tracking is governed by the shape of the trochlear groove, and to a lesser extent by the soft tissues which give stability to the patella. The activation curves had the greatest influence on the quadriceps tendon tension when compared to the other soft tissues that were considered. This was also expected since the quadriceps tendon serve as the "connection" between the patellofemoral joint and the quadriceps muscles. The largest error occurred in the patellofemoral contact load prediction. The maximum error (patellofemoral contact load), was below 20 %, and the mean error only 4.38 %. The analysis time for the first set of activation curves, was twice as long as the analysis time when the second set was implemented. It was decided that the error was negligible when the second set was to be used.

Appendix F: Graphical representation of mediolateral patella tilt and shift during knee flexion

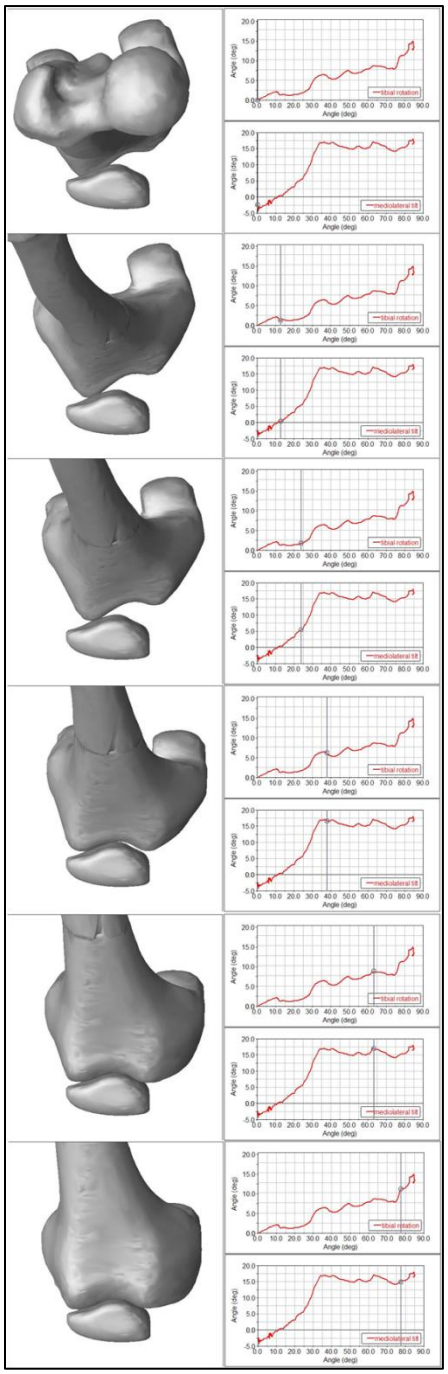

Figure F.1: Patella tilt and tibial rotation as a function of knee flexion (Volunteer One).

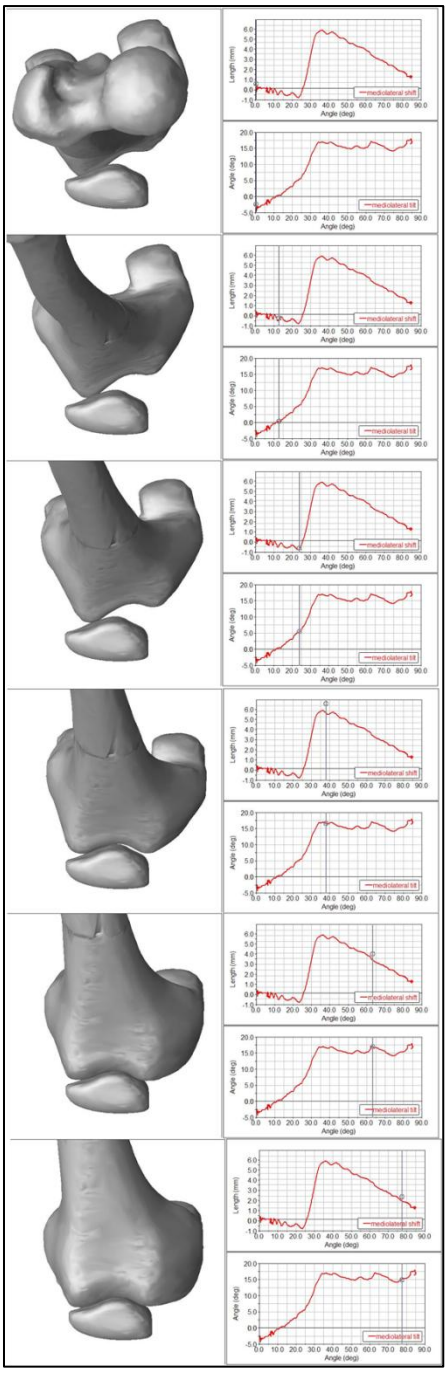

Figure F.2: Patella shift and tilt as a function of knee flexion (Volunteer One).

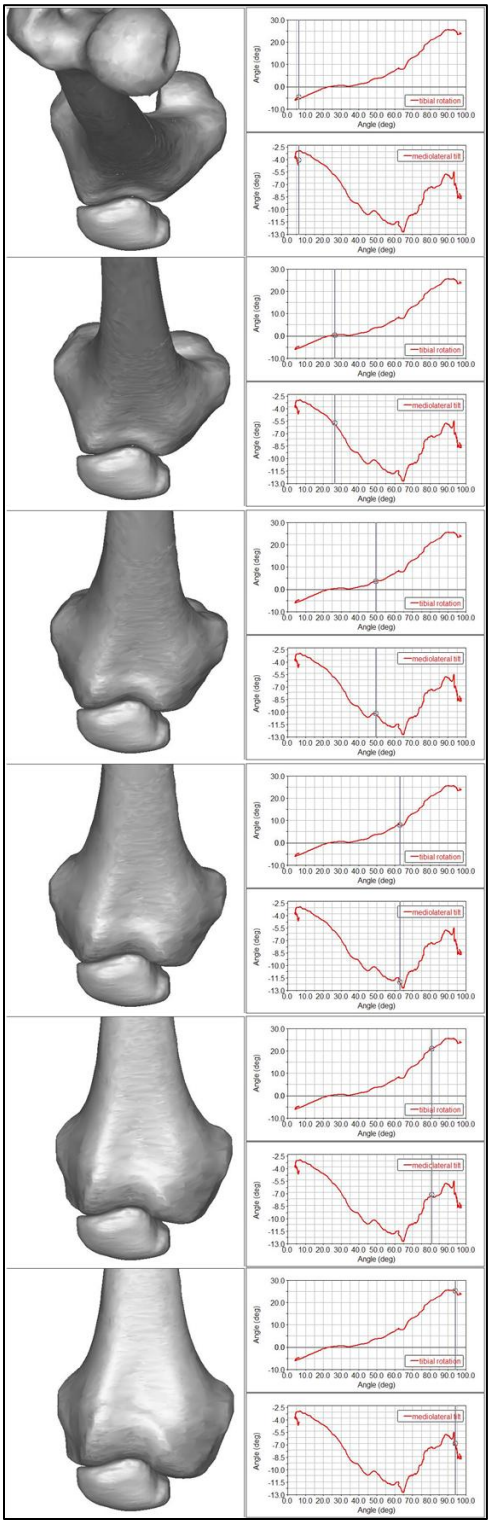

Figure F.3: Patella tilt and tibial rotation as a function of knee flexion (Volunteer Two).

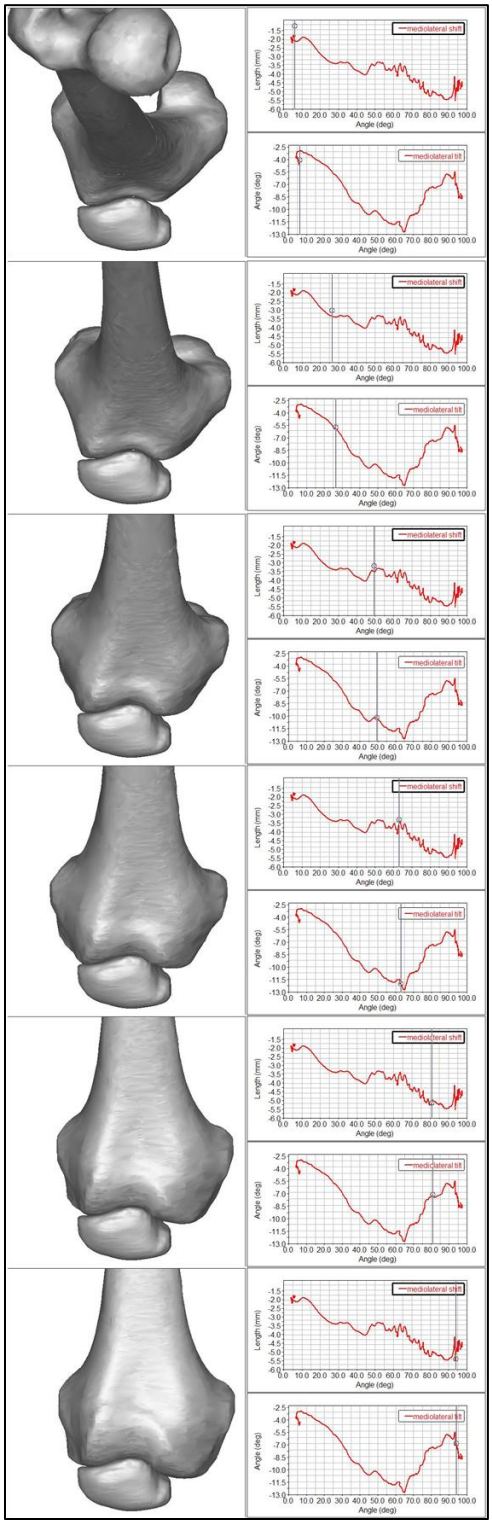

Figure F.4: Patella shift and tilt as a function of knee flexion (Volunteer Two).

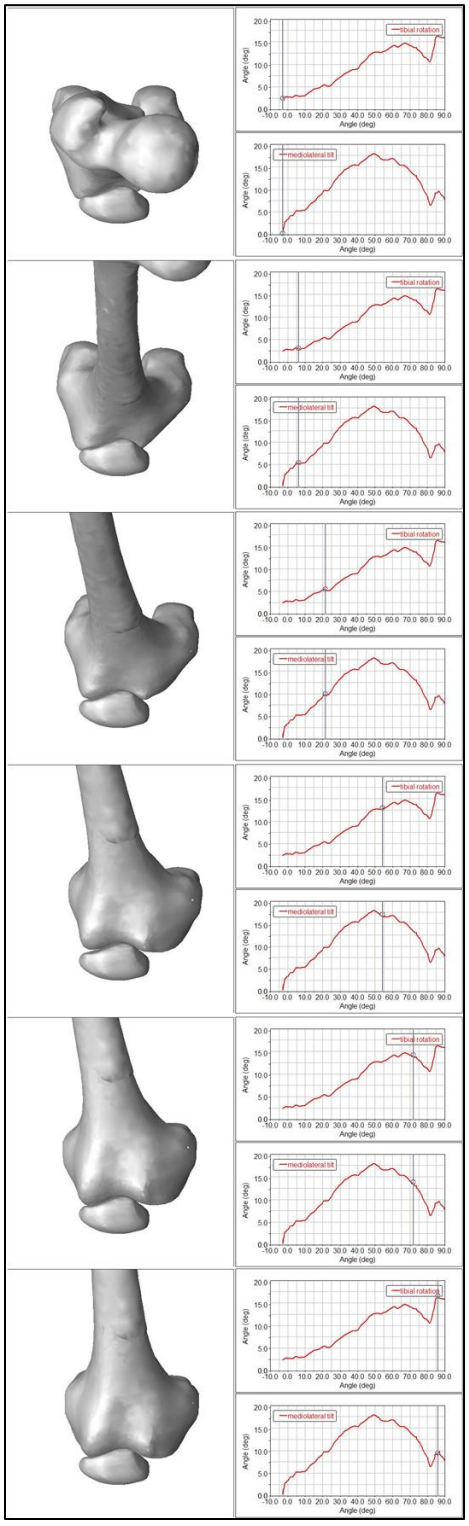

Figure F.5: Patella tilt and tibial rotation as a function of knee flexion (Volunteer Three).

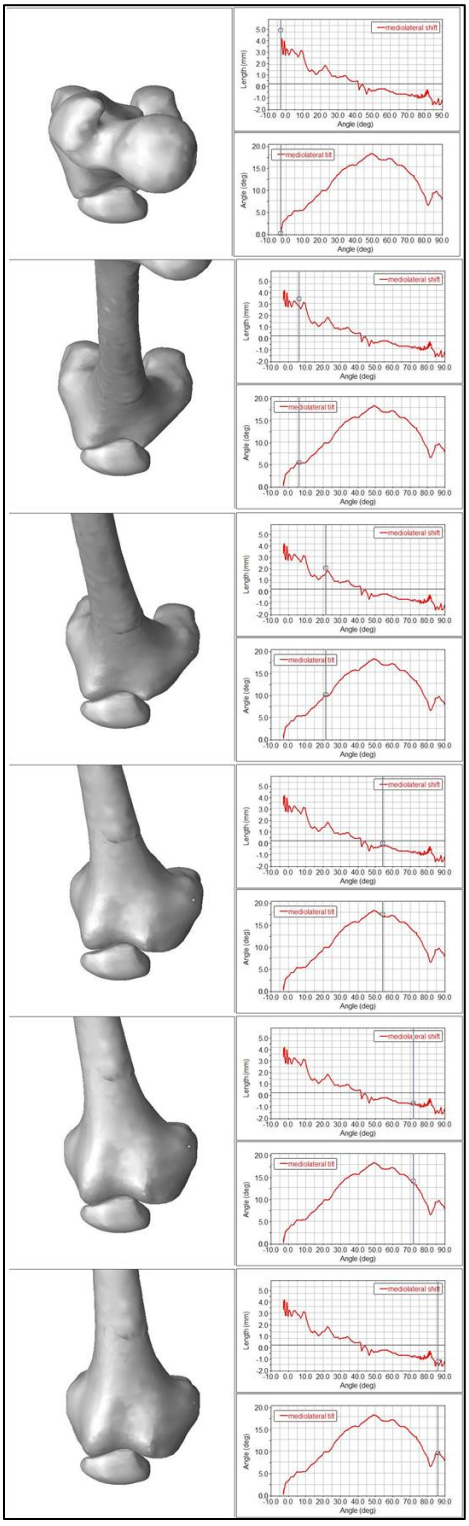

Figure F.6: Patella shift and tilt as a function of knee flexion (Volunteer Three)

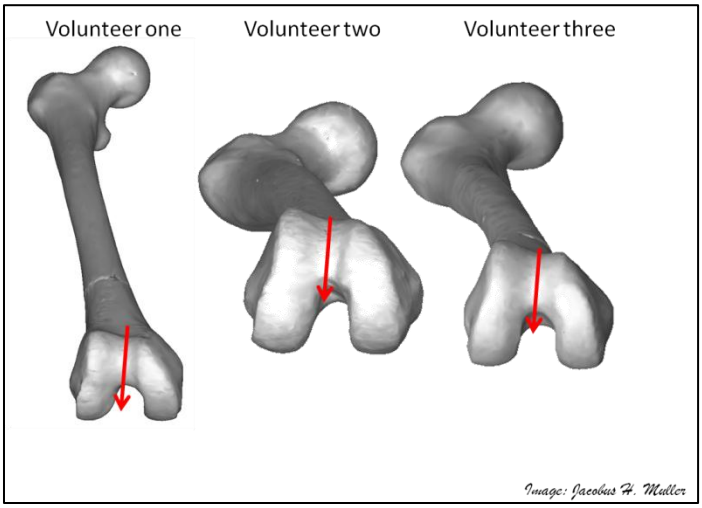

Figure F.7: Trochlear groove orientation.

Appendix G: Patellofemoral pressure distribution as a function of tibial tubercle position

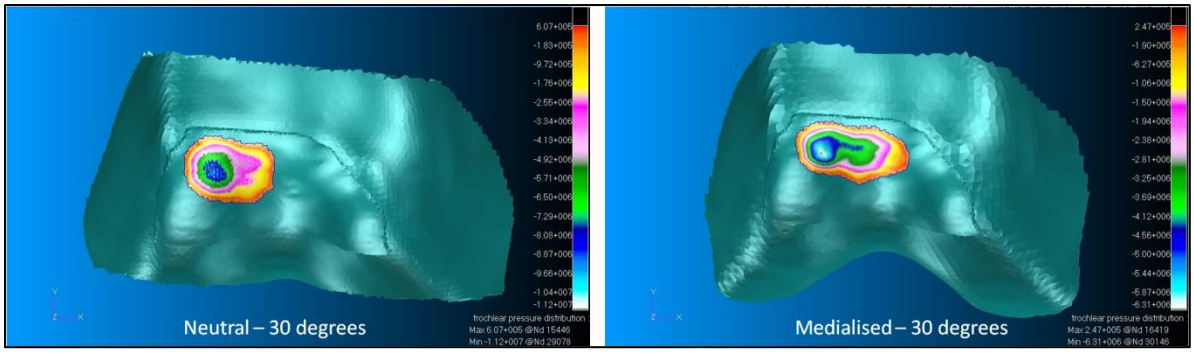

Figure G.1: Pressure distribution across the trochlear groove of Volunteer One (Pressure in Pa).

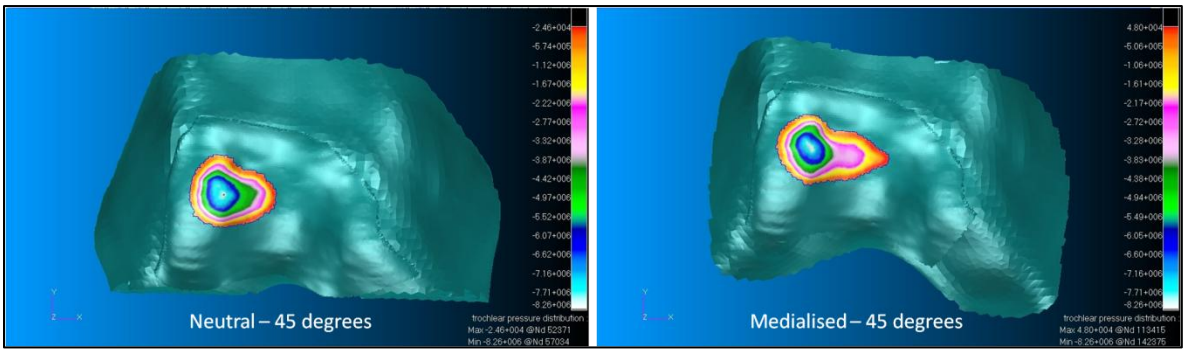

Figure G.2: Pressure distribution across the trochlear groove of Volunteer One (Pressure in Pa).

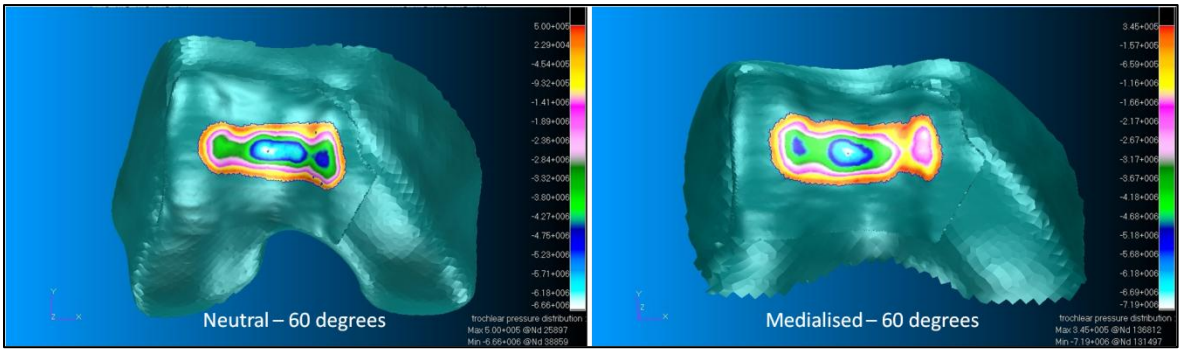

Figure G.3: Pressure distribution across the trochlear groove of Volunteer One (Pressure in Pa).

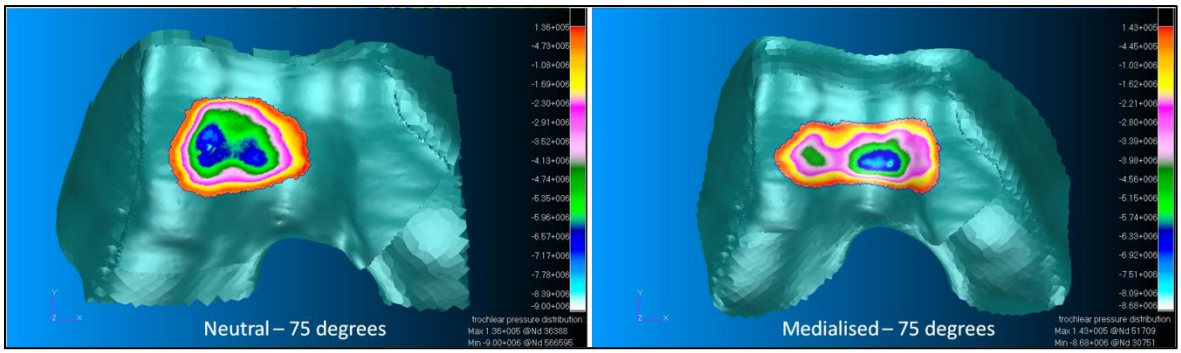

Figure G.4: Pressure distribution across the trochlear groove of Volunteer One (Pressure in Pa).

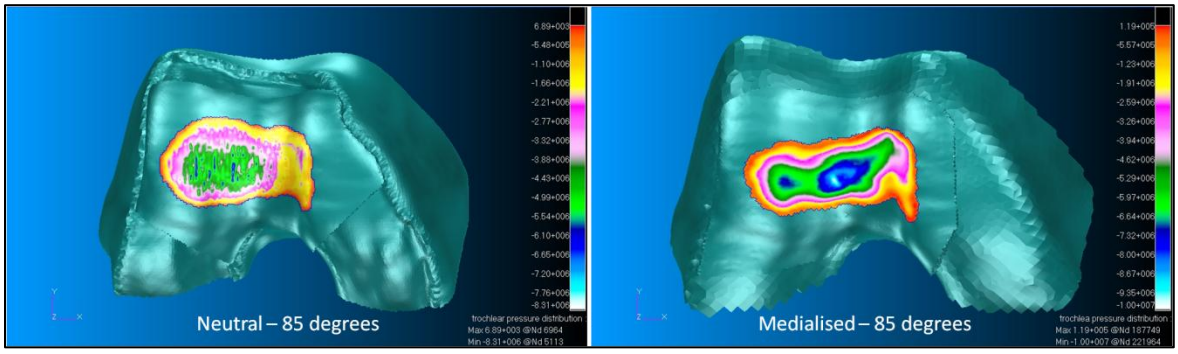

Figure G.5: Pressure distribution across the trochlear groove of Volunteer One (Pressure in Pa).

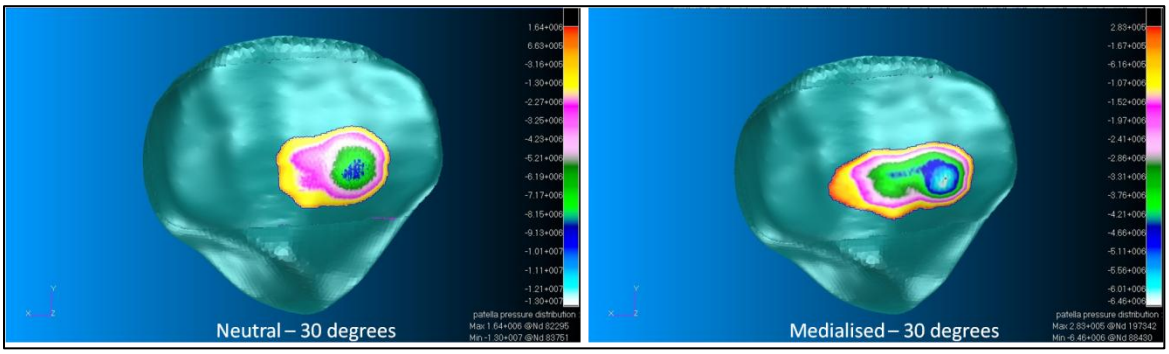

Figure G.6: Pressure distribution across the patella of Volunteer One (Pressure in Pa).

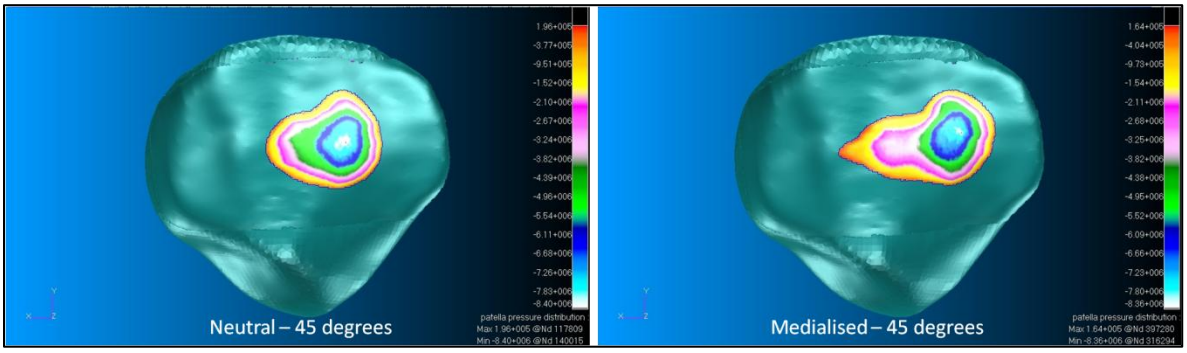

Figure G.7: Pressure distribution across the patella of Volunteer One (Pressure in Pa).

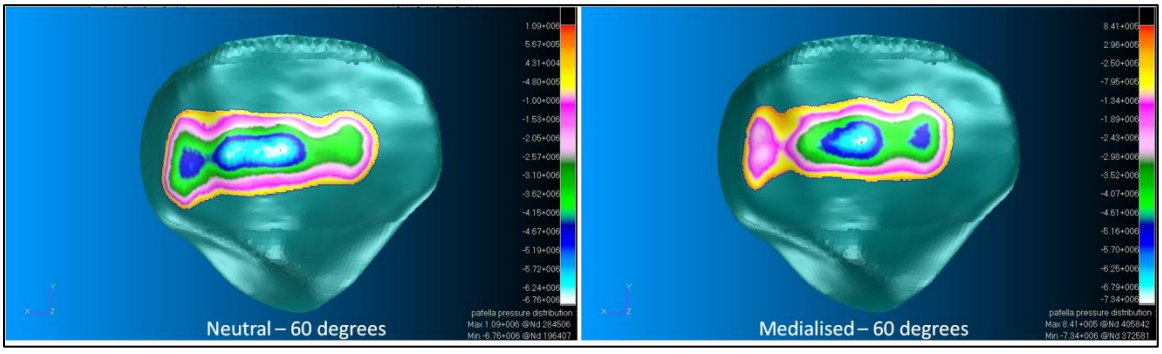

Figure G.8: Pressure distribution across the patella of Volunteer One (Pressure in Pa).

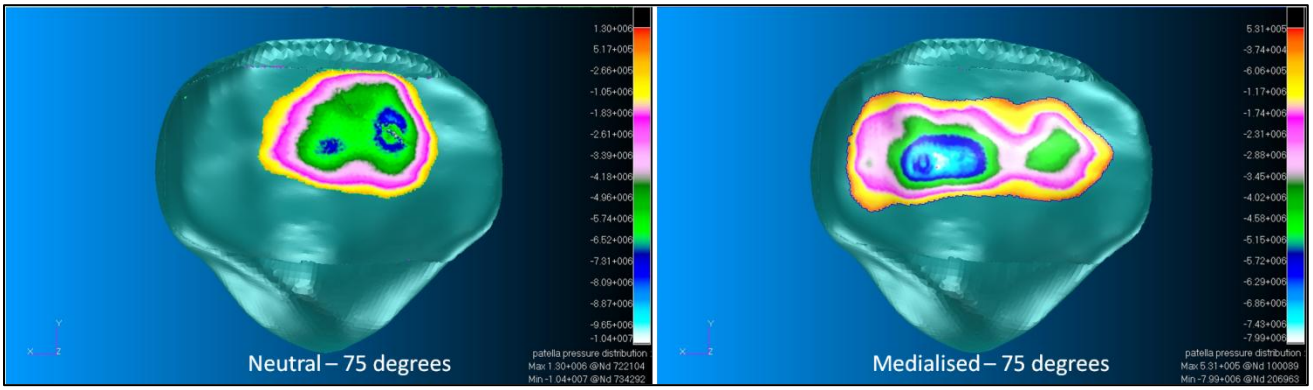

Figure G.9: Pressure distribution across the patella of Volunteer One (Pressure in Pa).

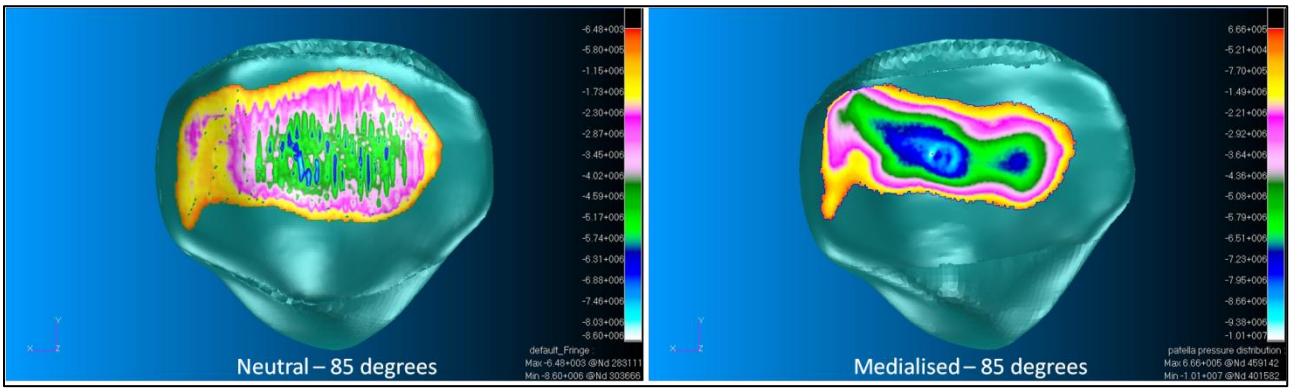

Figure G.10: Pressure distribution across the patella of Volunteer One (Pressure in Pa).

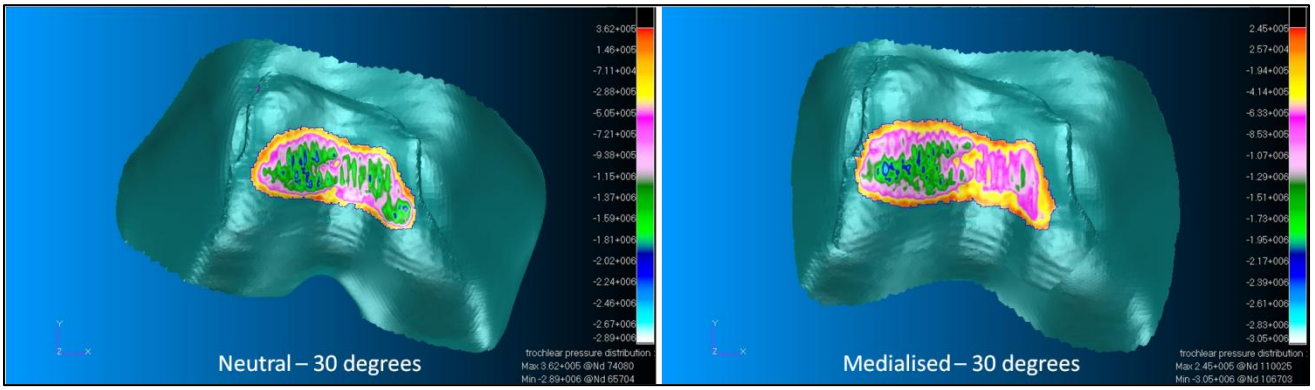

Figure G.11: Pressure distribution across the trochlear groove of Volunteer Two (Pressure in Pa).

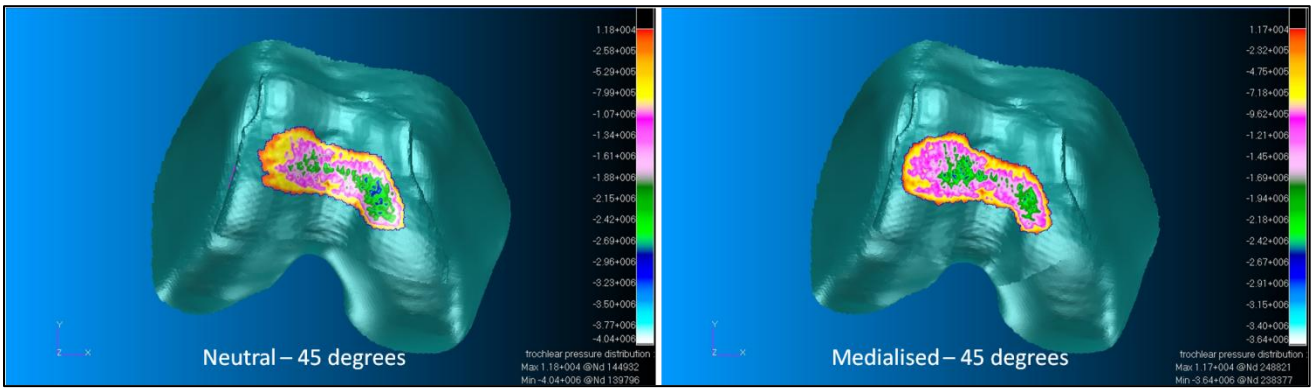

Figure G.12: Pressure distribution across the trochlear groove of Volunteer Two (Pressure in Pa).

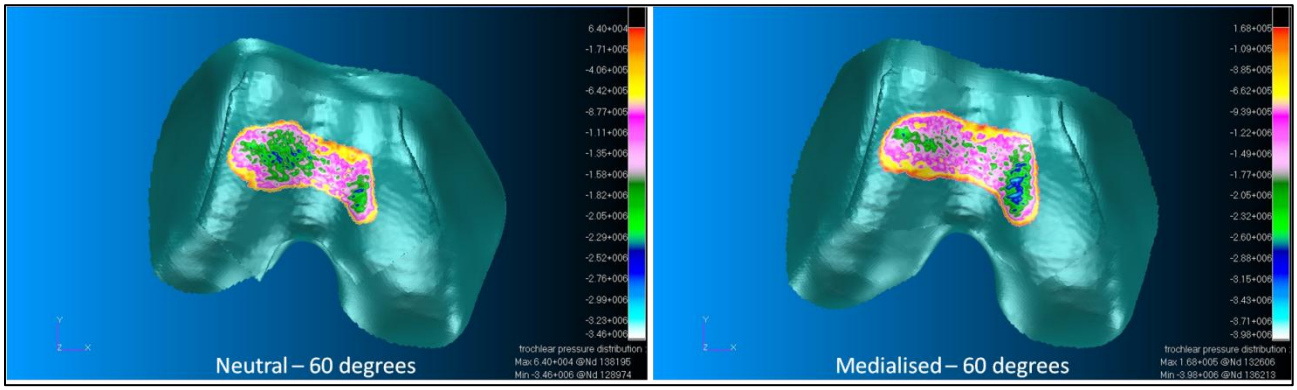

Figure G.13: Pressure distribution across the trochlear groove of Volunteer Two (Pressure in Pa).

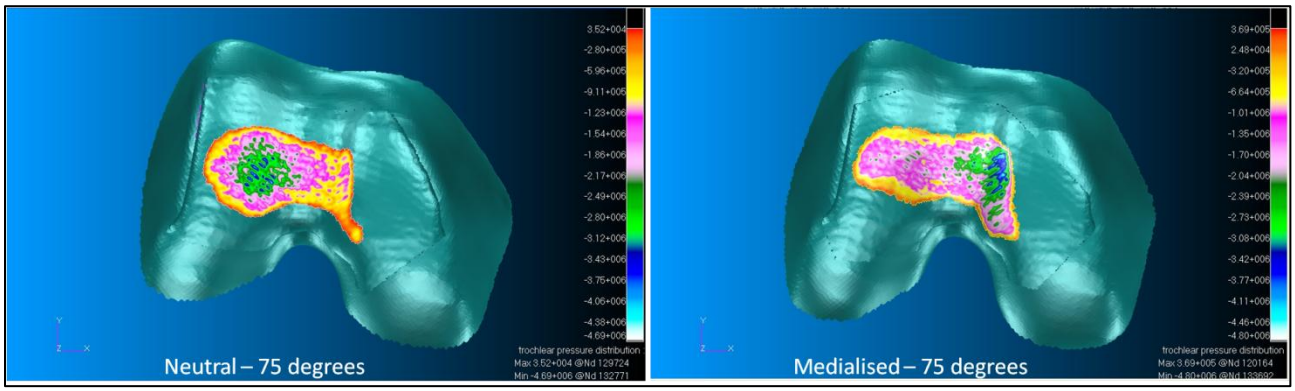

Figure G.14: Pressure distribution across the trochlear groove of Volunteer Two (Pressure in Pa).

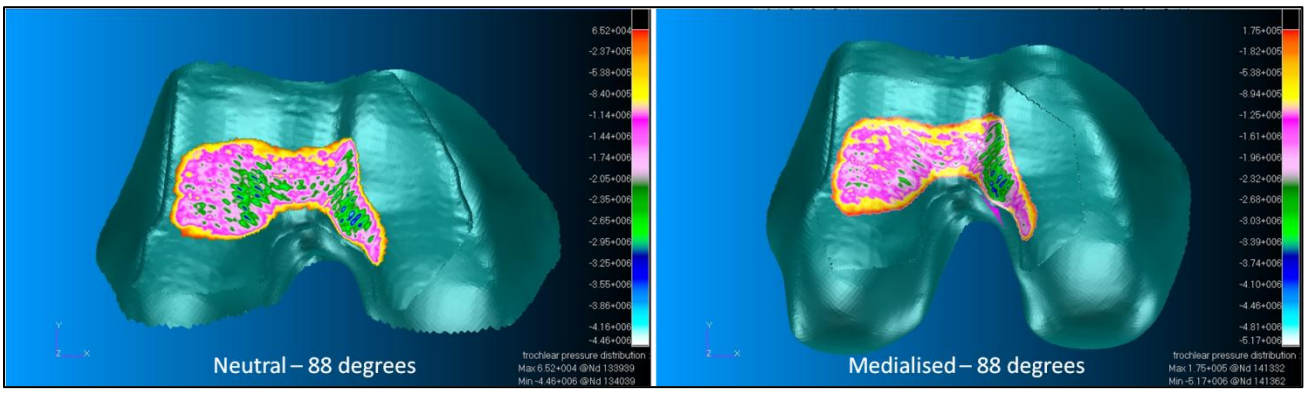

Figure G.15: Pressure distribution across the trochlear groove of Volunteer Two (Pressure in Pa).

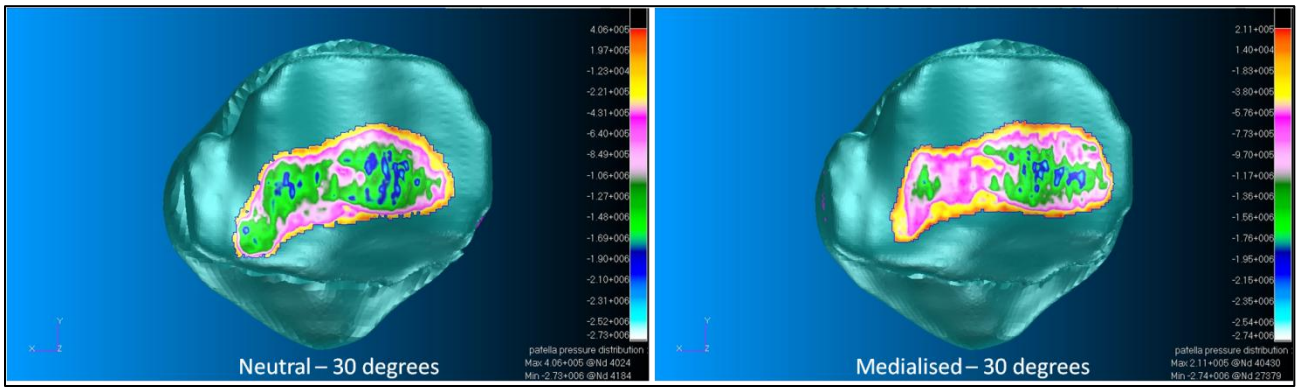

Figure G.16: Pressure distribution across the patella of Volunteer Two (Pressure in Pa).

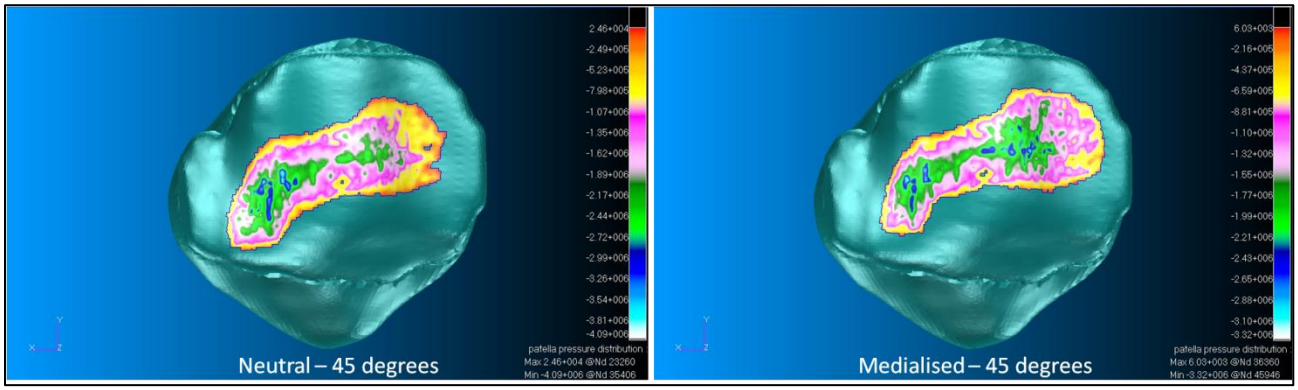

Figure G.17: Pressure distribution across the patella of Volunteer Two (Pressure in Pa).

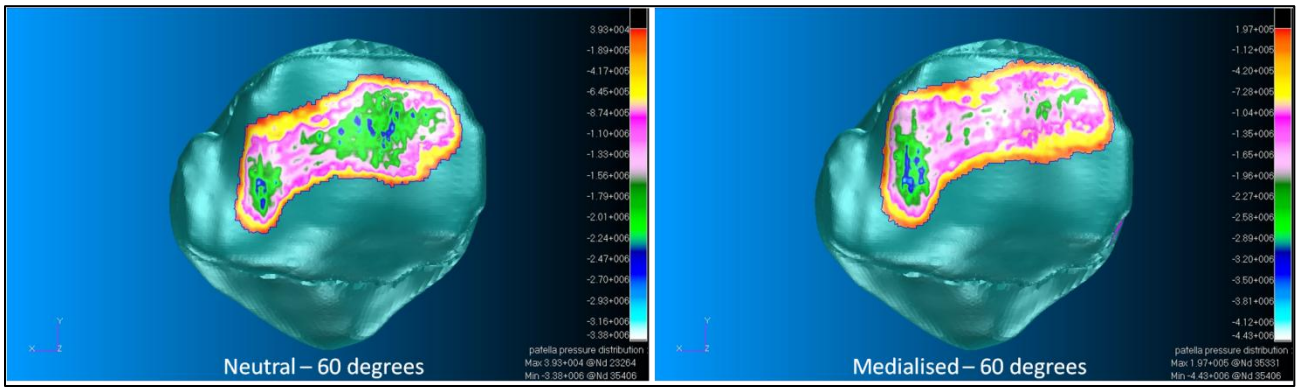

Figure G.18: Pressure distribution across the patella of Volunteer Two (Pressure in Pa).

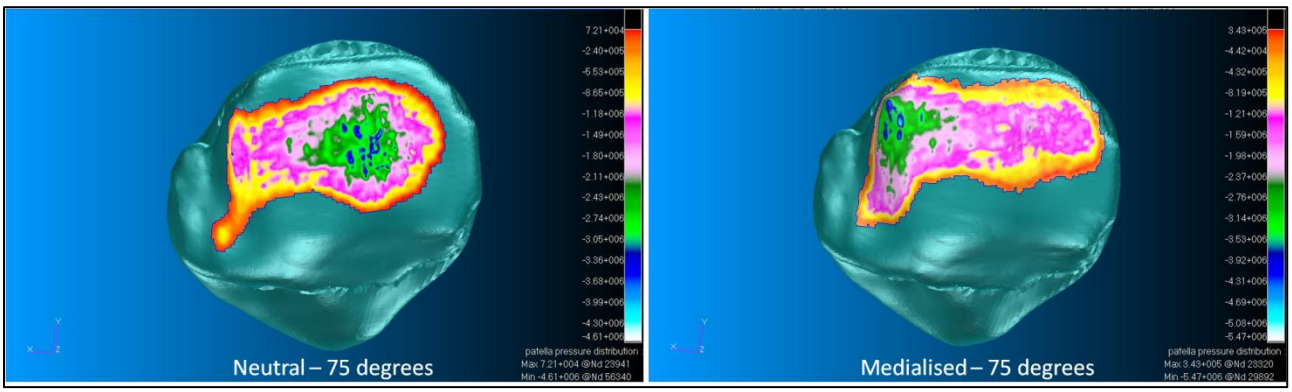

Figure G.19: Pressure distribution across the patella of Volunteer Two (Pressure in Pa).

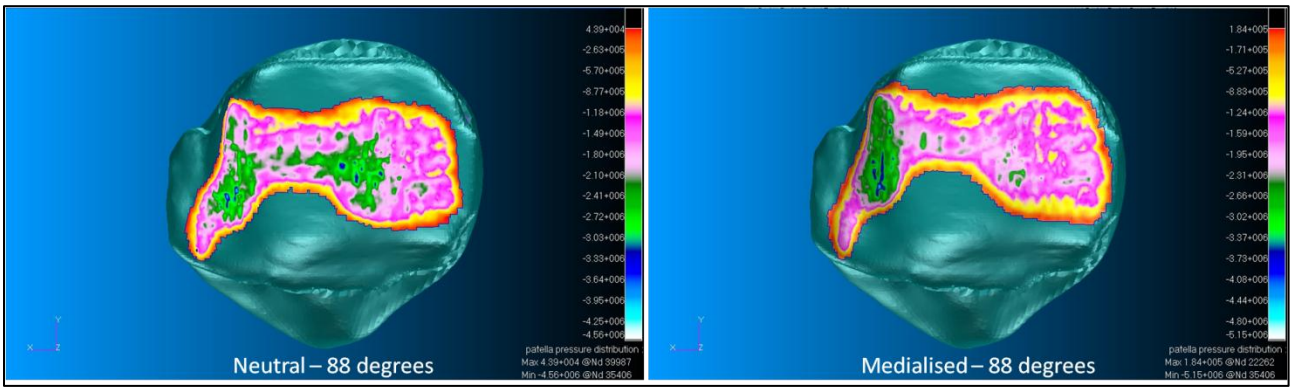

Figure G.20: Pressure distribution across the patella of Volunteer Two (Pressure in Pa).

Table G.1: Boxplot graphs of the principal pressure distributions on Volunteer One's trochlear groove at 30, 45, 60, 75 and 85 degrees knee flexion.

Flexion angle	Trochlear groove	Patella
30	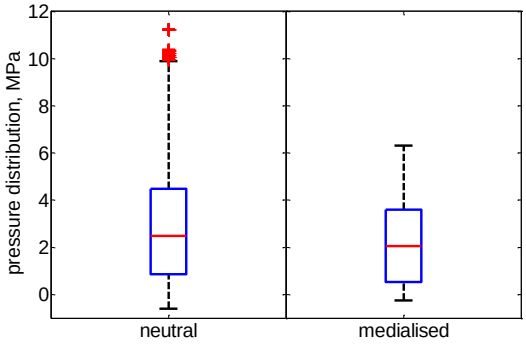	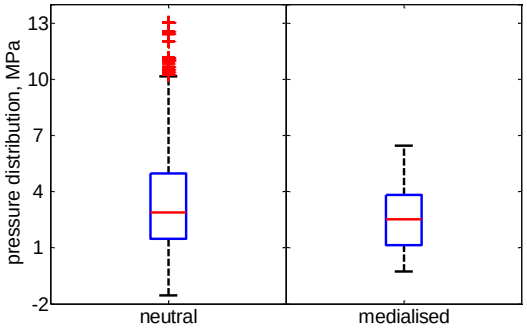
45	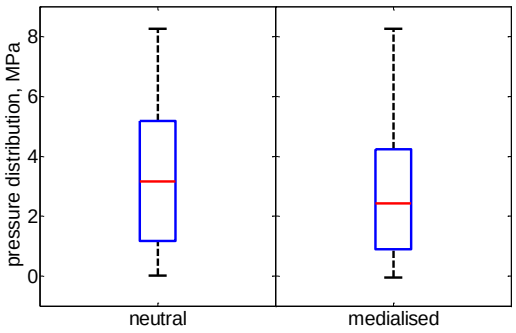	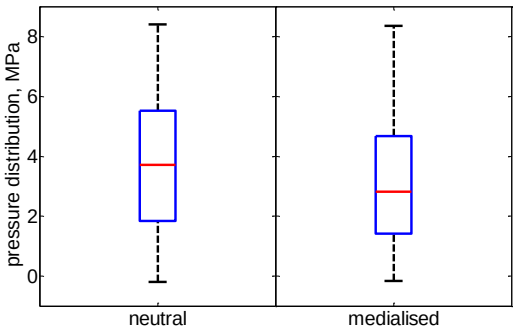
60	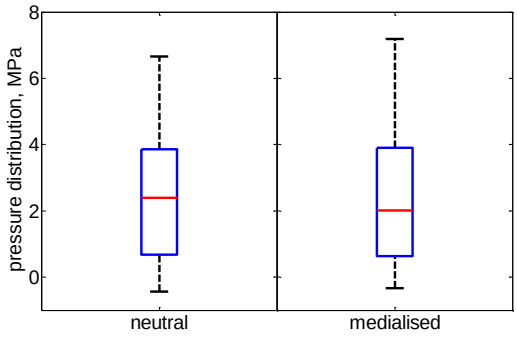	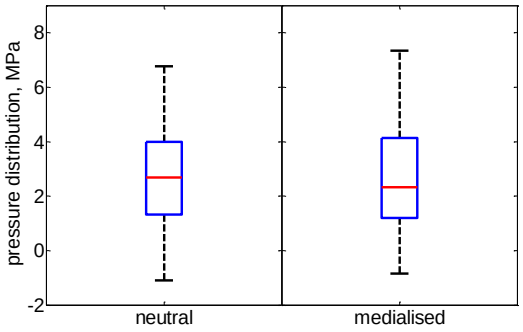
75	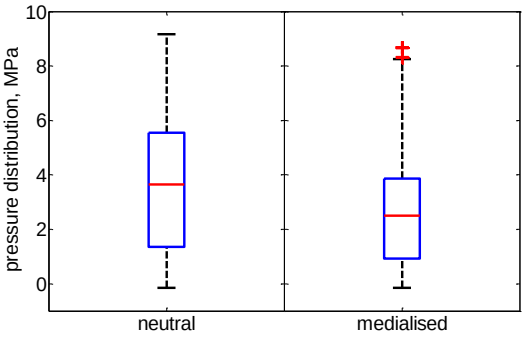	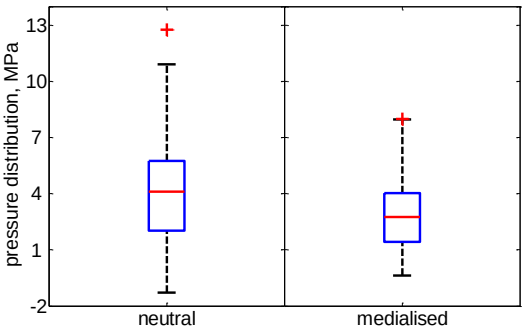

85	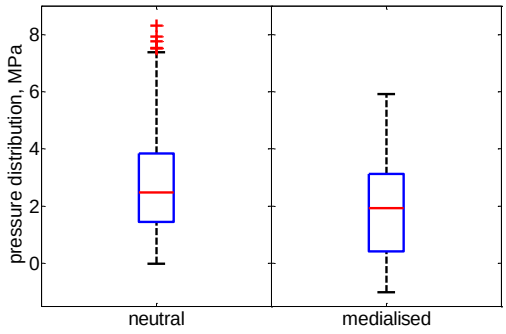	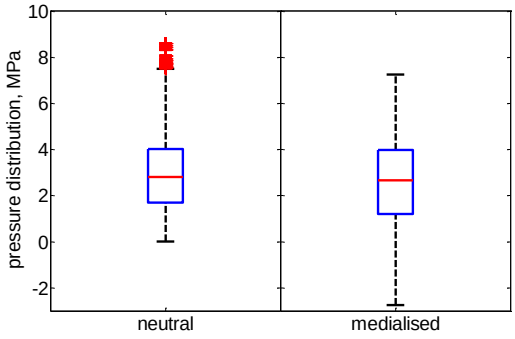

Table G.2: Boxplot graphs of the principal pressure distributions on Volunteer Two's trochlear groove at 30, 45, 60, 75 and 85 degrees knee flexion.

Flexion angle	Trochlear groove	Patella
30	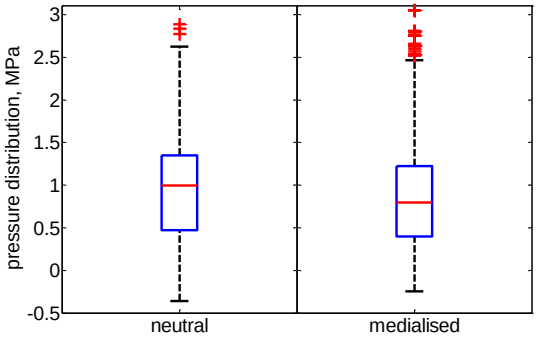	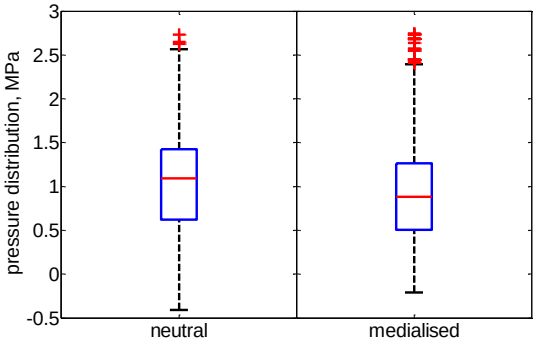
45	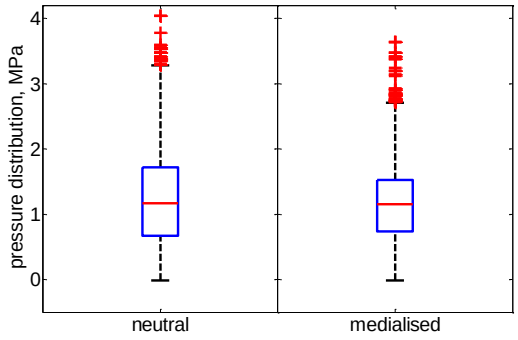	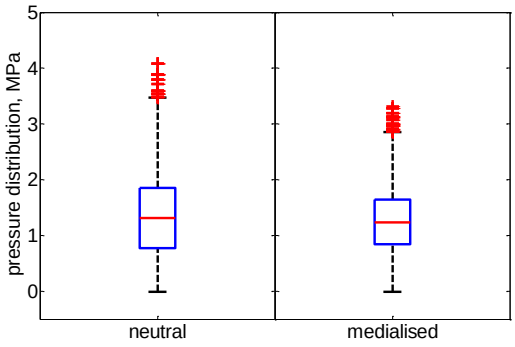
60	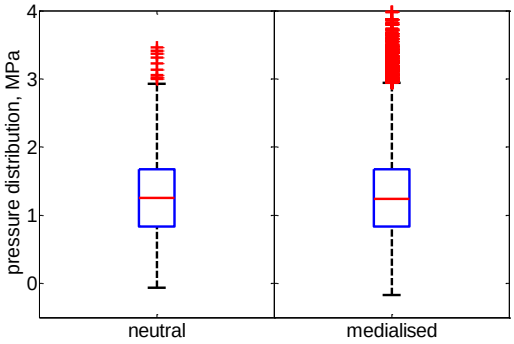	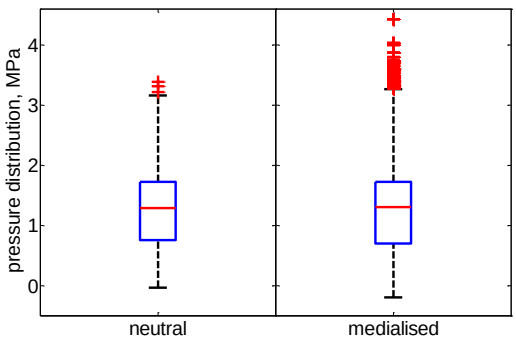

75

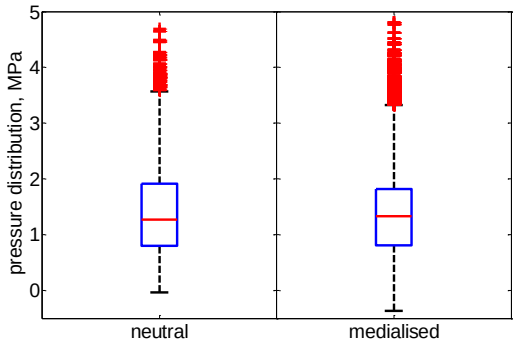
pressure distribution, MPa
0
1
2
3
4
5
neutral
medialised

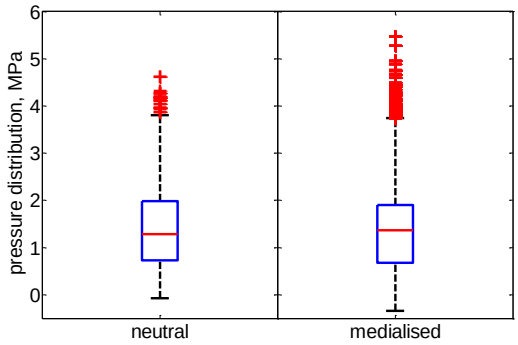
pressure distribution, MPa
0
1
2
3
4
5
6
neutral
medialised

88

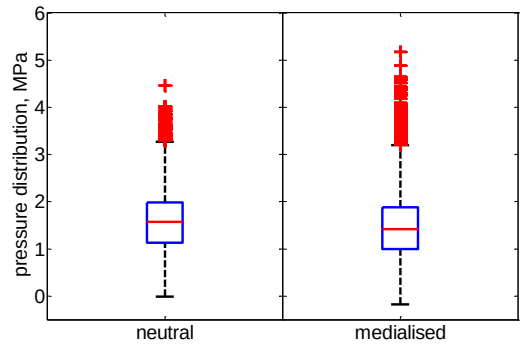
pressure distribution, MPa
0
1
2
3
4
5
6
neutral
medialised

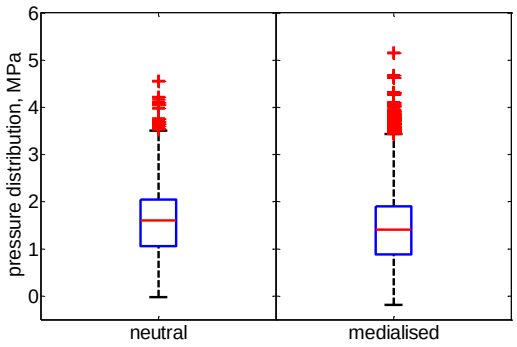
pressure distribution, MPa
0
1
2
3
4
5
6
neutral
medialised

Appendix H: Approximation of cartilage stiffness with a two-dimensional finite element model

H.1 Introduction

The purpose of this investigation was to derive an approximate cartilage stiffness value which could be used in the musculoskeletal models to model the patellofemoral contact. A two-dimensional FE model was assembled with which the stiffness of the cartilage having a modulus (E = 15 MPa) and a Poisson ratio (ν = 0.45) could be approximated.

H.2 Model setup

An uniformly distributed load equal to 2 N was applied on the right border while the cartilage was constrained on left border (Figure H.1). The bottom and top borders were constrained to translate only in the loading direction. Eight-node quadrilateral elements were used and the element size was determined from a convergence analysis.

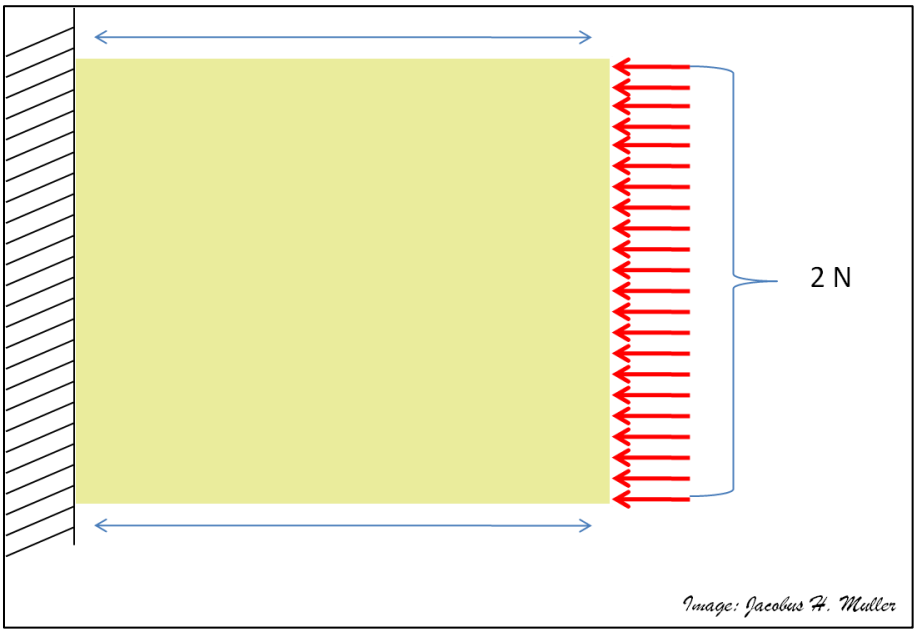

Figure H.1: Finite element model setup of two-dimensional cartilage material.

Pre-processing and post-processing was done in MSC Patran, while the MSC MARC processor was used. The 2 N load was applied over a one second period. The cartilage stiffness was calculated by dividing the applied load by the maximum compression distance.

H.3 Results

The cartilage was compressed (0.114 millimetres) after the load was applied (Figure H.2). The blue box indicates the geometry before application of the load, while the red mesh represents the deformed geometry. The approximate stiffness of the cartilage (E = 15 MPa, ν = 0.45) for this case was 17.5 N/mm.

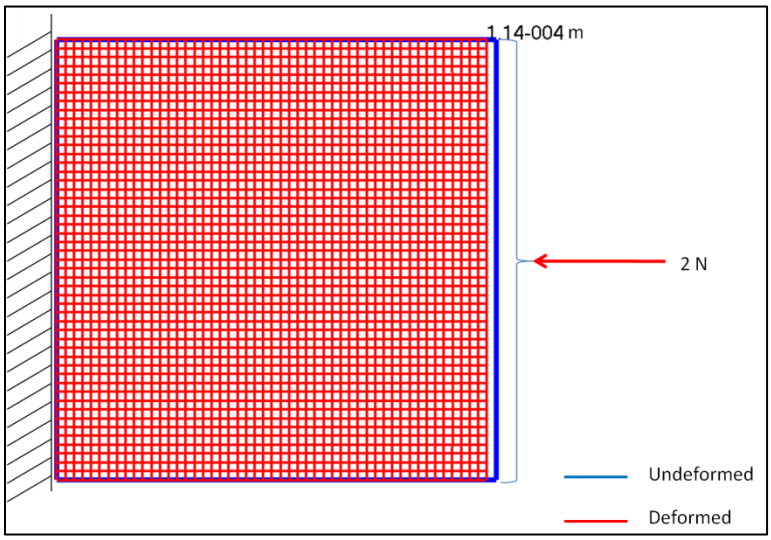

Figure H.2: Cartilage compression.

H.4 Conclusion

The two dimensional FE model provided a simple way with which a cartilage stiffness value could be derived. This is however a very crude approximation. The cartilage was assumed to be isotropic and elastic, while in reality it is a viscoelastic anisotropic material. The approximation made is however warranted since the fluid contents of the cartilage will only start to play a significant role when the loads are applied for prolonged times (Fernandez *et al.* (2008)). In this application (both FEA and dynamic computational model) the loads are applied only for short periods (< 3 seconds).

Appendix I: Illustration of the finite element model boundary conditions

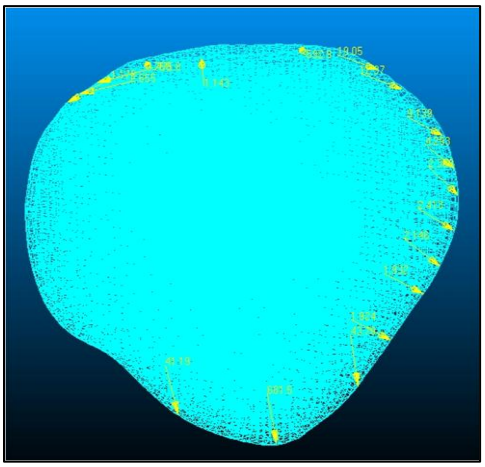

Figure I.1: Patella mesh with soft tissue stabiliser load vectors (yellow arrows).

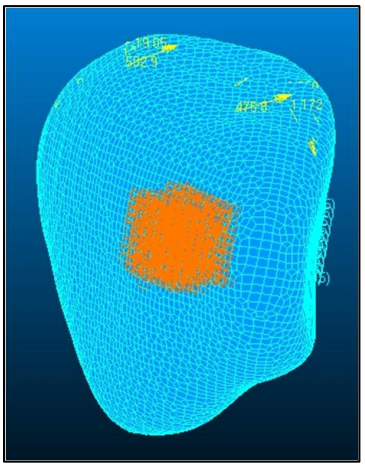

Figure I.2: Patella mesh with displacement boundary condition.

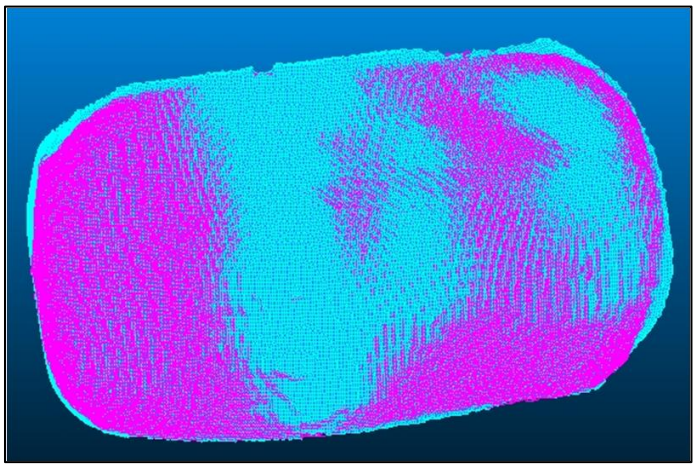

Figure I.3: Patella cartilage mesh with the contact defined (pink circles).

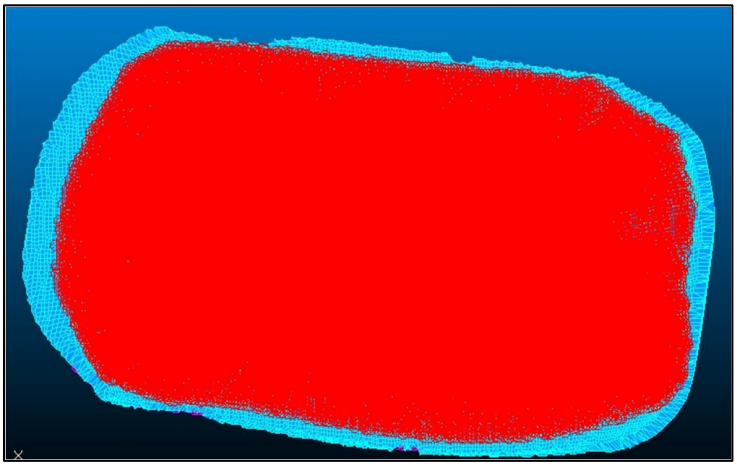

Figure I.4: Patella cartilage mesh with the rigid MPC (red circles).

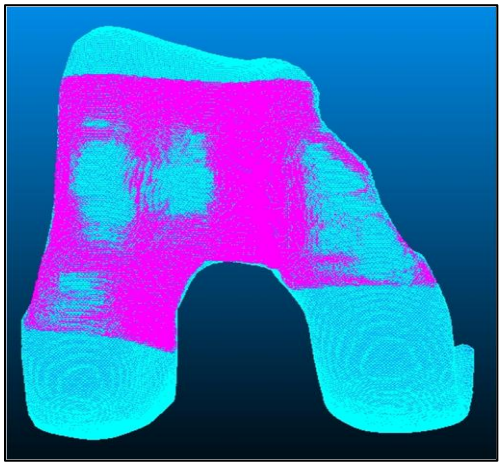

Figure I.5: Femoral cartilage mesh with the contact defined (pink circles).

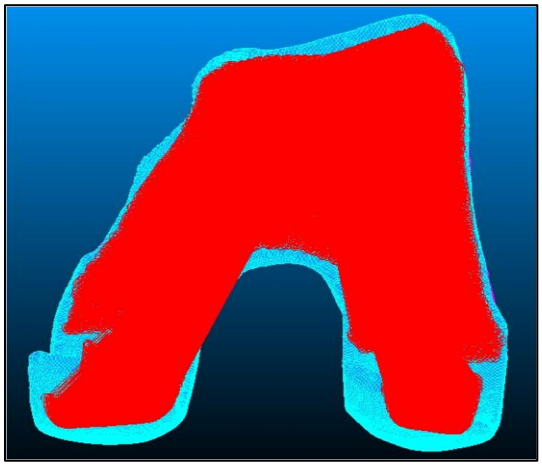

Figure I.6: Femoral cartilage mesh with the rigid MPC (red circles).

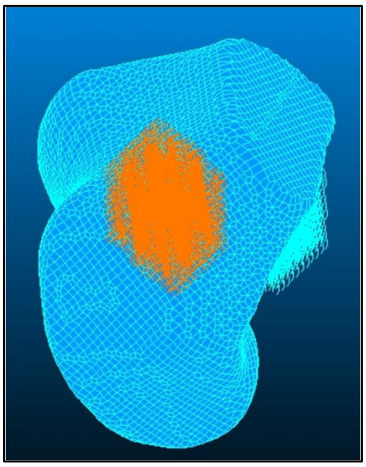

Figure I.7: Femoral mesh with displacement boundary condition.